2012

Investigations into the Role of Humic Acid in Biomembrane Permeability and the Effects of Naturally Formed Gold and Silver Nanoparticles on These Interactions

Loice Marklyne Ojwang
Louisiana State University and Agricultural and Mechanical College

INVESTIGATIONS INTO THE ROLE OF HUMIC ACID IN BIOMEMBRANE PERMEABILITY AND THE EFFECTS OF NATURALLY FORMED GOLD AND SILVER NANOPARTICLES ON THESE INTERACTIONS

A Dissertation

Submitted to the Graduate Faculty of the
Louisiana State University and
Agricultural and Mechanical College
In partial fulfillment of the
requirements for the degree of
Doctor of Philosophy

in

The Department of Chemistry

by
Loice M. Ojwang'
B. S., Moi University Chepkoilel Campus, 2005
August 2012

Dedication

This dissertation is dedicated to my family.

My parents Maurice and Benta
To my husband Richard

Acknowledgments

I would like to acknowledge the funding agent for funding that made this study possible.

- Dr. Robert Cook, my supervisor, for offering me an opportunity to conduct research in his group and for his guidance, direction, support, and patience while conducting this research of vesicle preparations and leakage studies.
- Dr. Naser Elayan for introducing me first to this project and offering me early training.
- My committee members, Dr. Isiah Warner, Dr. Dough Gilman, Dr. Bin Chen and Dr. Mayank Tyagi, for their advice and helpful comments.
- Dr. Dale Treleaven and Dr. Thomas Weldeghoirghis for training me on NMR and helping me with NMR measurements.
- Jameycia Teno for synthezing and characterizing the nanoparticles with me.
- Dr. Elizabeth Cook for editing my thesis.
- Dr. George Stanley for helping me during a difficult time in graduate school.
- Dr. Charisma Lattao, Caroline Schneider, Paulina Kolic, Ugwumsinachi Nwosu, and Balamurugan Subramanian for being such excellent group mates and for their moral support.
- In particular, I would like to thank Caroline for her patience and a lot of dedication in editing my thesis and her unwavering support in my entire time in graduate school and all other unlimited support she offered in the lab throughout my time in graduate school. I am very grateful.

Table of Contents

List of Tables

List of Figures

List of Abbreviations

CMC	critical micelle concentration
CP	cross polarization
Cryo-TEM	cryogenic transmission electron microscopy
DLS	dynamic light scattering
ENPs	Engineered Nanoparticles
MAS	magic angle spinning
FA	fulvic acid
FPHA	Florida Peat humic acid
HA(s)	humic acid(s)
HIX	humification index
IHSS	International Humic Substance Society
LAHA	Leonardite humic acid
LUVs	large unilamellar vesicles
MLVs	multilamellar vesicles
NMR	nuclear magnetic resonance
NOM	natural organic matter
POPC	1-palmitoyl-2-oleoyl-Sn-glycero-3-phosphatidylcholine
Ramp-CP	Ramped-Amplitude cross polarization
SPRP	surface plasmon resonance peaks
SRB	sulforhodamine-B
SUVA	specific ultraviolet sbsorbance
SUVs	small unilamellar vesicles
SWHA	Suwannee River humic acid

UV-Vis	ultraviolet – visible (wavelengths)
TEM	transmission electron microscopy
TX-100	t-octyl-phenoxy polyethoxy ethanol
WAMAs	weakly associated molecular assemblies
HSAB	hard and soft acid base
SA	soft acid

Abstract

The mechanism and kinetics of the interaction of humic acids (HAs) with a 1-palmitoyl-2-oleoyl-Sn-glycero-3-phosphatidylcholine (POPC) large unilamellar vesicle (LUV) model biomembrane system were studied by fluorescence spectroscopy. All three HAs studied induced a perturbation to the biomembrane bilayer structure at pH 4.8. Concentration dependence studies revealed that biomembrane perturbation increased with increasing HA concentrations for Suwannee River HA (SWHA) from 0 to 20 mg C/L. For both Leonardite HA (LAHA) and Florida Peat HA (FPHA) aggregation influenced biomembrane perturbation at concentrations above 5 and 7.5 mg C/L, respectively. Temperature studies over the environmentally relevant ranges of 10 to 30 °C revealed that biomembrane perturbation increased with decreasing temperature for all three HAs studied. Kinetic data established that adsorption and absorption occurred within seconds to minutes and the complex absorption process consisted of both fast and slow components. The slow component was fitted to first order kinetics; however, the fast component could not be fitted with either first or second order kinetics. A mechanism based on "lattice errors" within the biomembranes was proposed to explain the fast and slow components as well as the concentration and temperature findings.

The aromatic moieties within HAs were shown to be responsible for the interactions of HAs with biomembranes and the major biomembrane disruptors for the chemically edited HAs studied.

Au and Ag nanoparticles (NPs) were synthesized using the same chemically diverse and chemically edited HAs at environmentally relevant temperature and pH conditions. Stable particles with narrow size distributions for Au NPs and wider distributions for Ag NPs were formed. The NPs synthesized with HAs at pH 4.8 were polydisperse while the NPs synthesized with HAs at pH 7.6 were monodisperse. The interactions of Au and Ag NPs, synthesized and

stabilized by chemically diverse HAs, with POPC LUVs contributed to greater biomembrane perturbation at pH 4.8 compared to 7.6, as observed by fluorescence leakage experiments and cryo-TEM imaging.

Chapter 1. Introduction

1.1 Humic Substances

Natural organic matter (NOM) refers to the organic acids that are prevalent throughout the environment including terrestrial, aquatic and coal areas. NOM occurs naturally in the environment following microbial breakdown of plant matter containing proteins, cellulose, lignin, lipids, cutins and cutans in the environment [1-3]. NOM are classified into two major categories; non-humic substances and humic substances (HSs). HSs form the major components of natural organic matter and were first discovered by Achard in 1786 through the isolation of a dark precipitate by acidifying an alkali extract of peat [4]. HSs can be best described as complex, heterogeneous and polydisperse mixture of decayed organic matter [5].

As their aqueous solubility is dependent upon pH, HSs are further categorized into three major fractions as follows: humin is insoluble in water at all pH values, fulvic acid (FA) is soluble in water at all pH values, and humic acid (HA) is soluble at pH values higher than 2; as a result the aquatic environment is mostly dominated (50-80%) by the fulvic and HA components of HSs [6].

1.1.1 Sources of HAs

HAs are mainly found in soil in terrestrial, aquatic, and marine environments. They are normally extracted from peat, manure, lignite coal. HAs from different sources have different physical and chemical properties as illustrated in Tables 1.1, 1.2, and 1.3 below. The percent chemical composition of HAs depends on the source material from which it is derived, for example, HAs extracted from a microbial source have more aliphatic moieties than those from higher plants [7]. It has also been shown that HAs extracted from soil are less polar when compared to those extracted from aquatic environments [8, 9].

The structural characteristics and size of HAs are dependent upon the nature of the source material and the extent of diagenesis that occurred during the formation of HA [10, 11]. As a result, HAs from different sources are expected to interact differently with model biomembranes and will also have different potentials to reduce metal salts. In the investigations covered in this thesis, HAs from three different sources (aquatic, terrestrial and coal peat) were studied.

1.1.2 Components of HAs

HAs are made up of components from which they are formed. Terrestrial HAs form in the environment and are derived from mainly plants containing lignins and tannins [10]. HAs found in the aquatic environments are mainly derived from simple aquatic plants and organisms such as algae and bacteria. Generally, HAs are made up three main components: the aliphatic hydrocarbons, the aromatic moieties; with phenolic, carboxylic and methoxyl functionalities mainly derived from lignins, tannins, and carbohydrates [12]. Structural characterization of HAs using various techniques have demonstrated that HAs have a very complex structure with multiple functionalities as can be seen in Figure 1.1 below.

Table 1.1 The relative amount of functionalities within HAs from different sources determined by ^{13}C NMR [13].

	Carbonyl (200-190 pm)	Carboxyl (190-165 pm)	Aromatic (165-110 ppm)	Acetal (190-90 ppm)	Heteroaliphatic (90-60 ppm)	Aliphatic 60-0 ppm)
SWHA	8	19	37	9	7	21
FPHA	5	20	47	4	5	19
LAHA	8	15	58	4	1	14

Table 1.2 The dissociation constant K_a of HAs from various sources [14].

	Carboxyl (meq/g C; 1)	Log K1	Phenolic (meq/g C; 2)	Log K2	Methionine (umol/g)	Cysteine (umol/g)	Total Carbohydrate (umol/g)
SWHA	9.59	4.42	4.24	9.68	1.3	nd	96.5
FPHA	9.01	4.22	1.91	9.86	4	nd	100
LAHA	7.46	4.59	2.31	9.72	0.1	nd	2.6

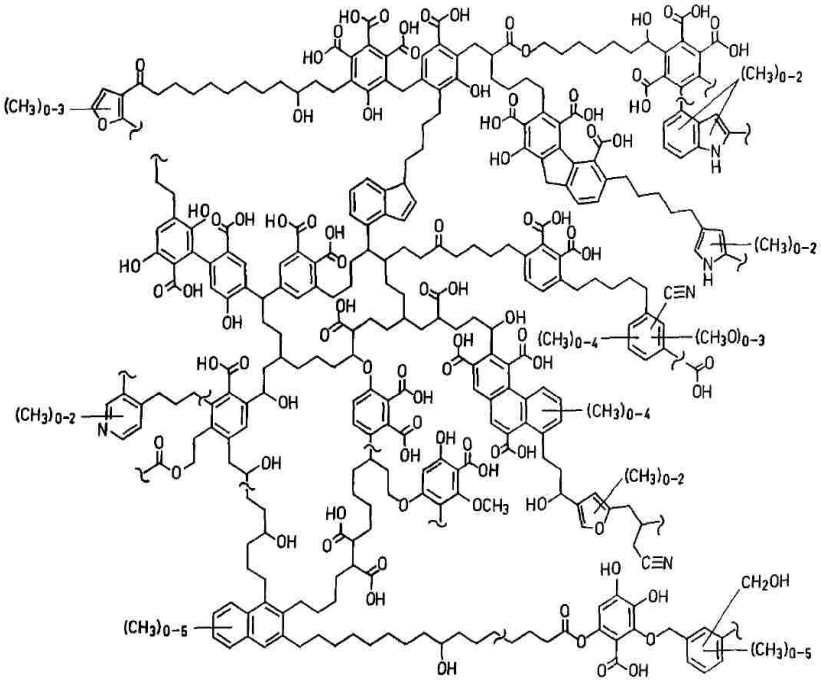

Figure 1.1 A hypothetical structure of humic acid. Molecular formula of $C_{308}H_{328}O_{90}N_5$ and molecular weight of 5540 Da [15].

Aromatic components of HAs

The aromatic components of HAs are either condensed or non-condensed depending on their formation. Non-condensed aromatic components mainly originate from lignins or tannins containing plants, while the condensed ones are via charring of plant materials in volcanic ash soils that yield either charred plant materials or charcoal [16]. Oxidative degradation of HA via

bleaching with NaClO has been reported to eliminate a significant amount of the non-condensed aromatic moieties from lignins or tannins within HAs [17, 18]. The condensed aromatic moieties are resistant to oxidation via bleaching [19]. Phenols, aldehydes and acids are released from lignins during microbial breakdown of parent plant matter and are converted to quinones via enzymatic reactions forming humic-like macromolecules [10].

Carbohydrate components of HAs

Carbohydrates in NOM originate mainly from plants in the form of cellulose, hemicellulose and simple sugars. They comprise approximately between 5-25% of soil organic matter (SOM). Carbohydrates play important roles in complexing metal ions and also bind inorganic soil aggregates. Soil carbohydrates can be classified into three main groups: polysaccharides, monosacharrides and oligosacharides. Acid hydrolysis has been reported to eliminate a significant fraction of extractable carbohydrates and amino acids from NOM [10, 20], with the exception of the non-hydrolyzable N-containing moieties which comprise between 20 to 35% of the total N in soils [10].

Aliphatic components of HAs

The aliphatic components of NOM are comprised of various components: alkenes, alkanes, n-alkyl, fatty acids, alcohols, polynuclear hydrocarbons, resins, terpenes, sterols, fats, and waxes [21] [22]. A major source of the aliphatic components are lipids where the typical concentrations of lipids in SOM range-between 1.2-6.3 % of total organic carbon [22]. Soil lipids are soluble in organic solvents such hexane, benzene or dichloromethane [23]. Soil lipids can partition into organic solvents and be extracted from the bulk soil. Specific lipid components that can be extracted with the organic solvents are long chain fatty acids, higher aliphatic alcohols, long chain alkanes, and esters [24], [21, 25, 26]. Lipid extraction is usually achieved using either

a combination of organic solvents such as a benzene:methanol azeotrope [27] toluene:methanol azaeotrope [21], chloroform:hexane azeotrope [23], or a single organic solvent such as ethanol [28]. Extraction using the benzene:methanol azeotrope has been shown to extract a wide range of lipids in HAs [24].

Sulfur in HAs

The sulfur content and its occurrence, whether organic or inorganic, varies with the environment where the HAs form. Aquatic HAs usually have the reduced form of organic sulfides [29] while terrestrial HAs have the oxidized form of organic sulfur [30]. The reaction of thiols with quinones and reducing sugars results in the formation of C-S-H complexes that occurs as structural components in HAs [10].

1.2 Interaction of HAs environmental components

HAs have a wide structural diversity including hydrophobic and hydrophilic domains. This endows HAs with the potential to interact with a range of environmental components including the living and nonliving components as described below. Interaction of HAs with cell membranes at acidic pHs has been shown to influence the permeability of cell membranes to lipophilic solutes and to pollutants [2, 31]. Adsorption of HAs to phytoplankton cells and fish gill at acidic pH has equally been demonstrated using the electrophoretic mobility of living cells [31]. In addition, HAs have been shown to adsorb to marine phytoplankton and influence the bioavailability of Pb [32]. Though the interaction of HAs with cell membranes at acidic pHs, it has been shown the mechanism governing these interactions is still an open question.

The presence of strong metal binding sites within HAs leads to the formation of HAs-metal cation complexes, this leads to HAs playing a major role in metal speciation and hence fate and transport within natural waters. Specific functional groups within HAs such as phenols,

carboxyls, and thiols have the potential to bind metals [33, 34]. HAs binding metals may lead to a decrease in the bioavailability and the toxicity of the metal as the metal will be in a complex form rather than free metal ion [35]. HAs have been shown to decreases the bioavailability of Cd [36-39] and Cu [39-42] to phytoplankton.

1.3 Oxidation-Reduction Reactions

HAs play a major role in redox reactions that occur naturally in the environment since they have redox potentials attributed to their functional groups, such as quinone-hydroquinone [43-48] as well as other non-quinone functional groups [49]. The redox potential of HAs varies with the origin of HAs (note it has been shown that fulvic acids can exist in an oxidized state in one environment and in reduced state in another environment [50]). The substituent's on the quinone groups play a role in the redox potential of a given HAs. The reduction of metal ions such as Cr^{4+} [51, 52], U^{4+} [53], and Fe^{3+} [54] by HAs have been previously demonstrated. The potential of HAs to reduce various other components such as substituted nitrobenzenes [55] and chlorinated aliphatic compounds has equally been shown [56, 57]. The electron transfer potential of HAs endows them with the potential to reduce oxidized metal ions. The electron-carrying capacity of HA is a measure of the redox potential and is measured as the number of the mole equivalents of electrons transferred from a donor to an acceptor per gram of HA and varies among HA samples [45, 46, 58, 59]. HAs have redox potentials of 0.5-07 V [60]. The redox potential of HAs endows them with the potential to reduce various environmental components, including metal ions, in addition to taking part in photochemical redox reactions in aquatic environments.

1.4 Aggregation of HAs

Aggregation of HAs mainly occurs at acidic pHs. The driving force for aggregation is mainly caused by thermodynamic stability and hydrophobic effects. At acidic pHs, HAs have a low overall negative charge which makes it less stable; as a result, the hydrophobic moieties within it interacts via hydrophobic interactions resulting in the aggregation of HAs molecules [61]. The formation of aggregates by HAs in solution at low pHs, high concentrations and high ionic strengths has been reported [62-64]. HAs aggregates have equally been observed using various techniques such as light scattering [65, 66], fluorescence spectroscopy [67], fluorescence correlation spectroscopy [68], atomic force microscopy [69], turbidimetry [70], and via predictions of molecular mechanics [62].

Protonation of HAs at acidic pHs has been shown to decreases the reactivity of carboxylic functional groups, hence decreasing electrostatic repulsion within HA macromolecule and enhancing the potential of HAs aggregation [71]. The information about the exact aggregate size and the stability of the aggregate is still a controversy. Despite this, several studies have demonstrated that the size of HAs aggregates increase with decreasing pH and decrease with increasing pH and that aggregation occurs in highly concentrated HAs solutions [65, 72, 73].

1.5 Analysis HAs

Elemental analysis of HAs is typically done by the determination of the percent carbon, hydrogen, oxygen nitrogen and sulfur. The amount of carbon is usually reported as total organic carbon; this is obtained after subtracting inorganic carbon from the total carbon. Elemental analysis data of HAs from the aquatic, terrestrial and coal HAs used in the work presented in this thesis is illustrated in Table 1.3 below.

Table 1.3 The percent elemental composition of HAs from various sources [74].

Humic acid	C (% Weight)	H (% Weight)	O (% Weight)	N (% Weight)	S (% Weight)
SWHA	52.55	4.4	42.53	1.19	0.58
FPHA	56.37	3.82	37.34	3.69	0.71
LAHA	63.81	3.7	31.27	1.23	0.76

The percent elemental composition of HAs from various sources differs as can be seen in Table 1.3 above. The carbon and the sulfur contents of Leonardite humic acid (LAHA) are greater than for Suwannee humic acid (SWHA) and Florida peat humic acid (FPHA). SWHA on the other hand has a higher content of hydrogen and oxygen, with the lowest content of carbon and sulfur. FPHA has the highest content of nitrogen. LAHA has a high H/C (17.25), followed by FPHA (14.76), while SWHA has the lowest (11.94). This implies that LAHA has the most aromatic character of the three followed by FPHA then SWHA. Based on the above table, the elemental make-up of HAs varies greatly with the source.

Analysis of HAs by use of UV spectroscopy is usually employed to approximate the concentration of HAs, which is typically achieved by measuring the absorbance of HAs at 254 nm [75]. However, due to the presence of multiple types of chromophores in the structure of HAs, a broad spectrum with no specific observable feature is always obtained. The aromatic content of HAs can be roughly estimated by the use of specific UV absorbance (SUVA), which is basically an absorbance at a specific wavelength divided by the dissolved organic carbon concentration. SUVA of HAs at 254 or 280 nm correlates well with aromatic carbon content, based on ^{13}C NMR, ^{1}H NMR and FTIR data [76-79].

Estimation of the molecular weight (MW) distributions of HAs is conventionally achieved by using high performance size exclusion chromatography. Size exclusion

chromatography is a separation technique in which larger molecules elute first, hence exhibiting a faster retention time while the smaller molecules interact with the stationary phase and are eluted much later [80]. HAs from different sources have been shown to have varying molecular weight (MW). For example soil HAs have a MW of approximately 79 kDa, while a coal-derived humic acid's MW is approximately 130 kDa [81]. Aquatic HAs have smaller MW than soil HAs and coal-derived HAs with MW values of approximately 17–57 kDa [82-84]. It has been shown that much lower MW values can be obtained through the addition of μM to mM concentrations of certain compounds that are capable of disrupting hydrophobic/hydrogen-bonding forces [82-84]. These findings agree with the supermolecular model of NOM and suggest that NOM is made of weak associations of low MW ($\leq$ 2 kDa) molecules, e.g. weak assemble molecular assemblies (WAMAs).

Studies have shown that HAs contain two major fluorophores attributed to protein-like and humic-like molecules [85] [80, 86-90]. The protein-like conclusion was arrived at by comparison to the characteristic excitation and emission wavelengths of tyrosine and tryptophan amino acids at approximately 240 to 325 nm and 300 to 400 nm, respectively. It has been proposed that the humic-like type of fluorophore may originate from quinone-like moieties. Cook, et al. showed that the quinone-like moieties with less conjugated humic materials emits fluorescence between approximately 375 to 475 nm upon excitation at approximately 240 to 325 nm whereas quinone-like moieties with a more conjugated nature emit at wavelengths of 450 to 550 nm upon excitation at 250 to 370 nm wavelength [90]. A highly humified NOM is characterized by high amount of quinone-like molecules, particularly the more conjugated type of quinones.

Nuclear Magnetic Resonance (NMR) has been widely used to identify the various structural components of humic acids. Analysis of HAs by use of ^{1}H NMR usually results in poorly resolved spectra due to the highly complex nature of HAs and the small chemical shift range of ^{1}H NMR when applied, whereas the use of liquid state ^{13}C NMR has difficulty in obtaining accurate quantitation and also requires long acquisition times for the analysis [91] [92]. Solid state ^{13}C NMR is more versatile and is the most preferred method for structural characterization of HAs [93]. This technique involves the use of cross-polarization (CP) which is associated with the following advantages: 1) faster acquisition time compared to the liquid state ^{13}C NMR; 2) a dry homogenized sample is used hence little sample preparation is necessary; 3) non-invasive; and 4) semi-quantitative data can be obtained [90-93].

^{13}C Ramp-CP NMR has been implemented for the analysis of humic acids. This technique involves the use of high magnetic fields as well as a fast sample rotation which significantly enhances the signal-to-noise ratio and the resolution [94] [91] [90, 92]. Ramp-CP studies have indicated that fulvic acid (FA) has high aliphatic moieties contents as well as polar components mainly attributed to carbohydrates and a substantial amount of unsubstituted aromatics [91, 92]. On the other hand, HA is comprised of a high proportion of large aliphatic groups and substituted aromatic moieties. This is consistent with the literature findings that FA contains more polar functionalities while HA is more reduced and more aromatic in nature [91] [90, 92]. Analysis of peat HAs with two-dimensional solid state ^{1}H-^{13}C HETCOR NMR hinted at the presence of significant amount of aromatic functionalities covalently-bonded methoxyl groups, this implies these HAs were derived from lignin containing plant materials, nonpolar alkyl moieties were also detected and the proximity of between O-alkyl domains and aromatic functionalities were determined [95, 96].

1.6 Membranes

Cell membranes play an important role in many biological processes as a regulatory barrier for the exchange of materials between the internal cell cytoplasm and the external cellular matrix via active and passive transport mechanisms. Cell membranes are typically made up of three main components: phospholipids, proteins and carbohydrates. The phospholipids are usually arranged as bilayers and are the main players in the structure and the functioning of the cell membrane while the carbohydrates are mostly found on the surface of the cell membrane and the proteins are either embedded or attached to the surface and offer structural roles for the cell membrane [97].

Investigations on the potential of toxins crossing over the cell membranes to the interior of the cell were traditionally carried out using real cells such as cell cultures and animal cells. However these studies have major drawbacks in regards to obtaining accurate quantitative results, reproducibility of the results, and the cost and the time involved in growing the cultures and the cells [98]. This therefore led to an effort to come up with a simplified model system that could mimic the real cell membranes in an attempt overcome the drawbacks of using real cell to gain insight into understanding the basic fundamental physicochemical properties of cell membranes [98].

Lipid vesicles, also known as liposomes, were first discovered by Sir Alec Bangham and collaborators in the early 1960's [99] when they discovered that amphiphilic molecules, such as phospholipids, self-assemble into sphere-shaped structures consisting of single or multiple bilayers when dispersed in an aqueous medium [99, 100]. The hydrocarbon tails usually form the internal hydrophobic core of the membranes while the hydrophilic regions are made up of the phosphate heads which are oriented at the surface of the membranes.

Liposomes have extensively been used as simple model system to mimic the cell membrane since they are similar to the cell membranes in regards to their self-closed structure which is similar to the plasma membrane structure of eukaryotic cells and in their capability to entrap and capture polar molecules [98]. In addition to their simplicity, it is possible to prepare liposomes with specific properties designed for specific application by varying the lipid composition, lamellarity, size, and surface charges. The use of liposomes as cell membranes models dates back to 1968 [100] and have been applied in food technology [101], analytical purposes [102], pharmaceutical [101], artificial cell studies [103], and among others. They have been widely used to study the interaction of membranes with different types of molecules such as small water-soluble molecules, peptides, complexes, macromolecules and ribosomes [104], Their wide applicability is a result of the ease involved in their preparation, their handiness and the easy with which molecules can be entrapped into their interior.

In general, different cell types have different membrane composition and charges. Studies have shown that it is possible to prepare a lipid vesicle that mimics a particular organism or tissue especially if the tissue or organism lipid composition is known. A good example is the preparation of the antimicrobial peptides that target various bacteria [105]. The choice of the phospholipid is usually based on the charge and the main-phase transition temperature of the vesicles targeted. Vesicles are mostly prepared from phosphatidylcholines, since they are zwitterionic, i.e. carry no net charge, and are most abundant in eukaryotic cells. Similarly, most of the lipids in the plasma membranes of prokaryotes and eukaryotes are made up of acyl chains [98].

In vesicle preparation, it is important to ensure that the vesicles are mostly monolamellar and have a monodisperse size distribution. In addition, the stability and the encapsulation

efficiency of the vesicles should equally be high. Vesicles can be prepared by dispersing phospholipids in an aqueous solution, which results to the formation of the multilamellar vesicles (MLVs). Large unilamellar vesicles (LUVs) of 100-200 nm are generated from the MLVs by extrusion of the MLVs through a pore membrane of an appropriate size [106, 107]. Small unilamellar vesicles (SUVs) with diameters of 20 nm to less than 100 nm can be prepared by sonication methods, while giant vesicles of sizes ranging between 5–200 mm can be prepared by electroformation which involves a controlled swelling of the lipid film in an aqueous solution under the influence of an electric field [108]. The size, lamellarity and charge of the vesicles can be determined by dynamic light scattering, electron microscopy, zeta potential measurements, or electrophoretic mobility [107].

It has been shown that vesicles with varying degrees of complexity that mimic the complexity of cell membranes of organelles in eukaryotic cells can be prepared by either modulating the vesicles membrane surface charge or composition of the phospholipid in various ways [98] [109]. However, these kinds of systems are rather inappropriate for the determination of fundamental mechanistic information especially at a molecular level. Lipid vesicles, which are very simplified models, can yield fundamental molecular level mechanistic information in a much simpler way as compared to complex systems [98] and could help determine the mechanism of interaction of HAs with biomembranes based on the mechanisms that are justified and relevant to the molecular system on or in the liposome.

Membrane permeability, as a result of the interaction of vesicles with various components, can be investigated by fluorescence spectroscopy using entrapped fluorescent molecules to investigate a possible change in the vesicle permeability [6]. These studies monitor increased membrane permeability usually indicated by dye leakage as an indicator of membrane

perturbation. This approach was used in this study to investigate the interaction of HAs with biomembranes by monitoring leakage of a fluorescence probe as induced by the interaction of HAs with biomembranes. A more detailed discussion is presented below.

Lipid bilayers exist in various lamellar and nonlamellar phases as a result of factors such as temperature, pressure and the surrounding solvent [110]. It has been shown that weak first-order processes dominate the main phase transition of the lipid bilayers [111]. Melting of the crystalline phospholipid lattice and acyl chains occurs at the T_m resulting to a change in the lipid bilayer phase, from solid crystalline phase to liquid crystalline phase [112] [113].

The permeability of a one-component phospholipid bilayer to small water soluble molecules, such as fluorescent dye molecules, is higher at the main phase transition temperature (T_m) and decreases at temperatures above and below the T_m when the bilayers are either all-gel or all-fluid [114-120]. At the T_m the gel and the liquid crystalline phases coexist in the vesicle membrane thus resulting in packing defects in the phase boundaries between these coexisting gel and liquid crystalline phases. These packing defects occur as a result of either fluctuations in the lateral compressibility of the bilayers at T_m [120-123] or acyl chain packing mismatches at the boundary between gel and fluid domains [114, 116, 117, 124]. At the T_m, higher leakage occurs in phospholipids with shorter acyl chain length, and vice versa (at T_m $C_{14} > C_{16} > C_{18} > C_{20}$) [118]. The lipid molecules at the domain interfaces are subject to lateral density fluctuations, which are inversely proportional to the acyl chain length; this causes a maximum in the bilayer permeability at T_m [120, 122, 123] [121]. The POPC palmitoyl chain is usually disordered in liquid crystalline phase due to constrain constraint caused by direct bonding of at least one oleyl chain among its nearest neighbors [125]. For this study POPC phospholipids were used to mimic the biomembranes of simple unicellular organisms since they are neutral and they form a

significant fraction of the phospholipids in eukaryotic cells [98], as well as its phase behavior in term of T_m. POPC has a phase transition temperature of T_m of -2.5 ±2.4.[126]. POPC, has a molecular formula of $C_{42}H_{82}NO_8P$ with a molecular weight 760 and an acyl chain of C 16:0 – 18:1 shown below in Figure 1.2.

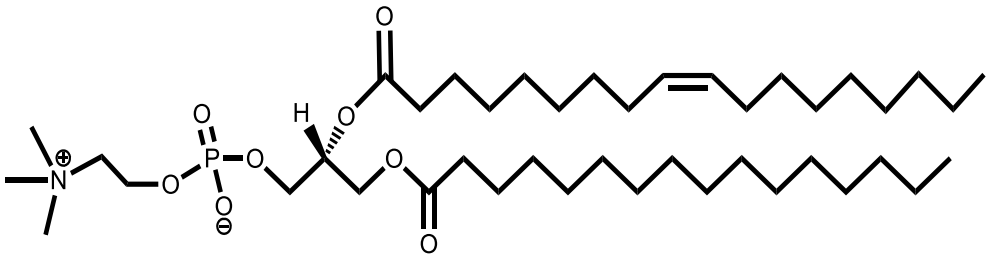

Figure 1.2 The structure of 1-palmitoyl-2-oleoyl-sn-glycero-3-phosphocholine (POPC)

Investigations into the interaction of HAs with model biomembranes using wide-line ^{31}P NMR at varying temperatures indicated that HAs absorb to the biomembranes surface influencing the permeability of the biomembrane and altering the structure of the membrane via interactions with its lipid components. This study further revealed that at temperatures above the T_m melting of the acyl chain takes place, resulting to less head group packing, utilizing fluorescence leak experiments (see discussion below).

1.7 Nanoparticles

Nanoparticles (NPs) are basically defined as particles with at least one dimension below 100 nm in size. This definition places NPs in the same size domain as natural colloids [127]. The presence of both NPs and colloids in the environment has been studied by several groups [128, 129]. NPs may occur naturally in the environment, such as with soil colloids [129], or may be formed unintentionally and introduced into the environment in which case they are usually referred to as incidental NPs. For example, incidental clusters of NPs could be generated during

milling, combustion, welding or grinding. In addition, NPs with specific properties are designed and synthesized for specific applications. These NPs are referred to as engineered nanoparticles (ENPs).

ENPs have found wide applications in various sectors such as in industry, electronics, and the medical field as well as in consumer products [130-132]. It was estimated that the production and use of NPs was at 10 billion in 2010 and is projected to rise to one trillion by 2015 [133, 134]. This therefore implies that significant amounts of ENPs will eventually end up in the environment either as waste or spills during production, transport and use of the nanoproducts.

The wide application of NPs is due to their unique properties that are derived from their high surface area to volume ratio. The reactivity of materials is dependent on its surface area which increases with decreasing particle size. This means that NPs have different properties from their bulk counterparts; a good example of this is gold. Bulk gold metal is chemically inert while gold NPs are very reactive and are used in industries for catalysis [135, 136]. Interest in the production and use of engineered nanoparticles (ENPs) is growing at a rapid rate due to the wide applicability of these particles in various sectors.

NPs are typically made up of three main parts, namely the core, which is metal and is responsible for the unique properties of NPs, a shell, and a cap. NPs are named based on the core identity. A shell may be added around the NPs core. To control the growth of the NPs during their synthesis and to prevent them from aggregating, they are usually coated with ligands, or surfactant which binds to NPs surface via attractive interactions such as electrostatic attraction, chemisorptions, or hydrophobic interaction attributed to the ligand head group. The surface of NPs is very important as all the chemistry of the NPs occurs on the NPs surface and is dependent

on the surface area to volume ratio of the NPs. In addition, the NPs' surface is usually the one that is in contact with other components such as with biomembranes or other environment components. The composition of the surface of NPs is chosen to suit the application of the NPs. In addition from a toxicity perspective the surface of the NPs has the potential to reduce or increase toxicity of the NPs in question [137].

Upon aggregation or precipitation, NPs lose their size properties as they no longer have the larger surface area to volume ratio. In order for NPs to stay suspended in solution, they are usually coated with a molecule, surfactant or an ion bound to the surface of the NPs to enhance their dispersion in solution. Metal NPs can be prepared via two main methods; chemical means or physical means. The later involves generation of NPs from bulk metal via different distribution techniques. Chemical means on the other hand involves the formation NPs by reducing a metal salt in solution chemically using various reducing agents followed by the stabilization of the NPs formed [138-142]. Stabilization of the NPs can be achieved by electrostatic repulsion or steric hindrance mechanisms.

Both gold and silver NPs can be prepared via the chemical method discussed above. Gold or silver metal ions are reduced to zero valences then stabilized with appropriate stabilizing agent to prevent their aggregation. Various components have been used to reduce gold and silver such as sodium borohydride [143], ascorbic acid [144], aliphatic amines [145], HAs [146], H_2 gas [147], ethylene glycols [148], ethanol [149], and Tollen's reagent [150] just to mention a few. Similarly various molecules have been used to stabilize Au and Ag NPs [151, 152]. Sodium citrate and alkanethiols are the most commonly used generating particles with size ranging between 13–100 nm [140, 153, 154] and between 5–10 nm [139, 155] respectively.

NPs of noble metals such as gold and silver are characterized by intense colors. These colors are attributed to surface plasmon resonance SPR, which occur as a result of the interactions between oscillating delocalized electrons on the NPs surface with an electromagnetic field [156]. NPs of gold and silver display surface plasmon resonance peaks (SPRPs) in the UV-Vis region when irradiated by light [157]. Stabilized gold NPs have a characteristic deep red color, which present a surface plasmon resonance peak at 550 nm [152, 156, 158], while stabilized silver NPs have a yellow color and presents a surface plasmon resonance peak at 414 nm [153]. The position and width of the SPR peak varies with size of the NPs [159]. As a result the SPRP can be used to determine the NPs size upon interaction with other molecules [160]. A decrease in NPs size results in a blue-shifted SPR peak and an increase in NPs size results in a red-shifted SPR peak [161].

Silver NPs have been shown to be toxic to aquatic and terrestrial organisms. Several studies have investigated silver toxicity to bacteria [162] [163-166]. In spite of their toxicity, Ag NPs are used widely in industry and in a variety of consumer products [167] [168]. As such they are likely to be released into the environment in significant amounts [169]. Thus understanding their natural formation and their interaction with organisms in the environment is very important. Although gold as a bulk metal is inert, Au NPs have unique size-related and tunable electronic, magnetic and optical properties [152]. In addition they are relatively inert and stable. Gold NPs were used in these studies to provide a base understanding to help in future work in relation to their potential to influence the bioavailability of nutrients [170, 171] and contaminants [172, 173] that could be adsorbed to their surface coating to aquatic organisms as they could be also present in the environment in significant amount as a result of their wide applicability and from various natural sources.

1.8 Methods of HAs, Nanoparticles and Biomembranes Analysis

1.8.1 Fluorescence Spectroscopy

Fluorescence spectroscopy is a sensitive, non-destructive and relatively inexpensive technique that is typically used to study HAs and membrane permeability [6]. Fluorescence is a form of luminescence that occurs mainly from an excited state thermally equilibrated fluorophore [174]. Upon excitation of a fluorophore with light of appropriate wavelength, the fluorophore absorbs a photon which promotes an electron to higher energy level, e.g. to an excited state, from where it relaxes via the emission of a photon. The processes involved in fluorescence occurs in different time frames; light absorption by molecules in ground state occurs in approximately 10^{-15} seconds, relaxation of the excited state molecule to a thermally equilibrate state takes place in about 10^{-12} seconds and the emission of a photon via fluorescence occurs in 10^{-8} seconds. Apart from emitting fluorescence a fluorophore in a thermally equilibrated singlet excited state could cross over to the triplet state from where it could emit a photon in 10^{-3} to 10^{-6} seconds. Emission from the triplet state is referred to as phosphorescence; however, these emissions are very rare as they are of lower energy and they take longer time than fluorescence since these electronic transitions are forbidden. Processes that take place in fluorescence directly from the absorption of light to the emission of light are illustrated by a Jablonski diagram as shown below in Figure 1.3 [174].

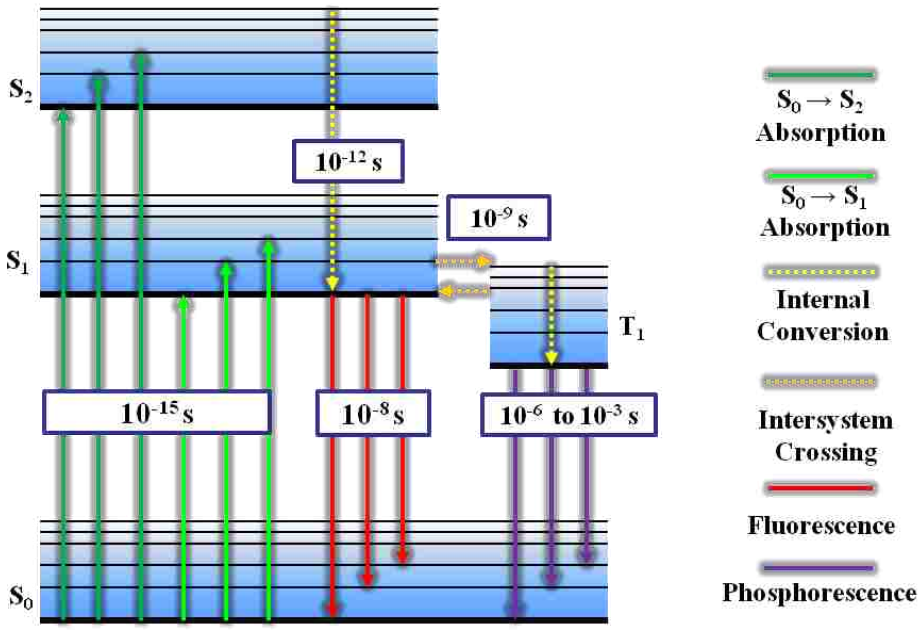

Figure 1.3 The Jablonski diagram illustrating the transitions that occur between absorption of a photon to the emission of the photon.

Fluorescence emission occurs at a longer wavelength than the excitation wavelength. An excitation spectrum is usually measured at a single emission wavelength and an emission spectrum is measured at a single excitation wavelength. A shift between excitation and emission occurs resulting to the wavelength of fluorescent light being greater than the wavelength of the exciting light [174]. This shift is mostly caused by loss of energy due to molecular re-arrangements that come about in order to minimize the energy of the excited state and ground state after the electron is excited and relaxes, respectively as well as associated vibrational losses, this shift phenomenon is called the Stokes shift and was first noted by George Gabriel Stokes in 1952 [174]. The absorption and the emission spectra of most fluorescent molecules are mirror images of each other with a few exceptions in cases where transitions are not vertical. In the case of these molecules the mirror image rule does not occur as a result of change in position of nuclei in the excited state.

Excitation of a fluorophore may involve the use of a continuous source light to measure instant emission in which case these measurements are called fluorescence steady state measurements or a pulsed source of light may be used to measure decay in intensity or anisotropy. These types of measurements are the fluorescence lifetime measurements. The most common type of fluorescence measurement is the steady state measurement, which uses a steady continuous source of light. Various fluorescence experiments have been used to analyze HAs such as fluorescence excitation-emission matrix, fluorescence emission and synchronous scans [175]. Encapsulation of a fluorescent probes within the vesicles makes it possible to investigate the molecular interactions of HAs with model biomembranes via fluorescence leakage experiments. Campbell and coworkers investigated the permeability of model membranes in presence of HAs using fluorescence leakage experiments [31]. The studies presented in this thesis probes HAs biomembranes perturbation mechanisms and kinetics and the interactions between HAs and model biomembranes and the natural NPs using steady state fluorescence measurements.

Leakage of sulforhodamine-B (SRB)

The investigations involving the mechanism of interactions HAs and chemically edited HAs with model biomembranes were probed by monitoring the leakage of the fluorescent probe SRB using fluorescence spectroscopy. These experiments were performed by encapsulating SRB inside the vesicles and upon interaction with HAs, chemically edited HAs and NPs formed with the same HAs, and monitoring the leakage of SRB dye into the surrounding solution as measured by fluorescence spectroscopy. Complete rupture of the vesicles can be attained using a detergent. LUVs were used in this study since they are stable as compared to SUVs in addition to their size of 100 nm which is close to the size of simple unicellular organisms such as bacteria. SRB dye

was used in this study because of its high aqueous solubility over a wide range of pH values and its chemical stability as well as it high molar absorptivity approximately 120 000 at 565 nm [176].

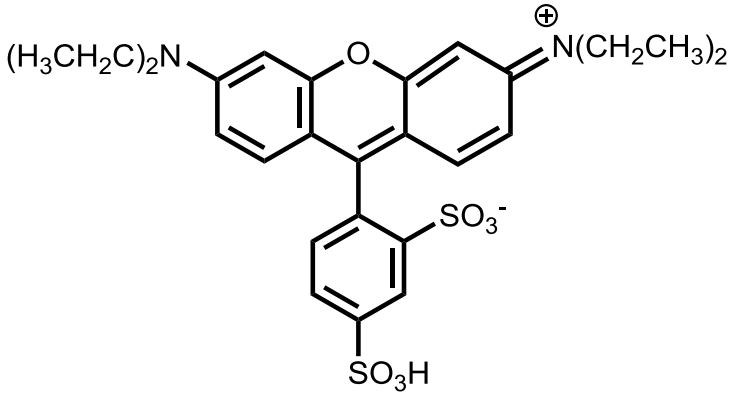

Figure 1.4 Structure of sulforhodamine-B ($C_{27}H_{30}N_2O_7S_2$), formula weight =558.66 g/ mol

As mentioned above, detergents are known to disrupt the molecular ordering of lipid bilayers and have been used to disrupt lipid membrane of various biological samples [6, 177] Triton X-100 (t-octyl-phenoxy polyethoxy ethanol) is a part of the surfactant amphiphilic pollutants family commonly found in the environment as a result of industrial use. TX-100 is also non-fluorescent. TX-100 was used in these studies mainly because it is a non-fluorescent surfactant and its non selectivity in dispruting membranes [178]. The critical micelle concentration (CMC) of TX-100 is 0.24 mM. Other properties of TX-100 includes: nontoxicity, hydrophilicity, and high degradablilty and it is also neutral [177]. TX-100 has been used extensively in other literature studies of disruption of biomembranes [6].

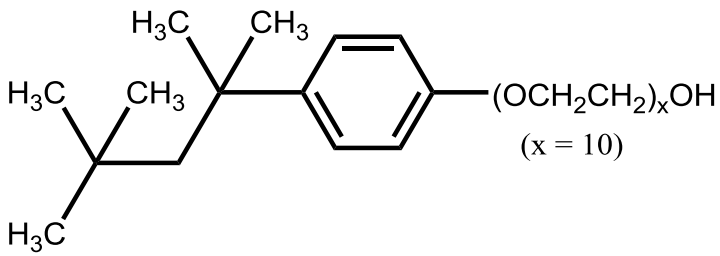

Figure 1.5 The structure of TX-100 (t-octyl-phenoxy polyethoxy ethanol)

1.8.2 Dynamic Light Scattering

When small particles are illuminated by light, they scatter light in all directions via Rayleigh scattering, causing fluctuations in the intensity of the scattered light by the particles. The mean particle size can then be determined by measuring the fluctuations in the intensity of the scattered light at a particular scattering angle; (θ) by a photon detector [179]. DLS is a conventional method used to determine the mean size distribution profile of liposomes in the nm range [6]. A typical commercial DLS instrument has the potential to measure mean particles sizes of between 1 nm to 250 nm. The scattered light undergoes either constructive or destructive interference by the surrounding particles. The decay time distribution for auto-correction functions is determined and the hydrodynamic diameter is calculated using Einstein relation as shown in equation 1.1.

$$RH = KT/6\pi\eta D \qquad 1.1$$

Where

RH is hydrodynamic ratio,

K is the Boltzmann constant,

T is the temperature of the sample,

η is the solvent viscosity

D is the diffusion coefficient.

1.8.3 Solid State Ramp Cross-Polarization Magic Angle spinning (CP MAS) ^{13}C NMR

The use of ^{13}C NMR for the analysis of HAs dates back to the 1970's. ^{13}C NMR is a much less sensitive technique compared to ^{1}H NMR yet it is the method of choice for elucidating the structure of organic molecules in solid samples. Solid state ^{13}C NMR has previously been used to characterize HAs. However, the spectra generated usually have poor signal-to-noise ratios since ^{13}C is less abundant in nature, approximately 1.1%. In addition, these experiments take longer to obtain a decent NMR spectrum since there are no strong homonuclear dipolar interactions to induce relaxation transitions.

Line broadening is the main cause of poor resolution in a ^{13}C NMR spectrum as it either eliminates or obscures the individual NMR peaks. Line broadening is caused by a combination of both dipolar interactions between ^{13}C spins and ^{1}H spins and also by chemical shift anisotropy. Chemical shift anisotropy occurs as a result of changes in chemical shift due to the orientation of the molecule or part of the molecule with respect to the external magnetic field.

Line broadening can be eliminated by magic angle spinning which involves rotating the sample rapidly at frequencies higher than 2 kHz at 54.7º with respect to the applied magnetic field. Long acquisition times can be overcome by the use of cross-polarization techniques since the recycling delay is dependent upon the spin-lattice time T_1, or relaxation of the abundant ^{1}H spins, which are much shorter than T_1 of ^{13}C [93]. Although magic angle spinning helps in eliminating line broadening, it is associated with complicating the Hartmann-Hahn match condition, shown mathematically below, and significantly disrupts cross polarization transfer when the spinning rate approaches the dipolar coupling constant [180].

The Hartmann Hahn equation

$$\gamma_H \omega_H = \gamma_C \omega_C \qquad 1.2$$

where:

γ_H is the gyromagnetic ratio of ^{1}H

ω_C is the gyromagnetic ratio of ^{13}C

ω_H, is the radio frequency field on the ^{1}H

ω_C radio frequency field on the ^{13}C

Due to a combination of all of the above factors, a ramped amplitude contact pulses on one of the spins is usually used to increase the cross-polarization efficiency under magic angle spinning [181, 182]. The use of ramped amplitude cross-polarization in combination with magic angle spinning results in enhanced intensity and less susceptibility to fluctuations in the Hartmann-Hahn match. Therefore solid state ramp-CP MAS **^{13}C** NMR was used in the characterization of the chemically edited HAs.

In a typical solid state Ramp-CP MAS ^{13}C NMR experiment (illustrated in Figure 1.6), a 90° pulse is applied to the abundant ^{1}H spins. This induces the magnetization of these spins. During cross-polarization (CP) a Hartmann-Hahn match is achieved, and magnetization from ^{1}H spins are transferred to ^{13}C spins. Dipole-dipole interactions between the same nuclei (homonuclear) and between different nuclei (heteronuclear) dipolar couplings also occur during the CP process, where the homononuclear dipolar coupling of ^{1}H are much more significant than those of ^{13}C which can be neglected as homonuclear dipolar couplings depends on the natural abundances of spin ½ nuclei [183]. The final step of the CP process involves the removal of the heteronuclear dipolar couplings during acquisition by irradiating the proton resonance frequency with a strong radio frequency field. Protons from the same molecule or from a different molecule are responsible for the transfer of magnetization in the CP process.

Cross-polarization also results in a signal enhancement of approximately 4x, since $\frac{\gamma_H}{\gamma_C}$ = 4, in addition to the faster acquisition times. Spinning the sample at the magic angle reduces line-broadening effects that are primarily caused by chemical shift anisotropy [91, 93] that are common in aromatic, carbonyls, and alkene carbons, as compared to other carbon types [184] [91]. In addition, homonuclear and heteronuclear dipolar couplings are greatly suppressed because they contain a $(1 - 3\cos^2\theta)$ term which goes to zero at the magic angle when the sample is spun rapidly. It has been reported that the dipolar coupling is reduced by 50% when sample is rapidly spinned under a spin-lock field [185].

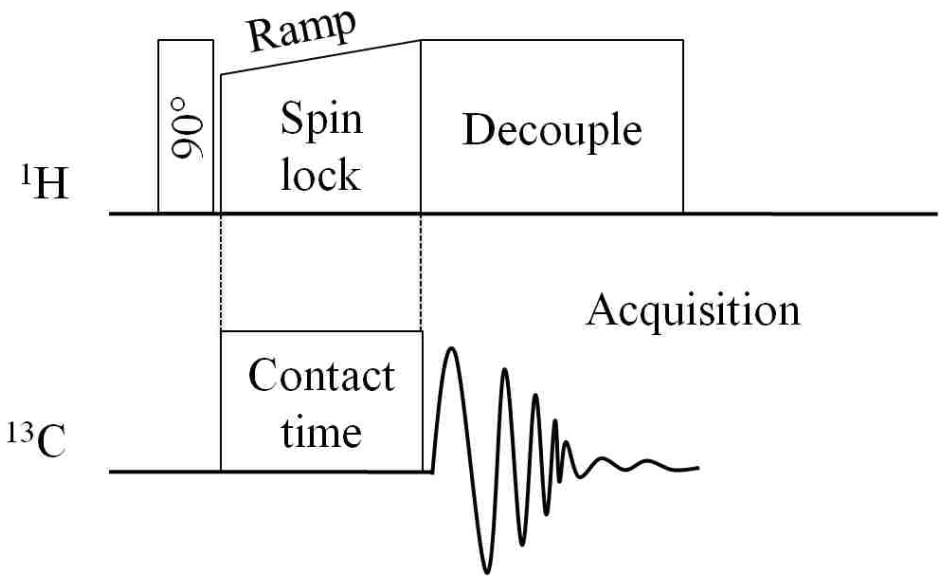

Figure 1.6 The pulse order of a typical solid state Ramp-CP-MAS ^{13}C NMR

A Ramp-CP experiment is associated with the following advantages: 1) an exact Hartmann-Hahn match is achieved, even with highly complex samples such as NOM; 2) this exact match improves resolution, because it allows for cross-polarization for the different carbon types present; and 3) this overcomes the narrowing of the Hartman-Hehn condition at high sample spinning speeds [91, 93].

1.8.4 Transmission electron microscopy (TEM)

TEM was developed in Germany by Max Knoll and Ernst Ruska in 1931. TEM imaging of NPs gives information about the size, size distribution, morphology, and the shape of the NPs. Resolution down to atomic level can be obtained as a result of short de-Brogli wavelength of electron. TEM is composed of three main components; an electron gun for generating electrons, electromagnetic lenses for focusing the electron beam, and a detector for recording the image. A beam of electrons from the electron gun is focused onto a sample and the transmitted electrons are projected onto a detector. The image formed is then focused, magnified and detected. TEM imaging is done under a high vacuum to prevent deflection of electrons by gas molecules. Resolution in TEM can be improved by increasing the acceleration voltage of the electrons since the increase in voltage decreases the wavelength of electrons; this, however, worsens the contrast since the scattering of the electrons is inversely proportional to their velocity. A high contrast is only possible in samples with high electron density [186].

Cryo-TEM

The instrumentation and the operation principles of cryo-TEM are very similar to that of a conventional TEM except it images specimens in a frozen hydrated state while the conventional TEM images dry specimens. As such, it has an additional component: a special sample holder that has small dewar for liquid nitrogen used for cooling the sample, this is what makes characterization of samples with a cryo-TEM a success because inadequate cooling of the vitrified sample damages the sample [187]. Cryo-TEM has been used by other research groups as well to characterize liposomes [187]. In the studies covered in this thesis, cryo-TEM was used determine the size and shape of the lipososmes as a complementary technique to fluorescence spectroscopy to visually investigate the interactions of HAs and naturally formed NPs with

model biomembranes. Conventional TEM was used to characterize the Au and Ag NP formed in the presence of HAs and chemically edited HAs.

1.8.5 UV-Vis Spectroscopy

UV-Vis spectroscopy measures the absorbance of ultra-violet and visible light by molecules at different wavelengths. UV-Vis spectroscopy has been used previously to confirm the formation of NPs of noble metals such as gold and silver. An absorption spectrum shows absorption bands corresponding to particles of different sizes. NPs of different sizes absorb UV-Vis radiation of different wavelengths, as discussed above for Au and Ag NPs. UV-Vis absorbance was used in this study to confirm the formation of gold and silver NPs and to determine their polydispersity and the aggregation by monitoring the characteristic SPRP. In addition it was used to quantify the amount of NPs formed as absorbance (A) is directly proportional to concentration (c) as long as the path length (b) and the extinction coefficient (ε) are constants following Beer's Law.

1.9 References

1. Nakashima, K.; Xing, S. Y.; Gong, Y. K.; Miyajima, T. Characterization of humic acids by two-dimensional correlation fluorescence spectroscopy. *Journal of Molecular Structure.* **2008,** *883,* 155-159.

2. Elayan, N. M.; Treleaven, W. D.; Cook, R. L. Monitoring the effect of three humic acids on a model membrane system using ^{31}P NMR. *Environ. Sci. Technol.* **2008,** *42* (5), 1531-1536.

3. Duval, J. F. L.; Wilkinson, K. J.; Van Leeuwen, H. P.; Buffle, J. Humic substances are soft and permeable: Evidence from their electrophoretic mobilities. *Environ. Sci. Technol.* **2005,** *39* (17), 6435-6445.

4. Frimmel, F. H. Aquatic Humic Substances. biopolymers online: 2005.
5. Buffle J. Complexation reactions in aquatic systems: an analytical approach. Ellis Harwood, : Chester, UK, , 1998.

6. Vigneault, B.; Percot, A.; Lafleur, M.; Campbell, P. G. C. Permeability changes in model and phytoplankton membranes in the presence of aquatic humic substances. *Environ. Sci. Technol.* **2000,** *34* (18), 3907-3913.

7. McKnight, D. M.; Aiken, G. R.; Smith, R. L. Aquatic Fulvic-acids in microbially based ecosystems- results from 2 desert lakes in antarctica. *Limnol. Oceanogr.* **1991,** *36* (5), 998-1006.

8. Gauthier, T. D.; Seitz, W. R.; Grant, C. L. Effects of structural and compositional variations of dissolved humic materials on pyrene KOC values. *Environ. Sci. Technol.* **1987,** *21* (3), 243-248.

9. Chin, Y. P.; Weber, W. J. Estimating the effects of dispersed organic polymers on the sorption of contaminants by natural solids .1. A predictive thermodynamic humic substance organic solute interaction-model. *Environ. Sci. Technol.* **1989,** *23* (8), 978-984.

10. Stevenson, F.J. Humus chemistry: Genesis, composition, reactions. *John Wiley and Sons, Stillerman*. **1994.**

11. Cronan, C. S.; Aiken, G. R. Chemistry and transport of soluble Humic substances in forested watersheds of the Adirondack park New-York. *Geochim. Cosmochim. Acta*. **1985,** *49* (8), 1697-1705.

12. Simpson, A. J.; Kingery, W. L.; Hayes, M. H. B.; Spraul, M.; Humpfer, E.; Dvortsak, P.; Kerssebaum, R.; Godejohann, M.; Hofmann, M. Molecular structures and associations of humic substances in the terrestrial environment. *Naturwissenschaften.* **2002,** *89* (2), 84-88.

13. Schulten, H. R.; Schnitzer, M. A state of-the-art structural concept for humic substances. *Naturwissenschaften.* **1993,** *80* (1), 29-30.

14. Thorn, K. A., Folan, D.W., MacCarthy, P. Characterization of the IHSS Standard and Reference Fulvic and Humic Acids by Solution State 13C and 'H NMR Spectrometry. *U.S. Geological Survey, Water-Resources Investigations Report.* **1989,** *89-4196*.

15. Ritchie, J. D.; Perdue, E. M., *Geochim. Cosmochim. Acta.* **2003,** *67*, 85-96.

16. Shindo, H.; Matsui, Y.; Higashi, T. Humus composition of charred plant residues. *Soil Science and Plant Nutrition.* **1986,** *32* (3), 475-478.

17. Sonnenberg, L. B.; Johnson, J. D.; Christman, R. F. Chemical degradation of humic substances for structural characterization. *Acs Symposium Series.* **1989,** *219*, 3-23.

18. Wise, L. E.; Murphy, M.; Daddieco, A. A. Chlorite holocellulose, its fractionation and bearing on summative wood analysis and on studies on the hemicelluloses. *Technical Association Papers.* **1946,** *29* (JUN), 210-218.

19. Chefetz, B.; Salloum, M. J.; Deshmukh, A. P.; Hatcher, P. G. Structural components of humic acids as determined by chemical modifications and carbon-13 NMR, pyrolysis-, and thermochemolysis-gas chromatography/mass spectrometry. *Soil Science Society of America Journal.* **2002,** *66* (4), 1159-1171.

20. Preston, C. M.; Schnitzer, M. Effects of chemical modifications and extractants on the C-13 NMR-spectra of humic materials. *Soil Science Society of America Journal.* **1984,** *48* (2), 305-311.

21. Wu, Q. G.; Schleuss, U.; Blume, H. P. Investigation on soil lipid extraction with different organic-solvents. *Z. Pflanzen. Bodenk.* **1995,** *158* (4), 347-350.

22. Stevenson, F.J. Humus chemistry: Genesis, composition, reactions. Wiley-Interscience, New York., 1982.

23. Bergman, W. Geochemistry of lipids. Organic Geochemistry., ed. I.A.E. In: Breger, Organic and Geochemistry. Pergamon Press, New York. **1963.**

24. Lodygin, E. D.; Beznosikov, V. A., Influence of soil moisture on concentrations and C-13 NMR profiles of lipids in three Albeluvisols. *Geoderma.* **2005,** *127* (3-4), 253-262.

25. Guignard, C.; Lemee, L.; Ambles, A. Lipid constituents of peat humic acids and humin. Distinction from directly extractable bitumen components using TMAH and TEAAc thermochemolysis. *Org. Geochem.* **2005,** *36* (2), 287-297.

26. Schnitzer, M.; Schulten, H. R. Pyrolysis-soft ionization mass- spectrometrometry of aliphatics extracted from a soil clay and humic substances. *Sci. Total Environ.* **1989,** *81-2*, 19-30.

27. Rice, J.; Maccarthy, P. Isolation of humin by liquid-liquid partitioning. *Sci. Total Environ.* **1989,** *81-2*, 61-69.

28. Grimalt, J. O.; Saizjimenez, C. Lipids of soil humic acids.1.The Hymatomelanic acid fraction. *Science of the Total Environment.* **1989,** *81-2*, 409-420.

29. Urban, N. R.; Ernst, K.; Bernasconi, S. Addition of sulfur to organic matter during early diagenesis of lake sediments. *Geochim. Cosmochim. Acta.* **1999,** *63* (6), 837-853.

30. Lehmann, J.; Solomon, D.; Zhao, F. J.; McGrath, S. P. Atmospheric SO_2 emissions since the late 1800s change organic sulfur forms in humic substance extracts of soils. *Environ. Sci. Technol.* **2008,** *42* (10), 3550-3555.

31. Campbell, P. G. C.; Twiss, M. R.; Wilkinson, K. J. Accumulation of natural organic matter on the surfaces of living cells: implications for the interaction of toxic solutes with aquatic biota. *Canadian Journal of Fisheries and Aquatic Sciences.* **1997,** *54* (11), 2543-2554.

32. Sanchez-Marin, P.; Beiras, R. Adsorption of different types of dissolved organic matter to marine phytoplankton and implications for phytoplankton growth and Pb bioavailability. *Journal of Plankton Research.* **2011,** *33* (9), 1396-1409.

33. Tipping, E.; Rey-Castro, C.; Bryan, S. E.; Hamilton-Taylor, J. Al(III) and Fe(III) binding by humic substances in freshwaters, and implications for trace metal speciation. *Geochim. Cosmochim. Acta* **2002,** *66* (18), 3211-3224.

34. Bryan, S. E.; Tipping, E.; Hamilton-Taylor, J. Comparison of measured and modelled copper binding by natural organic matter in freshwaters. *Comp. Biochem. Physiol. C-Toxicol. Pharmacol.* **2002,** *133* (1-2), 37-49.

35. Campbell, P. G. C. Interactions between trace metals and aquatic organisms: a critique of the free-ion activity model; In Tessier, A.; Turner, D. R., Eds.; Metal Speciation and Bioavailability in Aquatic Systems. *John Wiley & Sons, New York*. **1995**, 45–102.

36. Pempkowiak, J.; Kosakowska, A. Accumulation of cadmium by green algae Chlorella vulgaris in the presence of marine humic substances. *Environment International.* **1998,** *24* (5-6), 583-588.

37. Vigneault, B.; Campbell, P. G. C. Uptake of cadmium by freshwater green algae: Effects of pH and aquatic humic substances. *Journal of Phycology.* **2005,** *41* (1), 55-61.

38. Koukal, B.; Gueguen, C.; Pardos, M.; Dominik, J. Influence of humic substances on the toxic effects of cadmium and zinc to the green alga Pseudokirchneriella subcapitata. *Chemosphere.* **2003,** *53* (8), 953-961.

39. Lamelas, C.; Slaveykova, V. I. Comparison of Cd(II), Cu(II), and Pb(II) biouptake by green algae in the presence of humic acid. *Environ. Sci. Technol.* **2007,** *41* (11), 4172-4178.

40. De Schamphelaere, K. A. C.; Vasconcelos, F. M.; Heijerick, D. G.; Tack, F. M. G.; Delbeke, K.; Allen, H. E.; Janssen, C. R. Development and field validation of a predictive copper toxicity model for the green alga Pseudokirchneriella subcapitata. *Environmental Toxicology and Chemistry.* **2003,** *22* (10), 2454-2465.

41. Sunda, W. G.; Lewis, J. A. M. Effect of complexation by natural organic-ligands on toxicity of copper to a unicellular alga, monochrysis-lutheri. *Limnology and Oceanography.* **1978,** *23* (5), 870-876.

42. Srna, R. F.; Garrett, K. S.; Miller, S. M.; Thum, A. B. Copper complexation capacity of marine water samples from southern- california. *Environ. Sci. Technol.* **1980,** *14* (12), 1482-1486.

43. Klapper, L.; McKnight, D. M.; Fulton, J. R.; Blunt-Harris, E. L.; Nevin, K. P.; Lovley, D. R.; Hatcher, P. G. Fulvic acid oxidation state detection using fluorescence spectroscopy. *Environ. Sci. Technol.* **2002,** *36* (14), 3170-3175.

44. Fimmen, R. L.; Cory, R. M.; Chin, Y. P.; Trouts, T. D.; McKnight, D. M. Probing the oxidation-reduction properties of terrestrially and microbially derived dissolved organic matter. *Geochim. Cosmochim. Acta.* **2007,** *71* (12), 3003-3015.

45. Struyk, Z.; Sposito, G. Redox properties of standard humic acids. *Geoderma.* **2001,** *102* (3-4), 329-346.

46. Scott, D. T.; McKnight, D. M.; Blunt-Harris, E. L.; Kolesar, S. E.; Lovley, D. R. Quinone moieties act as electron acceptors in the reduction of humic substances by humics-reducing microorganisms. *Environ. Sci. Technol.* **1998,** *32* (19), 2984-2989.

47. Nurmi, J. T.; Tratnyek, P. G. Electrochemical properties of natural organic matter (NOM), fractions of NOM, and model biogeochemical electron shuttles. *Environ. Sci. Technol.* **2002,** *36* (4), 617-624.

48. Cory, R. M.; McKnight, D. M. Fluorescence spectroscopy reveals ubiquitous presence of oxidized and reduced quinones in dissolved organic matter. *Environ. Sci. Technol.* **2005,** *39* (21), 8142-8149.

49. Ratasuk, N.; Nanny, M. A. Characterization and quantification of reversible redox sites in humic substances. *Environ. Sci. Technol.* **2007,** *41* (22), 7844-7850.

50. Fulton, J. R.; McKnight, D. M.; Foreman, C. M.; Cory, R. M.; Stedmon, C.; Blunt, E. Changes in fulvic acid redox state through the oxycline of a permanently ice-covered Antarctic lake. *Aquatic Sciences* **2004,** *66* (1), 27-46.

51. Nakayasu, K.; Fukushima, M.; Sasaki, K.; Tanaka, S.; Nakamura, H. Comparative studies of the reduction behavior of chromium(VI) by humic substances and their precursors. *Environmental Toxicology and Chemistry.* **1999,** *18* (6), 1085-1090.

52. Wittbrodt, P. R.; Palmer, C. D. Reduction of Cr(VI) by soil humic acids. *European Journal of Soil Science.* **1997,** *48* (1), 151-162.

53. Gu, B. H.; Chen, J. Enhanced microbial reduction of Cr(VI) and U(VI) by different natural organic matter fractions. *Geochimica Et Cosmochimica Acta.* **2003,** *67* (19), 3575-3582.

54. Deiana, S.; Gessa, C.; Manunza, B.; Rausa, R.; Solinas, V. Iron(III) reduction by natural humic acids-a potentiometric and spectroscopic study I. *European Journal of Soil Science.* **1995,** *46* (1), 103-108.

55. Dunnivant, F. M.; Schwarzenbach, R. P.; Macalady, D. L. Reduction of substituted nitrobenzenes in aqueous-solutions containing natural organic-matter. *Environ. Sci. Technol.* **1992,** *26* (11), 2133-2141.

56. Kappler, A.; Haderlein, S. B. Natural organic matter as reductant for chlorinated aliphatic pollutants. *Environ. Sci. Technol.* **2003,** *37* (12), 2714-2719.

57. Curtis, G. P.; Reinhard, M. Reductive dehalogenation of hexachlorethane, carbon-tetrachloride, and bromoform by anthrahydroquinone disulfonate and humic-acid. *Environ. Sci. Technol.* **1994,** *28* (13), 2393-2401.

58. Lovley, D. R.; Blunt-Harris, E. L. Role of humic-bound iron as an electron transfer agent in dissimilatory Fe(III) reduction. *Applied and Environmental Microbiology.* **1999,** *65* (9), 4252-4254.

59. Bauer, M.; Heitmann, T.; Macalady, D. L.; Blodau, C. Electron transfer capacities and reaction kinetics of peat dissolved organic matter. *Environ. Sci. Technol.* **2007,** *41* (1), 139-145.

60. Skogerboe, R. K.; Wilson, S. A. Reduction of ionic species by fulvic-acid. *Anal. Chem.* **1981,** *53* (2), 228-232.

61. Leppard, G. G.; Buffle, J.; Baudat, R. A description of the aggregation properties of aquatic pedogenic fulvic-acids - combining physicochemical data and microscopic observations. *Water Res.* **1986,** *20* (2), 185-196.

62. Schulten, H. R.; Leinweber, P. New insights into organic-mineral particles: composition, properties and models of molecular structure. *Biology and Fertility of Soils.* **2000,** *30* (5-6), 399-432.

63. Clapp, C. E.; Hayes, M. H. B. Sizes and shapes of humic substances. *Soil Sci.* **1999,** *164* (11), 777-789.

64. Swift, R. S. Macromolecular properties of soil humic substances: Fact, fiction, and opinion. *Soil Sci.* **1999,** *164* (11), 790-802.

65. Pinheiro, J. P.; Mota, A. M.; dOliveira, J. M. R.; Martinho, J. M. G. Dynamic properties of humic matter by dynamic light scattering and voltammetry. *Anal. Chim. Acta.* **1996,** *329* (1-2), 15-24.

66. Tombacz, E.; Rice, J. A.; Ren, S. Z. Fractal structure of polydisperse humic acid particles in solution studied by scattering methods. *Ach-Models in Chemistry.* **1997,** *134* (6), 877-888.

67. Engebretson, R. R.; von Wandruszka, R. Kinetic aspects of cation enhanced aggregation in aqueous humic acids. *Environ. Sci. Technol.* **1998,** *32* (4), 488-493.

68. Lead, Jr.; Wilkinson, K. J.; Starchev, K.; Canonica, S.; Buffle, J. Determination of diffusion coefficients of humic substances by fluorescence correlation spectroscopy: Role of solution conditions. *Environ. Sci. Technol.* **2000,** *34* (7), 1365-1369.

69. Balnois, E.; Wilkinson, K. J.; Lead, Jr.; Buffle, J. Atomic force microscopy of humic substances: Effects of pH and ionic strength. *Environ. Sci. Technol.* **1999,** *33* (21), 3911-3917.

70. Senesi, N.; Rizzi, F. R.; Dellino, P.; Acquafredda, P. Fractal humic acids in aqueous suspensions at various concentrations, ionic strengths, and pH values. *Colloids and Surfaces a-Physicochemical and Engineering Aspects.* **1997,** *127* (1-3), 57-68.

71. Avena, M. J.; Wilkinson, K. J. Disaggregation kinetics of a peat humic acid: Mechanism and pH effects. *Environ. Sci. Technol.* **2002,** *36* (23), 5100-5105.

72. Milne, C. J.; Kinniburgh, D. G.; Dewit, J. C. M.; Vanriemsdijk, W. H.; Koopal, L. K. Analysis of proton binding by a peat humic-acid using a simple electrostatic model. *Geochim. Cosmochim. Acta* **1995,** *59* (6), 1101-1112.

73. Pinheiro, J. P.; Mota, A. M.; Goncalves, M.; van Leeuwen, H. P. The pH effect in the diffusion coefficient of humic matter: influence in speciation studies using voltammetric techniques. *Colloid Surf. A-Physicochem. Eng. Asp.* **1998,** *137* (1-3), 165-170.

74. Elemental Composition and Stable Isotopic Ratios of IHSS Sample. (Accessed **04/30/2012)**; Available from: http://www.humicsubstances.org/elements.html

75. Najm, I. N.; Patania, N. L.; Jacangelo, J. G.; Krasner, S. W. Evaluating surrogates for disinfection by-products. *J. Am. Water Work Assoc.* **1994,** *86* (6), 98-106.

76. Weishaar, J. L.; Aiken, G. R.; Bergamaschi, B. A.; Fram, M. S.; Fujii, R.; Mopper, K. Evaluation of specific ultraviolet absorbance as an indicator of the chemical composition and reactivity of dissolved organic carbon. *Environ. Sci. Technol.* **2003,** *37* (20), 4702-4708.

77. Chin, Y. P.; Aiken, G.; Oloughlin, E. Molecular-weight, polydispersity and spectroscopic properties of aquatic humic substances. *Environ. Sci. Technol.* **1994,** *28* (11), 1853-1858.

78. Kalbitz, K.; Geyer, W.; Geyer, S. Spectroscopic properties of dissolved humic substances - a reflection of land use history in a fen area. *Biogeochemistry.* **1999,** *47* (2), 219-238.

79. McKnight, D. M.; Harnish, R.; Wershaw, R. L.; Baron, J. S.; Schiff, S. Chemical characteristics of particulate, colloidal, and dissolved organic material in Loch Vale Watershed, Rocky Mountain National Park. *Biogeochemistry.* **1997,** *36* (1), 99-124.

80. Leenheer, J. A.; Croue, J. P. Characterizing aquatic dissolved organic matter. *Environ. Sci. Technol.* **2003,** *37* (1), 18A-26A.

81. Rausa, R.; Mazzolari, E.; Calemma, V. Determination of molecular -size distributions of humic acids by high-performance size-exclusion chromatography. *Journal of Chromatography.* **1991,** *541* (1-2), 419-429.

82. Piccolo, A. The supramolecular structure of humic substances: A novel understanding of humus chemistry and implications in soil science. *Advances in Agronomy*. **2002,** *75 57-134.*

83. Piccolo, A.; Conte, P.; Trivellone, E.; Van Lagen, B. Reduced heterogeneity of a lignite humic acid by preparative HPSEC following interaction with an organic acid. Characterization of size-separates by Pyr-GC-MS and (1)H-NMR spectroscopy. *Environ. Sci. Technol.* **2002,** *36* (1), 76-84.

84. Conte, P.; Piccolo, A. Conformational arrangement of dissolved humic substances. Influence of solution composition on association of humic molecules. *Environ. Sci. Technol.* **1999,** *33* (10), 1682-1690.

85. Coble, P. G.; Green, S. A.; Blough, N. V.; Gagosian, R. B. Characterization of dissolved organic-matter in the black-sea by fluoresence spectroscopy. *Nature.* **1990,** *348* (6300), 432-435.

86. Coble, P. G. Characterization of marine and terrestrial DOM in seawater using excitation emission matrix spectroscopy. *Mar. Chem.* **1996,** *51* (4), 325-346.

87. Chen, W.; Westerhoff, P.; Leenheer, J. A.; Booksh, K. Fluorescence excitation - Emission matrix regional integration to quantify spectra for dissolved organic matter. *Environ. Sci. Technol.* **2003,** *37* (24), 5701-5710.

88. Stedmon, C. A.; Markager, S.; Bro, R. Tracing dissolved organic matter in aquatic environments using a new approach to fluorescence spectroscopy. *Mar. Chem.* **2003,** *82* (3-4), 239-254.

89. Ariese, F.; van Assema, S.; Gooijer, C.; Bruccoleri, A. G.; Langford, C. H. Comparison of Laurentian Fulvic Acid luminescence with that of the hydroquinone/quinone model system: Evidence from low temperature fluorescence studies and EPR spectroscopy. *Aquat. Sci.* **2004,** *66* (1), 86-94.

90. Cook, R.L. NMR Application in Environmental Research of Anthropogenic Compounds. In: IUPAC series on biophysico-chemical processes in environmental systems, volume 3 Biophysico – chemical processes of Anthropogenic Organic Compounds in Environmental Systems, Xing, B.; Senesi, N.; Huang, P. M. Eds. **2009**.

91. Cook, R. L.; Langford, C. H.; Yamdagni, R.; Preston, C. M. A modified cross-polarization magic angle spinning ^{13}C NMR procedure for the study of humic materials. *Anal. Chem.* **1996,** *68* (22), 3979-3986.

92. Cook, R. L.; Langford, C. H. Structural characterization of a fulvic acid and a humic acid using solid state ramp-CP-MAS ^{13}C nuclear magnetic resonance. *Environ. Sci. Technol.* **1998,** *32* (5), 719-725.

93. Cook, R. L. Coupling NMR to NOM. *Anal. Bioanal. Chem.* **2004,** *378* (6), 1484-1503.

94. Dria, K. J.; Sachleben, J. R.; Hatcher, P. G. Solid-state carbon-13 nuclear magnetic resonance of humic acids at high magnetic field strengths. *J. Environ. Qual.* **2002,** *31* (2), 393-401.

95. Lattao, C.; Birdwell, J.; Wang, J. J.; Cook, R. L. Studying organic matter molecular assemblage within a whole organic soil by nuclear magnetic resonance. *J. Environ. Qual.* **2008,** *37* (4), 1501-1509.

96. Mao, J. D.; Xing, B. S.; Schmidt-Rohr, K. New structural information on a humic acid from two-dimensional ^{1}H -^{13}C- correlation solid-state nuclear magnetic resonance. *Environ. Sci. Technol.* **2001,** *35* (10), 1928-1934.

97. Wolfgang K, H. P. V. Physicochemical kinetics and transport at the biointerface: Setting the stage. *John Wiley & sons.* **2004**, 1-15.

98. Zepik, H. H.; Walde, P.; Kostoryz, E. L.; Code, J.; Yourtee, D. M. Lipid vesicles as membrane models for toxicological assessment of xenobiotics. *Critical Reviews in Toxicology.* **2008,** *38* (1), 1-11.

99. Bangham, A. D.; Standish, M. M.; Watkins, J. C., Diffusion of univalent ions across lamellae of swollen phospholipids. *Journal of Molecular Biology.* **1965,** *13* (1), 238-252.

100. Sessa, G.; Weissman.G, Phospholipid spherules (liposomes) as a model for biological membranes. *Journal of Lipid Research.* **1968,** *9* (3), 310-318.

101. Lasic, D. D. Novel applications of liposomes. *Trends in Biotechnology.* **1998,** *16* (7), 307-321.

102. Goral, V. N.; Zaytseva, N. V.; Baeumner, A. J. Electrochemical microfluidic biosensor for the detection of nucleic acid sequences. *Lab on a Chip.* **2006,** *6* (3), 414-421.

103. Luisi, P. L.; Ferri, F.; Stano, P. Approaches to semi-synthetic minimal cells: a review. *Naturwissenschaften.* **2006,** *93* (1), 1-13.

104. Jain, M.K. Introduction to Biological Membranes. **1988**.

105. Epand, R. F.; Schmitt, M. A.; Gellman, S. H.; Sen, A.; Auger, M.; Hughes, D. W.; Epand, R. M. Bacterial species selective toxicity of two isomeric alpha/beta-peptides: Role of membrane lipids. *Molecular Membrane Biology.* **2005,** *22* (6), 457-469.

106. Mui, B.; Chow, L.; Hope, M. J. Extrusion technique to generate liposomes of defined size. *Liposomes, Pt A.* **2003,** *367*, 3-14.

107. Walde, P. Preparation of vesicles (liposomes). *American Scientific Publishers, Los Angeles.* **2004.**

108. Angelova, M., Giant Vesicles,Perspectives in Supramolecular Chemistry*: Liposome Electroformation*. A.P.W.E. In: P.L. Luisi ed.; *John Wiley and Sons, Chichester,* **2000**.

109. Bolinger, P. Y.; Stamou, D.; Vogel, H. Integrated nanoreactor systems: Triggering the release and mixing of compounds inside single vesicles. *Journal of the American Chemical Society.* **2004,** *126* (28), 8594-8595.

110. Alakoskela, J. M. I.; Kinnunen, P. K. J. Probing phospholipid main phase transition by fluorescence spectroscopy and a surface redox reaction. *J. Phys. Chem. B* **2001,** *105* (45), 11294-11301.

111. Mouritsen, O. G. Theoretical-models of phospholipid phase-transitions. *Chem. Phys. Lipids.* **1991,** *57* (2-3), 179-194.

112. Alonso, A.; Villena, A.; Goni, F. M. Lysis and reassembly of sonicated lecithin vesicles in the presence of Triton X-100. *Febs Letters.* **1981,** *123* (2), 200-204.

113. Parente, R. A.; Lentz, B. R. Phase-behaviour of large unilamellar vesicles composed of synthetic phospholipids. *Biochemistry.* **1984,** *23* (11), 2353-2362.

114. Marsh, D.; Watts, A.; Knowles, P. F. Evidence for phase boundary lipid- permeability of tempocholine into dimyristoylphosphatidylcholine vesicles at phase-transition. *Biochemistry.* **1976,** *15* (16), 3570-3578.

115. Elmashak, E. M.; Tsong, T. Y. Ion selectivity of temperature-induced and electric-field induced pores in dipalmitoylphosphatidylcholine vesicles. *Biochemistry.* **1985,** *24* (12), 2884-2888.

116. Papahadj.D; Jacobson, K.; Nir, S.; Isac, T. Phase- transitions in phospholipid vesicles-fluorescence polarization and permeability measurements concerning effect of temperature and cholesterol. *Biochimica Et Biophysica Acta* .**1973,** *311* (3), 330-348.

117. Vanhoogevest, P.; Degier, J.; Dekruijff, B. Determination of the size of the packing defects in dimyristoylphosphatidylcholine bilayers, present at the phase transition temperature. *FEBS Lett.* **1984,** *171* (2), 160-164.

118. Bramhall, J.; Hofmann, J.; Deguzman, R.; Montestruque, S.; Schell, R. Temperature-dependence of membrane ion conductance analzed by using the amphiphilic anion 5/6-carboxyfluorescein *Biochemistry.* **1987,** *26* (20), 6330-6340.

119. Blok, M. C.; Vanderneutkok, E. C. M.; Vandeenen, L. L. M.; Degier, J. Effect of chain-length and lipid phase-transitions on selective permeability properties of liposomes. *Biochimica Et Biophysica Acta.* **1975,** *406* (2), 187-196.

120. Georgallas, A.; Macarthur, J. D.; Ma, X. P.; Nguyen, C. V.; Palmer, G. R.; Singer, M. A.; Tse, M. Y. The diffusion of small ions through phospholipid-bilayer. *Journal of Chemical Physics.* **1987,** *86* (12), 7218-7226.

121. Linden, C. D.; Wright, K. L.; McConnel.Hm; Fox, C. F. Lateral phase separations in membrane lipids and mechanism of sugar transport in escherichia-coli. *Proceedings of the National Academy of Sciences of the United States of America.* **1973,** *70* (8), 2271-2275.

122. Doniach, S. Thermodynamic fluctuations in phospholipid bilayers. *Journal of Chemical Physics.* **1978,** *68* (11), 4912-4916.

123. Nagle, J. F.; Scott, H. L. Lateral compressibility of lipid monolayers and bilayers theory of membrane-permeability. *Biochimica Et Biophysica Acta.* **1978,** *513* (2), 236-243.

124. Kanehisa, M. I.; Tsong, T. Y. Cluster model of lipid phase-transitions with application to passive permeation of molecules and structure relaxations in lipid bilayers. *Journal of the American Chemical Society.* **1978,** *100* (2), 424-432.

125. Curatolo, W.; Sears, B.; Neuringer, L. J. A calorimetry and deuterium NMR-study of mixed model membranes of 1-Palmitoyl-2-Oleylphosphatidylcholine and saturated phosphatidylcholines. *Biochimica Et Biophysica Acta.* **1985,** *817* (2), 261-270.

126. Koynova, R.; Caffrey, M. Phases and phase transitions of the phosphatidylcholines. *Biochim. Biophys. Acta-Rev. Biomembr.* **1998,** *1376* (1), 91-145.

127. SCENIHR, Request for a scientific opinion on the appropriatenessof existing methodologies to assess the potential risks associated with engineered and adventitious nanotechnologies, **2005.**

128. Wigginton, N. S.; Haus, K. L.; Hochella, M. F. Aquatic environmental nanoparticles. *Journal of Environmental Monitoring.* **2007,** *9* (12), 1306-1316.

129. McCarthy, J. F.; Zachara, J. M. Subsurface transport of cantaminants- mobile colloids in the subsurface environment may alter the transport of contaminants. *Environ. Sci. Technol.* **1989,** *23* (5), 496-502.

130. Sharma, V. K.; Yngard, R. A.; Lin, Y. Silver nanoparticles: Green synthesis and their antimicrobial activities. *Adv. Colloid Interface Sci.* **2009,** *145* (1-2), 83-96.

131. Mills, A.; LeHunte, S. An overview of semiconductor photocatalysis. *J. Photochem. Photobiol. A-Chem.* **1997,** *108* (1), 1-35.

132. Elghanian, R.; Storhoff, J. J.; Mucic, R. C.; Letsinger, R. L.; Mirkin, C. A. Selective colorimetric detection of polynucleotides based on the distance-dependent optical properties of gold nanoparticles. *Science.* **1997,** *277* (5329), 1078-1081.

133. Roco, M. C. International strategy for nanotechnology research and development. *J. Nanopart. Res.* **2001,** *3* (5-6), 353-360.

134. Roco, M. C.; Bainbridge, W. S. Converging technologies for improving human performance: Integrating from the nanoscale. *J. Nanopart. Res.* **2002,** *4* (4), 281-295.

135. Roco, M. C.; Bainbridge, W. S. Converging technologies for improving human performance: Integrating from the nanoscale. *J. Nanopart. Res.* **2002,** *4* (4), 281-295.

136. Bond, G. C. Gold: a relatively new catalyst. *Catal. Today.* **2002,** *72* (1-2), 5-9.

137. Turkevich, J.; Stevenson, P. C.; Hillier, J. A study of the nucleation and growth processes in the synthesis of colloidal gold. *Discussions of the Faraday Society.* **1951,** (11), 55-75.

138. Brust, M.; Walker, M.; Bethell, D.; Schiffrin, D. J.; Whyman, R. Synthesis of thiol-derivatized gold nanoparticles in a 2-phase liquid-liquid system. *Journal of the Chemical Society-Chemical Communications.* **1994,** (7), 801-802;

139. Frens, G. Controlled nucleation for regulation of particle-size in monodisperse gold suspensions. *Nature-Physical Science.* **1973,** *241* (105), 20-22.

140. Bajpai, S. K.; Mohan, Y. M.; Bajpai, M.; Tankhiwale, R.; Thomas, V. Synthesis of polymer stabilized silver and gold nanostructures. *Journal of Nanoscience and Nanotechnology.* **2007,** *7* (9), 2994-3010.

141. Schmid, G.; Corain, B. Nanoparticulated gold: Syntheses, structures, electronics, and reactivities. *European Journal of Inorganic Chemistry.* **2003,** (17), 3081-3098.

142. Lee, P. C.; Meisel, D. Adsorption and surface-enhanced raman of dyes on silver and gold sols. *J. Phys. Chem.* **1982,** *86* (17), 3391-3395.

143. Kashiwagi, Y.; Yamamoto, M.; Nakamoto, M. Facile size-regulated synthesis of silver nanoparticles by controlled thermolysis of silver alkylcarboxylates in the presence of alkylamines with different chain lengths. *J. Colloid Interface Sci.* **2006,** *300* (1), 169-175.

144. Rao, C. R. K.; Trivedi, D. C. Biphasic synthesis of fatty acids stabilized silver nanoparticles: Role of experimental conditions on particle size. *Mater. Chem. Phys.* **2006,** *99* (2-3), 354-360.

145. Dos Santos, D. S.; Alvarez-Puebla, R. A.; Oliveira, O. N.; Aroca, R. F. Controlling the size and shape of gold nanoparticles in fulvic acid colloidal solutions and their optical characterization using SERS. *Journal of Materials Chemistry.* **2005,** *15* (29), 3045-3049.

146. Evanoff, D. D.; Chumanov, G. Size-controlled synthesis of nanoparticles. 1. "Silver-only" aqueous suspensions via hydrogen reduction. *J. Phys. Chem. B* **2004,** *108* (37), 13948-13956.

147. Iyer, K. S.; Raston, C. L.; Saunders, M. Continuous flow nano-technology: manipulating the size, shape, agglomeration, defects and phases of silver nano-particles. *Lab Chip.* **2007,** *7* (12), 1800-1805.

148. Amendola, V.; Polizzi, S.; Meneghetti, M. Free silver nanoparticles synthesized by laser ablation in organic solvents and their easy functionalization. *Langmuir.* **2007,** *23* (12), 6766-6770.

149. Fernandez, E. J.; Garcia-Barrasa, J.; Laguna, A.; Lopez-de-Luzuriaga, J. M.; Monge, M.; Torres, C. The preparation of highly active antimicrobial silver nanoparticles by an organometallic approach. *Nanotechnology.* **2008,** *19* (18).

150. Templeton, A. C.; Hostetler, M. J.; Kraft, C. T.; Murray, R. W. Reactivity of monolayer-protected gold cluster molecules: Steric effects. *Journal of the American Chemical Society.* **1998,** *120* (8), 1906-1911.

151. Daniel, M. C.; Astruc, D. Gold nanoparticles: Assembly, supramolecular chemistry, quantum-size-related properties, and applications toward biology, catalysis, and nanotechnology. *Chem. Rev.* **2004,** *104* (1), 293-346.

152. Doty, R. C.; Tshikhudo, T. R.; Brust, M.; Fernig, D. G. Extremely stable water-soluble Ag nanoparticles. *Chemistry of Materials.* **2005,** *17* (18), 4630-4635.

153. Brown, K. R.; Walter, D. G.; Natan, M. J. Seeding of colloidal Au nanoparticle solutions. 2. Improved control of particle size and shape. *Chemistry of Materials.* **2000,** *12* (2), 306-313.

154. Hostetler, M. J.; Wingate, J. E.; Zhong, C. J.; Harris, J. E.; Vachet, R. W.; Clark, M. R.; Londono, J. D.; Green, S. J.; Stokes, J. J.; Wignall, G. D.; Glish, G. L.; Porter, M. D.; Evans, N. D.; Murray, R. W. Alkanethiolate gold cluster molecules with core diameters from 1.5 to 5.2 nm: Core and monolayer properties as a function of core size. *Langmuir.* **1998,** *14* (1), 17-30.

155. Noguez, C. Surface plasmons on metal nanoparticles: The influence of shpae and physical environment. *Journal of Physical Chemistry C.* **2007,** *111* (10), 3806-3819.

156. Tolaymat, T. M.; El Badawy, A. M.; Genaidy, A.; Scheckel, K. G.; Luxton, T. P.; Suidan, M. An evidence-based environmental perspective of manufactured silver nanoparticle in syntheses and applications: A systematic review and critical appraisal of peer-reviewed scientific papers. *Sci. Total Environ.* **2010,** *408* (5), 999-1006.

157. Grabar, K. C.; Brown, K. R.; Keating, C. D.; Stranick, S. J.; Tang, S. L.; Natan, M. J. Nanoscale characterization of gold colloid monolayers: A comparison of four techniques. *Analytical Chemistry.* **1997,** *69* (3), 471-477.

158. Thomas, S.; Nair, S. K.; Jamal, E. M. A.; Al-Harthi, S. H.; Varma, M. R.; Anantharaman, M. R. Size-dependent surface plasmon resonance in silver silica nanocomposites. *Nanotechnology.* **2008,** *19* (7).

159. Diegoli, S.; Manciulea, A. L.; Begum, S.; Jones, I. P.; Lead, J. R.; Preece, J. A. Interaction between manufactured gold nanoparticles and naturally occurring organic macromolecules. *Science of the Total Environment.* **2008,** *402* (1), 51-61.

160. Van Hyning, D. L.; Zukoski, C. F. Formation mechanisms and aggregation behavior of borohydride reduced silver particles. *Langmuir.* **1998,** *14* (24), 7034-7046.

161. Lee, K. J.; Nallathamby, P. D.; Browning, L. M.; Osgood, C. J.; Xu, X. H. N. In vivo imaging of transport and biocompatibility of single silver nanoparticles in early development of zebrafish embryos. *ACS Nano.* **2007,** *1* (2), 133-143.

162. Pal, S.; Tak, Y. K.; Song, J. M. Does the antibacterial activity of silver nanoparticles depend on the shape of the nanoparticle? A study of the gram-negative bacterium Escherichia coli. *Appl. Environ. Microbiol.* **2007,** *73* (6), 1712-1720

163. Sondi, I.; Salopek-Sondi, B. Silver nanoparticles as antimicrobial agent: a case study on E-coli as a model for Gram-negative bacteria. *J. Colloid Interface Sci.* **2004,** *275* (1), 177-182.

164. Shahverdi, A. R.; Fakhimi, A.; Shahverdi, H. R.; Minaian, S. Synthesis and effect of silver nanoparticles on the antibacterial activity of different antibiotics against Staphylococcus aureus and Escherichia coli. *Nanomed.-Nanotechnol. Biol. Med.* **2007,** *3* (2), 168-171.

165. Harper, S.; Usenko, C.; Hutchison, J. E.; Maddux, B. L. S.; Tanguay, R. L. In vivo biodistribution and toxicity depends on nanomaterial composition, size, surface functionalisation and route of exposure. *J. Exp. Nanosci.* **2008,** *3* (3), 195-206.

166. Kim, J. S.; Kuk, E.; Yu, K. N.; Kim, J. H.; Park, S. J.; Lee, H. J.; Kim, S. H.; Park, Y. K.; Park, Y. H.; Hwang, C. Y.; Kim, Y. K.; Lee, Y. S.; Jeong, D. H.; Cho, M. H. Antimicrobial effects of silver nanoparticles. *Nanomedicine-Nanotechnology Biology and Medicine.* **2007,** *3* (1), 95-101.

167. Jeon, H. J.; Yi, S. C.; Oh, S. G. Preparation and antibacterial effects of Ag-SiO_2 thin films by sol-gel method. *Biomaterials.* **2003,** *24* (27), 4921-4928.

168. Eckelman, M. J.; Graedel, T. E. Silver emissions and their environmental impacts: A multilevel assessment. *Environ. Sci. Technol.* **2007,** *41* (17), 6283-6289.

169. Buffle, J. The key role of environmental colloids/nanoparticles for the sustainability of life. *Environmental Chemistry.* **2006,** *3* (3), 155-158;

170. Huang, P. M.; Wang, M. K.; Chiu, C. Y. Soil mineral-organic matter-microbe interactions: Impacts on biogeochemical processes and biodiversity in soils. *Pedobiologia.* **2005,** *49* (6), 609-635.

171. Lyven, B.; Hassellov, M.; Turner, D. R.; Haraldsson, C.; Andersson, K. Competition between iron- and carbon-based colloidal carriers for trace metals in a freshwater assessed using flow field-flow fractionation coupled to ICPMS. *Geochim. Cosmochim. Acta.* **2003,** *67* (20), 3791-3802.

172. Lead, J. R.; Hamilton-Taylor, J.; Davison, W.; Harper, M. Trace metal sorption by natural particles and coarse colloids. *Geochim. Cosmochim. Acta* . **1999,** *63* (11-12), 1661-1670.

173. Lakowicz, J. R. Principles of Fluorescence, *3rd ed. Springer Science+Business Media, LLC: NewYork.* **2006**, 5.

174. Sierra, M. M. D.; Giovanela, M.; Parlanti, E.; Soriano-Sierra, E. J. Fluorescence fingerprint of fulvic and humic acids from varied origins as viewed by single-scan and excitation/emission matrix techniques. *Chemosphere.* **2005,** *58* (6), 715-733.

175. Oconnell, J. P.; Campbell, R. L.; Fleming, B. M.; Mercolino, T. J.; Johnson, M. D.; McLaurin, D. A. A highly sensitive immunoassay system involving antibody-coated tubes and liposome-entrapped dye. *Clinical Chemistry.* **1985,** *31* (9), 1424-1426.

176. Park, M. J.; Chung, Y. C.; Chun, B. C. PEG-based surfactants that show high selectivity in disrupting vesicular membrane with or without cholesterol. *Colloids and Surfaces B-Biointerfaces* . **2003,** *32* (1), 11-18.

177. Marcelino, J.; Lima, J.; Reis, S.; Matos, C. Assessing the effects of surfactants on the physical properties of liposome membranes. *Chemistry and Physics of Lipids.* **2007,** *146* (2), 94-103.

178. Berne B. J.; Pecora R. Dynamic light scattering. *Dover Publications, Mineola.* **2000.**

179. Herzfeld, J.; Berger, A. E. Sideband intensities in NMR-spectra of samples spinning at the magic angle. *J. Chem. Phys.* **1980,** *73* (12), 6021-6030.

180. Peersen, O. B.; Wu, X. L.; Kustanovich, I.; Smith, S. O. Variable-amplitude cross-polarization NMR. *J. Magn. Reson. Ser. A* **1993,** *104* (3), 334-339.

181. Metz, G.; Wu, X. L.; Smith, S. O. Ramped-amplitude cross-polarization in magic-angle-spinning NMR. *J. Magn. Reson. Ser. A* **1994,** *110* (2), 219-227.

182. Rovnyak, D. Tutorial on analytic theory for cross-polarization in solid state NMR. *Concepts Magn. Reson. Part A* **2008,** *32A* (4), 254-276.

183. Brown, S. P.; Emsley, L. The 2D MAS NMR spin-echo experiment: the determination of ^{13}C-^{13}C J couplings in a solid-state cellulose sample. *J. Magn. Reson.* **2004,** *171* (1), 43-47.

184. Brus, J.; Petrickova, H.; Dybal, J. Potential and limitations of 2D ^{1}H-^{1}H spin-exchange CRAMPS experiments to characterize structures of organic solids. *Mon. Chem.* **2002,** *133* (12), 1587-1612.

185. Rose, H. H. Optics of high-performance electron microscopes. *Sci. Technol. Adv. Mater.* **2008,** *9* (1).

186. Kuntsche, J.; Horst, J. C.; Bunjes, H. Cryogenic transmission electron microscopy (cryo-TEM) for studying the morphology of colloidal drug delivery systems. *Int. J. Pharm.* **2011,** *417* (1-2), 120-137.

Chapter 2. Spectroscopic Study of the Mechanism by which Humic Substances Interact with Biomembranes

2.1 Introduction

Humic substances (HSs) are the major components of natural organic matter (NOM). They are prevalent throughout the environment, including terrestrial, aquatic and coal areas, where they play diverse and significant environmental roles. They are formed as a result of the microbial breakdown of plant matter that contains proteins, cellulose, lignin, lipids, cutins and cutans. This leads to the formation of a complex, heterogeneous and polydisperse mixture with diverse functional groups ranging from hydrophobic moieties, such as aliphatic, aromatic, aldehyde, methoxyl, ketone, and thiol groups, to hydrophilic moieties, such as phenolic, quinolic, carboxylic and hydroxylic moieties [1-4]. This endows them with unique properties, such as the potential to interact with organic substances, metals, nutrients and biological surfaces [1, 5]. In addition, the amphiphilic nature of HSs favors their aggregation in solution [6] and their accumulation on surfaces [5]. As a result, HSs interact with hydrophobic organic compounds, thus strongly affecting the fate and transport of these compounds, as well as their bioavailability within the environment [7, 8]. It is therefore clear that one of the key processes controlling the transport, bioavailability and, hence, the toxic effect of xenobiotic pollutants to living organisms is the interaction of these pollutants with HSs.

The interactions of HAs with biomembranes and its influence on the bioavailability and toxicity of both inorganic and organic pollutants are of importance and interest to the environmental community. It has been found that HAs can both decrease and increase the bioavailability and toxicity of xenobiotic pollutants in the environment. The pollutants in these cited studies range from metal ions [9-16] and to organic molecules [17, 18] to nanoparticles [19]. In parallel, the interactions of HAs with biological surfaces have been monitored by several

techniques including electrophoretic mobility measurements [5, 20], adsorption isotherms [21, 22] and transmission electron microscopy [5]. These techniques have been used to investigate various types of biological surfaces such as those of fungi [23], bacteria [24], fish gills [5], and phytoplankton [5, 25]. Adsorption of HAs to living cells was illustrated by the physiological interaction of HAs with soil bacteria by using dielectric measurements to compare the properties of HAs with synthetic surfactants [7]. The pH dependent ability of HAs to increase plant membrane permeability to xenobiotic pollutants has also been demonstrated from a soil perspective [26-28]. Investigations of the effects of pH on the adsorption behavior of HAs to living cells revealed that adsorption prevails at lower pH values (i.e., pH 5 and below) leading to a controversial conclusion that HAs adsorb to biomembranes via hydrogen bonding [5]. Similar studies demonstrated greater adsorption of fulvic acid (FA) of different molecular weights at pH 5 and below, leading to the conclusion that adsorption behavior is mainly governed by hydrophobic interactions [21]. ^{31}P NMR studies led to the proposal of an adsorption/absorption mechanism, whereby, at acidic pH conditions, HAs initially adsorbs onto the biomembranes surface via hydrogen or cation bridging between the functional groups of the HAs and the head groups of the phospholipids, followed by an absorption step via hydrophobic interactions [2, 5, 21]. Although all these studies have led to important insights, they have left a number of open questions, such as: (i) what is the effect of temperature and (ii) what are the kinetics of these interactions. Also, the aforementioned studies have either focused on aquatic or terrestrial HAs but not on determining whether a universal behavior for HAs can be found.

In this study, the interaction with model biomembranes, the kinetics of these interactions, and the effects of various environmental parameters, including temperature, pH, and humic acid concentration were investigated with the use of three standard humic acids (HAs) from terrestrial

and aquatic sources. The model POPC LUV biomembranes used for this study mimic real biomembranes of such unicellular organisms as blue green algae in structure [20, 29] and in their ability to form a self-closed bilayer structure of vesicles that resembles the plasma membrane compartment of all eukaryotic cells [30].

2.2 Experimental Section

Chemicals and Materials

POPC was purchased from Avanti Polar Lipids (Alabaster, AL); Florida Peat Humic Acid (FPHA), Leonardite Humic Acid (LAHA), and Suwanee River Humic Acid (SWHA) were purchased from the International Humic Substances Society (IHSS, St. Paul, MN). Methanol and chloroform and were purchased from Fisher Scientific Company (Somerville, NJ). Nitrogen gas was supplied by the Chemistry department (upon being sourced from Capital Welders Supply Co.). Sulforhodamine-B and Triton X-100 (TX-100) were obtained from Sigma Aldrich (Milwaukee, WI), while Sephadex G-50 GE was obtained from Healthcare Biosciences (Piscataway, NJ). High quality (18MΩ) deionized water was obtained in our laboratory using an apparatus manufactured by US Filter.

Sample Preparation

The sulforhodamine-B (SRB) vesicles were prepared in accordance with the method developed by Ladokhin, et al.[31] and Graslund, et al. [32]. In short, 100 mg POPC was dissolved in 132 µL methanol and 264 µL chloroform. A rotary evaporator with no applied vacuum was used for thorough mixing of the lipid in the organic solvents for 30 min, followed by the evaporation of the solvents under nitrogen gas for 35-45 min and dried under vacuum overnight resulting in the formation of a thin lipid film. The film was dissolved in 10 mL of 50 mM SRB in 0.01 M phosphate buffer at two studied pHs: 4.8 and pH 7.6, then vortexed using

Vortex Genie series (G560) for 30 min. The sample was then heated in a water bath for another 5 min, and then placed in liquid nitrogen until the mixture was completely frozen, to be subsequently heated to 40 °C. This process was repeated six times, generating a pink heterogeneous mixture of large multilamellar vesicles. The solution was then extruded three times through a 100 nm-pore Whatman Nuclepore polycarbonate track-etched membrane at ambient temperatures using Lipex Lipid Extruder (North Lipids, Vancouver, BC, Canada), generating large unilamellar vesicles (LUVs). The non-encapsulated dye was separated from the encapsulated dye by gel filtration five times using a column packed with Sephadex G-50 resin (column diameter: 1 cm; length: 15 cm; applied sample volume: 2 mL) and 10 mM phosphate buffer at either pH 4.8 or 7.6 as an elution buffer.

HAs stock solutions were prepared by dissolving 8.6 mg of HA in 100 mL of 0.01 M phosphate buffer at pH 4.8 or 7.6, then adjusted to a basic pH using NaOH to dissolve all HAs, then adjusted back to pH 4.8 using HCL and diluted to 100.0 mL with phosphate buffer at pH 4.8. 5mL of a HA stock solution was then added to 5mL of the LUV solution to carry out the fluorescence leakage experiments. The solution pH was confirmed to be either 4.8 or 7.6 at all stages of the analysis. The one notable exception was during the kinetic runs in which the pH of the two mixing solutions was confirmed just before the mixing step and the end of the run.

Fluorescence Leakage Measurements

All fluorescence measurements were carried out using a Horiba Jobin Yvon Fluorolog 3 spectrofluorimeter with a FL1073 detector, Spectra Acq computer, and a model LFI3751 temperature control. SRB-loaded LUVs were exposed to FPHA, LAHA, and SWHA to investigate the perturbation effect of HAs on the model biomembranes. This was accomplished by measuring 5.00 mL of SRB-loaded LUVS and adding 5.00 mL of 0.01 M phosphate buffer

solution for the blank and 5.00 mL of HAs in phosphate buffer for the test sample. The blank contained only the first two components. The leakage of SRB dye from the model biomembranes was monitored using steady state fluorescence spectroscopy. The excitation wavelength used was 565 nm and the emission was monitored from 570 nm to 700 nm with an integration time of 1 s. The excitation and emission slits were both set at 1.5 nm. For the kinetics measurements, emission was monitored at 588 nm with an integration time of 1 min. The signal generated was compared to the one obtained after the sample was spiked with 100 µL of 1% detergent TX-100. DLS and cryo-TEM were used to verify the sizes of the prepared LUVs and the completely lysed LUVs as induced by the TX-100. All measurements were done in triplicate and the results were plotted, as indicated in the results section below.

Leakage of the SRB dye was expressed as a percentage relative to the total amount of dye released by the addition of 100 µL of 1% TX-100, which represented 100% leakage and was calculated according to the equation [20]

$$\text{Percent release} = 100 \times (I_H - I_B) / (I_T - I_B)$$

where I_H is the fluorescence intensity after the addition of HAs solution, I_B is the background fluorescence of SRB-loaded vesicles before the addition of either HAs or TX-100 solutions, and I_T is the total fluorescence intensity after the complete rupture of the vesicles caused by the addition of TX-100.

UV-Visible Absorbance Measurements: All absorbance spectra were collected from 250-600 nm using a 1.0 cm quartz cell. A Cary 100 Bio UV-Visible spectrometer was used to obtain the UV spectra. Deionized water was used as blank. The UV-visible measurements were used for inner filter correction and to obtain the excitation wavelength applied for fluorescence measurements.

Dynamic Light Scattering (DLS): Dynamic light scattering data were obtained using a ZetaSizer Nano Series, Nano ZG with Gateway 842GM (Malven Instruments). Measurements were made at a scattering angle of 90° and the sample was maintained at 20±1 °C. The laser wavelength was 647.1nm.

Cryo-Transmission Electron Microscopy (Cryo-TEM) Imaging: LUVs were characterized using a cryo-TEM microscope. The samples were prepared using a vitrification robot (Vitrobot, FEI), in which the relative humidity was kept close to saturation. A 3 µL drop of the lipid suspension was placed on a carbon-coated lacey film supported by a TEM 300 mesh copper grid (Ted Pella). The drop was then blotted to the right thickness, and then rapidly plunged into liquid ethane at its freezing point. This resulted in a vitrified film. The vitrified sample was then transferred under a liquid nitrogen environment to a cryoholder (model 626, Gatan Inc., Warrendale, PA) and then into the electron microscope, Tecnai 20, Sphera (FEI), operating at 120 kV with a nominal underfocus of 2-4 µL. The working temperature was kept slightly below -175 °C, and the images were recorded on Gatan 794 MultiScan digital camera and processed with Digital Micrograph 3.6 software.

2.3 Results and Discussions

Size Verification of LUVs

The size of the prepared LUVs was verified using DLS. SRB-entrapped POPC LUVs of approximately 100 nm size were prepared. The DLS data in Figure 2.1 demonstrated LUVs' size of approximately 112 nm in mean diameter. Cryo-TEM image also demonstrated that LUVs prepared were mostly unilamellar and had diameters of about 100 nm in size with a few multilamellar vesicles, as illustrated in Figure 2.2. The addition of a detergent (100 µL of 1% TX-100) led to complete rupture of the POPC LUVs, and gave smaller LUVs'size of about 10

nm for the mean diameter of the POPC LUVs and a few aggregates of approximately 130 nm in diameter.

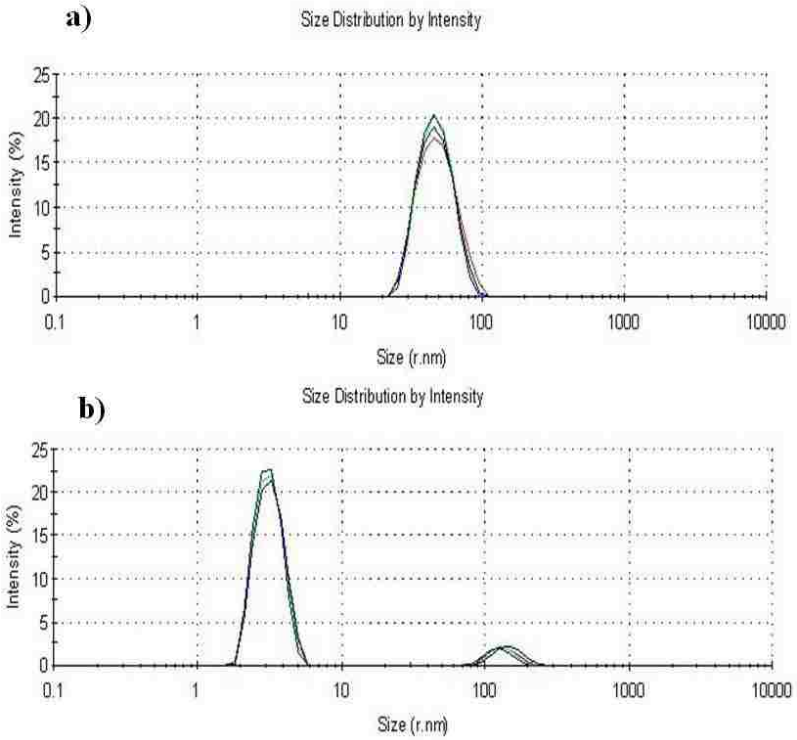

Figure 2.1 DLS of POPC LUVs a) POPC LUVs b) POPC LUVs spiked with TX-100.

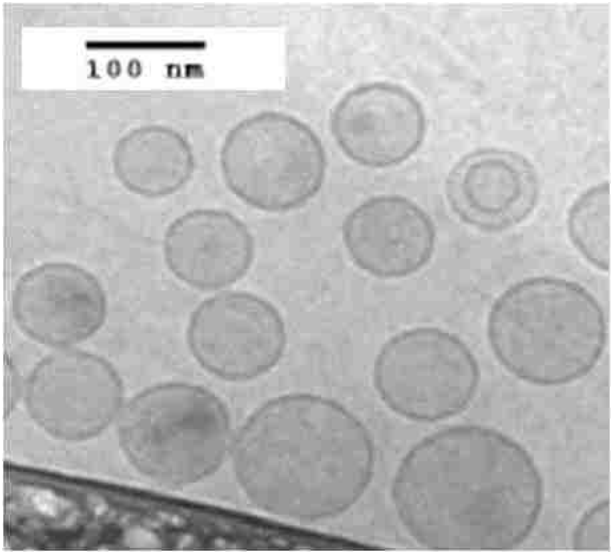

Figure 2.2 Cryo-TEM image of POPC LUVs.

2.3.1 Biomembrane Permeability Study using Steady State Fluorescence Spectroscopy

The interaction of HAs with large POPC unilamellar vesicle (LUVs) model biomembranes was investigated using steady state fluorescence spectroscopy. The spectra were collected at room temperature (25 °C). At this temperature, POPC LUVs phospholipids are in a liquid crystalline phase. SRB dye is known to self-quench at high molar concentrations, such as 50 mM, 70 mM and 80 mM, resulting in low fluorescence intensity, and to generate high fluorescence intensity at dilute concentrations (< 50 mM). Spiking the POPC LUVs with TX-100 leads to a complete rupture of the vesicles, releasing SRB dye out of the vesicles to the solution surrounding the vesicles, and thus, resulting in high fluorescence intensity.

2.3.2 Effects of concentration, pH, and temperature on the Interaction of FPHA with POPC LUVs

The percent SRB dye released from SRB-loaded POPC LUVs at two environmentally relevant pH and temperature conditions over a range of environmentally relevant concentrations of HA is illustrated in Figure 2.3. High fluorescence intensity is observed at pH 4.8, which implies that there is a high perturbation of the LUVs at acidic pH. These findings are in agreement with the literature and show that HAs interact with cell surfaces at acidic pH values [2, 5, 20]. The addition of FPHA at pH 7.6 to SRB-loaded POPC LUVs resulted in an average percent leakage of slightly less than 10% for the concentrations of FPHA investigated. This implies that the FPHA only perturbs the biomembranes at acidic pHs as the perturbation effect of HAs observed at pH 4.8 seems to be absent at pH 7.6. At pH 7.6 HAs are in their anionic forms and, as such, repel the negatively charged phosphates of the biomembrane, decreasing their rate of adsorption. These results are similar to what is reported in the literature and indicates that HAs both interact with and perturb the biomembranes only at acidic pH values [20].

As concentration of FPHA increases, so does the amount of membrane perturbation at both pH 4.8 and 7.6; however, the effect is much more prevalent at pH 4.8 as illustrated by the data. These findings are consistent with the previous work by Campbell and co-workers [20] for aquatic humic materials. The data in Figure 2.3 also appear to indicate that observed biomembrane perturbation may reach a plateau when FPHA increases to around 7.5 mg C/L. If we remained focused on the pH 4.8 data, it can also be seen that FPHA induces more leakage and hence greater membrane perturbation at 15 °C versus 25 °C; however, no such trend was seen for the pH 7.6 data. While the effects of both concentration and temperature are both interesting and important, and thus, require further investigation, it seems most appropriate to carry out further studies at acidic pH conditions.

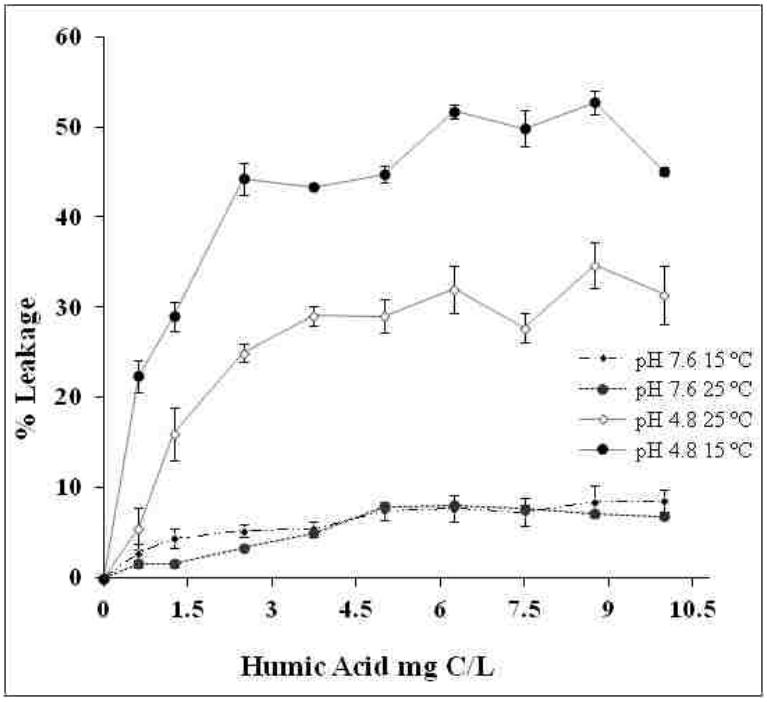

Figure 2.3 Concentration, pH, and temperature study on the interaction of FPHA with POPC LUVs.

2.3.4 Effects of Temperature on Leakage

The interaction of HAs with POPC LUVs was investigated at temperatures ranging between 10 and 30 °C, as shown in Figure 2.4 using the three HAs used in this study at a constant concentration of 5 mg C/L at pH 4.8, as already discussed. As seen in the dose study above, for the lower the temperature, the larger the difference the HAs ability to perturb biomembranes. These results indicate the largest amount of leakage at 10 °C, and the percent leakage decreases with increasing temperature, for all three HAs.

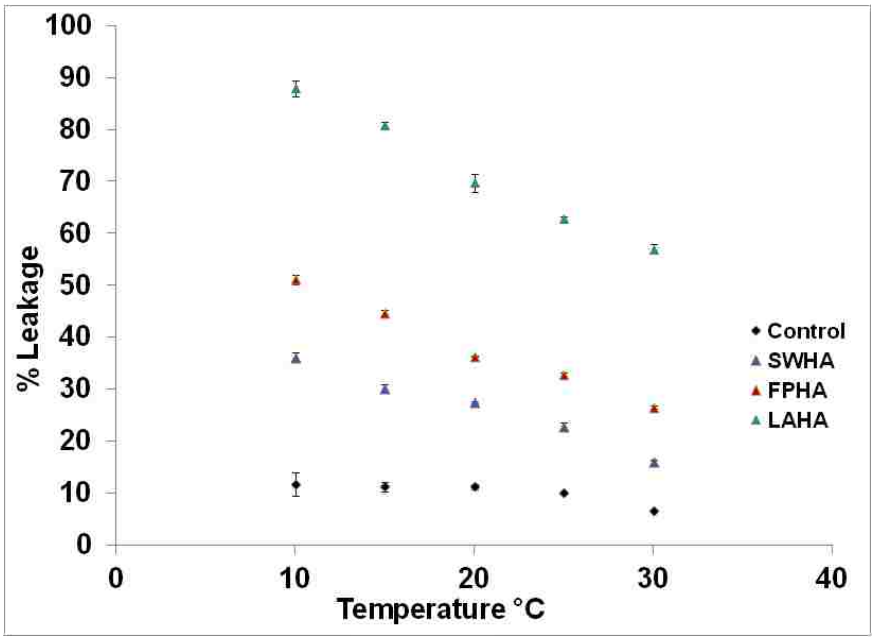

Figure 2.4 Effects of temperature on leakage of SRB dye as induced by 5 mg C/L of SWHA, FPHA and LAHA HAs at pH 4.8.

These results agree with the literature finding that maximum leakage occurs at the main phase transition temperature (T_m) and decreases at temperatures above and below the T_m when the bilayers are either all-gel or all-fluid [33-39]. POPC LUVs have their T_m of -2.5 ±2.4 [40], at 10 °C, a temperature near the T_m of POPC of the four temperatures investigated, the gel and the liquid crystalline phases could be coexisting in the vesicles' membrane, resulting in packing

defects in phase boundaries between these coexisting phases. Such packing defects occur as a result of either fluctuations in the lateral compressibility of the bilayers at T_m [38, 41-43] or due to the acyl chain packing mismatch at the interfacial region between gel and fluid domains [33, 35, 36, 44]. This, therefore, could be the reason for the high leakage observed as the temperature decreases from 30 °C to 10 °C. Of the three HAs investigated, SWHA had the lowest percent leakage followed by FPHA and LAHA. These differences in the leakage are attributed to structural differences in the HAs studied. LAHA has the most aromatic backbone, and hence, is more hydrophobic than FPHA, while SWHA has the least aromatic backbone, and thus, is the least hydrophobic [45.]. As a result, LAHA interacts more with the biomembranes, resulting in more leakage. Similar findings have been reported in the literature for liposomes [5].

2.3.3 Dose Response Study

Dose response studies have also been carried out at 25 °C using three different types of HAs at pH 4.8, see Figure 2.5. The HA concentrations in Figure 2.5 were selected to reflect the expected environmental concentrations for HAs in the lakes, rivers and marshes: 2.16 mg C/L, 6.97 mg C/L and 17.06 mg C/L, respectively [46]. HAs concentration is normally expressed in mg C/L or in ppm since it is a mixture of highly complex macromolecules. These data can be analyzed within at least two HA concentration ranges: 0-5 and 5-20 mg C/L. Within the first range, and for all three HAs studied, one observes an increase in dye leakage with increasing concentration. The ability of HAs to induce leakage, and hence, cause membrane perturbation follows the order LAHA>FPHA>SWHA. This trend directly correlates with the composition of these three HAs, and in particular with the concentration of aromatic moieties, as determined via ^{13}C NMR analysis (58, 47, and 31% for LAHA, FPHA, and SWHA, respectively). An inverse dependence is observed with respect to the polarity ((O+N)/C) (0.51, 073, and 0.83, as obtained

via elemental analysis for LAHA, FPHA, and SWHA, respectively) [47]. Even at a HA concentration as low as 5 mg C/L, the perturbation of LAHA is plateauing off. Within the second range (5-20 mg C/L), a number of interesting observations can be made. First of all, the leakage induced by LAHA decreasing with increasing HA concentration, this appears counterintuitive. One reasonable explanation is that at concentrations close to or higher than 5 mg C/L LAHA is starting to form aggregates [48-50]. For FPHA it can be seen that leakage increases until about 7.5 mg C/L, and causes more perturbation than LAHA at just below 7.5 mg C/L for the condition used in this work. After about 7.5 mg C/L, as discussed above, the leakage plateaus out with increasing FPHA concentration, again possibly due to aggregation. For SWHA there is an increasing leakage with increasing concentration for the entire concentration range studied here. These findings are consistent with the work of Campbell and co-workers [20].

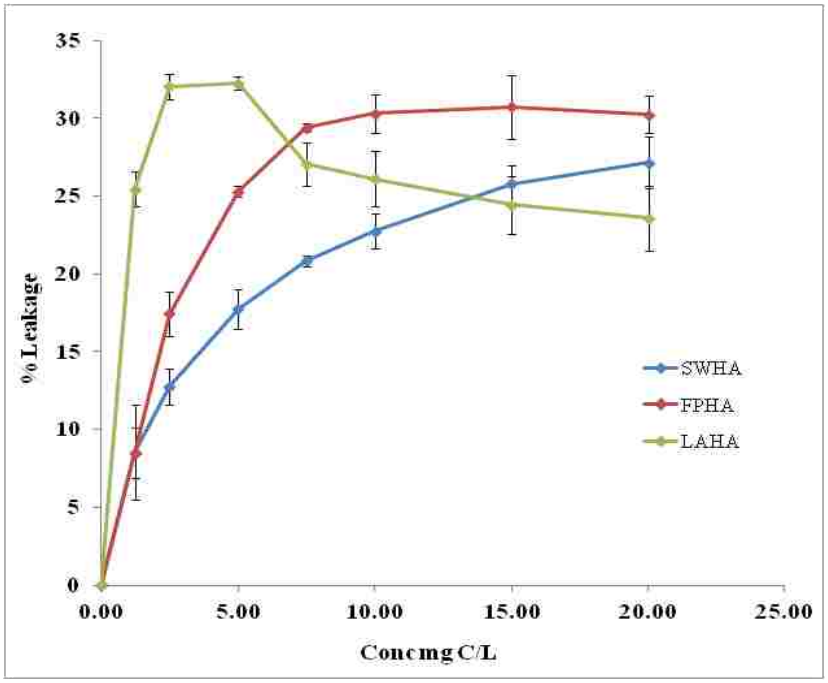

Figure 2.5 Dose response study of SWHA, FPHA and LAHA HAs at pH 4.8 measured at 25 °C.

For both LAHA and especially FPHA, the aggregation processes do not need to include the complete compliment of moieties within these two complex mixtures, but instead, just the most hydrophobic components. If the most hydrophobic components of these two HAs are aggregating, then they are less likely to interact with the model biomembrane system, and hence, induce less perturbation per unit C. For LAHA, it can be seen that the aggregation processes seems to reduce the number of moieties available for biomembrane perturbation, while for FPHA it appears that, once a certain concentration is reached, any additional membrane perturbing moieties introduced at higher concentrations are tied up in aggregation. The importance of this aggregation process will depend on a number of solution conditions, including concentration, temperature (see discussion below), ionic strength and pH (see discussion above). However, as shown with LAHA, it can lead to a decreased perturbation with increasing C concentration, and hence, each natural organic matter may have a different dose relationship and an optimal concentration, or range of concentrations, for inducing biomembrane perturbation.

2.3.5 Leakage Time Course Data and Kinetics

The time course data of leakage versus concentration are shown in Figures 2.6. From these data it is clear that LAHA induces the fastest, while SWHA induces the slowest membrane perturbation. If ones focuses only on the LAHA data, it can be seen that at the highest concentrations (7.5 and 10 mg C/L) full perturbation is established in less than 10 mins; however, at the lowest concentration (0.625 mg C/L) the perturbation is still ongoing even after 240 mins (4 hrs). It is also interesting to note that, as with the LAHA data from the dosage study, the leakage data starts to plateau at a concentration of 2.5 mg C/L, and that the onset of this effect is concentration dependent, with the most rapid onset corresponding to the highest concentration. Time course data for SWHA, on the other hand, show that the amount of dye

leakage at any time is greater the greater the concentration of SWHA is; however, there is no apparent plateua effect with time. The FPHA data are in between the LAHA and SWHA data, with an apparent plateauing appearing at between 7.5 and 10 mg C/L, and is the most apparent by the lower crossover point at approximately 120 mins. The findings reported for the leakage experiments are consistent with the dosage data and show that the aggregation phenomena discussed for the dosage data can also be used here to explain the differences among the different HAs discussed above. In fact, if points are taken at 10, 20, 40, and 60 mins and plotted as they were in Figures 2.6, the same trends are seen, but with greater leakage at longer times for SWHA and FPHA; however, for LAHA at about 6 mg C/L there is a convergence of the leakage data and a decrease in the amount of leakage with increasing HA concentration.

Table 2.1 presents a kinetic analysis of the time course data in Figure 2.6, and it can be seen that the leakage kinetics require two unique fits to be modeled for all three of the HAs investigated; and each of the three HAs yielded a first order rate constant for the slower component while the fast component cannot be fitted with first or second order kinetics.

The kinetic analysis of the time course data shows that there are at least two distinct mechanisms at work, namely a fast and slow mechanism. The slow mechanism can be fitted by first order kinetics in all cases and is highly concentration dependent, with increase in the rate with increasing concentration paralleling the plateauing or decreasing with concentration seen in the dosage studies for LAHA. These parallel findings imply that aggregation leads to a removal of available moieties within the HAs that are able to induce the slow membrane perturbation mechanism. Stated differently, the moieties within HAs that aggregate at the lowest concentration, and hence, in all likelihood are the most nonpolar moieties, are the moieties responsible for the slow biomembrane perturbation in this study. The fast component could not

be readily fitted to either first or second order kinetics. A very weak second order fit could be obtained if 1) only the first 5 to 10 mins of the time course data are were considered and 2) if it were assumed that the slow component, discussed above, is not in play i.e., the slow component requires a perturbation that takes longer than the first 5 to 10 mins. The fact that the fast component cannot be fitted to first or second order kinetics can be explained by more than one distinct process taking place, which this conclusion is consistent with complex heterogeneous nature of HA.

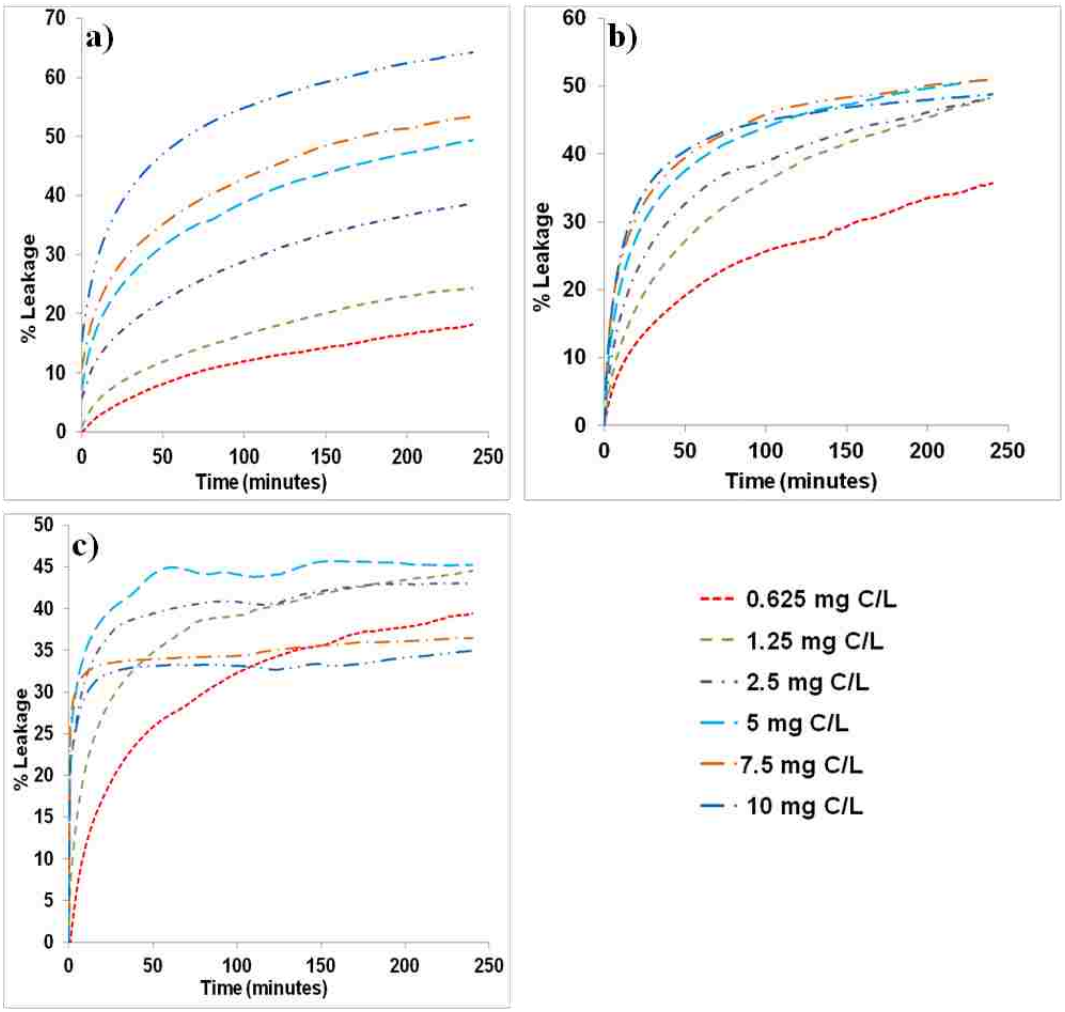

Figure 2.6 Kinetics of SRB dye leakage versus concentration of HAs at pH 4.8 a) is the leakage of SWHA, b) is the leakage of FPHA c) is the leakage of LAHA HAs. (Note that the scale on the y-axis is not consistent, this is to allow for clear observation of the percent leakage)

Table 2.1 First order kinetic rate constants for the slow component of the leakage studies. The rate constants for **a)** SWHA, **b)** FPHA, and **c)** LAHA HAs.

a)

Conc. (mg C/L)	Rate Constant s^{-1}	% Leakage fraction	R^2
0.625	-5.61E-05±0.71E-05	6.92±0.18	0.99 ±0.00
1.25	-5.13E-05±0.24E-05	9.68±0.92	0.98 ±0.01
2.50	-4.26E-05±0.95E-05	10.91±0.52	0.98 ±0.01
5.00	-3.22E-05±0.42E-05	11.47±1.46	0.97 ±0.01
7.50	-3.24E-05±0.77E-05	11.76 ±0.74	0.97 ±0.03
10.00	-2.34E-05±0.55E-05	10.46±0.67	0.97 ±0.01

b)

Conc. (mg C/L)	Rate Constant s^{-1}	% Leakage Fraction	R^2
0.625	-4.59E-05±0.57E-05	9.89±9.89	0.99±0.01
1.25	-4.65E-05±1.54E-05	13.22±13.22	0.98±0.01
2.50	-3.26E-05±0.92E-05	11.97±11.97	0.98±0.01
5.00	-2.28E-05±0.62E-05	10.28±10.28	0.97±0.01
7.50	-2.11E-05±1.10E-05	9.62±9.62	0.97±0.03
10.00	-1.36E-05±0.47E-05	6.91±6.91	0.97±0.01

c)

Conc. (mg C/L)	Rate Constant s^{-1}	% Leakage Fraction	R^2
0.625	-2.27E-05±0.22E-05	7.87±1.22	0.93±0.03
1.25	-1.08E-05±0.64E-05	4.04±2.33	0.85±0.18
2.50	-3.99E-06±0.56E-05	1.40±1.05	0.75±1.06
5.00	-3.82E-06±0.16E-06	1.40 ±0.47	0.63±0.20
7.50	-7.52E-06±0.57E-06	2.24±0.04	0.95±0.01
10.00	-6.52E-06±0.13E-06	2.08±0.54	0.79±0.02

2.3.6 Analysis of Leakage Kinetics

The leakage kinetics data were fitted to first-order kinetics as well as second-order kinetics using the following equations [51]

First order: $I_H = I_T(1 - e^{-kt})$

Second order: $I_H = \frac{I_T^2 kt}{1 + I_T kt}$

Where I_H is intensity at time *t* and I_T is maximum intensity after the addition of 100 µL of 1% TX-100. The data for the first rapid step and the slow step were each fitted to the second order kinetics equation as well as the first order kinetic equation. The fast component did not fit either the first or the second order kinetics equation. Fitting of the slow component data to the first order kinetic equation followed a straight line and the correlation coefficients were >0.9 for SWHA and FPHA and varied between 0.6 - 0.9 for LAHA as shown in Tables 2.1 above. The slopes were used to estimate the apparent rate constants, shown in Tables 2.1. The rate constants for the first order kinetics increase with increasing concentration of HAs for SWHA, and plateau at concentration beyond 2.5 mg C/L for FPHA and LAHA. The plateau denotes the completion of the first order reaction while plateau by FPHA and LAHA could be the attributed to the aggregation effect of at higher concentration [48-50]. This findings implies that the underlying leakage process can be formally described as a two-step process, a fast process and a slow process. The kinetics analysis above provides yet another evidence of a two-step process being involved in the interaction of HAs with biomembranes: an initial rapid release and then a slow release following first-order kinetics.

2.3.7 Mechanistic and Environmental Implication

The kinetic data and analysis allow for further insight into the mechansim by which HAs can interact with biomembrnanes. The use of vesicles in this study allows the highly complex of HA interactions with biomembrane to be simplified, as only passive processes are being monitored. This means that the observed perturbation is not a HA induced biochemical processes, such as apoptosis [52]. Our previous wideline ^{31}P NMR work has shown that HA can induce a structural perturbation within DPPC multilaminar vesicles, giving rise to the proposed

*ad*sorption/*ab*sorption mechanism [2]. The kinetic data indicate that these processes are even more complex than implied by the ^{31}P NMR data, as at least two distict processes are taking place in regards to absorption. The fast kinetic component discussed above as well as the data in Figure 2.5 illustrate that the membrane perturbation takes place on the minute (or faster) time scale, while the slow kinetic component suggests that membrane perturbation can take place over the course of hours. The pH dependence of the perturbation has been explained by a hydrogen bridge between the HA and the biomembrane surface. However, rather than looking at biomembrane as a homogenous surface, a better view point of the surface would be as a bilayer with "lattice" defects [53]. These defect sites can be viewed as initial *ad*sorption sites. Due to the fact that these defect sites locally reduce the thickness of phospholipids from a bilayer to a single layer, the hydrohobic domains of the HAs should be able to more directly interact with the hydrophobic tail groups of the phospholipids and lead to a rapid perturbation of the bilayer's stucture, and hence, intergrity.

This loss of bilayer stuctural intergrity could eventually lead to an increase in the premebaility of the bilayer, and hence, the rapid leakage of the dye induced by all three HAs in the kinetic studies described above. On the other hand, the slower component is more difficult to explain; nevertheless, the above-proposed mechansim is consistent with the hypothesis that at least two chemically distict groups of entites within the mixture that a humic acid constitutes are involved with the fast and slow steps observed above. The mechanism of this slow bilayer perturbation can be viewed as akin to the mechanism just discussed; however, rather than a direct *ad*soprtion step, the HA entity associated with the slower perturbation component diffuses over the bilayer surface until a condition is achieved in which it can absorb to a "lattice" defect site. This leads to the questions of what is this condition and why is there a much higher probability

of such a conditions for the HA entities involved with the fast component than with the slow component. We propose that the condition in question is the formation of a hydrogen bridge between the HA and the bilayer, which requires that the HA entity involved be able to support such a hydrogen bridge, strongly implying they have a high density of polar groups. On the other hand, HA entities with a low density of polar groups will have a much lower probability of achieving the hydrogen bridge condition. The HA concentration dependence of the kinetic data, along with the concentration dependence of the dosage data, support the polar group density argument, as the less polar the entity, the more likely it is to aggregate at higher HA concentrations, and hence, less likely to be able reach the hydrogen brideging condition. Stated differently, aggregated entities within a humic acid makes these entities much less available to induce bilayer perturbation, and the contribution of the slow perturbation component decreases for the more aromatic, and hence, more hydrophobic LAHA and FPHA at higher HA concentration.

The finding that temperature influences the amount of perturbation of the biomembranes by HAs has a large environmental implication in terms of the ever increasing average temperatures in the Northern and Southern ecosystems, but especially for the Northern hemisphere. The Northern hemisphere has larger land masses and higher carbon reservoirs, especially in the form of permafrost. As the global temperature, especially in the polar regions, continues to increase annually, permafrost regions will start to thaw and, in doing so, release their locked up carbon reserves. This release will increase the carbon content throughout associated watersheds, and hence, greatly increase the amount of dissolved organic matter with the aqueous phases, be it pore water, rivers, lakes, and estuaries. This, in turn, will induce a lowering of the water pH, similar to what has been found in Nordic waters during spring run-offs

when the wholesale snow melt leads to a large leaching of organic matter from the soils within the watershed and the pH of these Nordic waters decends to close to 4. According to the temperature and pH discussion above, both the low temperature and low pH of the run-off water increase the potential for membrane perturbation, the pertubations will be very high. The major questions are in regards to how much organic matter will be released and whether it will it be enough to induce aggregation, especially as the run-off water meets with the saline waters of the Artic Ocean as well as the northern Atlantic and Pacific oceans. A secondary question will be the chemical composition of the released organic matter since, as the above results show, different organic matters have different biomembrane perturbation potential., Nevertheless, for all organic matters tested in this work, biomembrane perturbation has been observed at acidic pHs at environmentally relevant organic matter concentrations. The kinetic data shows that this observed HA-induced perturbation is on the seconds to minutes time scale, and thus, is of environmental importance indeed. In addition, this process is complex and involves at least a two component *ab*sorption step, with the relative importance of these two components depending on the composition and concentration of the HA.

The results of this study are of concern as they illustrate that global climate change and the potential for wholesale organic matter release may lead to biomembrane perturbation of aquatic organisms, especially as this release will occur in very delicate and highly important nordic ecosystems. Although there is evidence that biomembrane composition can be adjusted for external environmental conditions, such as temperature, the concern is that the magnitude of organic matter release may fall outside the buffering capacity of the given ecosystem and lead to a highly damaging situation. The Nordic region is one of the major feeding grounds for a range of whales and fish, and any perturbation to these waters and the associated food web, as induced

by the perturbation of biomembranes of lower level organisms (e.g., algae) would be devastating to these large species, and hence, the oceans' health on a global scale. In addition, these findings have strong implications for the potential for nanoparticle bioavailability and toxicity, and may provide insight into the recent finding of Xing and co-workers that humic acids induce the internalization of CuO nanoparticles into blue-green algae [19].

2.3.8 Mechanism of Membrane Purtabation

Based on the kinetics studies and kinetics data analysis presented above and the previous ^{31}P NMR study [2] a mechanism of the interaction of HAs with model biomembranes is proposed. The mechanism involves an instant adsorption of HAs onto the biomembranes followed by a rapid then a slow absorption of HAs onto the biomembranes. The *ad*sorption step appears to be dependent on the concentration of HAs since the observed leakage increases with increasing concentration. The driving force for the adsorption process are the hydrogen bridging interactions between the phosphate groups and the negatively charged functional groups of HAs [2]. This interpretation has been further supported by the findings of Campbell and coworkers. Adsorption of HAs on biological surfaces has been reported in literature and was demonstrated directly by loss of DOM from solution, and indirectly by following changes in the electrophoretic mobility of individual cells in the presence or absence of DOM [20]. In this study we postulate that the adsorption of HAs to the biomembranes is a much faster process compared to the actual leakage. This assumption is based on literature findings that typical leakage in model membranes occur on the minute timescale while typical binding to model membranes occurs on the sub-second timescale [54, 55].

Adsorption of HAs to the biomembranes compromises the integrity of the biomembranes since packing defects are formed on the biomembranes around the adsorbed HAs [38, 41, 43].

The adsorption step is followed by the absorption step. The ***ab***sorption of HAs to the biomembranes occurs via hydrophobic interactions; this has been reported in the literature [2]. In addition to the two steps; the ***ad***sorption-***ab***sorption steps already proposed in the literature [2]. We, for the *first time* propose based on the kinetics studies that the ***ab***sorption step could involve more than one process depending on the lamellarity of the vesicles. In this study the absorption step is proposed to be a two-step process based on the kinetics analysis: a rapid absorption process resulting in the rapid leakage observed for the LUVs, followed by a slow absorption of HAs via first order kinetics resulting in the slow leakage. Leakage of vesicle contents via first order kinetics has previously been reported in literature [56]. The observed two-step *ad*sorption-*ab*sorption process above is consistent with our group's previous ^{31}P NMR work and illustrates that the mechanism of the interaction of HAs with the model biomembranes appears to be a two-step process of adsorption onto the biomembranes surface by hydrogen bridging interactions and is followed by absorption into the biomembranes hydrophobic domain by hydrophobic interactions [2].

2.4 Conclusions

In summary, we have successfully performed a series of studies using fluorescence spectroscopy. Fluorescence leakage studies have shown that HAs interacts with and perturbs model biomembranes at acidic pH values (4.8), thus making the model biomembranes permeable which is an effect lacking at a neutral pH (7.6). There is more leakage due to higher perturbations at temperatures closer to the T_m of POPC, due to the acyl chain packing mismatches at the interfacial region which is caused by the coexistence of both the gel and liquid crystalline phases in the phase boundaries. HAs concentrations as low as 0.3 mg C/L cause leakage; the leakage increases with increasing concentration of HAs.

The interaction of HAs with model biomembranes has been shown to occur in two main steps: (1) an initial instant *ad*sorption by hydrogen bridging between the phosphate group and the negatively charged functional groups of HAs followed by (2) a rapid *ab*sorption via hydrophobic interactions followed by a slow *ab*sorption via hydrophobic interactions following first order kinetics. These findings agree well with the literature and with the theoretical model postulated by Elayan, et al.[2] Overall, all three chemically diverse HAs studied here perturb the model biomembranes at acidic pHs.

2.5 References

1. Nakashima, K.; Xing, S. Y.; Gong, Y. K.; Miyajima, T. Characterization of humic acids by two-dimensional correlation fluorescence spectroscopy. *Journal of Molecular Structure.* **2008,** *883,* 155-159.

2. Elayan, N. M.; Treleaven, W. D.; Cook, R. L. Monitoring the effect of three humic acids on a model membrane system using P-31 NMR. *Environ. Sci. Technol.* **2008,** *42* (5), 1531-1536.

3. Duval, J. F. L.; Wilkinson, K. J.; Van Leeuwen, H. P.; Buffle, J. Humic substances are soft and permeable: Evidence from their electrophoretic mobilities. *Environ. Sci. Technol.* **2005,** *39* (17), 6435-6445.

4. Schulten, H. R.; Schnitzer, M. A state-of-the-art structural concept for humic substances. *Naturwissenschaften.* **1993,** *80* (1), 29-30.

5. Campbell, P. G. C.; Twiss, M. R.; Wilkinson, K. J. Accumulation of natural organic matter on the surfaces of living cells: implications for the interaction of toxic solutes with aquatic biota. *Canadian Journal of Fisheries and Aquatic Sciences.* **1997,** *54* (11), 2543-2554.

6. Wershaw, R. L. Model for humus in soil and sediments. *Environ. Sci. Technol.* **1993,** *27* (5), 814-816.

7. Visser, S. A. Physiological action of humic substances on microbial-cells. *Soil Biology & Biochemistry.* **1985,** *17* (4), 457-462.

8. Perminova, I. V.; Grechishcheva, N. Y.; Kovalevskii, D. V.; Kudryavtsev, A. V.; Petrosyan, V. S.; Matorin, D. N. Quantification and prediction of the detoxifying properties of humic substances related to their chemical binding to polycyclic aromatic hydrocarbons. *Environ. Sci. Technol.* **2001,** *35* (19), 3841-3848.

9. Lamelas, C.; Slaveykova, V. I. Comparison of Cd(II), Cu(II), and Pb(II) biouptake by green algae in the presence of humic acid. *Environ. Sci. Technol.* **2007,** *41* (11), 4172-4178.

10. Lamelas, C.; Wilkinson, K. J.; Slaveykova, V. I. Influence of the composition of natural organic matter on Pb bioavailability to microalgae. *Environ. Sci. Technol.* **2005,** *39* (16), 6109-6116.

11. Alstad, N. E. W.; Kjelsberg, B. M.; Vollestad, L. A.; Lydersen, E.; Poleo, A. B. S. The significance of water ionic strength on aluminium toxicity in brown trout (Salmo trutta L.). *Environmental Pollution.* **2005,** *133* (2), 333-342.

12. Guo, L. D.; Hunt, B. J.; Santschi, P. H.; Ray, S. M. Effect of dissolved organic matter on the uptake of trace metals by American oysters. *Environ. Sci. Technol.* **2001,** *35* (5), 885-893.

13. Sanchez-Marin, P.; Beiras, R. Adsorption of different types of dissolved organic matter to marine phytoplankton and implications for phytoplankton growth and Pb bioavailability. *Journal of Plankton Research.* **2011,** *33* (9), 1396-1409.

14. Matsuo, A. Y. O.; Playle, R. C.; Val, A. L.; Wood, C. M. Physiological action of dissolved organic matter in rainbow trout in the presence and absence of copper: Sodium uptake kinetics and unidirectional flux rates in hard and softwater. *Aquatic Toxicology.* **2004,** *70* (1), 63-81.

15. Klinck, J.; Dunbar, M.; Brown, S.; Nichols, J.; Winter, A.; Hughes, C.; Playle, R. C. Influence of water chemistry and natural organic matter on active and passive uptake of inorganic mercury by gills of rainbow trout (Oncorhynchus mykiss). *Aquatic Toxicology.* **2005,** *72* (1-2), 161-175.

16. Pan, J. F.; Wang, W. X. Comparison of the bioavailability of Cr and Fe bound with natural colloids of different origins and sizes to two marine bivalves. *Marine Biology.* **2002,** *141* (5), 915-924.

17. Haitzer, M.; Akkanen, J.; Steinberg, C.; Kukkonen, J. V. K. No enhancement in bioconcentration of organic contaminants by low levels of DOM. *Chemosphere.* **2001,** *44* (2), 165-171.

18. Yamamoto, H.; Liljestrand, H. M.; Shimizu, Y. Effects of dissolved organic matter surrogates on the partitioning of 17 beta-estradiol and p-nonylphenol between synthetic membrane vesicles and water. *Environ. Sci. Technol.* **2004,** *38* (8), 2351-2358.

19. Wang, Z. Y.; Li, J.; Zhao, J.; Xing, B. S. Toxicity and internalization of CuO nanoparticles to prokaryotic alga microcystis aeruginosa as affected by dissolved organic matter. *Environ. Sci. Technol.* **2011,** *45* (14), 6032-6040.

20. Vigneault, B.; Percot, A.; Lafleur, M.; Campbell, P. G. C. Permeability changes in model and phytoplankton membranes in the presence of aquatic humic substances. *Environ. Sci. Technol.* **2000,** *34* (18), 3907-3913.

21. Maurice, P. A.; Manecki, M.; Fein, J. B.; Schaefer, J. Fractionation of an aquatic fulvic acid upon adsorption to the bacterium, Bacillus subtilis. *Geomicrobiology Journal.* **2004,** *21* (2), 69-78.

22. Frost, P. C.; Maurice, P. A.; Fein, J. B. The effect of cadmium on fulvic acid adsorption to Bacillus subtilis. *Chemical Geology.* **2003,** *200* (3-4), 217-224.

23. Zhou, J. L.; Banks, C. J. Mechanism of humic-acid color removal from natural-waters by fungal biomass biosorption. *Chemosphere.* **1993,** *27* (4), 607-620.

24. Ongerth, J. E.; Pecoraro, J. P. Electrophoretic mobility of Cryptosporidium oocysts and Giardia cysts. *Journal of Environmental Engineering-Asce* .**1996,** *122* (3), 228-231.

25. Parent, L.; Twiss, M. R.; Campbell, P. G. C. Influences of natural dissolved organic matter on the interaction of aluminum with the microalga Chlorella: A test of the free-ion model of trace metal toxicity. *Environ. Sci. Technol.* **1996,** *30* (5), 1713-1720.

26. Chaminade, R.; Blanchet, R. Mecanisme delactionstimulante de lhumus sur la nutrition minerale des vegetaux. *Comptes Rendus Hebdomadaires Des Seances De L Academie Des Sciences.* **1953,** *237* (25), 1768-1770.

27. Lee, Y. S.; Bartlett, R. J. Stimulation of plant-growth by humic substances. *Soil Science Society of America Journal* .**1976,** *40* (6), 876-879.

28. Samson, G.; Visser, S. A. Surface-active effects of humic acids on patato cell- membrane properties. *Soil Biology & Biochemistry.* **1989,** *21* (3), 343-347.

29. Kalmanzon, E.; Zlotkin, E.; Cohen, R.; Barenholz, Y. Liposomes as a model for the study of the mechanism of fish toxicity of sodium dodecyl-sulfatein sea water. *Biochimica Et Biophysica Acta* .**1992,** *1103* (1), 148-156.

30. Zepik, H. H.; Walde, P.; Kostoryz, E. L.; Code, J.; Yourtee, D. M. Lipid vesicles as membrane models for toxicological assessment of xenobiotics. *Critical Reviews in Toxicology* .**2008,** *38* (1), 1-11.

31. Ladokhin, A. S.; Wimley, W. C.; White, S. H. Leakage of membrane vesicle contents: Determination of mechanism using fluorescence requenching. *Biophysical Journa* .**1995,** *69* (5), 1964-1971.

32. Barany-Wallje, E.; Gaur, J.; Lundberg, P.; Langel, U.; Graslund, A. Differential membrane perturbation caused by the cell penetrating peptide Tp10 depending on attached cargo. *Febs Letters.* **2007,** *581* (13), 2389-2393.

33. Perdue, E. M. R. J. D., Dissolved Organic Matter in Freshwaters. *Treatise on Geochemistry.* **2003,** *5*, 273–318.

34. Elemental Composition and Stable Isotopic Ratios of IHSS Sample. (Accessed **04/30/2012);** Available from: http://www.humicsubstances.org/elements.html .

35. Swift, R. S. Macromolecular properties of soil humic substances: Fact, fiction, and opinion. *Soil Sci.* **1999,** *164* (11), 790-802.

36. Clapp, C. E.; Hayes, M. H. B. Sizes and shapes of humic substances. *Soil Sci.* **1999,** *164* (11), 777-789.

37. Schulten, H. R.; Leinweber, P. New insights into organic-mineral particles: composition, properties and models of molecular structure. *Biology and Fertility of Soils.* **2000,** *30* (5-6), 399-432.

38. Papahadj.D; Jacobson, K.; Nir, S.; Isac, T. Phase-transitions in phospholipid vesicles-fluoresence polarizationand permeabilitymeasurements concerning effect of temperature and cholesterol. *Biochimica Et Biophysica Acta.* **1973,** *311* (3), 330-348.

39. Blok, M. C.; Vanderneutkok, E. C. M.; Vandeenen, L. L. M.; Degier, J. Effect of chain-length and lipid phase-transitions on selective permeability properties of liposomes. *Biochimica Et Biophysica Acta.* **1975,** *406* (2), 187-196.

40. Marsh, D.; Watts, A.; Knowles, P. F. Evidence for phase boundary lipid -permeability of tempo-choline into dimyristoylphossphatidylcholine vesicles at phase-transition. *Biochemistry.* **1976,** *15* (16), 3570-3578.

41. Vanhoogevest, P.; Degier, J.; Dekruijff, B. Determination of the size of the packing defects in dymyristoylphosphatylcholine bilayers present at the phase-transition temperature. *FEBS Lett.* **1984,** *171* (2), 160-164.

42. Elmashak, E. M.; Tsong, T. Y. Ion selectivity of temperature-induced and electric-field induced pores in dipalmitoylphosphatidylcholine vesicles. *Biochemistry.* **1985,** *24* (12), 2884-2888.

43. Georgallas, A.; Macarthur, J. D.; Ma, X. P.; Nguyen, C. V.; Palmer, G. R.; Singer, M. A.; Tse, M. Y. The diffusion of small ions through phospholipid-bilayers. *Journal of Chemical Physics.* **1987,** *86* (12), 7218-7226.

44. Bramhall, J.; Hofmann, J.; Deguzman, R.; Montestruque, S.; Schell, R. Temperature-dependence of membrane ion conductance analzed by using the amphiphilic anion 5/6-carboxyfluorescein *Biochemistry.* **1987,** *26* (20), 6330-6340.

45. Koynova, R.; Caffrey, M. Phases and phase transitions of the phosphatidylcholines. *Biochim. Biophys. Acta-Rev. Biomembr.* **1998,** *1376* (1), 91-145.

46. Linden, C. D.; Wright, K. L.; McConnel.Hm; Fox, C. F. Lateral phase separations in membrane lipids and mechanism of sugar transport in escherichia-coli. *Proceedings of the National Academy of Sciences of the United States of America.* **1973,** *70* (8), 2271-2275.

47. Doniach, S. Thermodynamic fluctuations in phospholipid bilayers. *Journal of Chemical Physics.* **1978,** *68* (11), 4912-4916.

48. Nagle, J. F.; Scott, H. L. Lateral compressibility of lipid monolayers and bilayers theory of membrane-permeability. *Biochimica Et Biophysica Acta.* **1978,** *513* (2), 236-243.

49. Kanehisa, M. I.; Tsong, T. Y., Cluster model of lipid phase-transitions with applicationto passive permeation of molecules at structure relaxations in lipid bilayers. *Journal of the American Chemical Society* **1978,** *100* (2), 424-432.

50. Thorn, K. A., Folan, D.W., MacCarthy, P. Characterization of the IHSS Standard and Reference Fulvic and Humic Acids by Solution State ^{13}C and 'H NMR Spectrometry. *U.S. Geological Survey, Water-Resources Investigations Report.* **1989,** *89-4196*.

51. Warren L. Erdahl, C. J. C., Richard W. Taylor,; Douglas R. Pfeiffer, Ca^{2+} Transport Properties of lonophores A23187, lonomycin, and 4-BrA23187 in a Well Defined Model System.*Biophysicocal journal.* **1994,** *66*.

52. Hseu, Y. C.; Lin, E.; Chen, J. Y.; Liua, Y. R.; Huang, C. Y.; Lu, F. J.; Liao, J. W.; Chen, S. C.; Yang, H. L. Humic Acid Induces G1 Phase Arrest and Apoptosis in Cultured Vascular Smooth Muscle Cells. *Environmental Toxicology.* **2009,** *24* (3), 243-258.

53. Segall, M. L.; Dhanasekaran, P.; Baldwin, F.; Anantharamaiah, G. M.; Weisgraber, K. H.; Phillips, M. C.; Lund-Katz, S. Influence of apoE domain structure and polymorphism on the kinetics of phospholipid vesicle solubilization. *J. Lipid Res.* **2002,** *43* (10), 1688-1700.

54. Sekharam, K. M.; Bradrick, T. D.; Georghiou, S. Kinetics of melittin binding to phospholipid small unilamella vesicles. *Biochimica Et Biophysica Acta.* **1991,** *1063* (1), 171-174.

55. Schwarz, G.; Gerke, H.; Rizzo, V.; Stankowski, S. Incorporation kinetics in a membrane, studied with the pore-forming peptide alamethicin. *Biophysical Journal.* **1987,** *52* (5), 685-692.

56. Shimanouchi, T.; Ishii, H.; Yoshimoto, N.; Umakoshi, H.; Kuboi, R. Calcein permeation across phosphatidylcholine bilayer membrane: Effects of membrane fluidity, liposome size, and immobilization. *Colloids and Surfaces B-Biointerfaces.* **2009,** *73* (1), 156-160.

Chapter 3. Spectroscopic Study of the Kinetics and the Mechanism of the Interaction of Chemically Diverse Humic Substances with Biomembranes

3.1 Introduction

Humic substances (HSs), which are the major components of natural organic matter (NOM), are a complex, heterogeneous and polydisperse mixture of decayed organic matter usually produced by microbial decomposition of dead plants and animal tissues in both terrestrial and aquatic environments [1-3]. HSs are made up of different moieties such as aliphatic acids, tannin and lignin, carbohydrates, amino acids, and other forms of heterocyclic and polyaromatic functionalities [4] [4, 5]. They are prevalent throughout the environment where they play various significant roles. It is well established that HAs, the water soluble fraction of HSs interact with biomembranes [2, 6-8]. The influence of HAs on biomembrane surfaces was previously investigated in regards to enhanced mineral uptake [9]. Similarly, the physiological interaction of HSs with the biomembranes of soil bacteria was indirectly illustrated by comparing HAs to synthetic surfactants through dielectric measurements [10]. Other studies have demonstrated the ability of HAs to interact with biomembranes in aquatic environments [6, 7, 11-13] [14]. Other studies focused on modeling the toxicity of metals to organisms, e.g. fish via metal binding to their gills [15, 16] [17, 18] [11, 15].

The ability of HAs to increase plant membrane permeability has also been demonstrated in soil science [14],[6],[19],[20],[21]. HAs have been shown to affect the permeability of biomembranes differently based upon pH and HAs origin by altering the biomembrane structure and fluidity, thus making the biomembranes more permeable to xenobiotic pollutants [19-22] [7]. In addition to this, it has been demonstrated that HAs affect biomembrane permeability to organic molecules, [7] [23] enabling these molecules to cross the membrane, hence indicating that HAs perturb the biomembrane. A model of the mechanism demonstrated that HAs interact

with biomembranes by first *ad*sorbing *onto* the biomembrane via hydrogen bridging and then *ab*sorbing *into* the biomembrane hydrophobic domains via hydrophobic interactions [2]. It is therefore clear that HAs interact with and perturb biomembranes. This, therefore, implies that HAs play a major role in the environmental toxicity issues, specifically, in determining the bioavailability of metal ions and xenobiotic pollutants within the environment.

Considering the complexity and polydispersity of HAs, it can be assumed that not all moieties within HAs play the same role or participate to the same extent in the in the perturbation of biomembranes. Understanding the roles of different moieties within HAs in the interaction of HAs with biomembranes can offer valuable information in regards to the mechanism of interaction of HAs with biomembranes. Developing this understanding requires the separation of these components from HAs by procedures that do not alter the remaining material. Lipids can be readily edited out from HAs using solvent extraction under relatively mild conditions. The aromatic components can be extracted by bleaching, while the carbohydrates can be edited out via hydrolysis. This work focuses on the contribution of the aromatic, lipids, and carbohydrates components to the mechanism of the interaction of HAs with biomembranes. The role of different moieties responsible for the interaction of HAs with biomembranes was investigated using fluorescent leakage experiments. Lipid vesicles, which are very simplified models, were used in this study to gain the fundamental molecular level understanding of the roles different moieties within HAs play in the interactions of HAs with biomembranes. The phospholipid POPC was used in this study due to its biological relevance as well as its phase behavior. POPC has a phase transition temperature (T_m) of -2.5 ±2.4°C at this temperature the acyl chains and the crystalline lattice of POPC phospholipid bilayers melts hence

causing phase changes in the lipid bilayer, from solid crystalline phase to liquid crystalline phase. This change of phase influences the permeability of phospholids [24].

3.2 Experimental Section

Chemicals and Materials

POPC was purchased from Avanti Polar Lipids (Alabaster, AL); Florida Peat Humic Acid (FPHA) and Leonardite Humic Acid (LAHA) were purchased from the International Humic Substances Society (IHSS, St. Paul, MN). Methanol, chloroform, benzene, hydrochloric acid, acetic acid and sodium chlorite were purchased from Fisher Scientific Company (Somerville, NJ). Nitrogen gas was obtained from the Chemistry department (Capital Welders Supply Co.) Sulforhodamine-B (SRB) was obtained from Sigma Aldrich (Milwaukee, WI). Sephadex G-50 GE was obtained from Healthcare Biosciences (Piscataway, NJ), and high quality 18MQ deionized water was obtained with the use of the US Filter apparatus situated in our laboratory.

Preparations of Chemically Edited HAs.

Specific structural components were edited out from HAs following three different chemical treatments. The lipid components of HAs were removed by treating HAs with benzene:methanol azeotrope in a 3:1 volume ratio for 72 hrs via Soxlet extraction the organic solvent was then evaporated [25]. HAs were hydrolyzed through mixing with 300 mL of 6 M HCl per gram of HAs and maintaining the system under reflux for 6 hrs [26]. Bleaching was achieved by treating HAs with 10 g of sodium chlorite, 10 mL of acetic acid, and 100 mL of deionized water per gram of HAs mixture and stirred overnight. The bleached supernatant was decanted and replaced with fresh solution; this process was repeated three times [27, 28]. The solid residue was then separated from the mixture by centrifugation at 4000*g* for 15 min and dialyzed using a Spectra/Por membrane (molecular weight cut-off 8000 Da). The bleached and

the hydrolyzed HAs samples were freeze-dried and stored for characterization and leakage studies.

Sample Preparation for NMR Experiment

The chemically edited HAs were freeze-dried and further ground with a mortar and pestle to ensure a homogeneous sample. The sample was then tightly packed into a 2.5 mm high resolution magic angle spinning zirconium rotor (Bruker) in order to achieve a homogeneous radio frequency field during the NMR analysis. It should be noted that the chemically edited HAs did not undergo any further chemical treatment prior to NMR analysis, in order to preserve the integrity of the chemically edited HAs.

^{13}C NMR Ramp CP-MAS

The NMR data were acquired using a ramp cross-polarization (CP) pulse program with magic angle spinning (MAS) on a Bruker Avance 400 MHz spectrometer. Spectra were acquired at a frequency of 400 MHz for ^{1}H and 100 MHz for ^{13}C for all NMR experiments. The sample MAS spinning rate was 26 kHz and a ramp cross-polarization contact time of 2 ms was used with a recycle delay time of 1 s. A total of 307,200 scans per experiment were collected. The resulting ^{13}C spectra were processed using 60 Hz line broadening. Prior to the application of the spectral collection for the chemically edited HAs sample, the performance of the pulse sequences was validated using tyrosine–HCl crystals. The NMR spectra are shown in Figure 3.1.

Preparation of Dye Encapsulated Vesicles

The sulforhodamine-B (SRB) vesicles were prepared in accordance with the method developed and optimized by Ladokhin, et al. [29, 30]. Briefly, 50 mg of POPC was dissolved in 66 µL methanol and 132 µL chloroform. A rotary evaporator with no applied vacuum was used for thorough mixing of the lipid in the organic solvents for 30 mins, followed by the evaporation

of the solvents under nitrogen gas for 35-45 mins and then dried further under vacuum overnight, resulting in the formation of a thin lipid film. The film was dissolved in 5 mL of 50 mM SRB in 0.01 M phosphate buffer at pH 4.8 and, then vortexed using Vortex Genie series (G560) for 30 mins. The sample was then heated in a 40 °C water bath for 5 mins, and then placed in liquid nitrogen until the mixture was completely frozen, and subsequently heated at 40 ^{o}C for another 5 mins. This freeze-thaw cycle process was repeated six times, generating a pink heterogeneous mixture of large multilamellar vesicles. The solution was then extruded three times through a 100 nm-pore Whatman Nucleopore polycarbonate track-etched membrane at ambient temperatures using Lipex Lipid Extruder (North Lipids, Vancouver, BC, Canada), generating large unilamellar vesicles (LUVs). The non-encapsulated dye was separated from the encapsulated dye by size exclusion chromatography five times using a column packed with Sephadex G-50 resin (column diameter: 2.5 cm; length: 60 cm; applied sample volume: 5 mL) with 10 mM phosphate buffer of an appropriate pH as an elution buffer.

Chemically edited stock solutions of humic acids were prepared by dissolving a bleached humic acid, e.g., 8.6 mg of FPHA, in 20 mL of 0.01 M phosphate buffer at pH 4.8, then adjusted to a basic pH using NaOH to dissolve all the HA, then adjusted back to pH 4.8 using HCl and diluted to 100.0 mL with phosphate buffer at pH 4.8 and were stirred in darkness for 24 hours to allow for sample equilibration. A similar procedure was followed for all the chemically edited HAs studied. All the solutions were protected from light and stored in the refrigerator until analyzed and were discarded after one week.

Fluorescence Leakage Measurements

All fluorescence measurements were carried out using a Horiba Jobin Yvon Fluorolog 3 spectrofluorimeter with a FL1073 detector, Spectra Acq computer, and a model LFI3751

temperature control. SRB-loaded LUVs were exposed to chemically diverse SWHA, FPHA and, LAHA, and used to investigate the perturbation effect of HAs on the model biomembranes. This was accomplished by measuring 5.00 mL of SRB-loaded LUVS and adding 5.00 mL of 0.01 M phosphate buffer solution for the blank and 5.00 mL of HAs in phosphate buffer for the test sample, the blank contained only the first two components. The leakage of SRB dye from the model biomembranes was monitored using steady state fluorescence spectroscopy. All emission spectra were collected at room temperature (25^{o}C). At this temperature, the phospholipids LUVs are in a liquid crystalline phase. The excitation wavelength used was 565 nm and the emission was monitored from 570 nm to 700 nm with an integration time of 1 s; the excitation and emission slits were both set at 1.5 nm. For the kinetics measurements, emission was monitored at 588 nm with an integration time of 1 min. The signal generated was compared to the one obtained after the sample was spiked with 100 µL of 1% detergent TX-100. DLS and cryo-TEM were used to verify the sizes of the prepared LUVs and the completely lysed LUVs, as induced by the TX-100. The solution pH was confirmed to be 4.8 at all stages of the analysis, with the exception of kinetic runs, during which the pH of the two mixing solutions was confirmed just before the mixing step and the pH of the monitored solution was confirmed at the end of the run. All measurements were done in triplicate and the results were plotted, as indicated in the results section below.

Leakage of the SRB dye was expressed as a percentage relative to the total amount of dye released by the addition of 100 µL of 1% TX-100 detergent, which represented 100% leakage and was calculated according to the equation [7]:

Percent release = $100 \times (I_H - I_B) / (I_T - I_B)$

I_H is the fluorescence intensity after the addition of HAs solution, I_B is the background fluorescence of SRB-loaded vesicles before the addition of either chemically diverse HAs or TX-100 solutions, and I_T is the total fluorescence intensity after the complete rupture of the vesicles by the addition of TX-100.

UV-Visible Absorbance Measurements All absorbance spectra were collected from 250-600 nm using a 1.0 cm quartz cell. A Cary 100 Bio UV-visible spectrometer was used to obtain the UV spectra. Deionized water was used as blank. The UV-visible measurements were used for inner filter correction and to obtain the excitation wavelength applied for fluorescence measurements.

Dynamic Light Scattering (DLS) Dynamic light scattering data were obtained using a ZetaSizer Nano Series, Nano ZG with Gateway 842GM (Malven Instruments). Measurements were made at a scattering angle of 90° and the sample was maintained at 20±1 °C. The laser wavelength was 647.1 nm.

Cryo-Transmission Electron Microscopy (Cryo-TEM) Imaging LUVs were characterized using cryo-TEM microscope. The samples were prepared using a vitrification robot (Vitrobot, FEI), in which the relative humidity was kept close to saturation. A 3 µL drop of the lipid suspension was placed on a carbon-coated lacey film supported by a TEM 300 mesh copper grid (Ted Pella). The drop was then blotted to the right thickness, and then rapidly plunged into liquid ethane at its freezing point. This resulted in a vitrified film. The vitrified sample was then transferred under a liquid nitrogen environment to a cryoholder (model 626, Gatan Inc., Warrendale, PA) into the electron microscope, Tecnai 20, Sphera (FEI), operating at 120 kV with a nominal underfocus of 2-4 µL. The working temperature was kept below about -175 °C,

and the images were recorded on Gatan 794 MultiScan digital camera and processed with Digital Micrograph 3.6 software.

3.3 Results and Discussion

3.3.1 NMR Analysis of the Chemically Edited HAs

Figure 3.1 shows the ^{13}C NMR spectra of the chemically edited HAs sample obtained by solid state ramp CP-MAS. The spectra suggest that the applied chemical treatment edited out the specifically targeted moieties and also resulted to the variation in the moieties distribution within HAs. Bleaching edited out a significant amount of the aromatic moieties, as illustrated in the 112-145 ppm chemical shift regions and in the relative aromaticity values in Table 3.1. The low signal observed for the bleached samples could be attributed to the aromaticity from charcoal-like components within HAs since charcoal is resistant to oxidative cleavage by sodium chlorite [31]. The bleaching treatment applied in this study effectively edited out the aromatic rings of lignin origin for all HAs studied [28]. The aromaticity values in Table 3.1 similarly indicate a decrease in the aromaticity values for the bleached samples and an increase in a romaticity values for the hydrolysed FPHA sample.

The hydrolysis treatment edited out most of the carbohydrate components, as illustrated by the decrease of intensity in the 50-112 ppm chemical shift region. This chemical shift range envelopes the different types of carbohydrate carbons. The carbon-6 and the ring carbons of polysaccharides produce signals in the 62-66 and 65-85 ppm chemical shift regions, respectively. The peaks centered at approximately 105 ppm are due to anomeric polysaccharides carbons. The decrease in the carbohydrate signal envelope leads to an apparent enhancement of the signals within the 112-145 (aromatic) and 29-33 ppm (lipids) chemical shift regions, as illustrated in Figure 3.1.

The lipid extraction edit resulted in a significant loss of the lipid components and an apparent enhancement of the carbohydrate and aromatic signals as shown in the Figure 3.1 NMR spectra. The signal within the 29-33 ppm chemical shift region corresponds to the polymethylene chains. While the HAs contain lipids from various compounds, such as alkanes, alkenes, fatty acids, n-alkyl, alcohols, terpenes, sterols, polynuclear, hydrocarbons, fats, waxes and resins [32, 33] [34], the lipids extracted in this study could be mainly aliphatic in nature, i.e., consisting of long-chain fatty acids and esters, long chain alkanes, and some aliphatic alcohols [32, 35-37] [34]. As can be seen from the above discussion, the chemical treatments produced appropriately edited HAs for the humic acids studied. This means that the influence of the different moiety classes, namely aliphatic (alkyl), carbohydrate (O-alkyl), and aromatic, can be investigated by samples with reduced or enhanced concentrations of these moiety families.

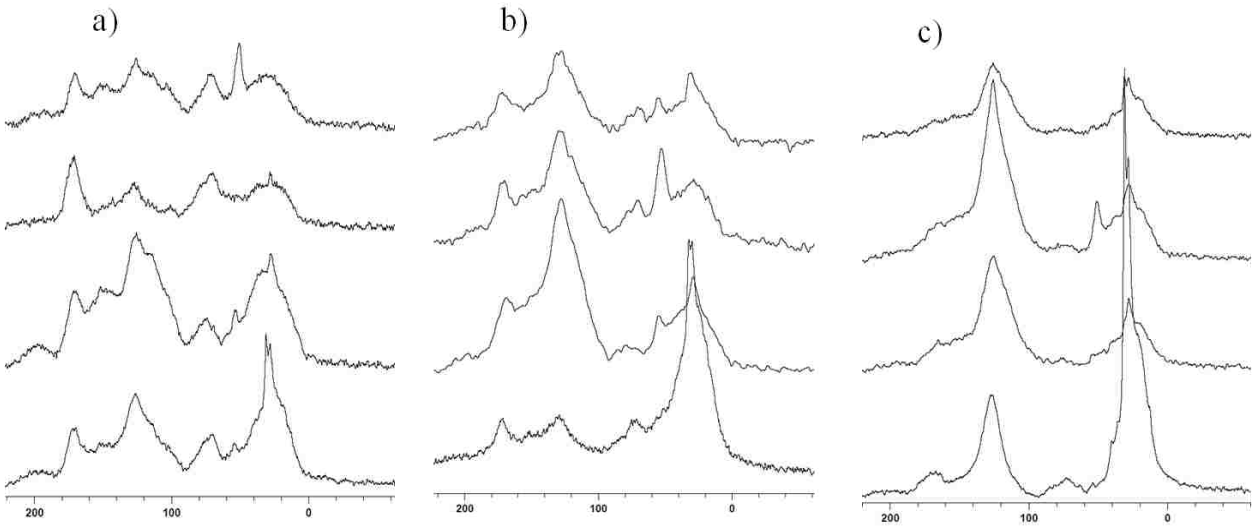

Figure 3.1 ^{13}C NMR spectra of chemically edited HAs. The spectra from the top to the bottom are; unedited, lipid extracted, hydrolyzed and bleached HAs a) is are the spectra for SWHA b) is are the spectra for FPHA and c) is are the spectra for LAHA HAs collected using solid state Ramp-CP MAS.

Table 3.1 ^{13}C NMR Percent relative areas and aromaticity of unedited and edited SWHA, FPHA and LAHA HAs.

SAMPLE	230-190ppm	190-165ppm	165-90ppm	165-110ppm	110-90ppm	90-60ppm	60-0ppm	Aromaticity
Florida Peat (FPHA)	2.49%	12.64%	45.80%	39.86%	5.94%	14.42%	24.64%	0.40
Suwannee HA (SWHA)	1.79%	9.85%	37.84%	31.04%	6.80%	14.64%	35.88%	0.31
Leonardite (LAHA)	0.88%	7.11%	55.03%	48.53%	6.50%	5.32%	31.65%	0.49
Hydrolysed FPHA	1.07%	11.95%	56.61%	50.46%	6.15%	8.54%	21.83%	0.50
Bleached FPHA	2.32%	8.53%	20.49%	17.15%	3.33%	15.88%	52.78%	0.17
Lipid extracted FPHA	1.95%	11.91%	39.89%	6.09%	17.21%	22.95%	0.00%	0.10
Hydrolysed LAHA	-0.48%	6.53%	55.58%	7.58%	3.55%	27.25%	0.00%	0.17
Bleached LAHA	-0.93%	3.75%	25.97%	-0.32%	2.46%	69.08%	0.00%	0.00
Lipid Extracted LAHA	0.76%	7.87%	53.43%	6.94%	6.96%	24.03%	0.00%	0.15
Hydrolysed SWHA	2.10%	10.35%	39.29%	9.47%	11.36%	27.42%	0.00%	0.16
Bleached SWHA	1.80%	17.40%	22.42%	5.30%	25.49%	27.59%	0.00%	0.07
Lipid Extracted SWHA	2.43%	11.27%	31.62%	8.60%	20.87%	25.21%	0.00%	0.13

3.3.2 Size Verification of LUVs

The size of the prepared LUVs was verified using DLS. SRB-entrapped POPC LUVs of approximately 100 nm size were prepared. The DLS data demonstrated LUV size of approximately 112 nm in mean diameter. Cryo-TEM images also demonstrated that LUVs prepared were mostly unilamellar and had a diameter of about 100 nm, with a few multilamellar vesicles also present. The addition of a detergent TX-100 led to the complete rupture of the LUVs, and gave a smaller size of about 10 nm for the mean diameter of the LUVs and a few aggregates of approximately 130 nm in diameter.

3.3.3 The Interaction of Chemically Diverse HAs with POPC Unilamellar Vesicles (LUVs)

Biomembrane perturbation through the interaction of three different HAs in their four different forms, namely: unmodified (reference), bleached, hydrolyzed, and lipid-extracted HA (12 in total) was monitored via the leakage of SRB from POPC LUV model biomembrane system using steady state fluorescence. Representative spectra for SWHA, FPHA, and LAHA are presented in Figures 3.2 (a), (b), and (c), respectively. In addition to the spectral data for the 12 HAs, two control data sets are presented, the first of which is simply labeled control; for this sample set, no HA is added. A low fluorescence intensity was obtained for the Control samples due self-quenching of SRB dye at high molar concentrations, such as 50 mM. Spiking the control samples with TX-100, yields the second set of control data, referred to as control TX. The addition of TX-100 leads to a complete rupture of the vesicles and results in the release of all the SRB dye from the vesicles. While the SRB is diluted in the surrounding solution–eliminating self-quenching–it yields the highest SRB solution concentration, and hence, the highest possible fluorescence.

3.3.4 Leakage Studies with HAs

Reference samples: The HAs studied are sourced from a range of origins, namely an aquatic, Suwannee River (SWHA); a terrestrial, Florida peat humic acid (FPHA); and a coal, Leonardite humic acid (LAHA). The ^{13}C NMR data presented in Figure 3.1 show that all three reference HAs have unique compositions, with SWHA being the most aliphatic in nature and LAHA being the most aromatic, with FPHA lying between these two extremes. As expected from the results in the previous chapter, LAHA resulted in the largest amount of SRB release, and hence, the largest amount of biomembrane perturbation, followed by FPHA, and with SWHA having yielded the smallest amount of perturbation. As discussed in the preceding chapter, this trend can

be related to aromatic content as well as bulk polarity of these three HAs; however, these correlations are highly empirical and require further validation due to the complex nature of HAs and natural organic matter as a whole. To this end, chemically edited humic acids (HAs) were used to greatly reduce the amount of families of different moieties within all three of the HAs studied here.

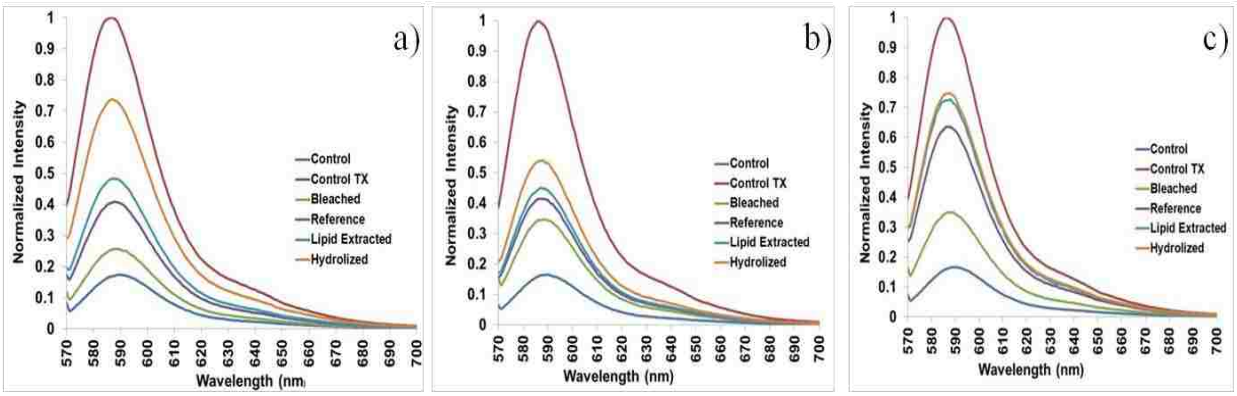

Figure 3.2 Normalized fluorescence emission spectra of SRB dye leakage as induced by chemically edited a) SWHA, b) FPHA and c) LAHA HAs (5 mg C/L, pH 4.8)

Chemically edited HAs: An increase in normalized fluorescence intensity was seen with the introduction of all nine chemically edited HAs, compared to the control. The hydrolyzed sample of SWHA had the highest fluorescence intensity, followed by the lipid-extracted samples and then the reference samples, which were the unaltered HAs. The lowest fluorescence intensity observed for the bleached sample was attributed to the limited interactions of the LUVs with the bleached samples. This yielded fewer perturbations, and hence, lower leakage, and thus, the lowest fluorescence intensity. Similar observations were made for chemically edited FPHA sourced samples where again, the bleached sample resulted in the lowest, while the hydrolyzed sample resulted in the highest fluorescence intensity. LAHA sources HAs had a similar trend to SWHA and FPHA sourced samples. The fact that, for all three HAs, the beached samples induce the least biomembrane perturbation further supports the conclusion made in the previous chapter

that the aromatic moieties–edited out during the bleaching process–appear to perturb the biomembrane the most. This is further supported by the fact that both the hydrolyzed and lipid-extracted samples induce greater perturbation than the reference samples, as both the hydrolysis and lipid extraction editing procedures increase the amount of aromatic moieties per gram of HA.

Source specific chemically edited HAs: If one looks further into the data presented in Figure 3.2 and link them to the NMR data, the trends just discussed are further emphasized. Comparison of the hydrolized samples with the reference samples reveals the largest difference in the steady state fluorescence leakage data for the SWHA sourced samples. The NMR data presented in Figure 3.1 show that the hydrolysis editing enhanced the aromatic content the most in the SWHA sourced sample. Using the same approach it can be seen that the difference between hydrolyzed and lipid-extracted samples follows the same trend. This further supports the finding that the aromatic moieties appear to be the major biomembrane perturbing moieties within all three HAs studied, regardless of source. If one now turns their attention to the bleached samples, the steady state fluorescence leakage data reveal that the largest loss of biomembrane perturbation ability occurs for the LAHA sourced sample, then the SWHA sourced sample; the FPHA sourced sample exhibits the smallest difference. While the NMR data show that the bleaching treatment reduced relative amount of aromatic moieties to the largest extent for the LAHA sourced sample, the difference seen so clearly in the fluorescence data is not as apparent in the NMR data for the SWHA or FPHA sourced samples. Aromatic moieties not being equivalent in their biomembrane perturbing potential may serve as a plausible interpretation of the above observation.

3.3.5 Leakage Kinetics with HAs

Kinetic studies of the release of SRB dye from LUVs are shown in Figures 3.3 (a), (b), and (c). The results clearly illustrate that the leakage of SRB dye from the vesicles was induced by HAs at pH 4.8 and was dependent on the exposure time and the chemical treatment applied to the HAs. The percent leakage of SRB dye increased with time and with the different chemically diverse HAs. The overall shape of the kinetic curves is similar to that we saw for the reference samples in the previous chapter, with two characteristic types of leakage being observed in this study, namely a rapid and slow leakage stages. This once again implies that more than one process is involved in the interaction of HAs with biomembranes. First, there is an initial rapid release of SRB dye, as indicated by the rapid increase in fluorescence intensity for a period of up to ~90 minutes, then a plateau followed by a slow release of SRB dye, as indicated by the slow increase in fluorescence intensity for a period of about three hours.

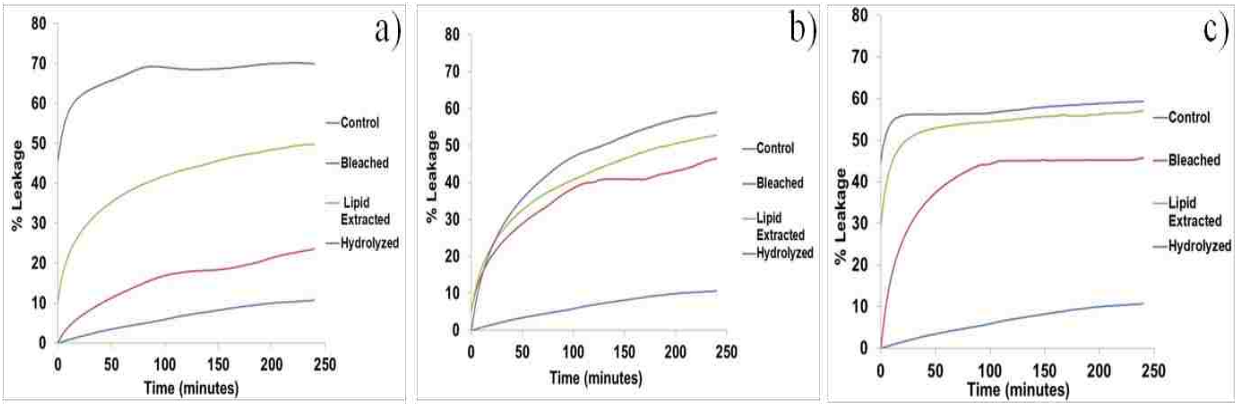

Figure 3.3 Kinetics of the percent leakage of SRB dye as Induced by chemically edited a) SWHA b) FPHA and c) LAHA HAs (5 mg C/L, pH 4.8)

Chemically edited HAs: For the three HAs, of different origins, the hydrolyzed samples induced the fastest overall leakage for the first hour and a half. This is very clear for both the SWHA and LAHA sourced samples, while for the FPHA sourced sample this becomes apparent already after the first 45 minutes. On the other hand, the bleached samples induced the slowest

overall leakage and, as with the hydrolyzed samples, the differences between chemically edited samples were the least apparent for the FPHA sourced sample. The kinetic data also reveal that over the course of 90 minutes and up to six hours the hydrolyzed HAs obtained from all three differently sourced HAs caused the largest perturbation, followed by the lipid-extracted HAs, with the bleached HAs inducing the least amount of perturbation for all three HAs of different origins.

Source specific chemically edited HAs: For the bleached HAs samples, SWHA sourced induced the slowest and the least significant perturbation, followed by bleached FPHA sourced, with bleached LAHA sourced inducing the fastest and largest amount of leakage. For the hydrolyzed HAs samples, the LAHA sourced sample induced the fastest perturbation followed by SWHA sourced, with the FPHA sourced hydrolyzed sample resulting in the slowest and the least amount of perturbation. For both the hydrolyzed SWHA and LAHA sourced samples a plateau is reached by 100 mins, and although LAHA induces the fastest perturbation for the time span studied, it appears that the SWHA sourced sample induces the largest overall perturbation, while even after 6 hours the hydrolyzed FPHA sourced sample is still inducing increase biomembrane perturbation. More homogeneous results were obtained for the lipid-extracted HAs, with the FPHA and SWHA sourced samples yielding very similar results and the LAHA sourced sample inducing somewhat faster and larger amount of perturbation. Once, again these results provide further evidence that it is the aromatic moieties within all three reference samples (unmodified HAs of different origins) that induce and are involved in the perturbation of biomembranes.

3.3.6 Mechanistic Insights and Environmental Significance

The combination of the NMR and fluorescence data collected from bleached, hydrolyzed, and lipid-extracted HAs strongly imply that it is the aromatic moieties within the three HAs, regardless of their origin, that induce and are involved in biomembrane perturbation. The data also show that even for the chemically edited HAs the perturbation process is complex and consists of both a fast stage and a slow stage; the slow component for the hydrolyzed and lipid-extracted LAHA sourced sample and the hydrolyzed SWHA sourced sample is minor, as can be seen by the kinetic data presented in Figure 3.3. The combined data also show that the aromatic moieties within the three HAs, from different sources, have a different potential to perturb biomembranes. This finding has mechanistic and environmental implications.

3.3.7 Mechanistic Implications

The mechanism presented in the previous chapter had a hydrogen bridge condition. This condition has been proposed previously in the literature [2] and, although not obvious, it is the only one that accounts for all the experimental observations, including those in the previous chapter. The results presented in this chapter and the apparent key role of aromatic moieties in the perturbation of biomembranes are completely consistent with this proposal and further adds to the development of the adsorption/absorption model, especially from a chemical perspective.

The requirement for a hydrogen bridge in the initial adsorption step of the adsorption/absorption model requires the presence of accessible hydrogen bonding entities on the natural organic matter (and the HS and HA subfractions) side of the HS/biomembrane couple. Within the mixture known as natural organic matter (NOM) and the HS and HA subfractions there are two major families of moieties that contain polar groups capable of hydrogen bonding, and hence, utilize hydrogen as a bridge, namely carbohydrates (O-alkyls) and aromatics. The

aromatic moieties are derived from lignin in plant material, and hence, inherently have phenol and methoxy groups, while the carbohydrate moieties are derived mainly from cellulose, and hence, have alcohol groups. During the natural degradation processes involving these starting materials, a range of carbonyl groups are produced within both the carbohydrate and aromatic functionalities [38], which provides the NOM the structural elements, such as an H atom at the end of a polar bond or a lone pair of electrons on an O atom, needed for the hydrogen bridge. With this in mind, one can now approach the results observed in this chapter.

The aromatic moieties within NOM and its HA subfraction posses the two characteristics needed to perturb a membrane's structure. The first is that it has the functional groups needed for the formation of the hydrogen bridge required for the adsorption step, as evidenced by the ^{13}C NMR signal envelope in the aromatic region between 137 to 160 ppm (C-O and C-N) in Figure 3.1. The NMR signal between 110-137 ppm is for C-C or C-H aromatic carbons, and hence, the NMR data show that there is a large fraction of the aromatic carbons that are not functionalized, and hence, are non-polar. Stated differently, there is evidence from the NMR data that, as a whole, aromatic moieties have enough functionality to allow for the hydrogen bridge condition of the adsorption step but, at the same time, there is a sufficient amount of hydrophobic aromatic moieties to allow for biomembrane perturbation via hydrophobic interactions in the absorption step of the adsorption/absorption mechanism.

The differences in biomembrane perturbation potential within the same type of edited HAs samples sourced from HAs from different origins once again point to a range of aromatic moieties within NOMs having the ability to perturb biomembranes, to a different extent. The kinetic studies also show complex behavior, for all HAs via chemical editing, along the lines of the complex behavior seen in the previous chapter for the unedited HAs. This is not surprising,

given that both the adsorption and absorption steps are required and the fact that HAs studied in the previous and this chapter, respectively, constitute complex mixtures of aromatic moieties.

The results presented here, combined with the data interpretation from the previous chapter, allow for a chemically refined adsorption/absorption model for the perturbation of membranes. Accordingly, aromatic moieties within NOM, in general, are adsorbed onto the biomembrane wall via a hydrogen bridge and then are absorbed into the biomembrane via hydrophobic interactions at "lattice" defects sites. It is the absorption step that induces the perturbation that, in turn, induces the increased permeability seen for the biomembrane systems in this study. An entire range of aromatic moieties can induce the observed biomembrane perturbation, as shown by the kinetic data, which also show a fast and slow component. Chemically, it is proposed that, due to their higher propensity to form the hydrogen bridge, the more functionalized aromatic moieties are responsible for the fast component, while the less functionalized aromatic moieties are responsible for the observed slow component, as they are more likely to just tumble along the biomembrane's surface and have a much lower probability of forming the required hydrogen bridge due to their very low density of functional groups.

3.3.8 Environmental Implications

The evidence presented above for the three HAs studied, implies that NOMs high in aromatic moieties, e.g., terrestrial NOM, have the potential to influence the permeability of biomembranes at acidic pHs. As discussed in the previous chapter, spring runoffs are high in terrestrial NOM, whose concentrations can be high enough to reduce the pH of the receiving waters to well below 5 [39, 40]. This terrestrial spring runoff of NOM in moderate to far Northern and Southern global regions have the potential to induce biomembrane permeability, and hence, increase the potential bioavailability and toxicity of both inorganic and organic

materials. As already discussed in the previous chapter, these findings have important implications for the thawing of permafrost and the release of the trapped soil organic matter reserves [39, 40]. In addition, modern agricultural practices, such as tilling, have led to a large loss of terrestrial NOM into local watersheds [41]. Such losses not only reduce the fertility of agricultural soils all over the world [41], but they may also make applied chemicals, such as pesticides, more bioavailable via the biomembrane perturbation mechanisms discussed above. As the vast majority of applied pesticides are hydrophobic [42], they have a high potential to associate with aromatic moieties within the terrestrial NOM [43].

The results in this chapter also imply that the removal of aromatic moieties via bleaching reduces the ability of the studied HAs to induce biomembrane perturbation. Serendipitously, within the environment, similar removal of aromatic moieties can take place via photochemical bleaching [44]. This means that, as the sun illuminates areas more intensely and for longer periods of the time during spring and then summer months, this photochemical bleaching of aromatic moieties is expected to take place in NOM that is shallow within the water column. This, along with the potential of aggregation, means that the situation involving surface runoff of terrestrial NOM aromatic moieties may not be as dire as one would first think.

3.4 Conclusions

Chemical treatment applied to the HAs investigated in this study generated specific structural modification on the HAs samples: bleaching eliminated a significant portion of the aromatic components; hydrolysis reduced most of the carbohydrates; and lipid extraction removed most of the lipids. The study has further demonstrated that the hydrolyzed HAs interact with the biomembranes more than the unmodified HAs, while the bleached HAs interact with biomembranes the least. Data presented in this study serve as strong evidence that aromatic

components within the HAs are the major biomembrane disruptors; however, direct evidence is impossible to due to the complex and heterogeneous nature of HAs and NOMs as a whole.

3.5 References

1. Nakashima, K.; Xing, S. Y.; Gong, Y. K.; Miyajima, T. Characterization of humic acids by two-dimensional correlation fluorescence spectroscopy. *Journal of Molecular Structure.* **2008,** *883*, 155-159.

2. Elayan, N. M.; Treleaven, W. D.; Cook, R. L. Monitoring the effect of three humic acids on a model membrane system using ^{31}P NMR. *Environ. Sci. Technol.* **2008,** *42* (5), 1531-1536.

3. Duval, J. F. L.; Wilkinson, K. J.; Van Leeuwen, H. P.; Buffle, J. Humic substances are soft and permeable: Evidence from their electrophoretic mobilities. *Environ. Sci. Technol.* **2005,** *39* (17), 6435-6445.

4. Hayes, M. H. B.; Clapp, C. E. Humic substances: Considerations of compositions, aspects of structure, and environmental influences. *Soil Science.* **2001,** *166* (11), 723-737.

5. Schnitzer, M. Soil organic-matter- the next 75 years. *Soil Science.* **1991,** *151* (1), 41-58.

6. Campbell, P. G. C.; Twiss, M. R.; Wilkinson, K. J. Accumulation of natural organic matter on the surfaces of living cells: implications for the interaction of toxic solutes with aquatic biota. *Canadian Journal of Fisheries and Aquatic Sciences.* **1997,** *54* (11), 2543-2554.

7. Vigneault, B.; Percot, A.; Lafleur, M.; Campbell, P. G. C. Permeability changes in model and phytoplankton membranes in the presence of aquatic humic substances. *Environ. Sci. Technol.* **2000,** *34* (18), 3907-3913.

8. Sanchez-Marin, P.; Beiras, R. Adsorption of different types of dissolved organic matter to marine phytoplankton and implications for phytoplankton growth and Pb bioavailability. *Journal of Plankton Research.* **2011,** *33* (9), 1396-1409.

9. Chenu C, S. G. Interactions between Microorganisms and Soil Particles: An Overview. In 'Interactions between Soil Particles and Microorganisms'. *John Wiley & Sons.* **2002**.

10. Visser, S. A. Physiological action of humic substances on microbial-cells. *Soil Biology & Biochemistry*. **1985,** *17* (4), 457-462.

11. Richards, J. G.; Burnison, B. K.; Playle, R. C. Natural and commercial dissolved organic matter protects against the physiological effects of a combined cadmium and copper exposure on rainbow trout (Oncorhynchus mykiss). *Canadian Journal of Fisheries and Aquatic Sciences.* **1999,** *56* (3), 407-418.

12. Knauer, K.; Buffle, J. Adsorption of fulvic acid on algal surfaces and its effect on carbon uptake. *Journal of Phycology.* **2001,** *37* (1), 47-51.

13. Alstad, N. E. W.; Kjelsberg, B. M.; Vollestad, L. A.; Lydersen, E.; Poleo, A. B. S. The significance of water ionic strength on aluminium toxicity in brown trout (Salmo trutta L.). *Environmental Pollution.* **2005,** *133* (2), 333-342.

14. Parent, L.; Twiss, M. R.; Campbell, P. G. C. Influences of natural dissolved organic matter on the interaction of aluminum with the microalga Chlorella: A test of the free-ion model of trace metal toxicity. *Environ. Sci. Technol.* **1996,** *30* (5), 1713-1720.

15. Lamelas, C.; Slaveykova, V. I. Comparison of Cd(II), Cu(II), and Pb(II) biouptake by green algae in the presence of humic acid. *Environ. Sci. Technol.* **2007,** *41* (11), 4172-4178.

16. Sanchez-Marin, P.; Lorenzo, J. I.; Blust, R.; Beiras, R. Humic acids increase dissolved lead bioavailability for marine invertebrates. *Environ. Sci. Technol.* **2007,** *41* (16), 5679-5684.

17. Pan, J. F.; Wang, W. X. Comparison of the bioavailability of Cr and Fe bound with natural colloids of different origins and sizes to two marine bivalves. *Marine Biology.* **2002,** *141* (5), 915-924.

18. Guo, L. D.; Hunt, B. J.; Santschi, P. H.; Ray, S. M. Effect of dissolved organic matter on the uptake of trace metals by American oysters. *Environ. Sci. Technol.* **2001,** *35* (5), 885-893.

19. Lee, Y. S.; Bartlett, R. J. Stimulation of plant-growth by humic substances. *Soil Science Society of America Journal.* **1976,** *40* (6), 876-879.

20. Chaminade, R.; Blanchet, R. Mecanisme de laction stimulante de lhumus sur la nutrition mineral des vegetaux. *Comptes Rendus Hebdomadaires Des Seances De L Academie Des Sciences.* **1953,** *237* (25), 1768-1770.

21. Samson, G.; Visser, S. A. *S*urface-active effects of humic acids on potato cell-membrane properties. *Soil Biology & Biochemistry.* **1989,** *21* (3), 343-347.

22. Visser, S. A. Acid functional-group content of aquatic humic matter - its dependence upon origin, molecular-weight and degree of humification of the material. *Journal of Environmental Science and Health Part a-Environmental Science and Engineering & Toxic and Hazardous Substance Control.* **1982,** *17* (6), 767-788.

23. Yamamoto, H.; Liljestrand, H. M.; Shimizu, Y. Effects of dissolved organic matter surrogates on the partitioning of 17 beta-estradiol and p-nonylphenol between synthetic membrane vesicles and water. *Environ. Sci. Technol.* **2004,** *38* (8), 2351-2358.

24. Koynova, R.; Caffrey, M. Phases and phase transitions of the phosphatidylcholines. *Biochimica Et Biophysica Acta-Reviews on Biomembranes.* **1998,** *1376* (1), 91-145.

25. Rice, J.; Maccarthy, P. Isolation of humin by liquid-liquid partitioning. *Sci. Total Environ.* **1989,** *81-2*, 61-69.

26. Almendros, G. Effects of different chemical modifications on peat humic-acid and their bearing on some agrobiological characteristics of soils. *Commun. Soil Sci. Plant Anal.* **1994,** *25* (15-16), 2711-2736.

27. Wise, L. E.; Murphy, M.; Daddieco, A. A. Chlorite holocellulose, its fractionation and bearing on summative wood analysis and on studies on the hemicelluloses. *Technical Association Papers* **1946,** *29* (JUN), 210-218.

28. Christman, R. F.; Norwood D.L.; Seo Y.; Frimmel F.H. *O*xidative degradation of humic substances from fresh water environments II. In search of structure ed.; *John Wiley & Sons, New York.* **1989.**

29. Ladokhin, A. S.; Wimley, W. C.; White, S. H. Leakage of membrane vesicle contents: Determination of mechanism using fluorescence requenching. *Biophysical Journal.* **1995,** *69* (5), 1964-1971.

30. Barany-Wallje, E.; Gaur, J.; Lundberg, P.; Langel, U.; Graslund, A. Differential membrane perturbation caused by the cell penetrating peptide Tp10 depending on attached cargo. *Febs Letters.* **2007,** *581* (13), 2389-2393.

31. Chefetz, B.; Salloum, M. J.; Deshmukh, A. P.; Hatcher, P. G. Structural components of humic acids as determined by chemical modifications and carbon-13 NMR, pyrolysis-, and thermochemolysis-gas chromatography/mass spectrometry. *Soil Science Society of America Journal.* **2002,** *66* (4), 1159-1171.

32. Wu, Q. G.; Schleuss, U.; Blume, H. P. Investigation on soil lipid extraction with different organic-solvents. *Z. Pflanzen. Bodenk.* **1995,** *158* (4), 347-350.

33. Stevenson, F.J. Humus chemistry: Genesis, composition, reactions. *Wiley-Interscience, New York*. **1982.**

34. Dinel H. M.S.; Mehuys G. R. Soil lIpids: Origin, Nature, Content, Decomposition, and Effect on Soil Physical Properties ed. S. *Biochemistry*. CRC Press**. 1990,** Mar 22

35. Guignard, C.; Lemee, L.; Ambles, A. Lipid constituents of peat humic acids and humin. Distinction from directly extractable bitumen components using TMAH and TEAAc thermochemolysis. *Org. Geochem.* **2005,** *36* (2), 287-297.

36. Schnitzer, M.; Schulten, H. R. Pyrolysis-soft ionization mass-spectrometry of aliphaticsextracted from a soil clay and humic substances. *Sci. Total Environ.* **1989,** *81-2*, 19-30.

37. Lodygin, E. D.; Beznosikov, V. A. Influence of soil moisture on concentrations and C-13 NMR profiles of lipids in three Albeluvisols. *Geoderma.* **2005,** *127* (3-4), 253-262.

38. Stevenson, F. J. H. C. G. Humus Chemistry: Genesis, composition, reactions. *John Wiley and Sons*, Stillerman. 1994.

39. Schaefer, K.; Zhang, T. J.; Bruhwiler, L.; Barrett, A. P. Amount and timing of permafrost carbon release in response to climate warming. *Tellus Series B-Chemical and Physical Meteorology.* **2011,** *63* (2), 165-180.

40. Edward A. G. Schuur, B. A., t and the Permafrost Carbon Network., High risk of permafrost thaw. *NATURE.* **2011,** *480*.

41. Montgomery, D.R., Dirt the erosion of civilization. 2008.

42. Gilliom, R. J. B., J. E.; Crawford, C. G.; Hamiton, P. A.; Martin, J. D.; Nakagaki, N.; Nowell, L. H.; Scott, J. C.; Stackelberg, P. E.; Thelin, G. P., Wolock, D. M. , 1992-2001. , The Quality of Our Nation's Waters. Pesticides in the Nation's Streams and Ground water. *National Water-Quality Assessment Program.* **2006.**

43. Pignatello, J.J. Interaction of Anthropogenic organic chemicals with organic matter in natural particles, ed. B.-c.P.o.A.O.C.i.E.S. In IUPAC series on Biophysico chemical processes in environmental systems. *IUPAC-sponsored Wiley Series*. **2009.**

44. Goldstone, J. V.; Pullin, M. J.; Bertilsson, S.; Voelker, B. M. Reactions of hydroxyl radical with humic substances: Bleaching, mineralization, and production of bioavailable carbon substrates. *Environ. Sci. Technol.* **2002,** *36* (3), 364-372.

Chapter 4. Gold and Silver Nanoparticles Formation using Chemically Diverse Humic Acids

4.1 Introduction

Nanoparticles (NPs) of metals, such as gold and silver, have been widely synthesized and characterized due to their broad industrial applicability, in particular in electronics and personal use products (silver NPs) and in the medical sector (gold NPs) [1-5]. While much of emphasis has been put on the laboratory synthesis and application of the NPs, the possibility of NP formation in the environment under natural environmental conditions, such as pH and temperature, has been explored to a much more limited extent [6-9]. The typical synthesis of gold and silver NPs involves the reduction of a metal salt by a reducing agent. Different reducing agents have been used in the synthesis of Ag and Au NPs, such as HAs [6-9], borohydrates, polysaccharides, alcohols, amines, carboxylic acids and fungi [5]. It has been shown that HAs interact with and stabilize aqueous suspensions of a range of these synthetic NPs [10]. These studies have demonstrated that lower concentrations of natural organic matter (NOM), including HAs, increase the stability of the NPs by coating their surface, whereas higher concentrations of NOM cause the aggregation of NPs [10]. Studies on the adsorption of NOM to NPs surfaces indicated that NOM plays an important role in stabilizing NPs in the environment [11].

HAs are the major component of NOM as a whole, and are formed in the environment as a result of microbial decomposition of plant matter. They are present everywhere in the environment and are made up of complex heterogeneous and polydisperse mixtures of decayed plant materials. They have a complex structure that comprises both hydrophobic and hydrophilic moieties. Functional groups within HAs, such as the thiols, [12] quinones, methoxy, hydroxyls, aldehydes, ketones, enols, and phenols [13] endow this macromolecule with the potential to interact with and reduce metal salts to metal NPs. The percent chemical composition of HAs

vary with their source, implying that the potential of a metal ion to become reduced by HAs will vary depending on the chemical composition of the HA. HAs originating from an aquatic environment (i) are less aromatic as they result from the degradation of mostly aquatic plants, such as algae; (ii) are polar in nature, and (iii) have a high content of aliphatic domains. HAs that form in the terrestrial and coal-rich areas are derived primarily from decomposing parent plant materials, which tend to be rich in lignin's and, as such, they are usually rich in aromatic components and, therefore, are more hydrophobic in nature [14]. As HAs are prevalent throughout the environment, and due to their chemical composition, it is believed that they may play a key role in the formation of NPs naturally in the environment.

Along these lines, a number of studies have been carried out to study the potential of HAs to reduce Au and Ag metal ions to form NPs. Machesky and co-workers [6] investigated the potential of HAs to form colloidal gold (NPs) with a range of peat derived HAs and fulvic acids. In this study, a range of environmental conditions were studied, such as HA and fulvic acid concentrations of (2-20 ppm carbon), Au concentration (5-50 μM), as well as pH ranging from 3.5 to 8.5. This study clearly showed that HAs can act as reducing agents and form colloidal Au (NPs). While thorough and pioneering, this study was rather limited in scope as it used HAs and fulvic acids sourced only from peats, studied only Au, and the characterization of the colloidal Au (NPs) was performed by UV/Vis at a single wavelengths only. This means the findings are very specific and little is known about the formed Au NPs other than that they were formed. Santos et al. [9] also investigated the ability of fulvic acids to form Au nanoparticles and showed that, over a FA concentration 25 to 250 ppm a range of different types of nanoparticles were formed, depending on the pH and fulvic acid concentrations. This study was systematic in approach with the successfully accomplished goal of using fulvic acid to form NPs. The study

was not aimed at the formation of NPs in the environment, and hence, used non-environmentally relevant conditions, such as Au concentration being as high as 500 ppm; only a single humic material was studied, and the temperature of the experiment was not discussed.

Humic acids have also been shown to reduce Ag to form NPs. The most comprehensive study, to date that we are aware of, is that by Shrama and co-workers [7], in which the authors study the formation of Ag NPs by HAs over a HA concentration range of 1 to 100 ppm, Ag concentration range of 10 to 1000 μM (1 mM), and temperature range of 22 to 95 ºC, utilizing HA from aquatic, soil, and sediment sources. The study clearly showed that Ag NPs could be formed at all conditions, studied, and characterized by a number of methods, including UV/Vis absorption spectroscopy, dynamic light scattering, atomic force microscopy, and transmission electron microscopy (TEM). Nevertheless, the vast majority of the study was on NPs formed at 90 °C, 1 mM silver concentration, and 100 ppm HA and only at single pH ranging between 7.4 and 8.1, depending on the HA studied. These conditions are at the extremes of environmental conditions, and hence, the study leaves a large territory for further investigation. Two other studies [8] [15] have looked at the potential of humic materials to form Ag NPs; however, these studies used Ag and humic material concentrations too high to be considered environmentally relevant to draw conclusions in regards to what might be taking place in the environment [16, 17].

Due to the environmental importance of humic materials in the fate, including bioavailability, and transport of metals within the environment there is a clear need to systematically study the role humic materials play in the formation of NPs. The work presented in this chapter explores, for the first time, the formation of Au and Ag NPs under natural environmental conditions in both acidic and basic media by reducing $HAuCl_4$ and $AgNO_3$ using

chemically diverse HAs. This study takes a systematic approach and focuses on 1) the potential of HAs from different sources to form Au and Ag NPs, 2) the determination of the role of environmentally realistic pH (both acidic and basic) conditions on the formation of Au and Ag NPs, as well as 3) the importance of both the metal and HA concentrations on the formation of Au and Ag NPs.

4.2 Experimental Section

Materials. Florida Peat Humic Acid (FPHA), Leonardite Humic Acid (LAHA), and Suwanee River Humic Acid (SWHA) were purchased from the International Humic Substances Society (IHSS, St. Paul, MN). Gold (III) chloride trihydrate ($HAuCl_4 \bullet 3H_2O$) and silver nitrate ($AgNO_3$), were obtained from Sigma Aldrich (Milwaukee, WI). High quality (18MΩ) deionized water was made in our laboratory using an apparatus manufactured by US Filter.

Preparation of HAs

HAs stock solutions were prepared by initially adding 8.6 mg of HA in 50 mL of 0.01 M phosphate buffer solutions at pH 4.8 or 7.6, followed by an alkalinization with NaOH for the purpose of dissolving all HAs, then adjusting the pH back to pH 4.8 or 7.6 with HCl, and finally, diluting the resulting solution to 100.0 mL with the appropriate phosphate buffer solution. All HAs stock solutions used in this study were prepared in a similar way. HAs stock solutions were diluted to environmentally relevant concentrations, ranging from 5 ppm HAs to 60 ppm, and their pH were confirmed to be either 4.8 and 7.6 prior to the synthesis of the NPs.

Synthesis of Au and Ag NPs

The preparation of Au NPs involved a modification of the literature method reported by Sharma and co-workers [7]. An aqueous solution of $HAuCl_4$ was mixed with the HA solutions at pH 4.8 and pH 7.6. The samples were sonicated at 60 °C. Ag NPs nanoparticles were prepared

by mixing aqueous solution of $AgNO_3$ with HA solutions at pH 4.8 and pH 7.6 and stirred on a hot plate, while gradually heated at 60 °C for 12 hours then allowed to sit on the bench. The concentrations of the metal salt reduced to NPs were 250 µM, 25 µM and 1 µM for both Au and Ag. Concentrations of HAs used in the reduction reactions were 2.5, 5, 10, 15, 20 and 30 ppm. The HA-induced reduction of $HAuCl_4$ to Au NPs and $AgNO_3$ to Ag NPs was monitored by observing the color change from pale yellow to deep red and to dark yellow, respectively. These solutions were allowed to cool and were stored in the dark. The nanoparticles were stable for use for approximately 3 months.

Characterization of Au and Ag NPs

UV-Visible Absorbance Measurements: Absorbance spectra were collected from 300-600 nm for Ag NPs and 400-700 nm for Au NPs using a 1.0 cm quartz cell. A Cary 100 Bio UV-visible spectrometer was used to obtain the UV spectra. Deionized water was used as blank.

TEM: The NPs formed were imaged using transmission electron microscopy.

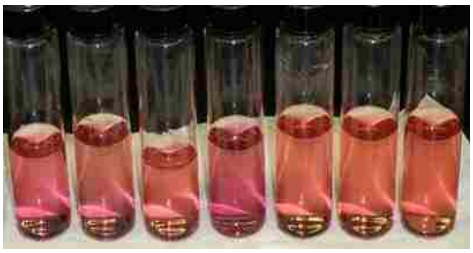

Figure 4.1 Au NPs solutions of different sizes

4.3 Results and Discussion

As mentioned above, stabilized Au NPs were prepared using chemically diverse HAs as both the reducing and the capping agents. Formation of Au NPs was indicated by the change of solution color from pale yellow to deep red Figure 4.1 and was further confirmed by the UV-Vis spectroscopic analysis via the characteristic surface plasmon resonance peak (SPRP) at ~540 nm

that is typical for gold NPs [18]. The surface plasmon resonance at ~540 nm is attributed to the excitation of surface plasmon vibrations. This characteristic plasmon peak was observed for all the HAs studied. Although a range of methods has been used to characterize Au NPs, as discussed above, the monitoring of the SPRP has proven to be a powerful method in characterising Au NP formation due to the SPRP dependence on 1) the NP size (the SPRP shifts to either lower wavelengths for smaller particles or higher wavelength for larger or aggregated particles); 2) the amount of NPs formed (the more NPs are formed, the more intense the SPRP is), and 3) the degree of dispersion (the more disperse the NPs are in size, the broader the SPRP).

4.3.1 Monitoring the formation of Au NPs via their SPRP

Figures 4.2 to 4.5 present the UV/Vis spectra for reactions containing the indicated concentration of HA under both acidic and basic conditions for Au metal concentrations of 1 μM, 25 μM, 75 μM, and 250 μM, respectively. From these data it can be seen that the metal concentration, humic acid concentration, and HA type all play a role in the amount and nature of the NPs formed. The lack of a SPRP in all the 1 μM Au spectra indicate that no Au NPs were formed at this Au concentration regardless of HA concentration or pH. When the Au concentration was raised to 25 μM, very different results are seen, especially for the acidic pH samples. For the SWHA samples it can be seen that, at all HA concentrations, a SPRP is clearly visible and is of similar intensity at a wavelength of 530 nm. These results indicate that, regardless of SWHA concentration, approximately the same amount and size of Au NPs are formed. On the other hand, FPHA at acidic conditions and at the same Au concentration gives rise to a more complex picture. As one goes from 2.5 ppm to 10 ppm HA, the SPRP narrows, indicating a narrower size distribution of the NPs formed. In addition, it can be seen that, while the intensity of the SPRP goes up with the HA concentration increase from 2.5 to 5 ppm, it then

decreases for the 10 ppm HA concentration, and subsequently steadly increases as the HA concentration increases from 10 to 30 ppm. At the same time, it can be seen in Figure 4.3 that the SPRP shifts to lower wavelengths as the concentration of the FPHA increases. In an effort to explain these observations, lets consider two phenomena that occur when the concentration of FPHA increases. The first is that, as the number of potential reducing sites increases, there are more sites for Ag NP formation, yielding smaller NPs. The second is that as the FPHA concentration increases, so does the possibility of conformational changes. This is particularly the case at lower pH values as a result of the reduction of repulsive forces within the FPHA supermolecular assembly due to the protonation of negatively charged functional groups. This change in the FPHA conformation may change the amount of accessible reducing sites. This can explain the up and down variation of the Ag NP SPRP between 2.5 and 10 ppm FPHA discussed above. HA conformational change with concentration also means that one may not neccesarily see a linear relationship between the intensity of the SPRP and HA concentration. A similar trend is seen for LAHA at a Au concentration of 25 μM and at a pH of 4.8, as seen in Figures 4.3, with the dip in the SPRP intensity occuring at 15 ppm, instead of the 10 ppm observed for FPHA, and with the same plausible explanation for this behavior as that offered above for FPHA.

Data collected at pH 7.6 for a Au concentration of 25 μM show that, only hints of NP formation is seen for all three HAs at the higher studied concentrations, with an exception for FPHA at a concentration of 20 ppm. This obseveration would seem to indicate that at this somewhat basic pH there are enough available binding sites within all three HAs to preferentially bind Au ions instead of forming Au NPs in amounts sufficient for the Au NPs' SPRP to emerge from the inherent UV/Vis spectra of the HA, except at 20 ppm FPHA. Why FPHA at 20 ppm is the exception is a question that requires further investigation.

When the concentration of Au is increased to 75 μM, different results are obatined than at a concentration of 25 μM Au. This can easily be seen by comparing the spectra in Figure 4.3 and 4.4. If one focuses on the acidic pH and starts off with SWHA, it can be seen that the two lowest HA concentrations yield very different spectra than the higher HA concentration samples. The Au NPs formed at the two lowest HA concentrations are much more polydisperse, as illustrated by the much broader SPRP. In addition, while there are fewer NPs formed, as can be seen by the lower intensity of the SPRPs, these sparse NPs are larger, as can be seen by the location of the SPRPs. As the HA concentration increases to10 ppm or higher, more NPs are formed and the NPs formed are smaller and more uniform, as evidenced by the increased intensity, decreased wavelength, and narrower width SPRP, respectively. If one considers the NPs formed by FPHA and LAHA at acidic pH, it can be seen that, in both cases, there is a minimum amount of NPs formed at a HA concentration of 10 ppm, while the largest NPs are fomed at HA concentrations of between approximately 15 and 10 ppm for FPHA and LAHA, respectively. As discussed above, conformational changes within the HAs offer the most logical explanation for these variations, and are expected to be more important for LAHA followed by FPHA, with SWHA being the least prone to these issues as it has the highest oxygen (a measure of polarity in HAs) content as well as carboxylic and phenolic content, which collectively hinder such transformations to very tightly packed conformation in aqueous solution.

The 75 μM Au data at the basic pH yield much more consistent as more easily understandable results than those discussed above for the acidic pH. For the NPs formed by SWHA it can be seen by the intensity (once one considers the underlying intensity of the HA) data in Figure 4.4 that, regardless of HA concentration, a consistent amount of Au NPs are formed and that these NPs have approximately the same polydispersity and size, as illustrated by

the wavelength data in Figure 4.4. Very similar results can be seen for FPHA, as illustrated by the data in Figure 4.4. When it comes to LAHA under the same conditions, different results are obtained. The first difference is that more Au NPs are formed at lower LAHA concentrations (2.5, 5.0 and 10 ppm) than at higher LAHA concentrations (15, 20, and 30 ppm). Secondly, while the sizes of the formed NPs are rather consistent with the NPs formed at the higher LAHA concentrations, they are more polydisperse, as can be seen by the wider SPRP in Figure 4.4. These results for LAHA can be explained once again by the conformational changes, including aggregation, of LAHA at higher concentrations.

A Au concentration of 250 μM produces very polydisperse and generally large as indicated by the broad peaks. NPs for all the HAs at the acidic pH, which is again, in all likelihood, a result of this high Au concentration inducing large scale aggregation of the HAs due to the scarsity of the negatively charged sites within the HAs. The fact that for none of the HAs did the higher HA concentrations result in the most NPs being formed is consistent with HA aggregation induced by the high concentration of Au. The aggregation assumption is consitent with SWHA showing the smallest and LAHA showing the largest effect, respectively. The basic pH data for all three HAs also show that there is a complex competition taking place between NP formation and HA aggregation due to Au binding.

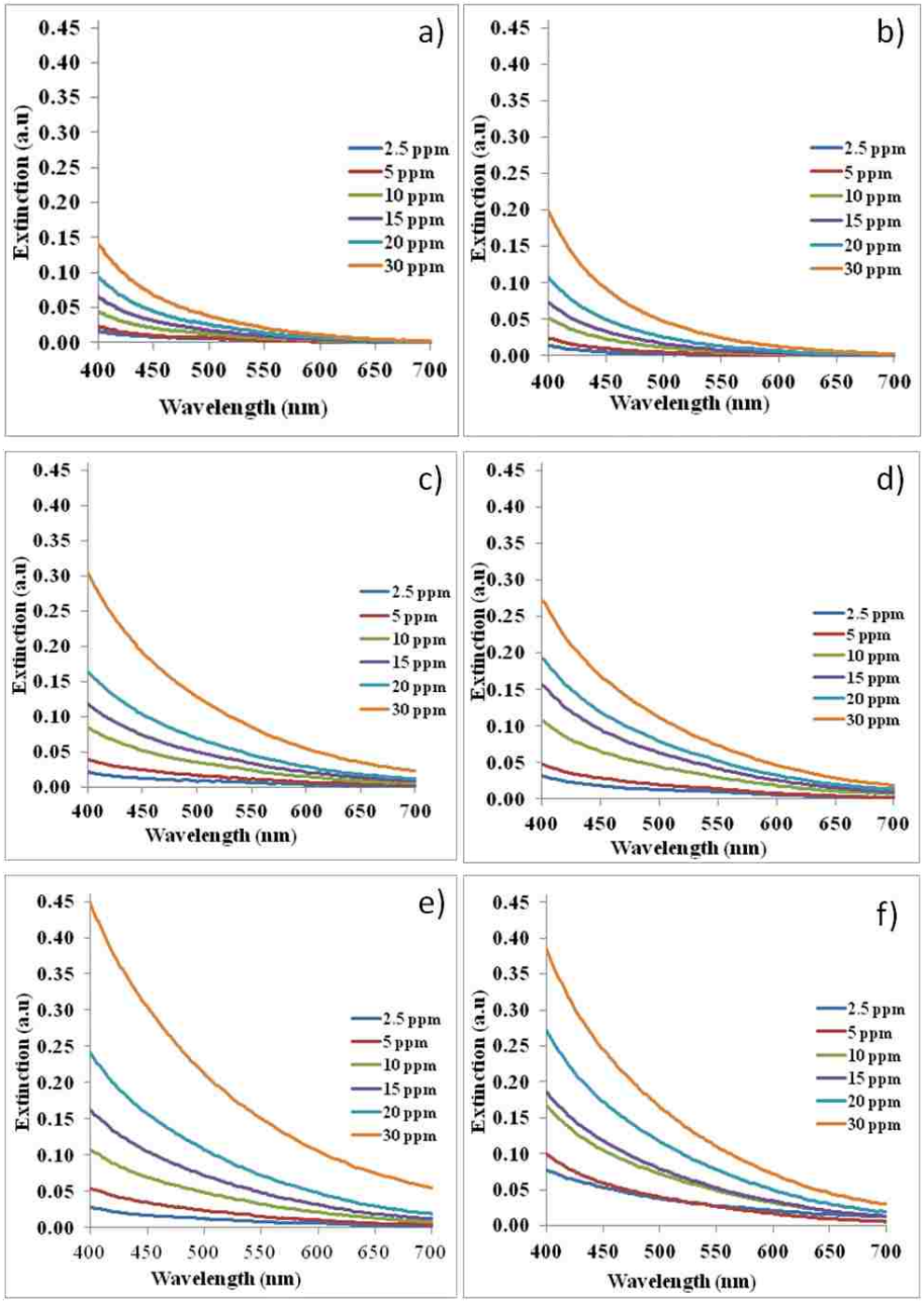

Figure 4.2 UV-Vis spectra of Au NPs formed at 1µm metal ion concentration and varying concentrations of HAs **a)** SWHA pH 4.8. **b)** SWHA pH 7.6. **c)** FPHA pH 4.8. **d)** FPHA pH 7.6. **e)** LAHA pH 4.8. and **f)** LAHA pH 7.6.

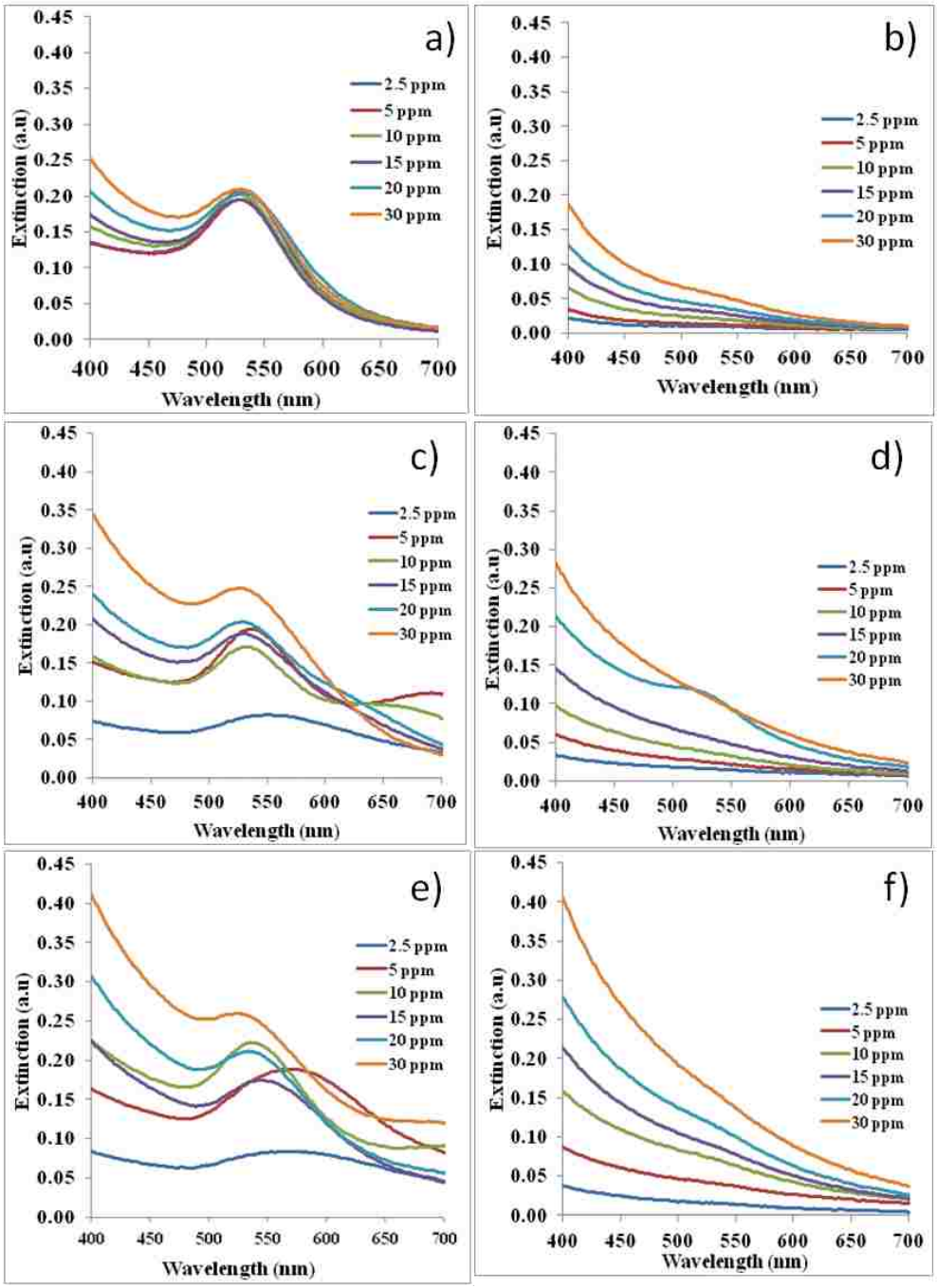

Figure 4.3 UV-Vis spectra of Au NPs formed at 25 µm metal ion concentration and varying concentrations of HAs **a)** SWHA pH 4.8. **b)** SWHA pH 7.6. **c)** FPHA pH 4.8. **d)** FPHA pH 7.6. **e)** LAHA pH 4.8. and **f)** LAHA pH 7.6.

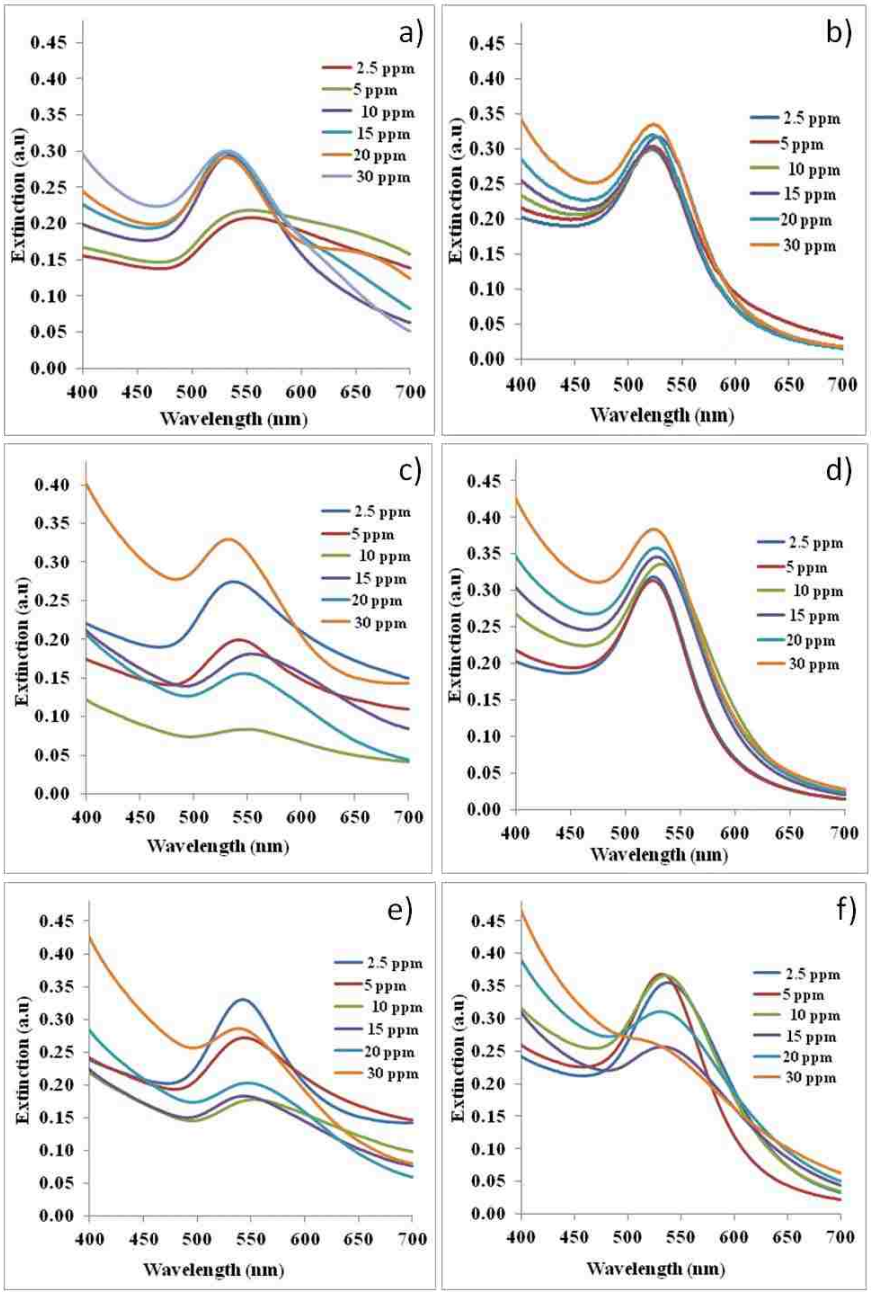

Figure 4.4 UV-Vis spectra of Au NPs formed at 75 µm metal ion concentration and varying concentrations of HAs **a)** SWHA pH 4.8. **b)** SWHA pH 7.6. **c)** FPHA pH 4.8. **d)** FPHA pH 7.6. **e)** LAHA pH 4.8. and **f)** LAHA pH 7.6.

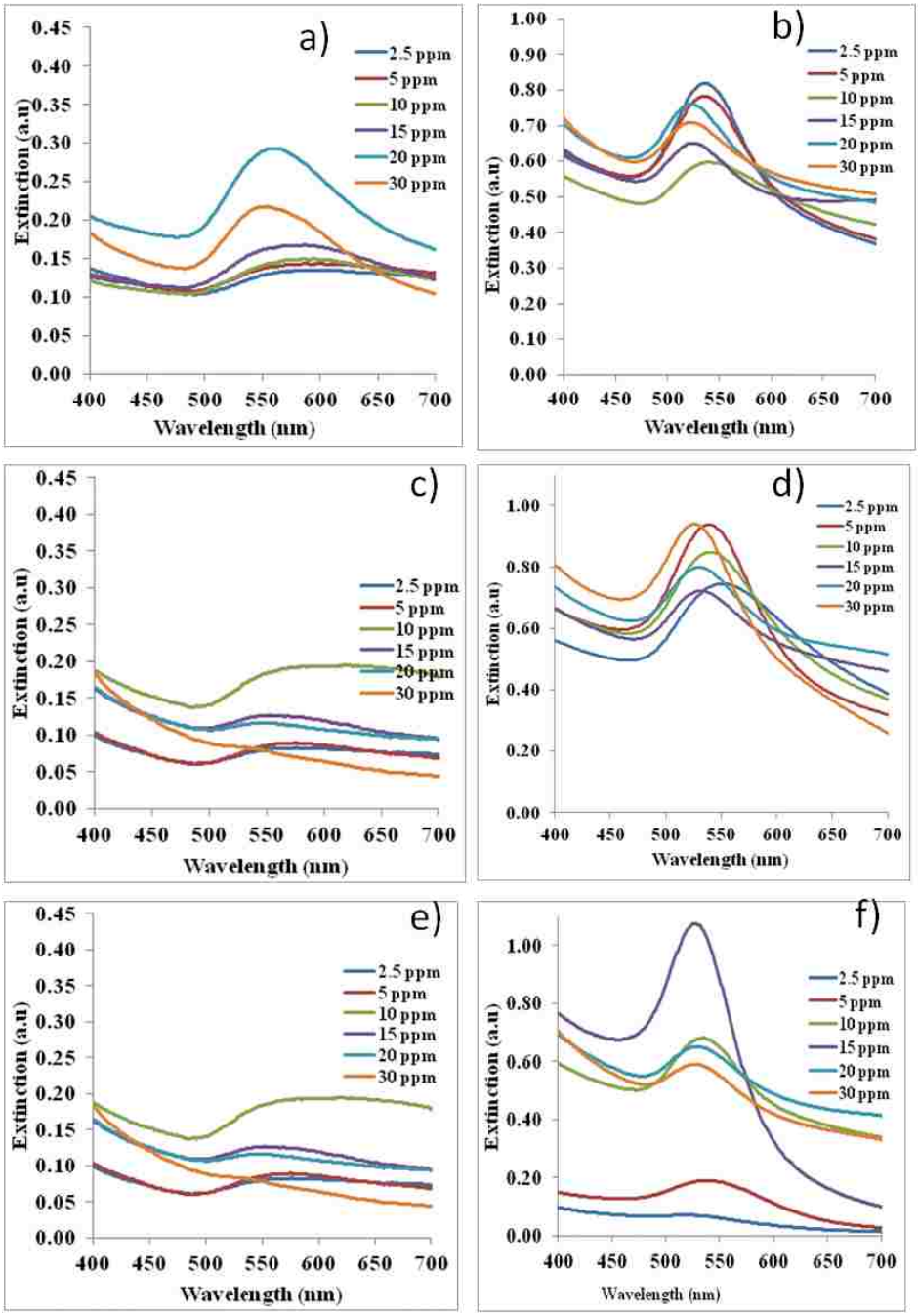

Figure 4.5 UV-Vis spectra of Au NPs formed at 250 µm metal ion concentration and varying concentrations of HAs **a)** SWHA pH 4.8. **b)** SWHA pH 7.6. **c)** FPHA pH 4.8. **d)** FPHA pH 7.6. **e)** LAHA pH 4.8. and **f)** LAHA pH 7.6.

4.3.2 Monitoring the formation of Ag NPs via their SPRP

Figures 4.6 to 4.8 present the UV/Vis spectra for reactions containing the indicated concentration of HA under both acidic and basic conditions for Ag metal concentrations of 1 μM, 25 μM, and 250 μM, respectively. From these data it can be seen that the metal concentration as well as HA concentration and type all play a role in the amount and nature of the NPs formed. The 1 μM Ag data show no evidence of NP formation at any of the tested HA concentrations for any of the HAs at either acidic or basic pH; the same holds true for the 25 μM Ag data at the acidic pH. At a Ag+ (aq) concentration of 25 μM at basic pH there is evidence of NP formation for 30 ppm SWHA and for all but the lowest LAHA concentration. For SWHA the evidence is a very clear shoulder at about 405 nm, while for LAHA, a weaker shoulder at ~405 nm (especially at the lower HA concentrations).

Clear SPRPs emerge for Ag NPs for the 250 μM Ag concentration at both acidic and basic pH for all three HAs studied. From the acidic pH data it can be seen that NPs are formed at HA concentration of 2.5, 5.0, and 10.0 ppm; however, it is difficult to clearly see any SPRP evidence at higher HA concentrations. At higher HA concentrations the UV/Vis signature of the HA may be overlaying the Ag NP SPRP signal. The most logical approach to overcome this would seem to simply remove the HA signal through the subtraction of the appropriate HA blank (no Ag). Due to the nature of the HA the situation is not this simple, as any silver bonded (NP forming or otherwise) to the HA will cause comformational as well supermolecular assembly changes, both of which have the potential to induce changes to the HA's spectral signature. It should also be noted that, as the SPRP peak gets weaker in comparison to the background signal, its location appears to migrate toward the HA spectral signal; in the cases being discussed here this means that the center of the SPRP will appear to move toward shorter wavelegths. Again,

this cannot be corrected for by subtracting a HA blank for the reason already discussed. The same holds for the Au results discussed above, giving rise to the qualititative nature of the discussion in this section.

Ag NPs are formed at all of the HA concentrations for both SWHA and FPHA at the basic pH and at an Ag+ (aq) concentration of 250 μM; however, for LAHA at the higher concentration (15 ppm and above) the Ag SPRP is weaker and is seen as a shoulder. The reasoning for the weaker NP signal at the higher LAHA concentration is due to aggregation processes. Evidence of the same phenomenon, i.e., the weaker SPRP signal, can be seen for the higher concentrations of both SWHA and FPHA. However, the data clearly show that much more Ag NPs are formed at the basic pH versus the acidic pH. The data also show that there is very little variation in the location of the SPRP, suggesting homogeneity in the size of the Ag NPs formed, regardless of HA concentration. The uniformity in size of the Ag NPs formed seems to be independent of HA concentration.

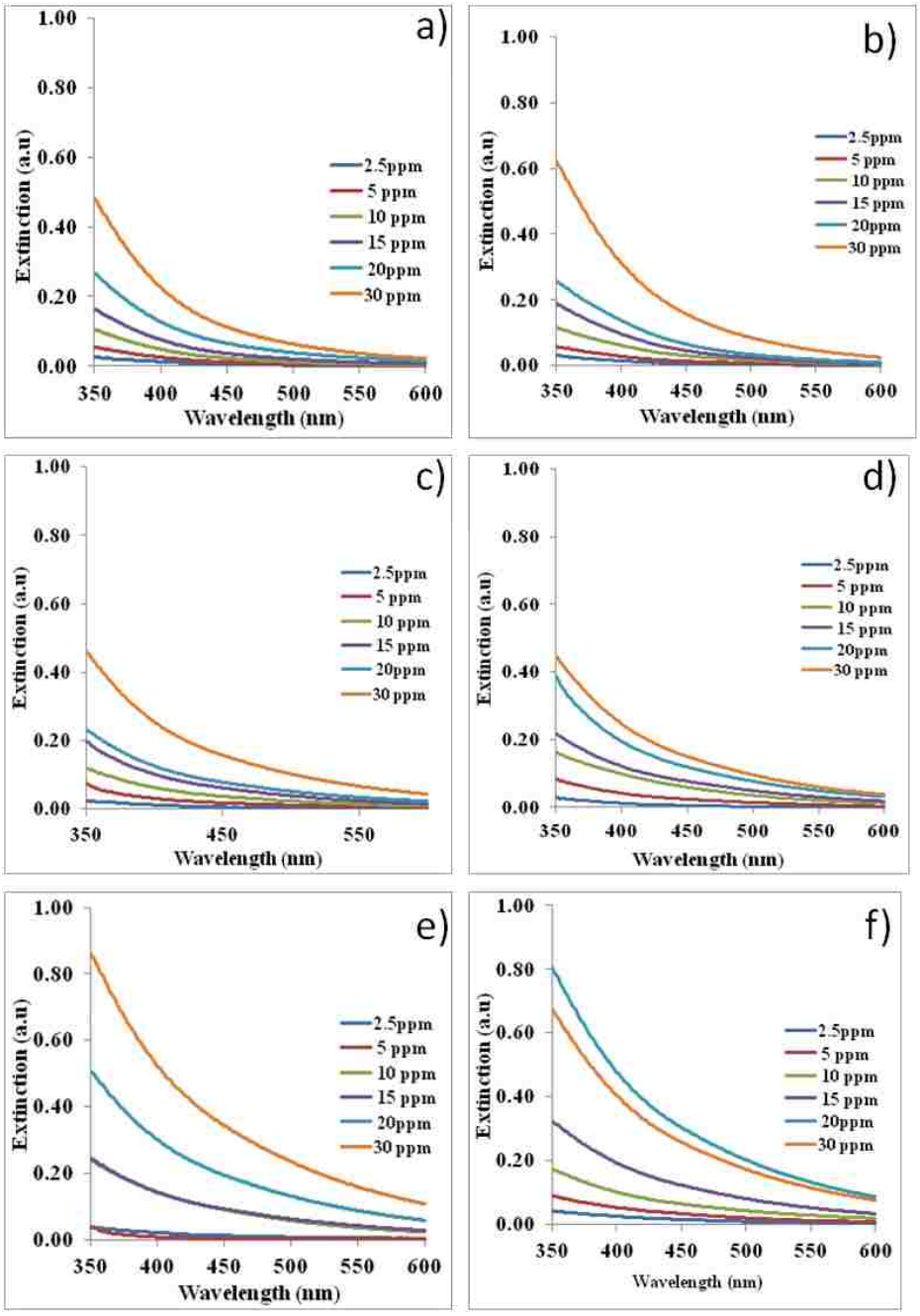

Figure 4.6 UV-Vis spectra of Ag NPs formed at 1 µm metal ion concentration and varying concentrations of HAs **a)** SWHA pH 4.8. **b)** SWHA pH 7.6. **c)** FPHA pH 4.8. **d)** FPHA pH 7.6. **e)** LAHA pH 4.8. and **f)** LAHA pH 7.6.

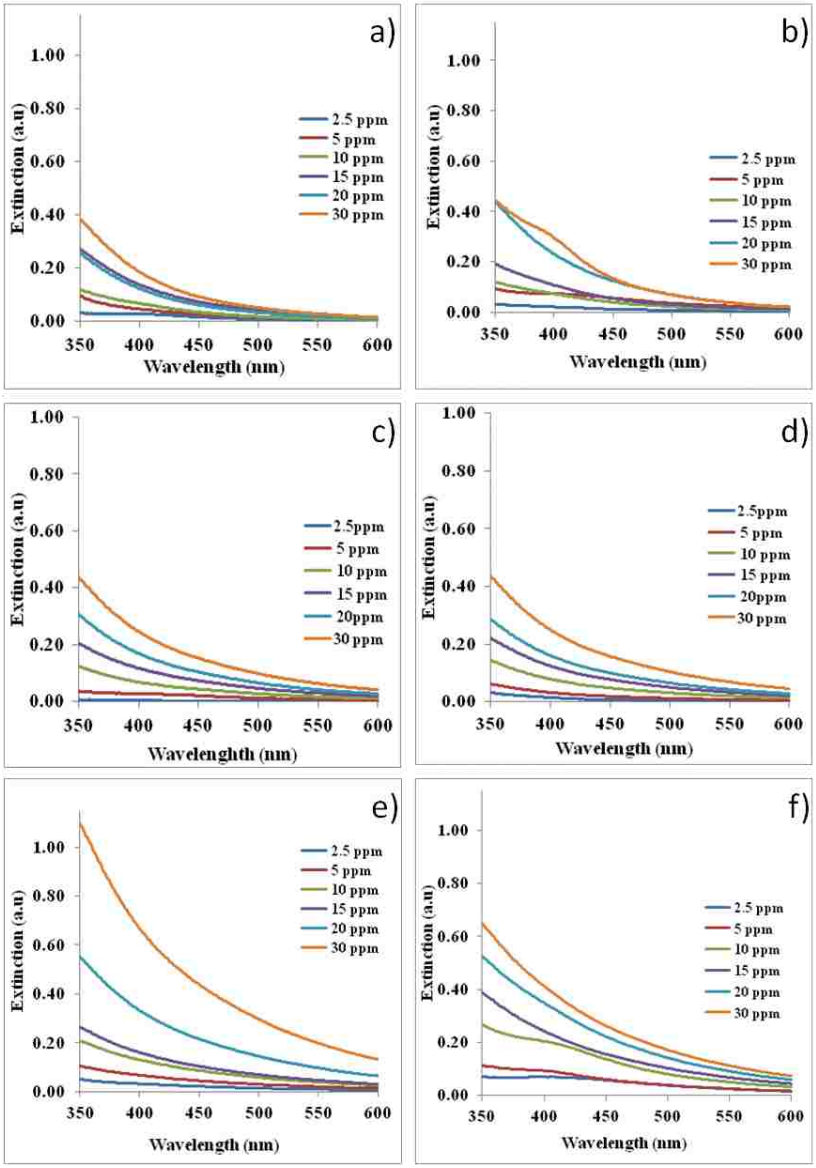

Figure 4.7 UV-Vis spectra of Ag NPs formed at 25 µm metal ion concentration and varying concentrations of HAs **a)** SWHA pH 4.8. **b)** SWHA pH 7.6. **c)** FPHA pH 4.8. **d)** FPHA pH 7.6. **e)** LAHA pH 4.8. and **f)** LAHA pH 7.6.

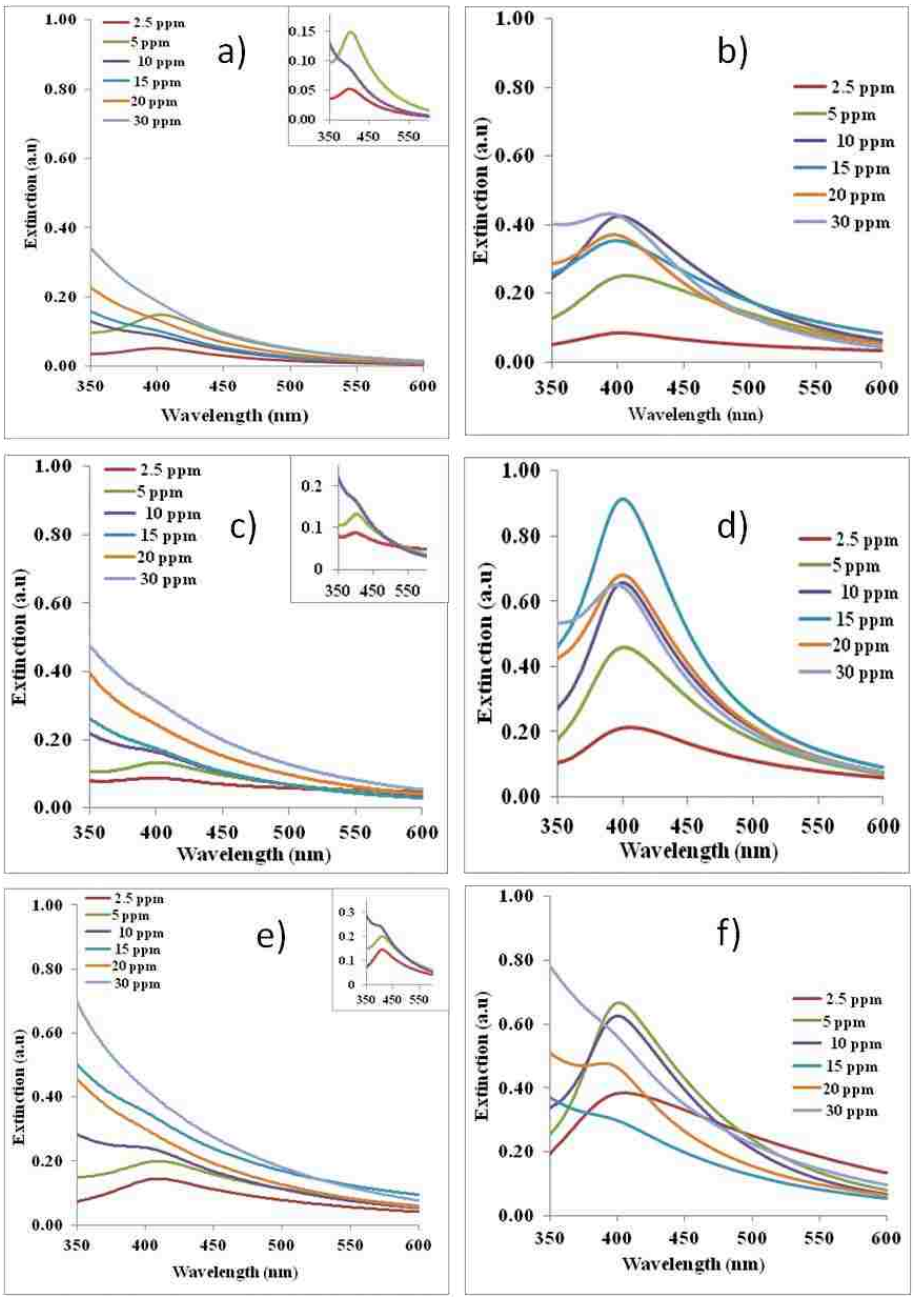

Figure 4.8 UV-Vis spectra of Ag NPs formed at 250 µm metal ion concentration and varying concentrations of HAs **a)** SWHA pH 4.8. **b)** SWHA pH 7.6. **c)** FPHA pH 4.8. **d)** FPHA pH 7.6. **e)** LAHA pH 4.8. and **f)** LAHA pH 7.6.

4.3.3 TEM Characterization of Au and Ag NPs

Although the analysis of the SPRPs of NPs by the UV/Vis spectroscopy can provide a large amount of useful data, it is a bulk analysis with a number of limitations, including those

discussed above. In particular, it yields no information as to the shape of the NPs formed. TEM images, on the other hand, do provide this information, but TEM data are statically challenged as they only sample a limited number of NPs and are resource instensive, limiting the number of samples that can be analyzed. However, due to the unique information that TEM can provide, and its complementary nature to the above UV/Vis analysis, a select subsampling of the NPs formed in this work were characterized by TEM. The obtained TEM images are presented in Figures 4.9 to 4.17.

The TEM images shown in Figures 4.9 to 4.13 are for the Au NPs formed with an Au concentration of 75 μM for both of the tested pH values and at HA concentrations of 5 and 10 ppm. For the SWHA samples at the acidic pH the TEM images show that at a HA concentration of the 5 ppm (Figure 4.9) there is a large variation in both the size and shape of the NPs. The size range is from <10 nm to >100 nm, and include spherical, triangular and trapezoid shapes, collectively giving rise to the very broad SPRP seen in the associated UV/Vis spectrum. If one examines the TEM image when the SWHA concentration is increased to 10 ppm, one see large differences. The first difference is that the size of the formed NPs is much more uniform and ranges between 10 and 30 nm. The second difference is that the NP are much more regular in shape, mainly spherical as well as some triangular. These findings are consistent with the narrower SPRP in the associated UV/Vis spectrum. The differences in both the size and shape of the formed NPs, seen here as a function of HA concentration, can be explained by there being a limited number of sites within the less concentrated HAs suitable for NP formation. On the other hand, at the higher HA concentrations, there are more such sites available, and hence, less of a potential for aggregation of Au NPs as they grow. Figure 4.10 shows the complementary basic pH TEM images for SWHA. Both the 5 and 10 ppm SWHA images show a higher degree of

monodispersity of the NPs in terms of both size and shape, which is consistent with the obtained SPRP profiles, as can be also seen from the corresponding UV/Vis spectra in Figure 4.4.

TEM images for the Au NPs formed by FPHA at both acidic and basic pH, as seen in Figure 4.11 and 4.12, once again show large differences in the sizes and shapes of the Au NPs. Focusing on the Au NPs formed at acidic pH, it can be seen that both the 5 and 10 ppm HA concentrations yield Au NPs that are polydisperse in both size and shape. As with SWHA, the shapes seen with FPHA range from spherical, triangular, and trapezoidal. The Au NPs formed at the basic pH with FPHA at both 5 and 10 ppm HA concentrations yield much more monodisperse NPs than those seen at the acidic pH, as was the case with SWHA. The quality (as measured by high shape or size uniformity or monodispersity), in terms of shape (the more uniform the better) and size distribution (the narrower the better) seems to be lower for FPHA than for SWHA. Figure 4.13 shows the TEM image of Au NPs formed at the acidic pH in a 10 ppm solution of LAHA; once again this HA yields NPs that are polydisperse in terms of size but rather uniform in shape. These and other conclusions drawn from TEM data must be made with caution due to the TEM imaging ability to sample only a small number of the particles formed. Nevertheless, the bulk UV/Vis analysis above does show a wide SPRP, which is consistent with the TEM observation, and hence, builds confidence in the above discussion of the TEM results.

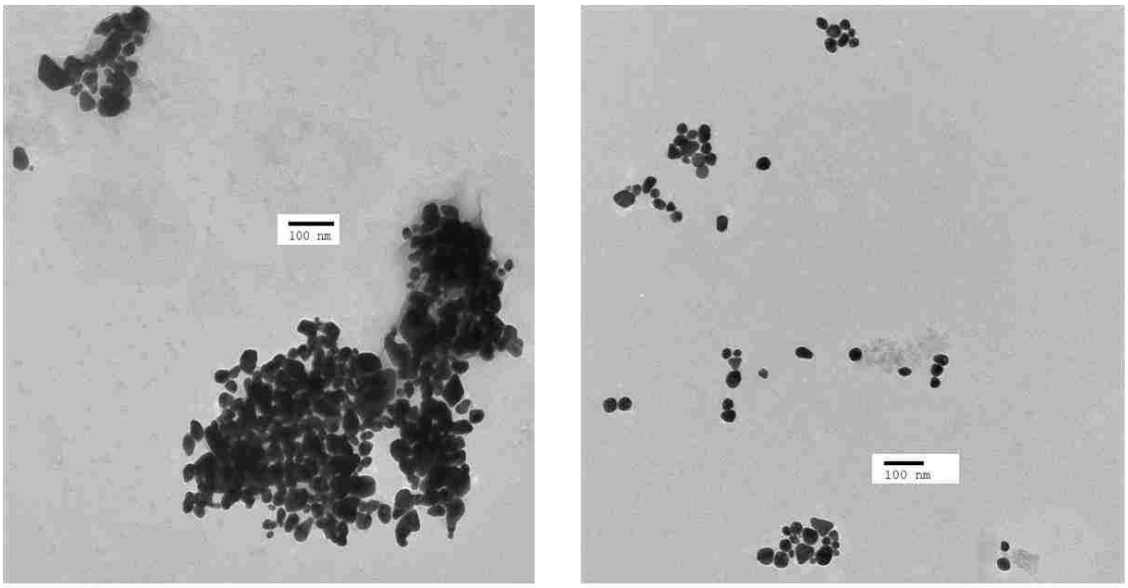

Figure 4.9 TEM images of Au NPs synthesized with 75 μM gold metal ion and SWHA at pH 4.8 **a)** 5ppm **b)** 10ppm HAs

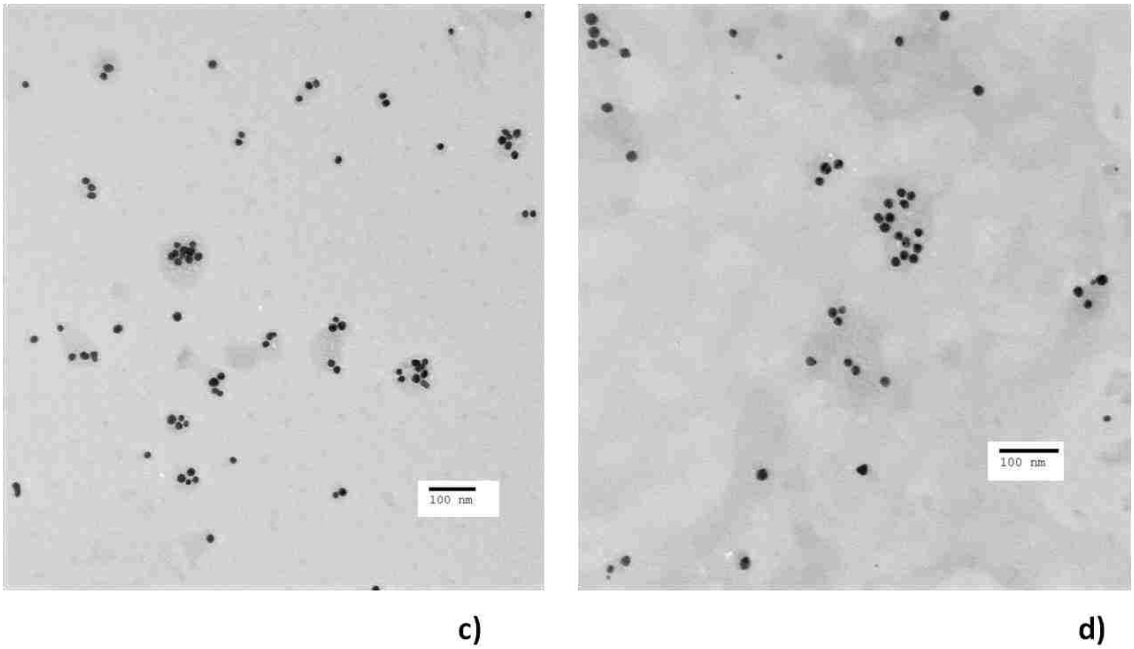

Figure 4.10 TEM images of Au NPs synthesized with 75 μM gold metal ion SWHA at pH 7.6 **a)** 5ppm **b)** 10ppm HAs

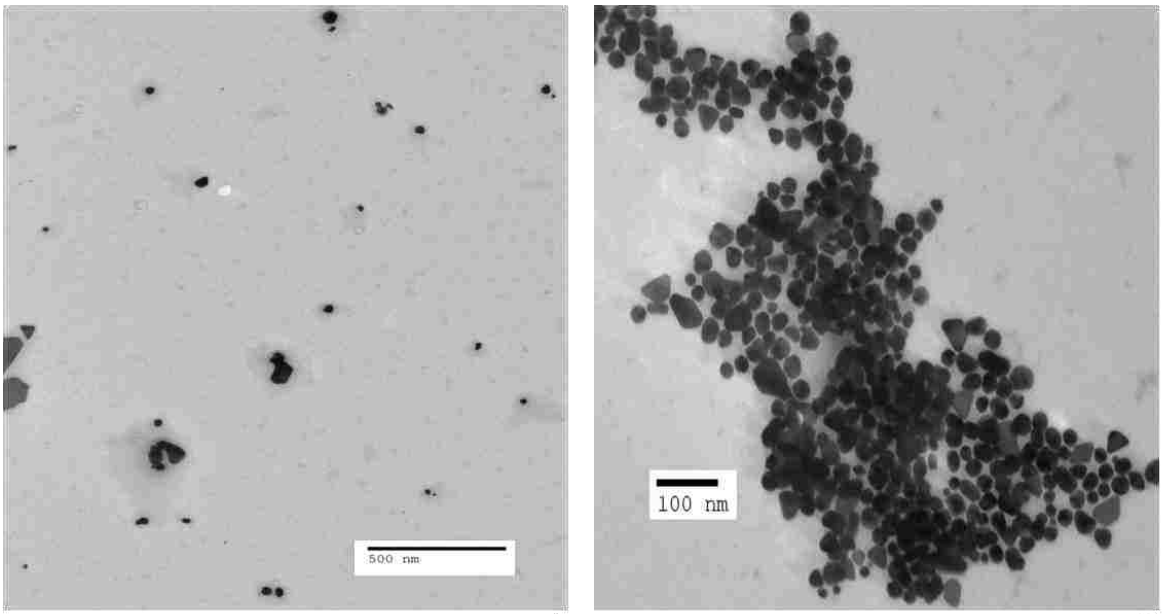

Figure 4.11 TEM images of Au NPs synthesized with 75 μM gold metal ion FPHA at pH 4.8 **a)** 5 ppm **b)** 10 ppm HAs

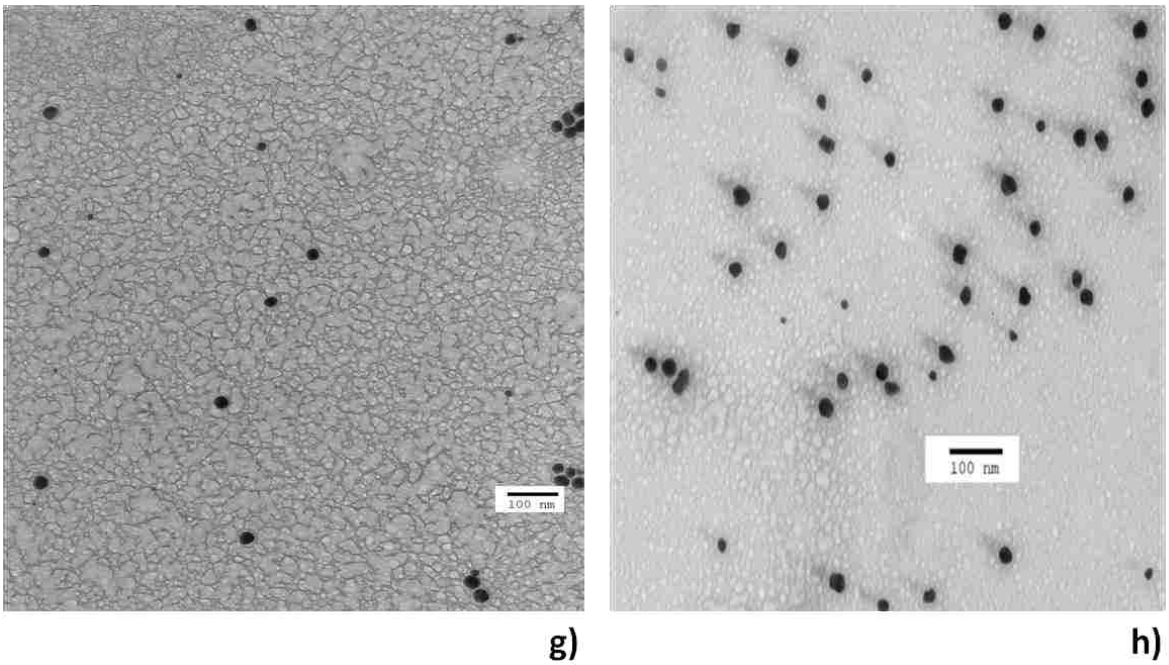

Figure 4.12 TEM images of Au NPs synthesized with 75 μM gold metal ion FPHA at pH 7.6 **a)** 5ppm **b)** 10ppm HAs

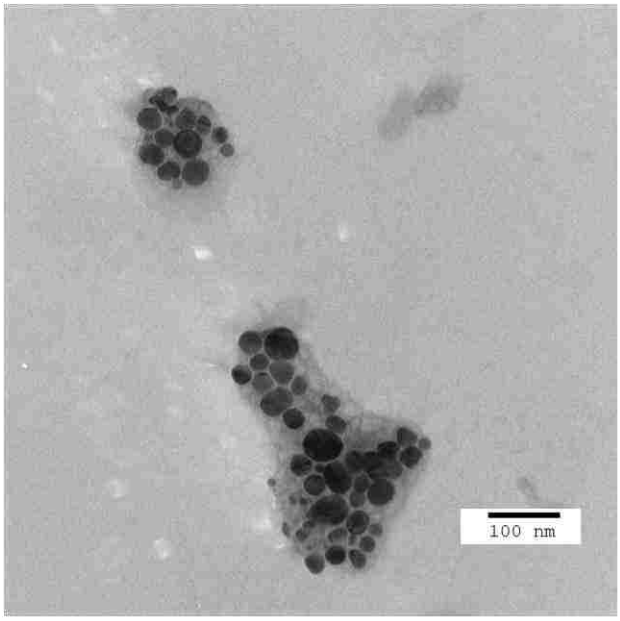

i)

Figure 4.13 TEM images of Au NPs synthesized with LAHA at pH 4.8, 10ppm HA

TEM images of the Ag NPs formed in solutions containing 250 μM Ag as well were collected at SWHA and FPHA concentrations of both 5 and 10 ppm. The TEM images for Ag NPs formed at acidic the pH for SWHA are presented in Figure 4.14. and Figure 4.15 for pH 7.6 From these images it can be seen that the Ag NPs are formed in a range of shapes and over a range of sizes, especially at 5 ppm SWHA, which is in agreement with the obtained UV/Vis spectra. It should be noted that at neither of the two concentrations were the formed NPs of high quality (uniform shaped particles). The TEM results show that the Ag NPs formed at the basic pH and at a SWHA concentration of 5 ppm are rather uniform in both size and shape (spherical) compared to those formed at the acidic pH under the same Ag and SWHA concentrations. The NPs formed at a 10 ppm SWHA concentration under the basic pH yielded more uniformly sized and shaped NPs when compared to their acidic pH counterparts, but less uniform NPs in terms of size and shape than those obtained at 5 ppm SWHA concentration. TEM images of the NPs

formed at the acidic pH in the presence of FPHA are presented in Figure 4.16 and Figure 4.17 for pH 7.6. From these images it can be seen that NPs are formed; however, they are polydipserse in terms of size (ranging from 20 to >100 nm) and shape at both FPHA concentrations. The Ag NPs formed at the basic pH are much smaller and less polydisperse in size and shape at both 5 and 10 ppm FPHA, when compared to their acidic pH counterparts. The Ag NPs formed at 5 and 10 ppm FPHA also appear to be very similar to each other.

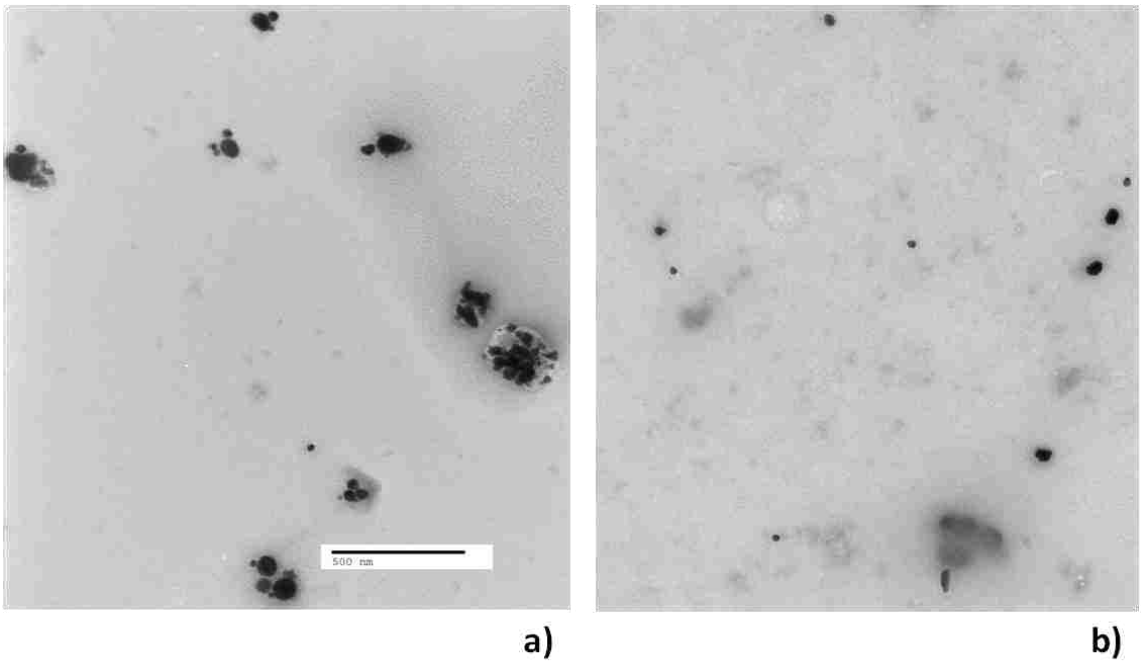

Figure 4.14 TEM images of Ag NPs synthesized with 250 μM silver metal ion SWHA at pH 4.8 a) 5ppm b) 10ppm HAs

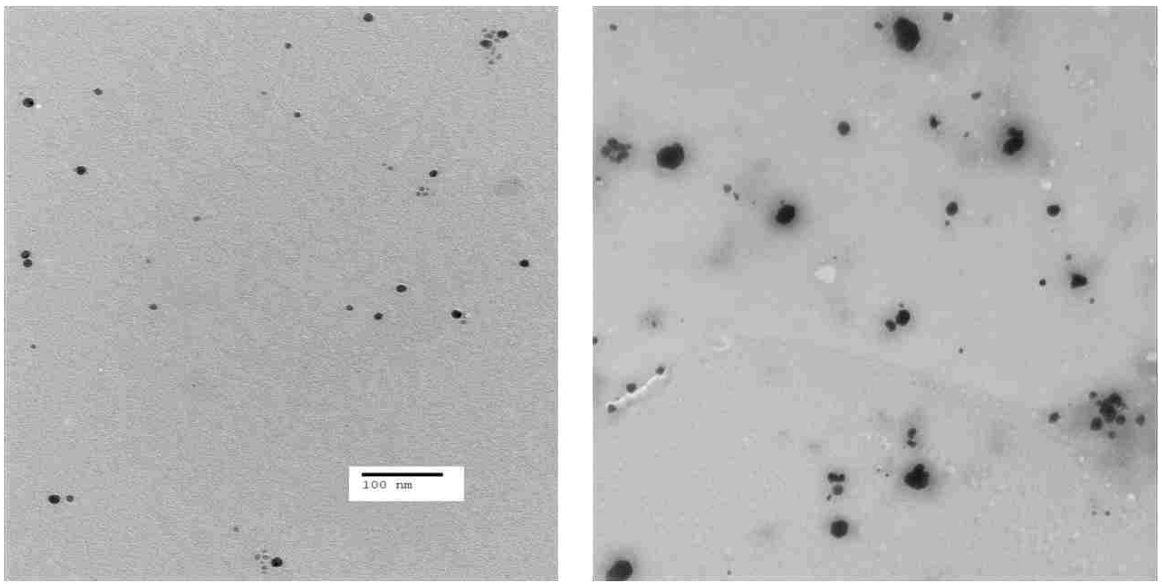

Figure 4.15 TEM images of Ag NPs synthesized with 250 μM silver metal ion SWHA at pH 7.6 a) 5ppm b) 10ppm HAs

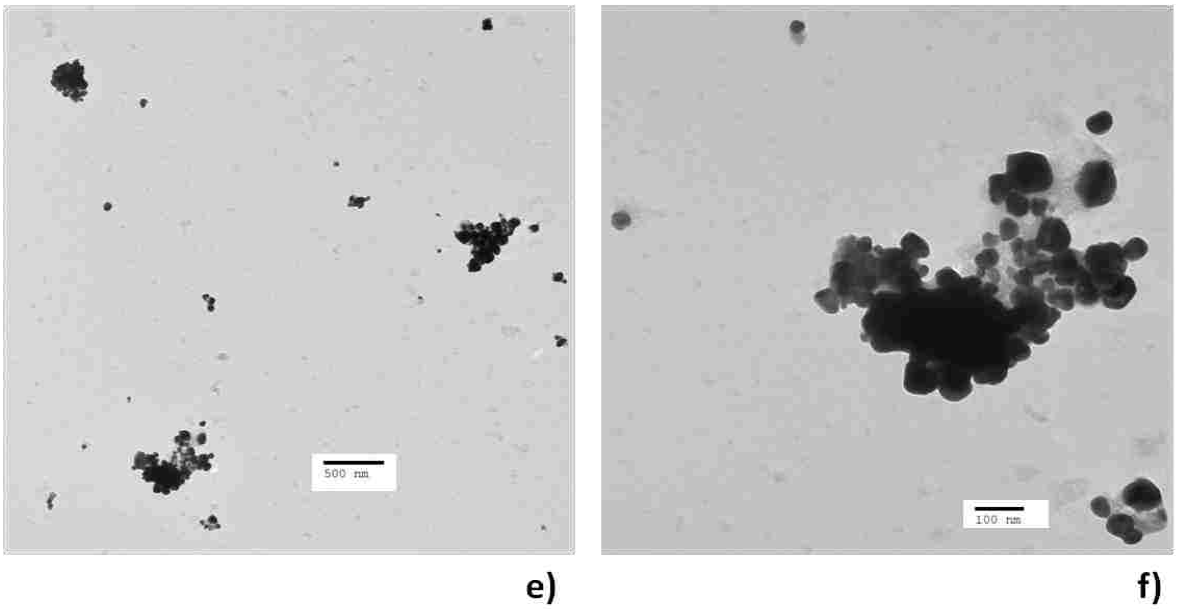

Figure 4.16 TEM images of Ag NPs synthesized with 250 μM silver metal ion FPHA at pH 4.8

a) 5ppm b) 10ppm HAs

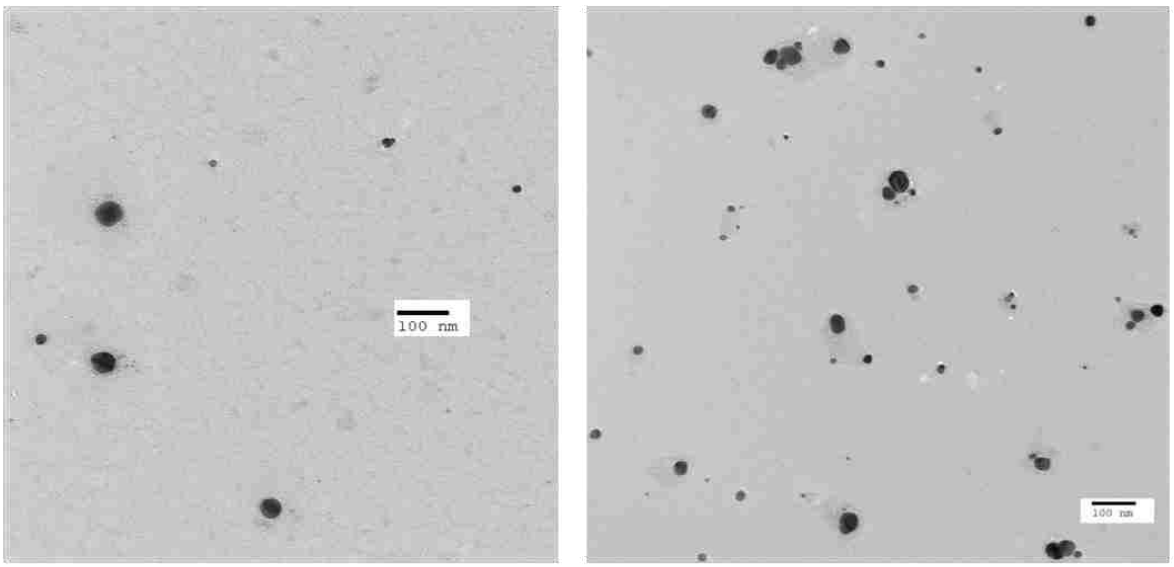

Figure 4.17 TEM images of Ag NPs synthesized with 250 μM silver metal ion FPHA at pH 7.6

a) 5ppm b) 10ppm HAs

4.3.4 The Role of pH and Concentration in the Formation of Au and Ag NPs

Due to the nature of HAs, pH as well as concentration play major roles in the conformation as well as aggregation of HAs. HAs can be viewed as supermolecular assemblies held together by weak non-covelent interactions, which will be, from now on, called weakly associated molecular assemblies (WAMAs) [19]. Due to the range of functional groups within HAs, different pH values and concentrations will give rise to a different way of balance between the repulsive and attractive forces provided by diverse functional group combinations. In addition to these non-covalent interactions, the so-called hydrophobic interactions need to also be considered. The higher the HA concentration, equivalent to an increase in the HA to water ration, the higher the probability of the HA interacting with itself, and the lower the probability of it interacting with water. This means that both pH and HA concentration will play a role in terms of the HA WAMAs conformations, and hence, the access metal ions in solution have to the available metal binding sites within the HA WAMAs. The binding of free metal ions will also

induce a range of changes within the conformation of HA WAMAs, as the binding of metals will reduce the number of negatively charged sites, changing the balance between the repulsive and attractive forces among various negatively and positively charged functional groups. In addition, metal ions with larger than a 1+ charges, can be bound to more than one binding site within the HA WAMAs, and hence, act as a bridge further affecting the conformation of the HA WAMAs, and hence, changing the distribution of accesible binding sites. Overall, this means that more condensed HA WAMAs with fewer available and more closely packed binding sites are expected at acidic pH conditions and at high HA and metal ion concentrations.

In terms of NP growth, two things must be considered. The first is that the HA does not have too many available binding sites to bind all, or the vast majority of, the metal ions, here Au and Ag. Consequently, a critical number of Au or Ag atoms are not available to cluster and form NPs. This situation appears to happen for both Au and Ag at the 1 μM concentration and, for Au at 25 μM at the basic pH as well as for Ag at 25 μM at both of the pH studied. The second extreme case is due to the HA WAMAs being so closely packed that they aggregate, forming highly constricted binding sites, as would be expected at low pH and high metal concentrations. The exact role of HA is complicated in that, while higher HA concentration potentially provides more binding sites, more HA contributes to more aggregated the HA WAMAs. The evidence of low pH and high metal and HA concentrations leading to a decrease in the amount of Au binding sites available can be inferred from the SPRP data collected for LAHA at the acidic pH at the Au concentration of 250 μM, where the SPRP intensity was at its maximum for the LAHA concentration of 5 ppm. In addition, such a HA WAMAs case would also lead to the potential aggregation of Au NPs, as can be seen by the longer wavelength signature in the SPRPs. The SPRP peaks for SWHA under the same condition show an increasing intensity occuring with

increasing SWHA concentration up to 20 ppm, indicating that more potential binding sites for Au NPs are available at higher SWHA concentrations up to 20 ppm.

The basic pH data at both 75 and 250 μM Au show much less aggregational effects, as can be seen by the more systematic increase in the SPRP intensity with increasing SWHA and FPHA concentration for 75 μM Au. This is especially true for SWHA and FPHA and, at the lower concentrations (2.5, 5, and 10 ppm), for LAHA as well. Shifting attention to the 250 μM data, it can be seen that more NPs are formed at the basic pH compared to the acidic pH for SWHA and FPHA as well as LAHA for the majority of the LAHA concentrations under investigation, indicating more available sites for the Au NP formation at the basic pH versus the acidic pH. This observation is consistent with the above discussion in regards to more sites being available at the higher pH due the decreased proton competition for the sites as well as a more open conformation with a higher amount of accessible sites. The 250 μM Ag SPRP data are consistent with the above findings for Au.

All TEM images collected at the acidic pH show possible HA aggregation. This aggregation can be seen by the clustering effect of the NPs, and, in a number of cases (e.g., on the TEM image of the LAHA Au NP in Figure 4.13), a lighter gray colored aura around the NPs. Also, based on the irregular shapes of the large NPs, it could be proposed that some of the NPs formed at the acidic pH could be due to the smaller NPs aggregating with larger NPs. This is also supported by the longer wavelengths of the SPRP of the NPs at the acidic pH as a whole, and example of this is shown in Figure 4.16.

Thus, the overall trend is that, lower pH and higher HA and metal concentrations, tend to yield larger NPs that are more polydisperse in terms of both size and shape.

4.3.5 The Role of Different HAs in the Formation of Au and Ag NPs

The three HAs used in this study are from very different sources and, as such, have different chemical compositions. This, in turn, means that they will interact with Au and Ag ions differently. Table 1.1 presented in Chapter 1 shows the differences among the HAs under consideration here. From those data it can be seen that these three HAs are diverse in regards to: 1) elemental composition, including O, N, and S content; 2) functional group content; and 3) radical spin content. However, all three HAs were able to reduce Au and Ag at both acidic and basic conditions. This implies, under the conditions studied, that the reduction of both Ag and Au are thermodynamically favorable. This means that all three HAs studied must have sites that have reduction potential lower than approximatley 0.8 V, based on the standard reduction potential of Ag (see discussion below on the role of metals). The redox properties of HAs have been previously studied and shown to be important in the reduction of chlorinated aliphatic compounds [20], substituted nitrobenzenes [21], oxidized metal ions [22] [23, 24] as well as in the ability of HAs to act as electron acceptors or donors during microbial respiration [24]. These studies have traditionally looked at the electron carrying capability (ECC) (μequiv/g HA) of different HAs. For the HAs studied here, SWHA has the highest ECC, followed by FPHA, with LAHA having the lowest ECC for the non quinone sites while LAHA has the highest followed by FPHA, with SWHA having the lowest ECC for the quinone sites [25]. This ECC ranking is based on more than a simple bulk number, as there are at least three distinct classes of redox sites within the three HAs studied [25]. The chemical nature of these three distinct redox sites can be summarized as non-quinone-like (NQL), quinone-like with electron withdrawing group next to the quinone-like group (QL1), and quinone-like with no substituents or with an electron donating group in the vicinity of the quinone-like group (QL2). NQL sites account for close to one half

(56% and 49%) of the ECC of both SWHA and FPHA, respectively, while for LAHA, the QL2 sites account for 50% of the observed ECC.

As thiols and disulfides are known to be capable of reversible redox cycling to sulfoxide, and both Au and Ag are known to preferentially bind to sulfur over the oxygen-containing sites within the HAs, it seem resonable to hypothesise that the NP formation sites within both SWHA and FPHA are sulfur based NQL sites. It should be noted that nitrogen containing species, in addition to sulfur functional groups, have also been proposed as redox sites within aquatically derived HAs [26] thus, in addition to sulfur-based sites, it also seems resonable to consider nitrogen-based NQL redox sites for SWHA and FPHA. If one combines this with the elemental data presented in Table 1.3, it can be concluded that SWHA and FPHA have large amounts of reduced sulfur compared to LAHA. On the other hand, reducing groups in LAHA are primarily of the QL2 type, and thus, the binding site for the metal ions may be oxygen-centered rather than sulfur-centered. This would seem to contradict the fact that, of the three HAs studied here, the LAHA has the highest percentage of sulfur, though it can be argued that not all sulfur sites within HAs are equivalent. In fact, it has been reported in the literature that, the more mature HAs (LAHA is the most mature of the HAs studied here), the more likely sulfur is to be in an oxidized form [27]. The complexity of HA means that, in all probability, there is a combination of NQL and QL2 sites that are involved, but the discussion above focuses on the major one for each HA investigated.

The ability of SWHA to yield more consistent in terms width, position, and intensity SPRPs for the NPs formed at acidic pH as a function of HA concentration may be attributed to more NP forming sites being accessible. This may be due to the SWHA being less aromatic in nature, and hence, having more flexible WAMASs [7]; however, given the complex nature of

HAs, a more systematic investigation is required to explore the specific roles of aliphatic, aromatic and carbohydrate moieties. Such a systematic study is presented in Chapter 5, and hence, further discussion on the roles of HA chemistry on Au and Ag NP formation will be left to Chapter 5.

4.3.6 The Role of the Metal in NP Formation Via HAs

The two metals used in this study were chosen as they are known to form NPs under a variety of conditions. However, even though they are in the same column (11) in the Periodic Table of Elements, they are unique in their chemistry. As stated above, one of the major criteria for Au and Ag NPs formation by HAs is that the HA must be able to reduce both metals, as shown below along with the associated standard reduction potentials [28]:

$$Au^{3+} + 3e^- \rightarrow Au(s) \qquad E°=1.50\ V \qquad (4.1)$$

$$Ag^{+} + e^- \rightarrow Ag(s) \qquad E°=0.80\ V \qquad (4.2)$$

It is worthwhile to note that, while the above gold and silver reduction potentials are at standard conditions, their relative order will be maintained at corresponding non-standard conditions. If this is taken into consideration–along with the fact that the SPRP data presented above clearly showed that it was much easier to make Au than Ag NPs at all but the highest metal concentration where the aggregation appeared to be a major problem–it can be concluded that the reduction potentials of all three HAs under most conditions is closer to, but still below Ag.

Traditionally, both Au and Ag are referred to as soft metals and, as such, their cations are more likely to bind to soft anions, such as sulfur-centered binding sites within HAs (e.g., thiols), compared to the hard binding sites, such as oxygen-centered ones (e.g., carboxyl functional groups). The concept of “soft” versus “hard” in this context is based on hard and soft acid-base

theory (HSAB), which has been developed through empirical observations [29], and showed that, while both Au and Ag are soft acids (SA), they form different precipitates and, as such, are classified as Group II and I, respectively. This classification is based on the fact that Ag forms a precipitate with 0.3 M HCl, while Au forms a precipitate in the presence of H_2S in acidic solution. Au and Ag can further be separately classified utilizing geochemical classification developed by Victor Goldschmidt [30] according to which, Au is considered to be a siderophile and Ag is considered to be a chalcophile. Accordingly, a chalcophile can be viewed as "sulfide-forming", while a siderophile can be viewed as "occurring as a noble metal". Stated differently, siderophiles are more likely to interact with themselves. This, plus the finding that Au NPs are formed more readily than Ag NPs in the presence of HAs, leads to the conclusion that, once a Au^{3+} ion is reduced, there is a higher probability of it attracting more gold ions that will, in turn, be reduced, forming and initial gold cluster. As more Au ions are assimilated, this cluster becomes a NP. On the other hand, since Ag is less likely to interact with itself there is a lower probability of Ag NPs formation, unless the Ag ion concentration is very high.

By combining the fact that there is a higher probability that HAs will have Au reducing sites (due to the higher reduction potential of Au) and the fact that Au is more likely to interact with itself compared to Ag, it becomes clear why Au NPs are more easily formed with HAs acting as the reducing agent, compared to the Ag NPs.

4.4 Conclusion

This study has demonstrated that all the three chemically diverse HAs studied here reduce metal salts to their NPs. The metal reduction reactions were faster in the reactions with SWHA, as compared to FPHA and LAHA, which required almost similar time. We have shown that the NPs formed at both pH 4.8 and pH 7.6 for both silver metal (for the first time at an acidic

pH and at environmentally relevant concentrations) and gold metal, and that the NPs formed at pH 4.8 were mostly aggregated, while the NPs at pH 7.6 were suspended in solution. This study has further demonstrated that the reduction reactions were faster for gold metal, as compared to silver metal, which required 4-5 weeks for complete synthesis. In addition, this study has demonstrated that reduction of metal salt to metal NPs is dependent on the metal salt concentration as well as the source and concentration of HAs, and that potentially, at extremely low concentrations, such 1 µM, metal salts may not be reduced to metal NPs in the natural environment.

4.5 Environmental Implications

Although this study shows that Au and Ag nanoparticles can be formed, a more appropriate question may be whether such nanoparticles have been found in the environment. The answer to this question is yes. For Au, there have been a number of reports from the Amazonian area of Brazil [31]. For Ag, reports include Ag NPs found in Zacatlan, Puebla, Mexico in the area of previously active silver mines [32] as well as within the Texian fluvial and estuarine waters [33]. It should be noted that all these areas can be viewed as warm to hot on a global scale, which is not surprising given the findings that Au and Ag NPs are more readily formed at higher temperatures (this work as well as [7]. This would imply that Au and Ag NP formation within the environment should be more problematic in warm to hot regions of the planet compared to cooler areas.

With the results presented above for the three HAs studied, it is evident that metal ions present in the environment can potentially be reduced to metal NPs by HAs and be stabilized at the same time. This study has further demonstrated that HAs of concentration ranges typical to those found to oceans, rivers, swamps, etc., [16] can reduce metal ions to metal NPs at

environmentally relevant pH conditions, such as 7.6 and 4.8, and temperature of 60 °C. The demonstration of the formation of the NPs at this temperature has important environmental implications in hot springs, where Ag NPs concentrations have been reported to be in the milimolar range [34].

There are a number of potential anthropogenic sources of Au and Ag, including mine run-offs and leaks during ore processing. Under these circumstances, it is anticipated that the associated mine run-off waters would be acidic, making receiving waters acidic, thus making our findings that both Au and Ag NPs can be formed at acidic pH environmentally relevant. In addition, on a whole, natural waters are naturally acidic due to the dissolved CO_2 and the subsequent carbonate buffer system formation, ubiquitous in the majority of waters, again, making our findings that Au and Ag NPs can be formed in the presence of HAs highly environmentally relevant. In addition to the natural leaching (documented in the Amazonian area of Brazil, as mentioned above) and mining run-offs, NPs enter the environment from a variety of medical uses (e.g., Au^{+} in the form of myocrism or chloro(triethylphosphine)gold(I) $\{(C_2H_5)_3P{:}AuCl\}$ and gold(I) thiomalate $\{[Au\text{-}S\text{-}CH(COO^{-}Na^{+})]_n\}$ electronics as well as jewelry manufacturing in which gold is used, and finally, dentistry in some areas of the world were gold dental work is popular. Sources of silver are natural (i.e., geological), mining, electroplating, film-processing wastes, disinfection of water, and medicinal (e.g., from the use of silver as an antibiotic agent) [29]. Thus, as can be seen by these lists, that there are a number of sources of both Au and Ag at environmental release points, and the concentrations of these metals may be high enough for the formation of NPs with humic materials present in the environment. Finally, it was found by color change, that NPs could be formed at room temperature by us and others (in this work, using color change as evidence as well as [7], that higher temperatures, as those found

in hot springs and discharges from nuclear plants are much more favorable for nanoparticle formation and, as pointed out by Akaigne et al., some natural hot springs have very high (mM) Ag concentrations [34]. when compared to other natural waters [7]. Since natural hot spring water is at the correct temperature, it is also usually acidic, once again makes our finding of Ag nanoparticles being formed at acidic pHs very environmentally relevant. The same holds true for natural deep sea vents in terms of high silver and concentrations.

The fact that HAs can reduce metal salts to metal NPs at acidic pH conditions has an important environmental implication, especially in regards to the bioavailability of the so-formed NPs to living organisms since we, as well as other research groups have shown that HAs interact and perturb the biomembranes at acidic pHs. This, therefore, means that metal NPs present in the environment could find their way into the living organisms in the environment, which may have major impact, in terms of bio concentrations. With wide applicability of Ag NPs in personal care products, it is likely that Ag^+ (aq) will find their way to the environment in large amount in the near future, where they can potentially degrade back to metal ions, which could eventually be reduced by HAs present in the environment to form metal NPs. This is particularly important since we have shown that concentrations of metal salts as low as 25 µM can be reduced to metal NPs at environmentally relevant conditions. These findings have important implications in the amount of NPs that may be bioavailable to living organisms through biomembrane perturbation mechanisms, as has been discussed in the chapters 2 and 6.

4.6 References

1. Mills, A.; LeHunte, S. An overview of semiconductor photocatalysis. *Journal of Photochemistry and Photobiology a-Chemistry*. **1997,** *108* (1), 1-35.

2. Bond, G. C., Gold: a relatively new catalyst. *Catalysis Today*. **2002,** *72* (1-2), 5-9.

3. Elghanian, R.; Storhoff, J. J.; Mucic, R. C.; Letsinger, R. L.; Mirkin, C. A. Selective colorimetric detection of polynucleotides based on the distance-dependent optical properties of gold nanoparticles. *Science.* **1997,** *277* (5329), 1078-1081.

4. Sharma, V. K.; Yngard, R. A.; Lin, Y. Silver nanoparticles: Green synthesis and their antimicrobial activities. *Adv. Colloid Interface Sci.* **2009,** *145* (1-2), 83-96.

5. Daniel, M. C.; Astruc, D. Gold nanoparticles: Assembly, supramolecular chemistry, quantum-size-related properties, and applications toward biology, catalysis, and nanotechnology. *Chemical Reviews.* **2004,** *104* (1), 293-346.

6. Machesky, M. L.; Andrade, W. O.; Rose, A. W. Interactions of gold (III) chloride and elemental gold with peat-derived humic substances. *Chemical Geology.* **1992,** *102* (1-4), 53-71.

7. Akaighe, N.; MacCuspie, R. I.; Navarro, D. A.; Aga, D. S.; Banerjee, S.; Sohn, M.; Sharma, V. K. Humic Acid-Induced Silver Nanoparticle Formation Under Environmentally Relevant Conditions. *Environ. Sci. Technol.* **2011,** *45* (9), 3895-3901.

8. Sal'nikov, D. S.; Pogorelova, A. S.; Makarov, S. V.; Vashurina, I. Y. Silver ion reduction with peat fulvic acids. *Russian Journal of Applied Chemistry.* **2009,** *82* (4), 545-548.

9. dos Santos, D. S.; Alvarez-Puebla, R. A.; Oliveira, O. N.; Aroca, R. F. Controlling the size and shape of gold nanoparticles in fulvic acid colloidal solutions and their optical characterization using SERS. *Journal of Materials Chemistry.* **2005,** *15* (29), 3045-3049.

10. Baalousha, M.; Manciulea, A.; Cumberland, S.; Kendall, K.; Lead, J. R. Aggregation and surface properties of iron oxide nanoparticles: Influence of pH and natural organic matter. *Environmental Toxicology and Chemistry.* **2008,** *27* (9), 1875-1882.

11. Stankus, D. P.; Lohse, S. E.; Hutchison, J. E.; Nason, J. A. Interactions between Natural Organic Matter and Gold Nanoparticles Stabilized with Different Organic Capping Agents. *Environmental Science & Technology.* **2011,** *45* (8), 3238-3244.

12. Urban, N. R.; Ernst, K.; Bernasconi, S. Addition of sulfur to organic matter during early diagenesis of lake sediments. *Geochimica Et Cosmochimica Acta.* **1999,** *63* (6), 837-853.

13. Stevenson, F. J. H. C. G. Humus chemistry genesis, composition, reactions. *John Wiley and Sons, Stillerman.* **1994**.

14. Sihombing, R.; Johnson, W. D.; Wilson, M. A.; Johnson, M.; Vassallo, A. M.; Alderdice, D. Origin of humus variation-effects of leaching and seasonal flooding on aromaticity. *Org. Geochem.* **1991,** *17* (1), 85-91.

15. Dubas, S. T.; Pimpan, V. Humic acid assisted synthesis of silver nanoparticles and its application to herbicide detection. *Mater. Lett.* **2008,** *62* (17-18), 2661-2663.

16. Perdue, E. M. R. J. D. Dissolved Organic Matter in Freshwaters. *Treatise on Geochemistry; Elsevier Ltd.: Atlanta, GA* **2003,** *5*, 273–318.

17. Kramer, J.R.B., G. Andren, A. W. Environmental chemistry of silver. In Silver in the Environment: Transport, Fate, and Effects. Bober, T. W., Eds. *SETAC Press, North Carolina*. **1993**.

18. Noguez, C. Surface plasmons on metal nanoparticles: The influence of shpae and physical environment. *Journal of Physical Chemistry C.* **2007,** *111* (10), 3806-3819.

19. Piccolo, A. The supramolecular structure of humic substances. *Soil Science.* **2001,** *166* (11), 810-832.

20. Kappler, A.; Haderlein, S. B. Natural organic matter as reductant for chlorinated aliphatic pollutants. *Environmental Science & Technology*. **2003,** *37* (12), 2714-2719.

21. Dunnivant, F. M.; Schwarzenbach, R. P.; Macalady, D. L. Reduction of substituted nitrobenzenes in aqueous-solutions containing natural organic-matter. *Environmental Science & Technology.* **1992,** *26* (11), 2133-2141.

22. Nakayasu, K.; Fukushima, M.; Sasaki, K.; Tanaka, S.; Nakamura, H. Comparative studies of the reduction behavior of chromium(VI) by humic substances and their precursors. *Environmental Toxicology and Chemistry.* **1999,** *18* (6), 1085-1090.

23. Wittbrodt, P. R.; Palmer, C. D. Reduction of Cr(VI) by soil humic acids. *European Journal of Soil Science.* **1997,** *48* (1), 151-162.

24. Gu, B. H.; Chen, J. Enhanced microbial reduction of Cr(VI) and U(VI) by different natural organic matter fractions. *Geochimica Et Cosmochimica Acta.* **2003,** *67* (19), 3575-3582.

25. Ratasuk, N.; Nanny, M. A. Characterization and quantification of reversible redox sites in humic substances. *Environ. Sci. Technol.* **2007,** *41* (22), 7844-7850.

26. Fimmen, R. L.; Cory, R. M.; Chin, Y. P.; Trouts, T. D.; McKnight, D. M. Probing the oxidation-reduction properties of terrestrially and microbially derived dissolved organic matter. *Geochim. Cosmochim. Acta.* **2007,** *71* (12), 3003-3015.

27. Lehmann, J.; Solomon, D.; Zhao, F. J.; McGrath, S. P. Atmospheric SO_2 emissions since the late 1800s change organic sulfur forms in humic substance extracts of soils. *Environ. Sci. Technol.* **2008,** *42* (10), 3550-3555.

28. Harris C. D. Quantitative chemical analysis. 5^{th} ed *W.H. Freeman and company, New York.* **1999**.

29. Wulfsberg, G. In organic Chemistry. **1994**.

30. Goldschmidt, V. M. The principles of distribution of chemical elements in minerals and rocks. The seventh Hugo Muller Lecture, delivered before the Chemical Society on March 17th. *Journal of the Chemical Society.* **1937**, 655-673.

31. Freise, F. W. The transportation of gold by organic underground solutions. *Econ. Geol.* **1931,** *26*, 421-431.

32. Liu, J. Y.; Sonshine, D. A.; Shervani, S.; Hurt, R. H. Controlled Release of Biologically Active Silver from Nanosilver Surfaces. *Acs Nano.* **2010,** *4* (11), 6903-6913.

33. Wen, L. S.; Santschi, P. H.; Gill, G. A.; Paternostro, C. L.; Lehman, R. D. Colloidal and particulate silver in river and estuarine waters of Texas. *Environ. Sci. Technol.* **1997,** *31* (3), 723-731.

34. Ambient Water Quality Criteria for Silver, H. o.-.; 80-071; United States Environmental Protection Agency: Washington; DC, w. e. g. w. c. Washington, DC, **1980**.

Chapter 5. Roles of Different Moieties within HAs in the Reduction of Metal Ions to Metal Nanoparticles

5.1 Introduction

Humic substances (HSs) are natural organic acids, ubiquitous in the environment, where they are formed through the decomposition of parent plant materials. They are made up of polydisperse complex heterogeneous mixtures of decaying plant matter. HSs are made up of different components, such as aromatic, aliphatic, carbohydrate and amino acid moieties, as well as other forms of heterocyclic and polyaromatic functionalities [1, 2]. Due to their nature HSs are traditionally separated into humic acid (HA), a fraction of humic substances, are soluble at pH 2 and above, fulvic acid (FA) is soluble in water at all pH values, and humin which is insoluble in aqueous solutions regardless of pH [3]. Humic acids are the most dominant in the natural environment, comprising about 50-80% of natural organic matter (NOM) in the environment [4].

The aromatic moieties within HAs are usually derived from slow decomposition of plants rich in lignins and tannins that are responsible for moieties such as quinones and phenol, and functional groups such as the methoxy and carboxylic acid [3]. On the other hand, the carbohydrate moieties within HAs mainly originate from plants rich in cellulose, hemicellulose, and simple sugars, and are comprised of functional groups, such as aldehyde, ketone and alcohol [3]. Cutins and cutans are the main source of lipids in HAs. Lipids are comprised mainly of alkenes, alkanes, n-alkyls, fatty acids, and alcohols [5] [6-9].

The chemical composition of HAs varies with their source; aquatic HAs, such as SWHA, is mainly composed of aliphatic moieties [10] in addition to the reduced organic sulfides [11]. Terrestrial HAs, on the other hand, are rich in aromatic backbones [10] and contain the oxidized form of organic sulfur [12]. Due to the presence of a variety of moieties in HAs, they are endowed with various chemical functionalities that could be involved in the reduction of

dissolved metals to metal nanoparticles, such as thiols [11] quinones, methoxy, hydroxyls, aldehydes, ketones, enols, and phenols [3].

Several studies have shown that HAs can reduce dissolved metals to metal NPs [13] [10, 14, 15]. The reduction of Au^{3+} (aq) to Au NPs using HAs under natural environmental conditions has been reported; [13] similarly, the reduction of Ag^{+} (aq) to Ag NPs using HAs under natural environmental conditions has been reported [10, 14]. The reduction of bulk Ag to Ag NPs has been reported [16]. Also, the ability of HAs from three different sources to reduce Au and Ag to form NPs was shown in Chapter 4. The major focus of these studies was on the reduction of metal salts to metal NPs at different conditions.

However, due to the complexity and the varied functionality of HAs, it is important to determine the specific moieties within HAs involved in the reduction of dissolved metals to metal NPs. The studies mentioned above have been focused on the formation of NPs, and hence, have been NP oriented. This means that they have merely implied the role of HA composition. The study presented below takes a forward step by investigating, using UV-Vis spectroscopy, the roles of aromatic, aliphatic (alkyl), and carbohydrate (O-alkyl) moieties within HAs in the formation of metal NPs with, and the stabilization of the formed NPs by, the three HAs from different environmental origins. The information generated from this study aids in determining the fate of dissolved metals in the aquatic and terrestrial environments by investigating the mechanism of their reduction to metal NPs under natural environmental conditions, along with the stabilization of the NPs formed.

5.2 Experimental Section

Chemicals and Materials

Suwannee River Humic Acid (SWHA), Florida Peat Humic Acid (FPHA) and Leonardite Humic Acid (LAHA) were purchased from the International Humic Substances Society (IHSS, St. Paul, MN). Methanol, benzene, hydrochloric acid, acetic acid and sodium chlorite were purchased from Fisher Scientific Company (Somerville, NJ). Gold (III) chloride trihydrate ($HAuCl_4 \cdot 3H_2O$) and silver nitrate ($AgNO_3$) were obtained from Sigma Aldrich (Milwaukee, WI), and high quality 18MQ deionized water was obtained with the use of the US Filter apparatus in our laboratory.

Chemical editing of HAs

Specific structural components within HAs were removed and the samples were characterized using ramp CP-MAS ^{13}C NMR; details of the chemical treatment and characterization of the chemically edited HAs are discussed in Chapter 3.

Synthesis of Au and Ag NPs

Au NPs and Ag NPs were prepared following procedures outlined in Chapter 4 except that chemically edited HAs were used in this synthesis instead of the original HAs. All the synthesized NPs were formed through the reduction of 250 μM $HAuCl_4$ and $AgNO_3$ to form Au NPs and Ag NPs, respectively. The reduction by HAs of $HAuCl_4$ to Au NPs and $AgNO_3$ to Ag NPs was monitored through the observation of the color change from light yellow to deep red and yellow for gold and silver NPs, respectively.

Characterization of Gold and Silver Nanoparticles:

UV-Visible Absorbance Measurements

Absorbance spectra were collected from 300-600 nm for Ag NPs and 400-700 nm for Au NPs using a 1.0 cm quartz cell. A Cary 100 Bio UV-visible spectrometer was used to obtain the UV-Vis spectra. Deionized water was used as blank.

5.3 Results and Discussion

As in Chapter 4, there will first be a discussion of the formed NPs, as viewed through their characteristic surface plasmon resonance peak (SPRP) visible in a UV/Vis spectrum. The use of SPRP here is based on the fact that, as was found in Chapter 4, such characterization is information rich and, for the HA NPs formed, the SPRP were consistent with the transmission electron microscopy (TEM) analysis across the board. In short, the SPRP shifted to either shorter (or longer) wavelengths with a decrease (or increase) in NPs size, and its absorbance increased (or decreased) with an increase (or decrease) in the number of NPs formed. This SPRP discussion will be followed by a discussion that addresses the influence of the different moieties within the three different HAs in the formation of Au and Ag NPs.

5.3.1 Formation of Au and Ag NPs by Chemically Edited HAs

The UV/Vis spectra characterization of the Au and Ag NP formed with the (i) bleached, (ii) hydrolyzed and (iii) lipid-extracted HAs are presented in Figures 5.1- 5.6. (Note that the scale on the y-axis is not consistent, this is to allow for clear observation of the SPRP). As a general trend, the formation of both Au and Ag NPs was more consistent at pH 7.6 than at pH 4.8.

Bleached SWHA (bSWHA)

The bSWHA sample at pH 7.6 formed Au NPs at all concentrations studied, except at 30 ppm. The SPRP shifted to shorter wavelengths with the increasing concentrations of bSWHA,

indicating that the NPs formed were stable, as there was sufficient HA to bind and stabilize them. In general, the greatest amount of NP formation occurred at 15 ppm bSWHA concentration. A subsequent decrease in NP formation at higher bSWHA concentration of HAs is illustrated by the decrease in the intensity of the plasmon peak. This could be attributed to the formation of a large number of NPs that rapidly aggregate and fall out of solution. At pH 4.8, the characteristic plasmon peak was observed at 10 ppm bSWHA and above. There appeared to be no further formation of NPs at the higher concentration as no further increase in the plasmon peak was observed. At pH 7.6, Ag NPs were only formed at high concentrations of the bSWHA, i.e., 15, 20 and 30 ppm. The formation of NPs decreased with the increasing concentration of this bleached humic acid. More NPs were formed at 15 ppm bSWHA. At pH 4.8, the characteristic plasmon absorbance band was observed at all the concentrations studied, except at 2.5 and 30 ppm bSWHA. Even then, the amount of NPs formed at this pH is very small, as indicated by the very weak SPRP. As discussed in the previous chapter, the lack of NP formation at some HA concentrations can be due to 1) the metal ion being bound to sites that are too isolated (high pH and HA concentration) or 2) aggregation of the HA due to either too much bridging by the metal ion (low HA concentration) or HA-induced aggregation (low pH and high HA concentration). These explanations have been discussed at length in the previous chapter, thus they will not be discussed here in detail. It should be stated, however, that the above pH and HA concentration trends are consistent with these mechanisms.

Bleached FPHA (bFPHA)

The formation of Au NPs with bFPHA formed at pH 7.6 depended upon the concentration of HA. At FPHA concentration greater than 10 ppm, there is clear evidence of NP formation. The maximum SPRP peak absorption was obtained at 15 ppm bFPHA, and then

decreased with the further increase in bFPHA concentration. This indicates that 15 ppm of bFPHA is sufficient to reduce Au^{3+} (aq) to Au NPs. The SPRP decreased with further increases in bFPHA concentration, indicating that this bleached humic acid could be aggregating at concentrations above 15 ppm. This would result in the formation of fewer Au NPs due to an insufficient amount of bFPHA in solution needed to reduce the dissolved metal to form Au NPs. Aggregation of bFPHA at high concentrations was also postulated in Chapter 2, 3, and 4 [17-20]. At the acidic pH of 4.8, more NPs were formed as the concentration of bFPHA increased from 10 ppm up to 30 ppm. It can be seen that, as one goes from 10 to 15 ppm in terms of bFPHA, there is a change in the SPRP in terms of it becoming both wider and shifted to a higher wavelength, indicating that more, larger in size and more polydisperse NPs are formed at 15 ppm bFPHA compared to 10 ppm. As the HA concentration increases, the SPRP further narrows, but remains centered at a higher wavelength, indicating larger Ag NPs are formed and that the transition takes place somewhere between 10 and 15 ppm. Bleached FPHA at pH 7.6 reduced Ag^{+} (aq) to Ag NPs at all the bFPHA concentrations investigated, except at two highest concentrations of 20 and 30 ppm. This finding is consistent with the results for the formation of Au NPs using bFPHA with the aggregation of bFPHA resulting in the potential loss of reduction sites within this humic acid needed to react with the aqueous metal to form metal NPs. On the other hand, at a pH of 4.8 the SPRP was only observed at 2.5 ppm bFPHA; again, this can be explained by HA aggregation at higher concentrations.

Bleached LAHA (bLAHA)

The bLAHA formed Au NPs at all bLAHA concentrations investigated, except with 2.5 ppm HAs at pH 7.6. The intensity of the SPRP increased and the peak broadened with increasing concentrations of bLAHA. While the higher SPRP intensity could be attributed to the formation

of more NPs with increasing concentration of bLAHA, peak broadening could be attributed to the increase in size of the NPs formed. At pH 4.8, the characteristic plasmon absorbance was observed at all the studied bLAHA concentrations; however, the peaks were broader at lower concentrations, specifically at 2.5 and 5 ppm, and narrower at 10 ppm and above. The SPRPs were shifted to shorter wavelengths at bLAHA concentrations above 5 ppm, indicating the formation of the stable Au NPs being smaller in size. The peaks increased in intensity and broadened with increasing bLAHA concentration, before decreasing at the 30 ppm bLAHA concentration. The increase and broadening in the SPRP with increasing concentration of this humic acid could be a result of the formation of more NPs and the coating of the NPs with excess HA. The reduction of Ag^{+} (aq) with bLAHA at pH 7.6 resulted in the formation of Ag NPs at lower bLAHA concentrations, as illustrated by the characteristic plasmon absorbance of the Ag NPs at 2.5, 5, and 10 ppm bLAHA concentrations. The absence of the plasmon peak at higher concentration of bLAHA could be attributed to aggregation of bLAHA, leaving an insufficient LAHA to reduce the aqueous metal. At a pH of 4.8, the only evidence of NP formation–obtained via the emergence of a SPRP–is at a bLAHA concentration of 2.5 ppm.

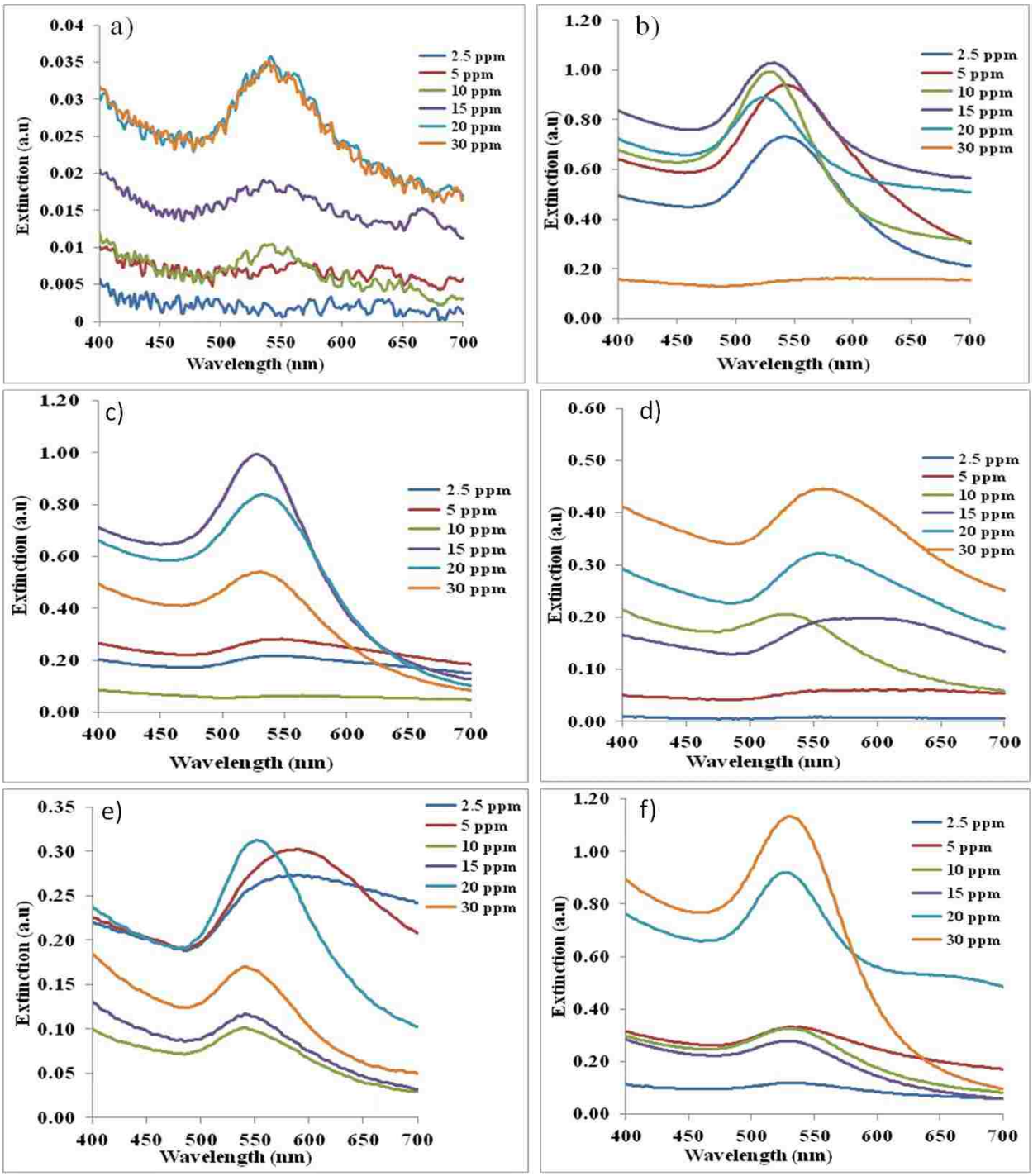

Figure 5.1 UV/Vis spectra of Au NPs formed with the bleached SWHA (bSWHA), FPHA (bFPHA) and LAHA (bLAHA) HAs at pH 4.8 a) c) e) and pH 7.6 b) d) f). (Note that the scale on the y-axis is not consistent, this is to allow for clear observation of the SPRP)

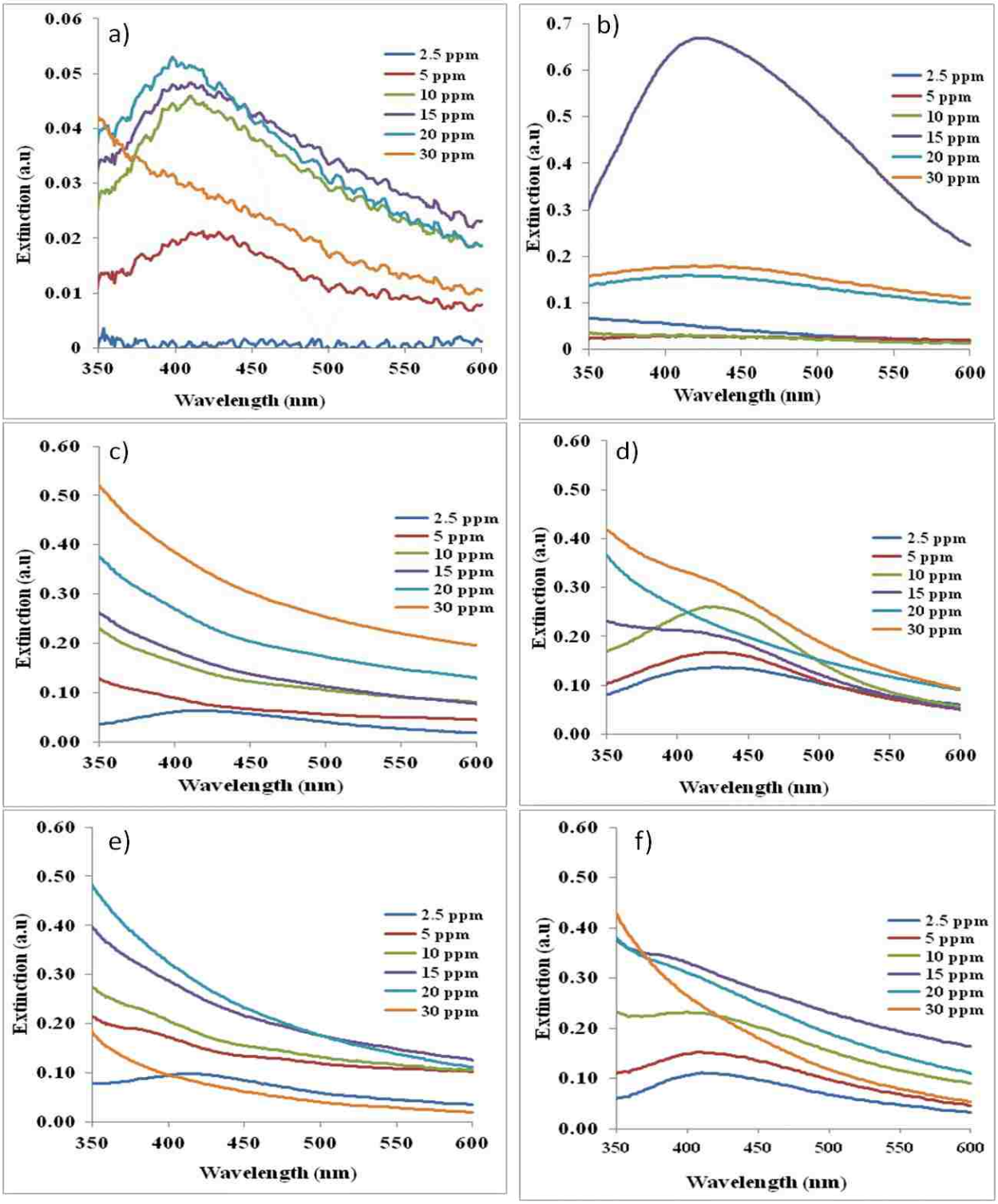

Figure 5.2 UV/Vis spectra of Ag NPs formed with the bleached SWHA (bSWHA) FPHA, (bFPHA), LAHA bLAHA at pH 4.8 a) c) e) and pH 7.6 b) d) f). (Note that the scale on the y-axis is not consistent, this is to allow for clear observation of the SPRP)

Hydrolyzed SWHA (hSWHA)

Hydrolyzed SWHA Figure 5.3 and Figure 5.4 yields very little Ag NP at either of the two pHs studied. At a pH of 7.6, it can be seen that NPs are best formed at the lowest hSWHA concentrations, namely 2.5 and 5 ppm and there is some evidence of very polydisperse NPs being formed at hSWHA concentrations of up to 20 ppm. One can also see that between 2.5 and 5.0 ppm, the size and polydispersity of the formed NPs decreases. If one looks at the pH 4.8 data, it can be seen that at Au NPs are only formed at the higher hSWHA concentrations of 20 and 30 ppm, with the size distribution decreasing with increasing HA concentration. The fact that Ag NPs are formed at the highest hSWHA concentration is counter to what one would normally expect due to aggregation processes, especially at this pH. This result can be explained by the fact that, at higher HA concentrations, there will be more sites for Ag reduction available to form the Ag NPs, thus it appears that at pH 4.8 this factor overrides aggregation processes. At the pH of 7.8, only the 10 ppm hSWHA concentration yields strong evidence of NP formation, i.e., a broad SPRP, while at 2.5 ppm there is only a hint of a SPRP. Why there is no evidence of a SPRP at 5 ppm is puzzling. At a pH of 4.8, there is no evidence of Ag NP formation at any of the hSWHA concentrations examined.

Hydrolyzed FPHA (hFPHA)

The hFPHA formed Au NPs at pH 7.6 at all the studied concentrations of this humic acid; however, the relationship between hFPHA concentration and the amount of NPs formed as well as their size and size polydispersity is very complex. For instance, there is an increase between 2.5 and 5 ppm, followed by a decrease between 5 and 10 ppm, followed by an increase between 10 to 15 ppm, followed by a decrease between 15 to 30 ppm. This zig-zag behavior would appear to indicate that there is a complex balancing act taking place involving the amount of Au

bound, the closeness of these sites so that NP aggregation may be induced, and the potential aggregation of the humic acid itself. With this said, it is clear that at this basic pH, the hFPHA is very capable of forming Au NPs throughout the studied concentration range. At pH 4.8, similar fluctuations in the amount of NP formed with the increasing HA concentration are observed, and therefore, can be explained using similar arguments. What is clear is that, at the higher HA concentrations of 20, 30, and especially 30 ppm, there is a clear and well defined SPRP, and the most Au NPs are formed at the hFPHA concentration of 30 ppm. The results for Ag are much more consistent. At a pH 7.6, Ag NPs are formed at all of the lower hFPHA concentrations up to and including 15 ppm. Between 2.5 and 5.0 ppm, a transition takes place, whereby a broad SPRP becomes a well defined one, indicating an increase in the quality of Ag NPs formed in terms of size distribution. Between 5 and 15 ppm there is a steady increase in the intensity of the SPRP, indicating an increasing number of Ag NPs being formed, and it appears that there is little change in their size or in size distribution. If one now considers the pH 4.8 data, it can be seen that NPs are being formed between 2.5 and 15 ppm, with an increasing intensity of the SPRP, and hence, an increase in the number of NPs formed.

Hydrolyzed LAHA (hLAHA)

Hydrolyzed LAHA samples at pH 7.6 resulted in the formation of Au NPs at all concentrations except at 30 ppm, as indicated by the plasmon peak. There was a steady increase in the SPRP's intensity as the hLAHA concentration increased from 2.5 to 15 ppm and a decrease when the hLAHA concentration increased from 15 ppm to 30 ppm (ultimately, with no SPRP peak at 30 ppm). It should be noted that the SPRP at both 10 and 20 ppm of the hLAHA concentrations are almost identical in intensity; however, the 20 ppm SPRP is centered at a lower wavelength, indicating that the NPs at this higher concentration are smaller in size. On the other

hand, at a pH of 4.8, the Au SPRP is only observed at the highest concentration of 30 ppm; however, the intensity of this SPRP is comparable to that seen for the highest SRPR at pH 7.8, thus indicating that approximately the same amout of Au NPs are formed. This implies that, when the conditions are correct for NP formation, then a large amount of NPs can be formed and that this condition may only exist in a narrow concentration range for this a single Au concentration constraint. In regards to Ag, it was found that at pH 7.6, NPs were formed at all but the highest hLAHA concentration, with a very weak and broad SPRP being visible at the lowest concentration of 2.5 ppm. At a pH of 4.8, Ag NP formation is only observed at the lowest hLAHA concentration. The lack of NP formation at the higher concentration can be explained once again by HA aggregation.

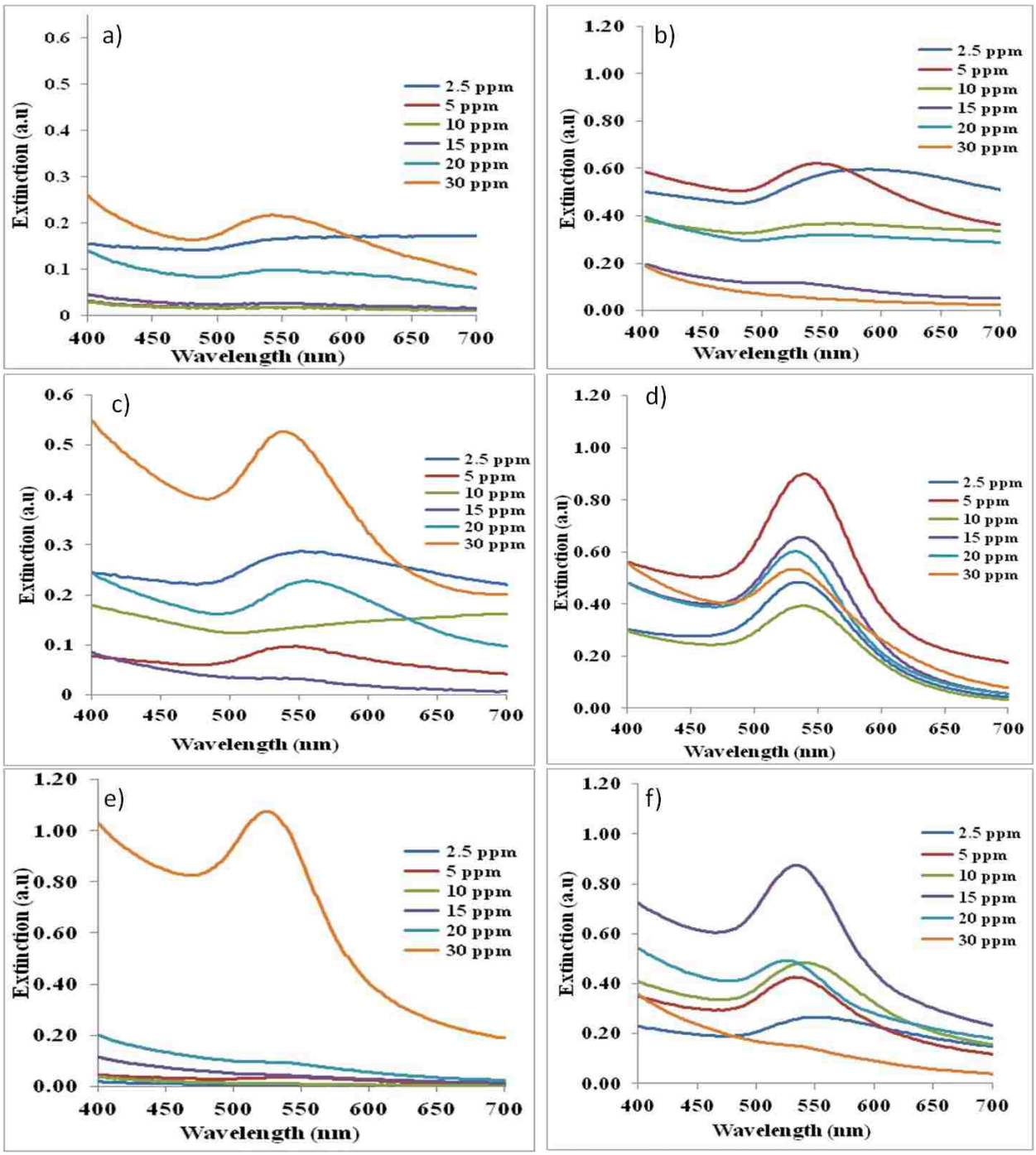

Figure 5.3 UV/Vis spectra of Au NPs formed with the Hydrolysed SWHA (hSWHA), FPHA, (hFPHA) and LAHA (hLAHA) HAs at pH 4.8 a) c) e) and pH 7.6 b) d) f). (Note that the scale on the y-axis is not consistent, this is to allow for clear observation of the SPRP)

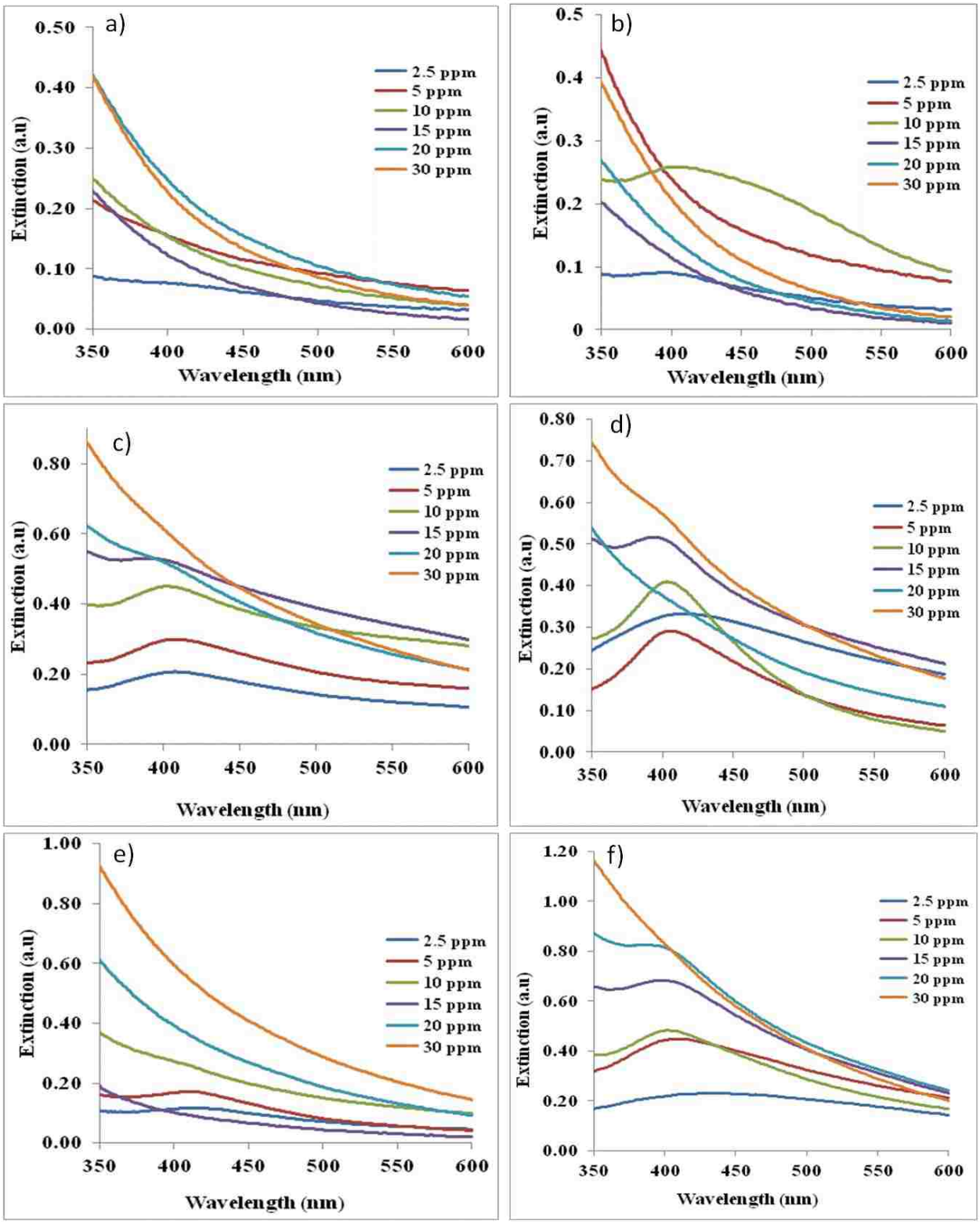

Figure 5.4 UV/Vis spectra of Ag NPs formed with the Hydrolysed SWHA (hSWHA), FPHA, (hFPHA) and LAHA (hLAHA) HAs at pH 4.8 a) c) e) and pH 7.6 b) d) f). (Note that the scale on the y-axis is not consistent, this is to allow for clear observation of the SPRP)

Lipid-extracted SWHA (leSWHA)

Lipid-extracted SWHA at pH 7.6 Figure 5.5 formed Au NPs with a narrow size distribution at a leSWHA concentration of 30 ppm HA. The SPRPs were broad at all the other concentrations of leSWHA, indicating that the NPs were mostly aggregated. At pH 4.8, the SPRP were broader than at pH 7.6, but otherwise similar observations to those at pH 7.6 were made in that the NPs appeared to have formed at 30 ppm and the SPRPs were broader at lower concentrations. Formation of Ag NPs with leSWHA showed a characteristic plasmon absorbance only at a leSWHA concentration of 2.5 ppm HA when the pH was 7.6. There was no SPRP observed for any of the concentrations at pH 4.8.

Lipid-extracted FPHA (leFPHA)

The formation of Au NPs with leFPHA samples depended on the HA's concentration: the intensity of the SPRP increased with increasing concentration for all studied concentrations. In addition, the plasmon peak appeared to shift to shorter wavelengths with increasing concentration of leFPHA indicating that NPs of smaller sizes were formed as the concentration of this lipid-extracted humic acid increased. At pH 4.8; however, Au NPs were only formed at higher leFPHA concentrations: 10 ppm and above. At 30 ppm there was a decrease in the intensity of the SPRP, indicating that fewer Au NPs were formed due to leFPHA aggregating at higher concentrations, such as at 30 ppm. This aggregation has been discussed thoroughly in Chapter 2. Lipid-extracted FPHA samples formed Ag NPs at all leFPHA concentrations studied, except at 30 ppm at pH 7.6; Ag NPs were only formed at a leFPHA concentration of 2.5 ppm at a pH of 4.8.

Lipid-extracted LAHA (leLAHA)

Lipid-extracted LAHA formed Au NPs at all the leLAHA concentrations investigated at pH 7.6. The SPRP appeared to shift to shorter wavelengths with increasing concentrations of leLAHA, namely at 10, 20 and 30 ppm. Au NPs with narrow size distributions were formed at a leLAHA concentration of 5 ppm, as indicated by the comparatively narrow SPRP at this concentration. At the acidic pH of 4.8, the only observed SPRP was at 2.5 ppm, and this peak was weak and very broad, indicating that the Au NPs that form at very low concentration of leLAHA are polydisperse and may be mostly aggregated. At pH 7.6, Ag NPs were formed using leLAHA at concentrations of ranging from 2.5 to 15 ppm. At the higher concentrations of leLAHA (20 and 30 ppm) the characteristic SPRP of Ag NPs was not observed, implying that the NPs were not formed at this concentration. At pH 4.8, the characteristic SPRP of Ag NPs was only observed at a leLAHA concentration of 2.5 ppm.

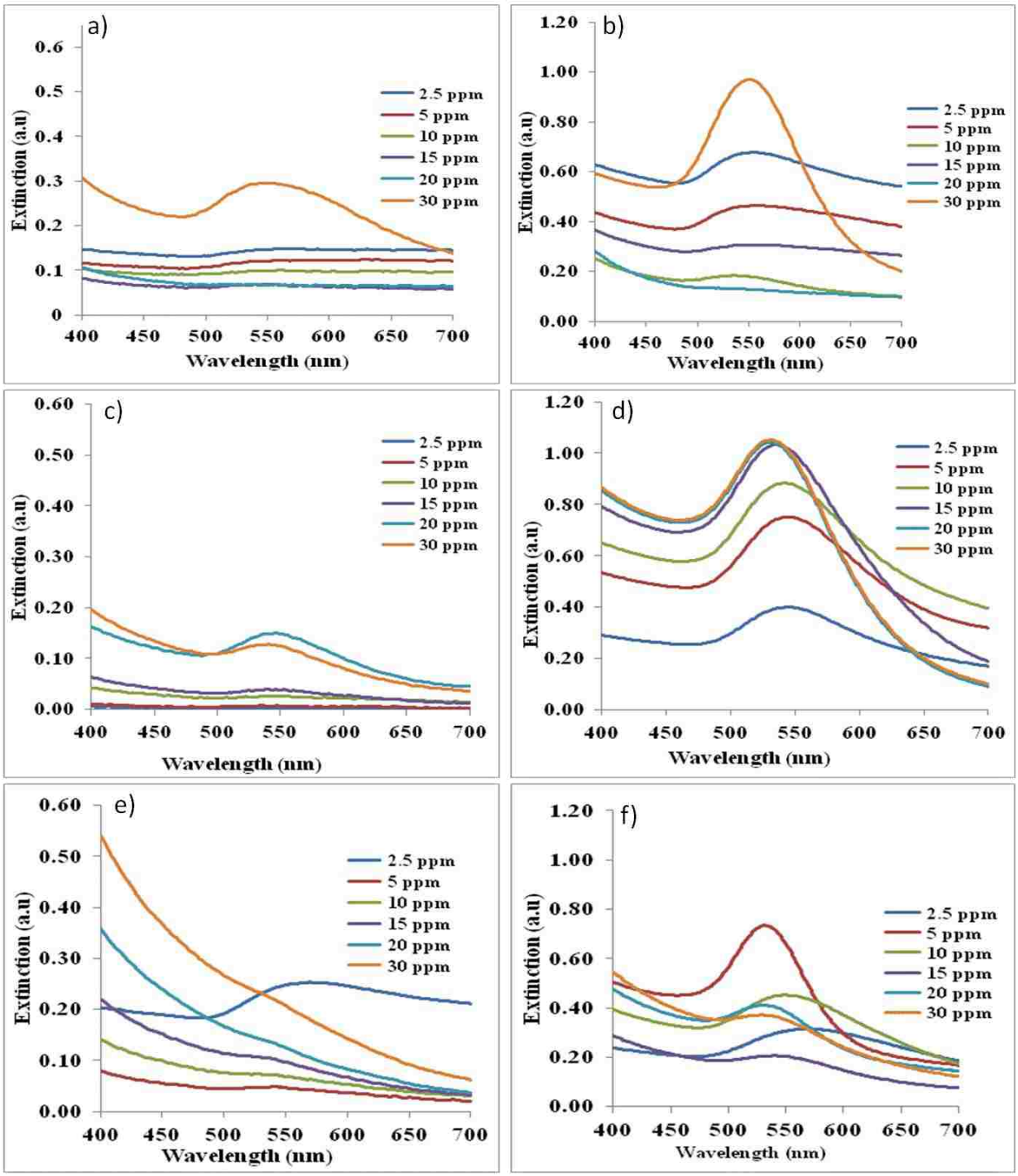

Figure 5.5 UV/Vis spectra of Au NPs formed with the lipid extracted SWHA (leSWHA), FPHA, (leFPHA) and LAHA (leLAHA) HAs at pH 4.8 a) c) e) and pH 7.6 b) d) f). (Note that the scale on the y-axis is not consistent, this is to allow for clear observation of the SPRP)

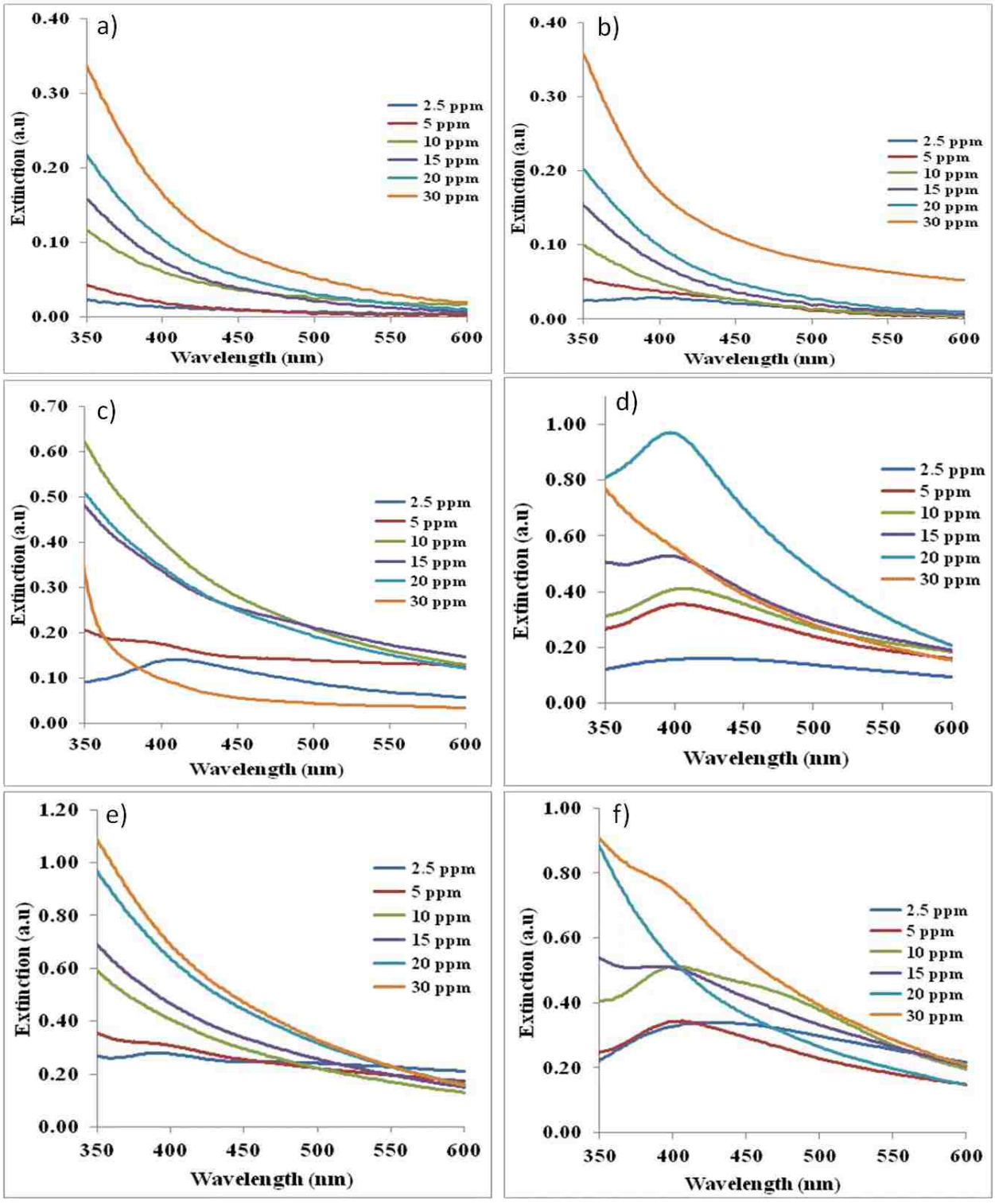

Figure 5.6 UV/Vis spectra of Ag NPs formed with the lipid extracted SWHA (leSWHA), FPHA, (leFPHA) and LAHA (leLAHA) at pH 4.8 a) c) e) and pH 7.6 b) d) f). (Note that the scale on the y-axis is not consistent, this is to allow for clear observation of the SPRP)

5.3.2 The Role of Different Chemical Moieties within HAs in the Formation of Au and Ag NPs.

The discussion in this section will compare overall summarization of the data presented in this chapter to the complementary results for the unedited HAs presented in Chapter 4. This *grosso modo* analysis of the data focuses on the role of aliphatic, aromatic, and carbohydrate moieties within the three studied HAs in the formation of Au and Ag NP.

The bleaching treatment of the HAs resulted in the removal of a significant fraction of the aromatic moieties and an enhancement of the O-alkyl functional groups, as was shown in chapter 3. It has also been reported in the literature that oxidative degradation of HAs via bleaching eliminates a significant amount of non-condensed aromatic moieties from lignins or tannins within HAs [21, 22]. Aromatic moieties within terrestrial HAs have been implicated in the formation of NPs [10] however, this notion was based purely on general knowledge of HA composition in regards to origin. The results discussed above indicate that the removal of the aromatic moieties by bleaching mainly influenced the formation of NPs for both FPHA and LAHA, while SWHA was less affected. These findings imply that the aromatic moieties present within HAs of terrestrial origin (FPHA and LAHA) play a significant role in the reduction of both Au^{3+} (aq) and Ag^{+}(aq) to their respective NPs. This finding is consistent with terrestrial HAs originating mainly from parent plants materials rich in lignins and tannins, which are the main source of the aromatic moieties in these HAs and have such functionalities as quinones, phenols, methoxy and carboxylic acid groups [3]. These functional groups are electron-rich and seem to be the ones (likely the quinone-like two (QL2) groups discussed in Chapter 4) involved in the reduction of Au^{3+} (aq) and Ag^{+} (aq) to their respective NPs. SWHA is of aquatic origin and consists of more microbially derived materials; it is rich in aliphatic as well as carbohydrate moieties, and (thus, is lower in aromatic components in comparison with terrestrial HAs. Instead,

it contains reduced organic sulfides [11]. With this in mind, and based on the above findings, it can be concluded that non-quinone like (NQL) groups, such as thiols are mainly involved in the reduction of both Au^{3+}(aq) and Ag^{+}(aq) to NPs.

Along the same thread of thought that implicated aromatic moieties in the formation of NPs by terrestrial HA, it has been implied that aliphatic and carbohydrate moieties within aquatic HAs are involved in the formation of NPs; however, once again, this was based purely on general knowledge of HA composition in regards to origin. The hydrolysis and lipid extraction results above address this more directly.

Acid hydrolysis has been reported to eliminate a significant fraction of carbohydrate and amino acid moieties [23] and can result in the loss of functionalities, such as aldehydes, and ketones within HAs [3]. From the results above in this Chapter it can be seen that hydrolysis greatly decreases the potential for SWHA to reduce Au^{3+} (aq) and Ag^{+} (aq) to their respective NPs. This strongly implies that the Au and Ag NP forming sites within SWHA are associated with the carbohydrate moieties, as the removal of these moieties would also lead to the removal of electron rich aldehyde and alcohol groups which could play major roles in the reduction of Au^{3+}(aq) and Ag^{+}(aq) to their respective NPs by SWHA. The removal of the carbohydrate moieties from both FPHA and LAHA also appears to affect the formation of NPs, but to a lesser extent. These findings also provide further evidence that the aromatic moieties within terrestrial HAs are major participants in Au and Ag NP formation, compared to the carbohydrate moieties.

Lipid extraction mainly eliminated the aliphatics comprising of long chain fatty acids, long chain aliphatic alcohols, long chain alkanes and esters, [5-8] and, in the context used here, allows one to investigate the role of aliphatic moieties. The removal of lipids in SWHA greatly reduced its potential to form both Au and Ag NPs. In fact, our results show that aliphatic

moieties in SWHA appear to play a role comparable to that of carbohydrate moieties suggesting that higher aliphatic alcohols in the aquatic HAs could be greatly involved in the reduction of Au^{3+}(aq) and Ag^{+}(aq) to their respective NPs. In regards to the terrestrial HAs, the removal of the aliphatic moieties influences the formation of both Au and Ag NPs in terms of the amount as well as size. These effects are much smaller than those observed for the SWHA, thus providing more evidence for the importance of aromatic moieties in the formation of Au and Ag NPs by terrestrial HAs.

5.4 Conclusions

Certain conclusions can be drawn from the data presented in this work although there is no conclusive evidence. This is due to the complex, heterogeneous and polydisperse nature of WAMAs humic substances form, conclusive statements, or answers, are currently not possible. The best way of looking at how to approach the presented results obtained for the HAs used in this work is by attempting to establish causes and their effects, and provide as much of corroborating evidence as possible. Accordingly, in all probability, aliphatic, aromatic, and carbohydrate moieties within HAs are involved in Au and Ag NPs formation. The weighting of the influences of these different moieties on the formation of Au and Ag NPs is different depending on the origin of the HA. The reason for the importance of these different moieties is due to the complex processes accompanying the formation of NPs by HAs, including binding and reduction of the metal cations by the HAs where, as illustrated by the metal and HA concentration data presented in this as well as the previous chapter, the secondary and tertiary structure of the HAs also play an equally important role.

5.5 Environmental Implications

In a natural environmental setting, removal of aromatic moieties within HAs occurs naturally in shallow waters as a result of photochemical bleaching of aromatic moieties by daily intense illumination by sun [24]. This fact reduces the role of HAs within surface aquatic systems with terrestrial inputs, due to run-off, especially the longer the terrestrial sourced HAs are in the surface waters. This is countered by the fact that photobleaching is believed to make HAs more bioavailable, and hence, increase the amount of microbially derived HAs within surface waters. The results above imply that the resulting microbial HA has the ability to reduce Au^{3+} (aq) and Ag^{+} (aq) cation to form NPs. On aggregate, there appears to be a number of moieties within HAs, depending on the origins of the HA, that can reduce Au^{3+} (aq) and Ag^{+} (aq) to form NPs, and that as terrestrial HA is photobleached, the removal of NP forming aromatic moieties is counter balanced by the addition of aliphatic and carbohydrate forming NPs moieties due to the microbially produced HA.

5.6 References

1. Hayes, M. H. B.; Clapp, C. E. Humic substances: Considerations of compositions, aspects of structure, and environmental influences. *Soil Science.* **2001,** *166* (11), 723-737.

2. Schnitzer, M. Soil organic-matter - the next 75 years. *Soil Science.* **1991,** *151* (1), 41-58.

3. Stevenson, F J. H. C. G. Humus chemistry genesis, composition, reactions. *John Wiley and Sons,* Stillerman. **1994**.

4. Vigneault, B.; Percot, A.; Lafleur, M.; Campbell, P. G. C. Permeability changes in model and phytoplankton membranes in the presence of aquatic humic substances. *Environ. Sci. Technol.* **2000,** *34* (18), 3907-3913.

5. Schnitzer, M.; Schulten, H. R. Pyrolysis-soft ionization mass-spectrometry of aliphatics extracted from a soil clay and humic substances. *Science of the Total Environment.* **1989,** *81-2*, 19-30.

6. Wu, Q. G.; Schleuss, U.; Blume, H. P. Investigation on soil lipid extraction with different organic-solvents. *Zeitschrift Fur Pflanzenernahrung Und Bodenkunde.* **1995,** *158* (4), 347-350.

7. Guignard, C.; Lemee, L.; Ambles, A. Lipid constituents of peat humic acids and humin. Distinction from directly extractable bitumen components using TMAH and TEAAc thermochemolysis. *Organic Geochemistry.* **2005,** *36* (2), 287-297.

8. Lodygin, E. D.; Beznosikov, V. A. Influence of soil moisture on concentrations and ^{13}C NMR profiles of lipids in three Albeluvisols. *Geoderma.* **2005,** *127* (3-4), 253-262.

9. C.Harris, D. Quantitative chemical analysis. 5th ed.; *W.H. Freeman and company New York.* **1999.**

10. Akaighe, N.; MacCuspie, R. I.; Navarro, D. A.; Aga, D. S.; Banerjee, S.; Sohn, M.; Sharma, V. K. Humic Acid-Induced Silver Nanoparticle Formation Under Environmentally Relevant Conditions. *Environ. Sci. Technol.* **2011,** *45* (9), 3895-3901.

11. Urban, N. R.; Ernst, K.; Bernasconi, S. Addition of sulfur to organic matter during early diagenesis of lake sediments. *Geochimica Et Cosmochimica Acta.* **1999,** *63* (6), 837-853.

12. Lehmann, J.; Solomon, D.; Zhao, F. J.; McGrath, S. P. Atmospheric SO_2 emissions since the late 1800s change organic sulfur forms in humic substance extracts of soils. *Environ. Sci. Technol.* **2008,** *42* (10), 3550-3555.

13. Machesky, M. L.; Andrade, W. O.; Rose, A. W. Interactions of gold (III) chloride and elemental gold with peat-derived humic substances. *Chemical Geology.* **1992,** *102* (1-4), 53-71.

14. Dos Santos, D. S.; Alvarez-Puebla, R. A.; Oliveira, O. N.; Aroca, R. F. Controlling the size and shape of gold nanoparticles in fulvic acid colloidal solutions and their optical characterization using SERS. *Journal of Materials Chemistry.* **2005,** *15* (29), 3045-3049.

15. Sal'nikov, D. S.; Pogorelova, A. S.; Makarov, S. V.; Vashurina, I. Y. Silver ion reduction with peat fulvic acids. *Russian Journal of Applied Chemistry.* **2009,** *82* (4), 545-548.

16. Wen, L. S.; Santschi, P. H.; Gill, G. A.; Paternostro, C. L.; Lehman, R. D. Colloidal and particulate silver in river and estuarine waters of Texas. *Environ. Sci. Technol.* **1997,** *31* (3), 723-731.

17. Leppard, G. G.; Buffle, J.; Baudat, R. *A* description of the aggregation properties of aquatic pedogenic Fulvic-acids-combining physicochemical data and microscopic observations .*Water Research.* **1986,** *20* (2), 185-196.

18. Clapp, C. E.; Hayes, M. H. B. Sizes and shapes of humic substances. *Soil Science* **1999,** *164* (11), 777-789.

19. Swift, R. S. Macromolecular properties of soil humic substances: Fact, fiction, and opinion. *Soil Science.* **1999,** *164* (11), 790-802.

20. Schulten, H. R.; Leinweber, P. New insights into organic-mineral particles: composition, properties and models of molecular structure. *Biology and Fertility of Soils.* **2000,** *30* (5-6), 399-432.

21. Wise, L. E.; Murphy, M.; Daddieco, A. A. Chlorite holocellulose, its fractionation and bearing on summative wood analysis and on studies on the hemicelluloses. *Technical Association Papers* **1946,** *29* (JUN), 210-218.

22. Christman, R. F.; Norwood, D.L.; Seo, Y.; Frimmel, F.H. Oxidative degradation of humic substances from fresh water environments II. In search of structure ed.; *John Wiley & Sons, New York.* **1989**.

23. Preston, C. M.; Schnitzer, M. Effects of chemical modifications and extractants on the C-13 NMR-Spectra of humic materials. *Soil Science Society of America Journal*. **1984,** *48* (2), 305-311.

24. Goldstone, J. V.; Pullin, M. J.; Bertilsson, S.; Voelker, B. M. Reactions of hydroxyl radical with humic substances: Bleaching, mineralization, and production of bioavailable carbon substrates. *Environmental Science & Technology*. **2002,** *36* (3), 364-372.

Chapter 6. Investigation into the Interaction of Biomembranes with Gold and Silver Nanoparticles Synthesized and Stabilized by Chemically Diverse Humic Acids

6.1 Introduction

Metal nanoparticles (NPs) have been and continue to be intensely studied due to their diverse probable and actual applications: in biolabeling [1, 2] and diagnostics, electronics and optics, [3, 4] catalysis, [5, 6] environmental remediation, pharmaceuticals and consumer products [7-9]. In particular, silver NPs have been incorporated into a variety of personal care products, while gold nanoparticles are being strongly considered for a range of biomedical applications. Owing to the numerous applications of metal NPs, there is a rapid growth in their production and use in the industrial and research sectors. It was estimated that 2,000 tons of NPs were produced and used in 2004. This production is projected to increase to 58,000 tons in 2011-2020[10]. Tons of NPs have already been released into the environment and these amounts are expected to dramatically increase in the near future.

Metal NPs may end up in the environment directly or indirectly via a number of potential release routes, such as product handling and transportation, the improper disposal of nanoproducts, the use of nanoparticles as fuel additives, as components of consumer products [11] and groundwater treatment agents, [12] through the excretion of non-metabolized nanomedicines as well as through industrial emissions, leaks or spills [13]. Thus, there is a strong probability that these metal NPs will be present in significant amounts in both aquatic and terrestrial environments in the future. At present, the information regarding the magnitude of probable release, distribution and transformation nanoparticles in the environment is inadequate [10].

HAs form in the environment as a result of microbial decomposition of plant matter. They are present everywhere in the environment and are made up of complex heterogeneous and

polydisperse mixtures of decayed plant materials. They have a complex structure that comprises both hydrophobic and hydrophilic moieties. Functional groups within HAs, such as the thiols, [14] quinones, methoxy, hydroxyls, aldehydes, ketones, enols, [15], and phenols endow this macromolecule with the potential to interact with, and reduce, metal ions to metal NPs. Since HAs are prevalent throughout the environment, they may play a key role in the formation and the fate and transport of HAs-metal NPs system in the environment.

The presence of colloidal silver in the environment was for the first time reported in the mid-1990s [16]. Studies have also shown that silver nanoparticles can be synthesized with HAs as both the reducing and the capping agent at environmentally relevant conditions such as pH, temperature and concentrations [17]. Capping is typically referred to as a process of binding ligands to the NPs formed to stop their growth and their aggregation. The first attempt to synthesize colloidal gold using humic substances was done by Machesky and coworkers, while investigating the possible mechanism of interaction of HAs with gold in the environment [18, 19]. In addition, gold nanoparticles of different sizes and shapes have been previously prepared using varying concentrations of fulvic acid at pH 5, 8 and 11 and at high temperatures[17, 19].

Apart from reducing metal ions to metal nanoparticle studies have shown that HAs interact with NPs synthesized and stabilized by other reducing and stabilizing agents [20]. These studies have demonstrated that lower concentrations of HAs increase the stability of the NPs by coating the surface of the NPs, whereas higher concentrations of HAs cause the aggregation of NPs [20] Pallem and coworkers have further shown that HAs further increase the stability of citrate-capped NPs by either replacing the citrate capping or overcoating the citrate capping. They also showed that HAs substitute's coatings composed of β-D-glucose molecules [21]. Other studies looked at natural organic matter (NOM), of which HAs comprise at least 60%.

Investigations into the adsorption of NOM to NP surfaces indicated that NOM plays an important role in stabilizing NPs in the environment [22]. Given that metal ions can be released from metal NPs, and that metal ions can be transformed back to metal NPs in the environment [17] metal ions from either the NPs or metal salt forms can be transformed into metal NPs in the environment, which then may lead to the formation of HAs-metal NPs systems in the environment. These studies further stress the likelihood of the presence of substantial amounts of HAs-metal NPs systems in the environment in the near future.

As metals are known to interact with HAs and with biomembranes, [23-29] we postulate that the HAs-metal NPs system could also have the potential to interact with biomembranes. Several studies have already shown that several NPs are toxic to organisms [30-32]. In a study that investigated the toxicity of CuO NPs to algae in the presence of dissolved organic matter (DOM), Suwannee River fulvic acid showed that toxicity of CuO NPs was enhanced in the presence of DOM [30]. Toxicity of CuO NPs to organisms has been studied on a range of organisms, from algae, bacteria, and protozoa, to crustaceans, further emphasizing the relevance of these kinds of studies [30, 32]. The study of the interaction of HAs-metal nanoparticles systems with biomembranes has not yet been explored. Taking into consideration that the production, commercialization and use of NPs is growing at an alarming rate, there is a crucial need to fully understand how these naturally-formed NPs interact with the biomembranes in the environment especially at a molecular level. This study therefore examines the association of natural HA capped NPs of Ag, and Au with model biomembranes utilizing fluorescence leakage and cryo-TEM.

6.2 Experimental Section

Materials. POPC was purchased from Avanti Polar Lipids (Alabaster, AL); Florida Peat Humic Acid (FPHA), Leonardite Humic Acid (LAHA), and Suwanee River Humic Acid (SWHA) were purchased from the International Humic Substances Society (IHSS, St. Paul, MN). Methanol and chloroform and were purchased from Fisher Scientific Company (Somerville, NJ). Nitrogen gas was supplied by the Chemistry department (upon being sourced from Capital Welders Supply Co.). Gold (III) chloride trihydrate ($HAuCl_4.3H_2O$), silver nitrate ($AgNO_3$), and Triton X-100 (TX-100) were obtained from Sigma Aldrich (Milwaukee, WI), Sulforhodamine-B was obtained from molecular probes while Sephadex G-50 GE was obtained from Healthcare Biosciences (Piscataway, NJ). High quality (18MΩ) deionized water was made in our laboratory using an apparatus manufactured by US Filter.

Sample Preparation of HAs

HAs stock solutions: These solutions were prepared by dissolving 8.6 mg of FPHA in 50 mL of 0.01 M phosphate solution at pH 4.8 or 7.6, then adjusted to a basic pH using NaOH in order to dissolve all HAs, then adjusted back to pH 4.8 or 7.6 with HCl and diluted to 100.0 mL with the phosphate buffer solution at pH 4.8 or 7.6.

LUVs: POPC vesicles of approximately 100 nm in diameter were prepared using extrusion method refer back to chapter 2

Humic acid capped NPs: NPs of Au and Ag were synthesized using chemically diverse HAs as the reducing and the capping agent refer back to Chapter 4. These NPs were used without purification to imitate an environmental setting.

Solutions for Fluorescence Leakage Experiments*:* dye encapsulated LUVs were exposed to chemically diverse HAs, metal salts and HA-coated NPs and used to investigate the perturbation

effect of HAs on the model biomembranes. Leakage measurements were done by measuring 5.00 mL of SRB-loaded LUVS and adding 5.00 mL of 0.01 M phosphate buffer solution for the blank and 5.00 mL of metal salt in phosphate buffer for the first control and 5.00 mL of HA for the second control. The test sample contained 5.00 mL of HA-NPs plus 5.00 mL of SRB-loaded LUVS refer back to Chapter 2

TEM Sample Preparation and Analysis: A vitrification robot was used to ensure that the relative humidity was kept close to saturation. A 3 μL drop of the lipid suspension was used for all the samples imaged refer back to Chapter 2.

6.3 Results and Discussion

6.3.1 Steady-State Fluorescence Study of the Interaction of HAs-Metal NPs with Biomembranes

The steady-state fluorescence emission spectra are presented in Figure 6.1 below. As can be seen from these spectra, four different controls were used in addition to the Ag and Au HAs capped nanoparticles. The spectra labelled “control”are the data for the large unilaminar vesicles (LUVs) at the appropriate pH value, and illustrate that there was background fluorescence signal coming from fluorescence dye that was not seperated from the LUVs in the size exclusion step and, as in Chapters 2 and 3. The next two sets of controls are the metal ions samples, labeled Ag and Au. In these samples the conditions are as for the LUV control (labeled “control”) sample with the addition of $AgNO_3$ or $HAuCl_4$ at the concentration used to make the HA-capped NPs. These controls were included to determine whether either of these to ions would induce leakage at pH 4.8 or 7.6 and, as can be seen from the data in Figure 6.1, either of these ions induced only a very minimal leakage, and hence, neither of these ions induced biomembrane perturbation on the level seen for the HAs and chemically edited HAs studied in Chapters 2 and 3, especially at pH 4.8. The final controls were the three HAs that both the Ag and Au NPs were capped with

and, as expected, the trends in the leakage induced by these HAs mirror those seen in Chapter 2; the reader is referred to Chapter 2 for a full discussion of the HA-induced biomembrane perturbations. HA and metal ions controls were not included for two reasons. First, as the data in Chapter 4 show, the mixing of the three HAs used in this study and $AgNO_3$ or $HAuCl_4$ ions yields NPs, hence there is a likelihood that there would be HA-capped NPs present or being formed, and hence, yielding a complex and potentially difficult situation. The second reason is that, as shown Chapter 4, the environmentally relevant condition is HA capped Ag and Au NPs. The non-HA-capped NPs were not included as controls for two major reasons. Firstly, Ag and Au NPs need to be capped in order to not aggregate and remain in solution; the chemical nature of the capping agent will determine the potential of the capped NPs to perturb biomembranes. Secondly, it has been shown in the literature that natural organic matter will coat capped NPs such as citrate capped NPs or substitute the capping agent made up of citrate or β-D-glucose molecules [21]. This means that biomembrane perturbing potential of these NOM-coated capped NPs will depend on the NOM that coats the capped NPs. Thus, for the environmental conditions we are studying, it will be the NOM that determine biomembrane perturbation potential rather than the NP capping agent.

In Chapter 2, HAs can induce biomembrane perturbation under environmental conditions, while in Chapter 4 it was shown that under environmental conditions HA-capped Au and Ag NPs can be formed. These two findings lead to the following question “can HA-capped NPs formed under environmentally relevant conditions perturb biomembranes?”. While the data presented in Figure 6.1 show that the answer to this question is “yes, they can”, they also point to the fact that the situation is more complicated than a simple “yes” or “no”.

The data in Figure 6.1 clearly indicate that the perturbation potential of HA-coated NPs depends on both the metal and the HA used to form the HA-coated NPs. SWHA-capped Ag NPs cause more leakage than SWHA-capped Au NPs at both pH 4.8 and 7.6, while for both FPHA and LAHA-capped NPs it is the Au-capped NPs that induce the largest amount of leakage at both pH 4.8 and 7.6. From a HA origin point of view, it is interesting to note that the terrestrial HAs gave the same trend in terms of the biomembrane perturbation and NP's metal, while the aquatic sourced HA had an oposite preference to the perturbation causing nanoparticle's metal.

As it is the capping agent that is on the exterior of the NP surface, it will be the capping agent that interacts with the biomembrane surface. This means that for the HA-capped NPs it will be the chemical nature of the HA on the NP surface that will induce biomembrane perturbation by HA-capped nanopaticles. However, once again the real situation is more complex as the HA NPs used in this study could not be separated from the HA solution used to make the NPs. This means that one must campare the observed leakage of the appropriate HA with that of the HA-capped NPs. For SWHA it can be seen that at pH 4.8 there is no difference in observed perturbation between the HA-capped Ag NPs versus and "simple" SWHA. In fact, the signals for these two cases directly overlap each other. On the other hand, for the same pH it can be seen that the formation of the HA-capped Au NPs reduce the potential for the SWHA that remained in solution to induce leakage, and hence, its potential for biomembrane perturbation. This is because most of HAs is consumed in the reduction and the capping of the NPs formed thus not much is available to interact with and perturb the biomembranes. At pH 7.6 the same result is seen for the formation of Au HA-capped NPs; however, for the formation of HA-capped Ag NPs the HA that remains in solution has a higher potential to peturb biomembranes. If one now shifts their attention to FPHA, it can be seen that, at pH 4.8, HA-capped Au NPs induce

more leakage than FPHA; however, the FPHA-capped Ag NPs induce less leakage. For pH 7.6 the same trend is seen for the FPHA-capped Au NPs, but the FPHA-capped Ag NPs also induce more leakage than FPHA alone. For NPs formed in the presence of LAHA, different results are yet seen. At pH 4.8, both LAHA-capped Au and Ag NPs induce less leakage than LAHA alone, while at pH 7.6 LAHA-capped Au NPs induce an almost identical level of leakage as LAHA but the LAHA-capped Ag NPs induced less leakage.

These results demonstrate that, after the formation of nanoparticles, the distribution of the residual HAs induces leakage, and hence, biomembrane perturbation. Based on the mechanism put forward in Chapter 2, it would seem that the formation of the Au and Ag NPs can either 1) change the potential of the HA present to form the needed hydrogen bridge or 2) change the potential of HA to absorb into the biomembrane through hydrophobic interactions. The trends in the pH data do not help in determining which one of these effects is taking place; however, given the bulk trend that more leakage is observed for HA-capped NPs at pH 4.8 compared to 7.6 (except for FPHA-capped Ag NPs), it can be postulated that it is the the formation of nanoparticles in the prescence of HA that results in 1) the remaining HA to have a higher potential to form a hydrogen bridge or 2) the HA that caps the nanoparticles has a higher potential for hydrogen bond formation. It is expected that functional groups capable of forming hydrogen bridges are also the ones involved in the initial binding of Ag and Au and the HA groups in question have a high potential to bind cations. Therefore it could be envisioned that the HA capping the nanoparticle surface would be more polar than the bulk HA, enhancing the probability of forming a hydrogen bond between the capping HA and the biomembrane; however, the leakage data also suggest that the capping HA has also enough hydrophobic nature to allow for the absorption step as well.

It would be ideal if one could separate the HA-capped NPs from the dissolved HA; however, this was not possible due to the small size and polydisperisty of the formed nanoparticles resulting in standard separation methods being inapplicable. In addition, any chemical separation may lead to chemical alteration of both the dissolved HA and the capping HA. Nevertheless, what can be concluded from the fluorescence data is that in an environment in which HAs produce nanoparticles, this NP forming process induces an alteration of the HA's potential to perturb biomembranes. As HAs have been found to be very good surrogates of natural organic matter, the above stated findings for HA in all probability applies to natural organic matter as a whole. In order to determine whether it is the HA-capped NPs that are associated with, and hence, in all likelihood perturbing the biomembranes, Cryo-TEM studies were carried out.

6.3.2 Cryo-TEM Study of the Interaction of HAs-Metal NPs System with Biomembranes

The discussion of the fluorescence data above shows the weakness of a bulk measurement when dealing with a mixture in which there is more than one possibility for the observed signal. Under such circumstances, an imaging approach may allow for a more specific view, and hence, conclusion. For the case here one must consider that we are trying to image very small objects (the nanoparticles) as well as a mixture of hard (nanoparticles) and soft (LUVs) materials, and thus, an appropriate imaging technique must be used. Cryo-TEM is such an imaging tool, with which to obtain pictorial evidence of membrane perturbation via its interaction with HA-coated Ag and Au NPs. In reality, this means that we are trying to capture a snapshot images of NPs interacting with the POPC LUVs and perturbed LUVs with the nanoparticles still interacting with the bilayer of the LUVs.

The results for the HA-metal NP systems exposed to model biomembranes are shown in the cryo-TEM images. The HA-metal NPs appear to be interacting less with the model biomembranes at pH 7.6 than at pH 4.8. This is illustrated by the presence of intact vesicles even in the presence of the NPs at this pH. However, at pH 4.8 most of the NPs appear to interact with the vesicles, as most of them are noticeably ruptured. In addition, some NPs can be seen in contact with the vesicles. The TEM images results complement the steady state fluoresence results, which showed more leakage, as indicated by the increase in the fluoresence intensity at pH 4.8. The Cryo-TEM images further illustrate that the pertabation of the vesicles in the presence of NPs is mainly attributed to the interactions of the HAs coatings on the NPs with the biomembranes, as the NPs appear to be in contact with the vesicles and not right inside the vesicles.

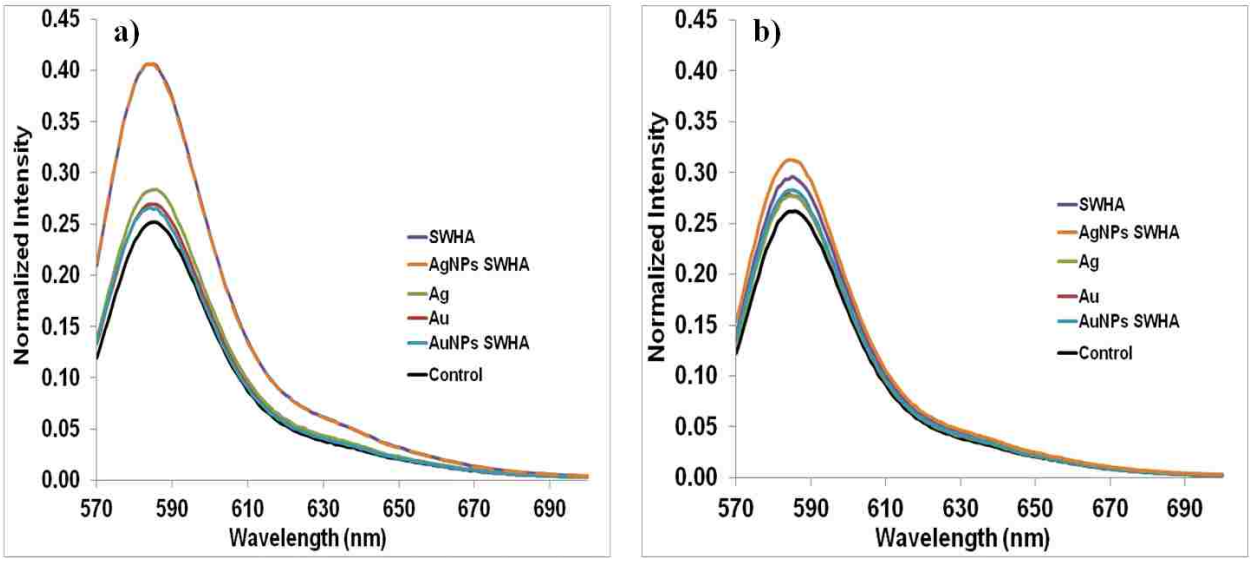

Figure 6.1 Fluorescence emission spectra of SRB dye leakage as induced by SWHA and NPs formed from SWHA a) is the leakage at pH 4.8 and b) is the leakage at pH 7.6.

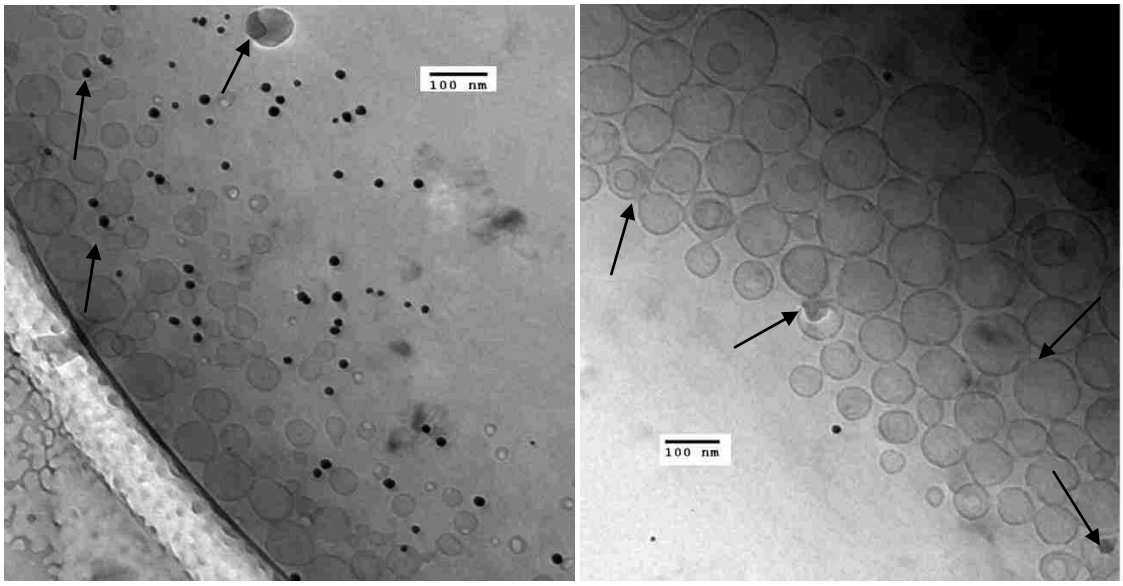

Figure 6.2 Cryo-TEM image of Au NP formed with SWHA at pH 7.6.

Some of the vesicles appear to be associating with the NPs, as shown by the arrows. A general dispruption is indicated by the smaller sizes of the vesicles and the irregularly shaped vesicles, which could be a result of interactions with HAs.

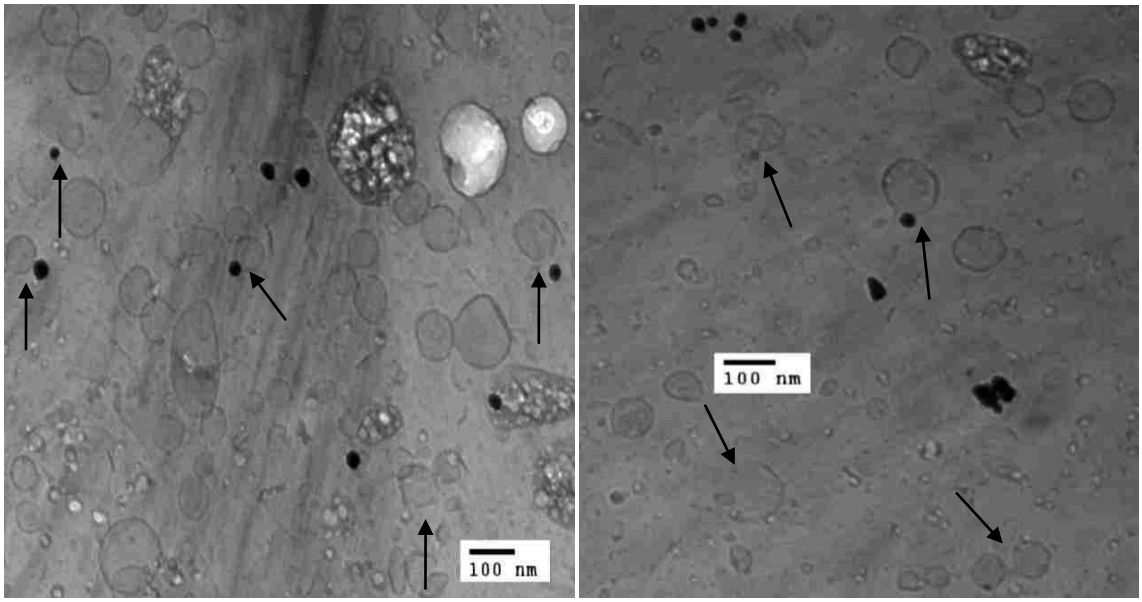

Figure 6.3 Cryo-TEM image of Au NP formed with SWHA at pH 4.8.

At pH 4.8 most of the vesicles above are raptured, as indicated by the arrows in the image above. Some vesicles also appear to be iteracting with the NPs.

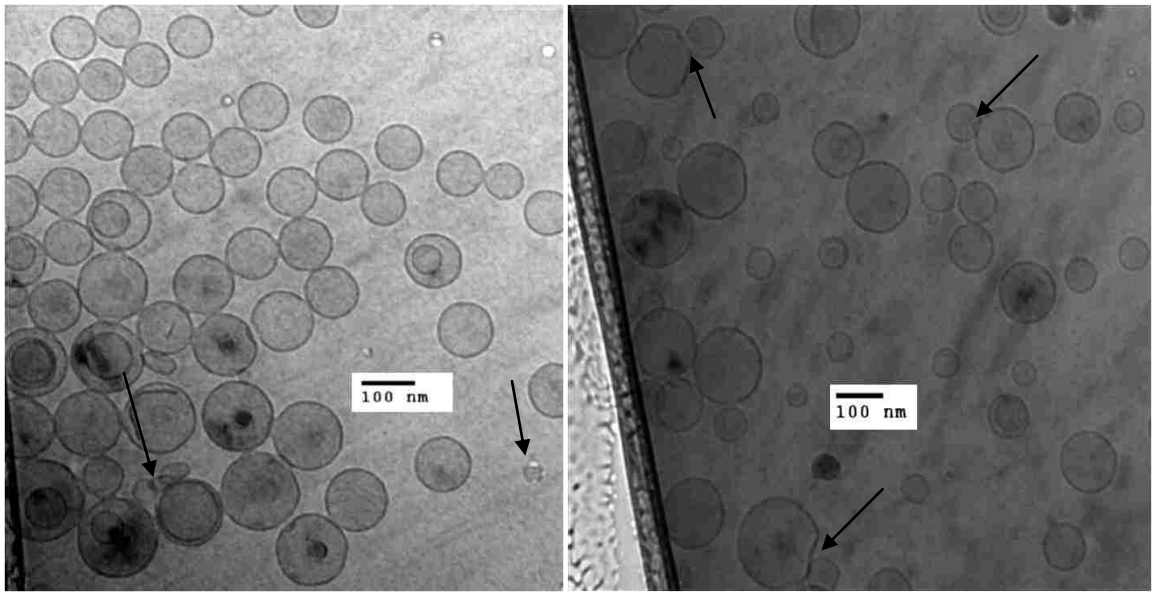

Figure 6.4 Cryo-TEM image of Ag NP formed with SWHA at pH 7.6

Most of the vesicles appear intact with a few exceptions that are of much smaller sizes, as shown by the arrow indicating that they may have been pertubed.

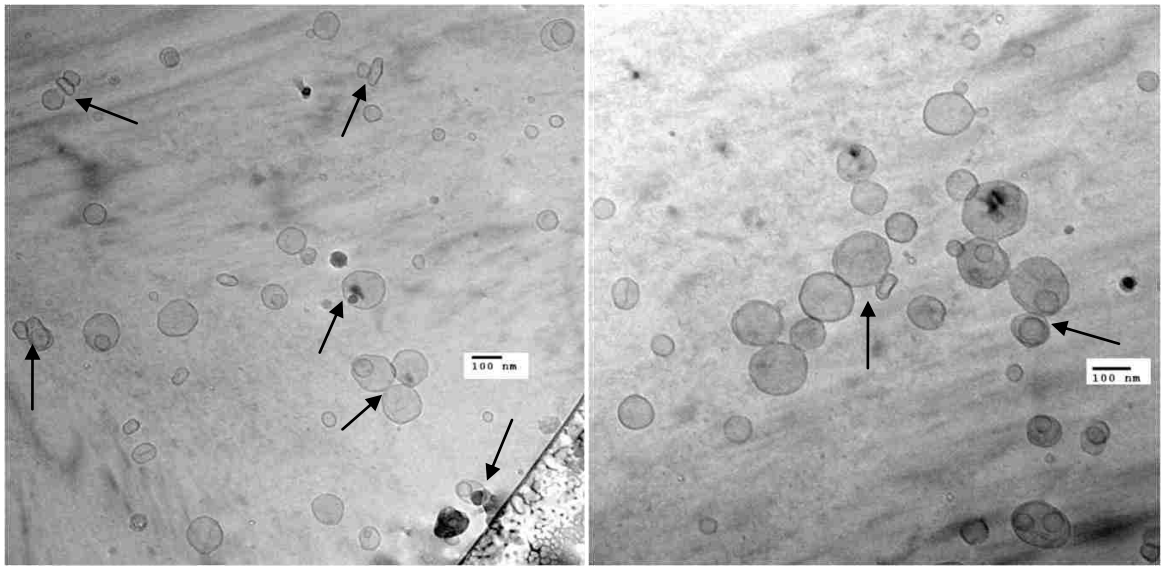

Figure 6.5 Cryo-TEM image of Ag NP formed with SWHA HA at pH 4.8

Some vesicles appear to be interacting with the NPs, as shown by the arrows, while other vesicles appear raptured, as illustrated by the smaller sizes of vesicles depicted in the image above.

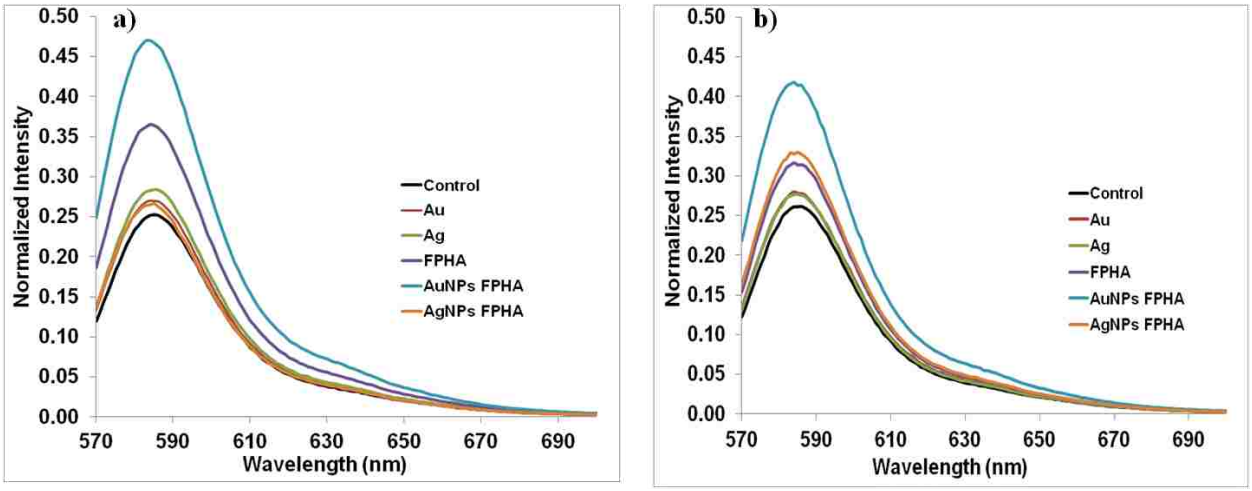

Figure 6.6 Fluorescence emission spectra of SRB dye leakage as induced by FPHA and NPs formed from FPHA, a) is the leakage at pH 4.8 and b) is the leakage at pH 7.6.

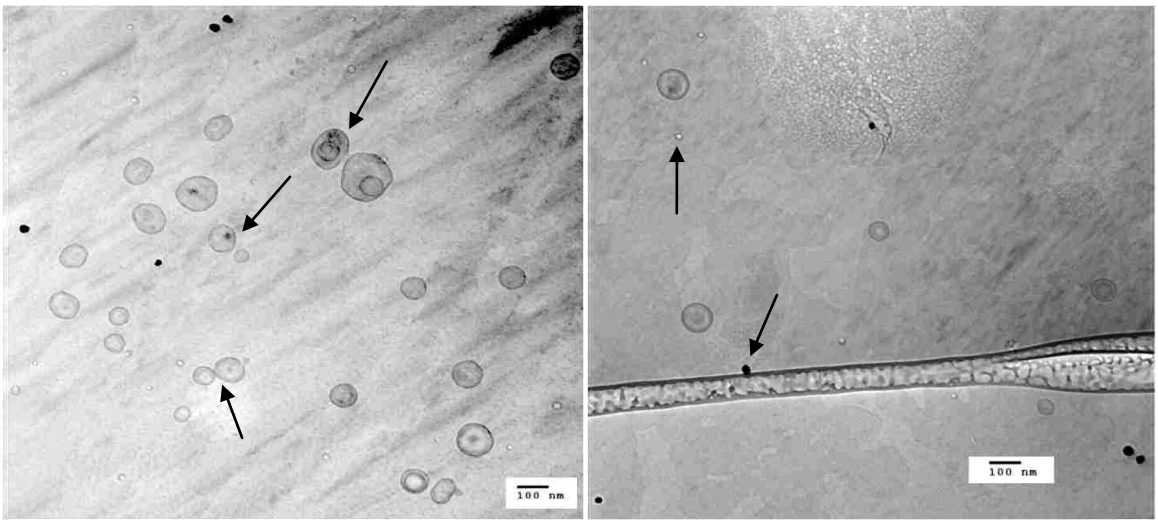

Figure 6.7 Cryo-TEM image of Au NPs formed with FPHA HA at pH 7.6

Most of the vesicles are intact, with a few exceptions of the pertubed ones, and the vesicles of smaller sizes, as shown by the arrows, indicating that they may have been pertubed. There is also

an indication of NPs interacting with the vesicle, as shown by the arrows in the cryo-TEM images.

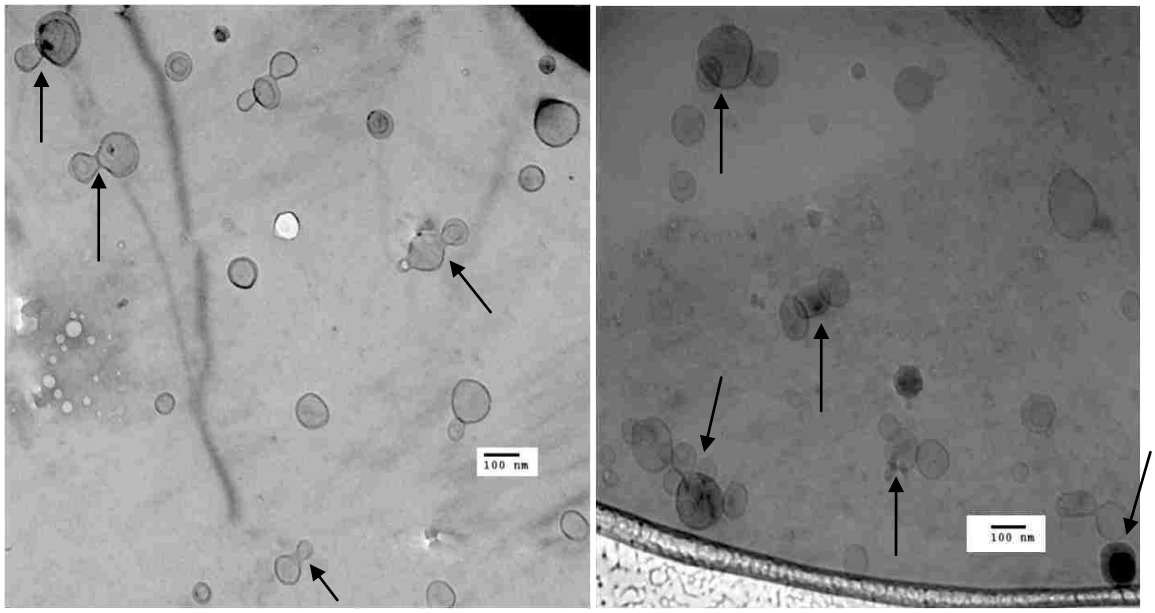

Figure 6.8 Cryo-TEM image of Au NPs formed with FPHA HA at pH 4.8

HAs appears to be forming hydrogen bridge between vesicles and gets absorbed by the vesicles, as depicted by the fusing of the vesicles. This, in turn, results in pertubation of the vesicles and dye leakage.

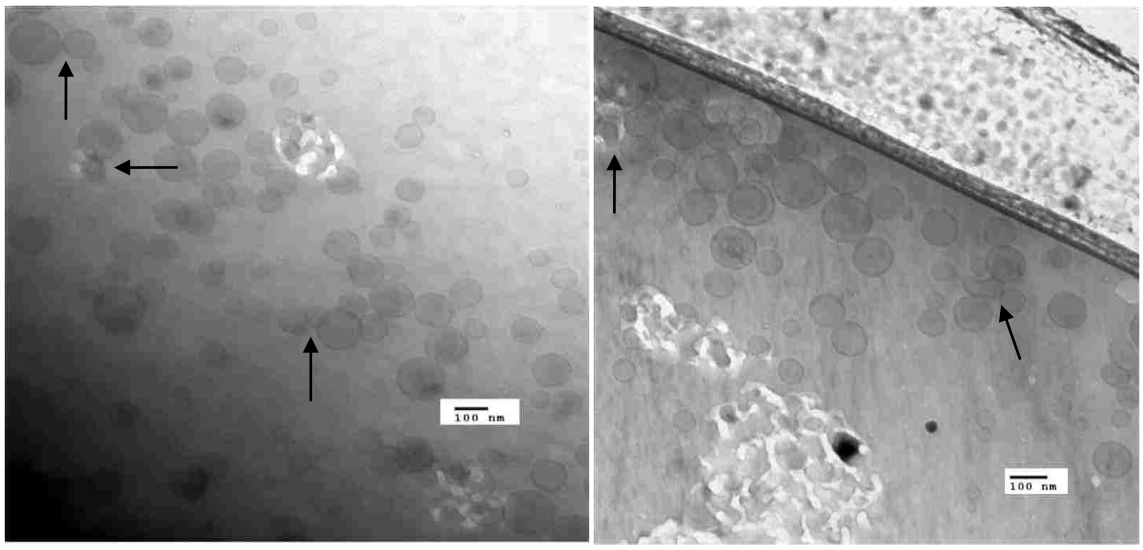

Figure 6.9 Cryo-TEM image of Ag NPs formed with FPHA HA at pH 7.6

There could be some form of slight interaction between the vesicles and HAs, as illustrated by the association of the vesicles with each other, as shown by the arrows.

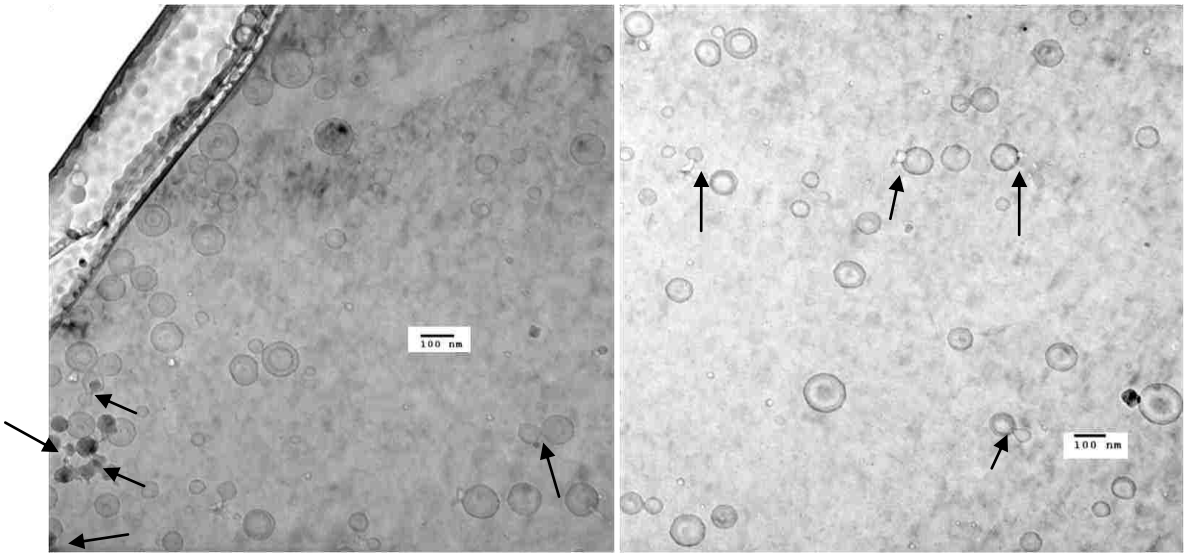

Figure 6.10 Cryo-TEM image of Ag NPs formed with FPHA at pH 4.8

HAs appears to be interacting with the vesicles, as depicted by the arrows and the aggregation of the vesicles, which could be attributed to the formation of hydrogen bridge between HAs and the vesicles, which in turn, results to pertubation of the vesicles and dye leakage. There also appears to be interactions between the NPs and the vesicles, as can be seen by the arrows.

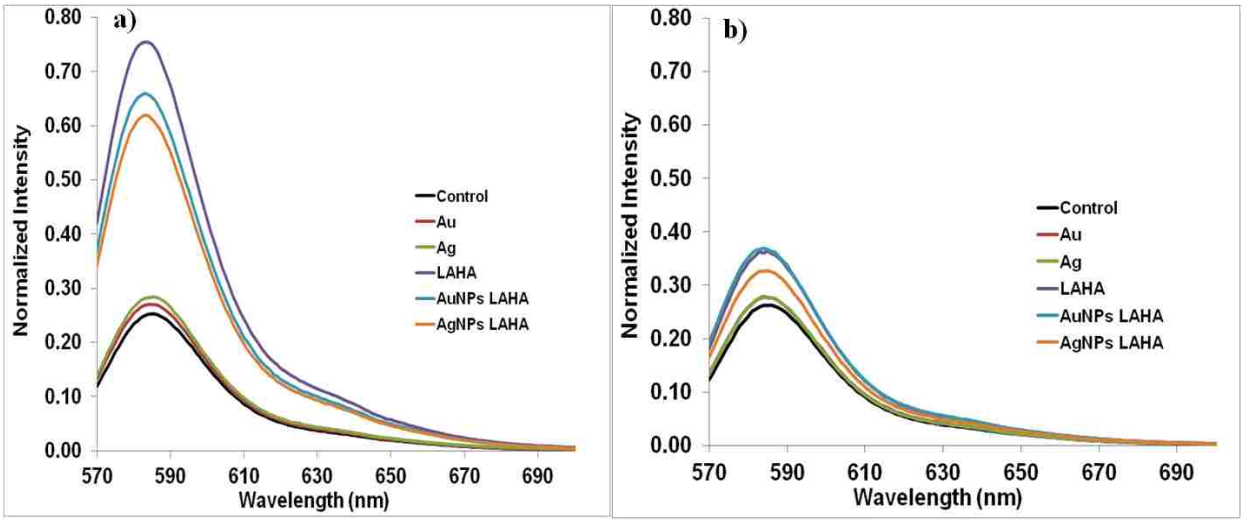

Figure 6.11 Fluorescence emission spectra of SRB dye leakage as induced by LAHA and NPs formed from LAHA a) is the leakage at pH 4.8 and b) is the leakage at pH 7.6.

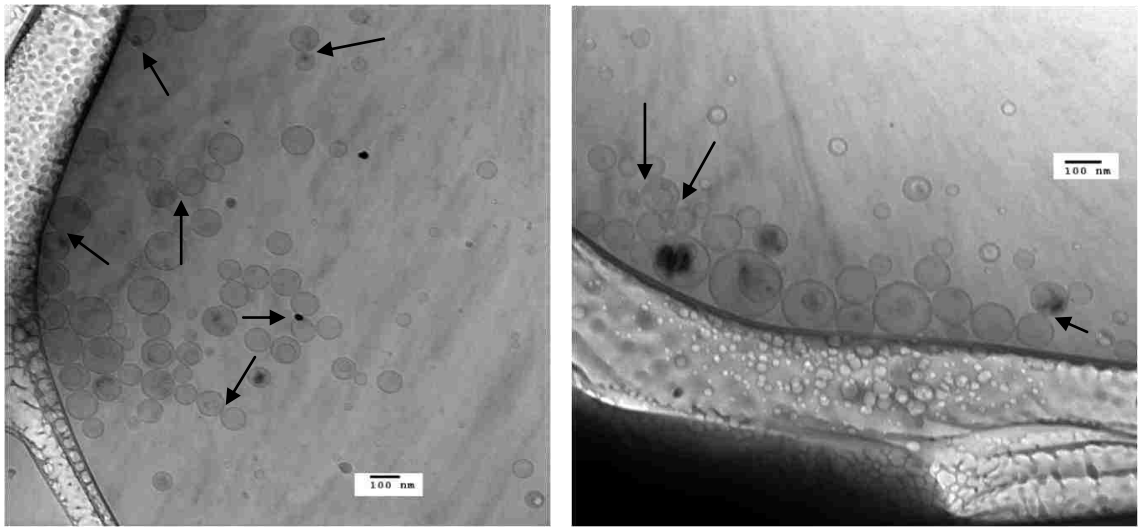

Figure 6.12 Cryo-TEM image of Au NPs formed with LAHA HA at pH 7.6

There appears to be slight interaction between the vesicles and HAs as illustrated by the association of the vesicles with each other as shown by the arrow. There also appears to be some sort of association of vesicles with NPs as illustrated by the arrows.

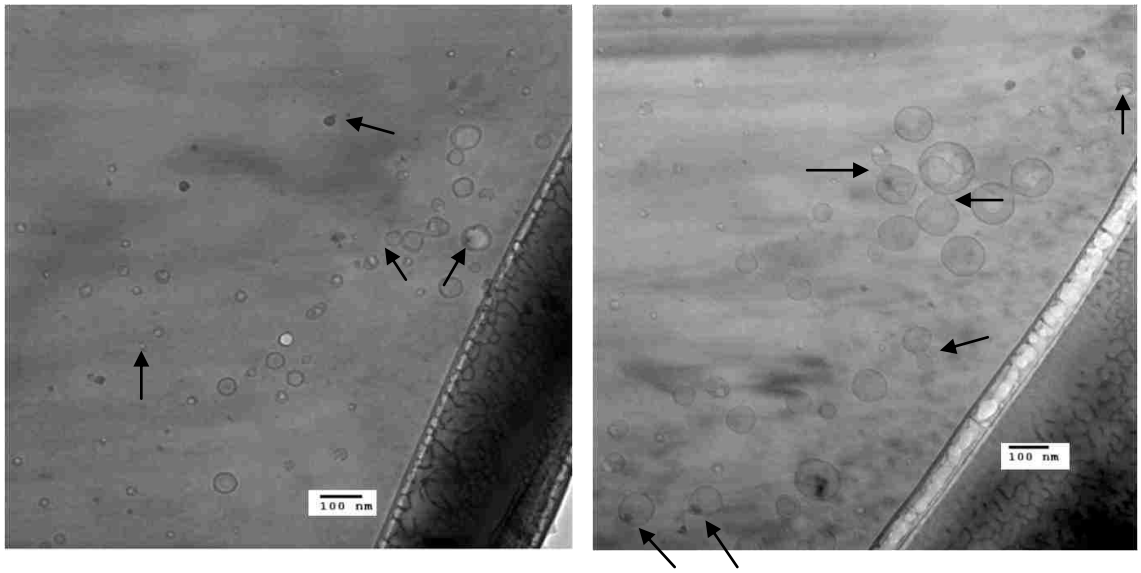

Figure 6.13 Cryo-TEM image of Au NPs formed with LAHA HA at pH 4.8

Some vesicles appear to be interacting with the vesicles, while some smaller sizes as shown by the arrow indicating that they may have been pertubed.

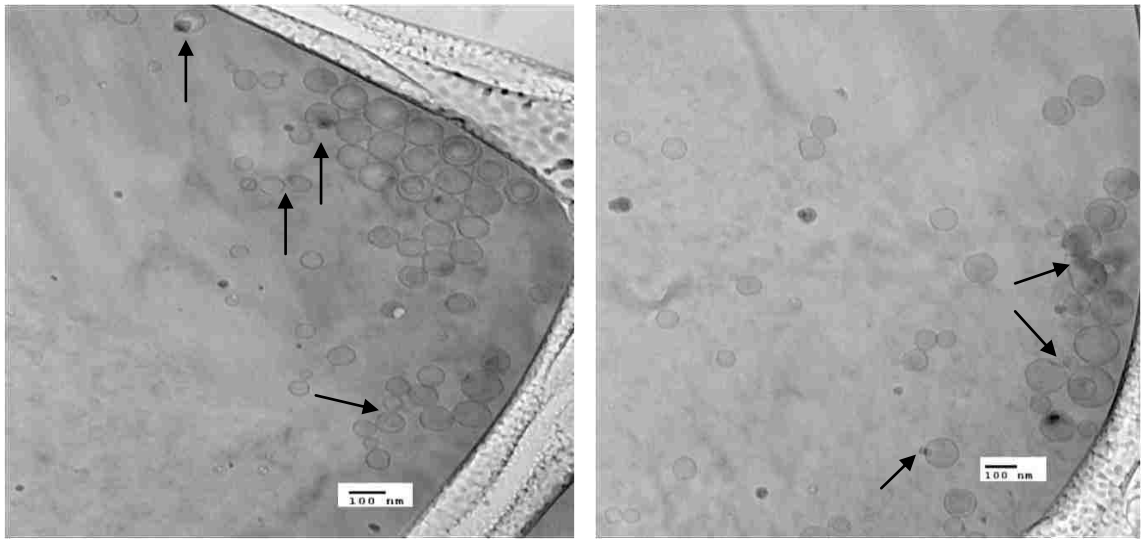

Figure 6.14 Cryo-TEM image of Ag NPs formed with LAHA at pH 7.6

Some vesicles appear to be interacting with the NPs as shown by the arrow while other vesicles appear raptured as illustrated by the smaller sizes of vesicles depicted in the image above.

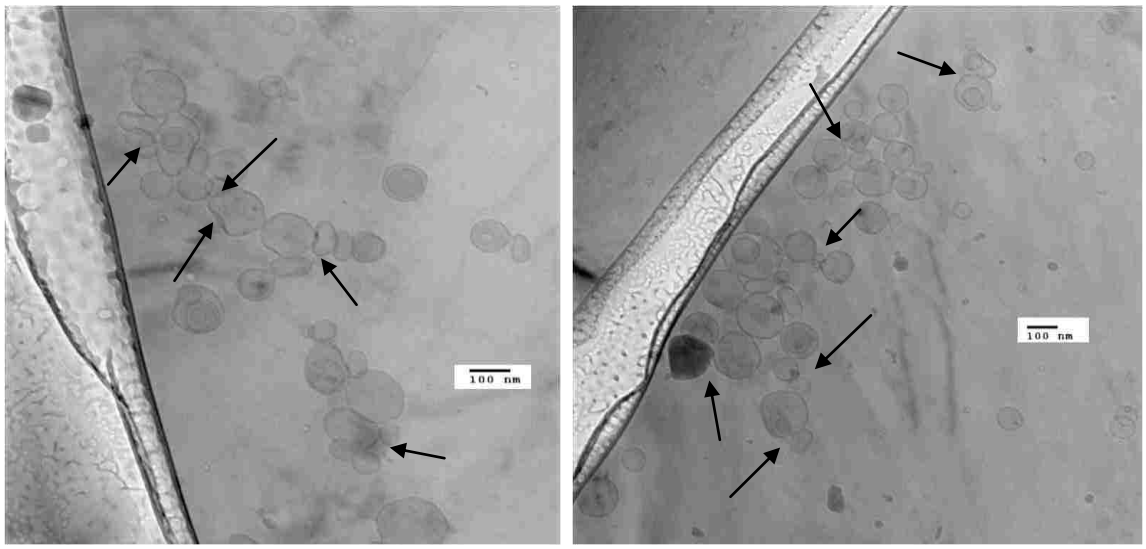

Figure 6.15 Cryo-TEM image of Ag NPs formed with LAHA HA at pH 4.8

Most of the vesicles above appear raptured as can be seen in the image above by the arrows. Some vesicles also appear to be interacting with the NPs. The aggregation of the vesicles could be an indication of the formation of hydrogen bridges between vesicles and HAs which inturn disrupts the vesicles resulting to dye leakage.

From the TEM images presented for the SWHA-capped NPs (Figure 6.2-6.5) it can be seen that, at pH 7.6, the majority of the imaged vesicles are spherical in shape, close to 100 nm in diameter, and unfused; however, there are some small and malformed vesicles visible for the Ag NPs. On the other hand, the pH 4.8 images show a number of malformed vesicles of various sizes, especially for the Ag NPs. As a whole, for the SWHA-capped NPs, the TEM results are in agreement with the fluorescence results, but there seems to be some discrepancy for the SWHA-capped Au NPs at pH 4.8. For the FPHA-capped Ag NPs, the TEM images at pH 7.6 in Figure 6.9, show the same behavior as did the SWHA-capped NPs in Figure 6.5, namely that the vesicles appear to be spherical in shape, close to 100 nm in diameter, and unfused. The images for the FPHA-capped Au NPs at pH 7.6 were different than their Ag counterparts in that they

formed a number of smaller vesicles, some of which were deformed. These pH 7.6 results are consistent with the fluorescence results in which the FPHA-capped Au NPs induced perturbation at this pH. The pH 4.8 images also show that, while the FPHA capped Ag NPs caused very little disruption of the imaged vesicles, their Au counterparts induced perturbation, as evidenced by malshaped vesicles as well as small vesicles and, in some cases, fused vesicles. Once again, these findings are consistent with the fluorescence results discussed above. For the LAHA-capped NPs at both pH conditions, both smaller and malshaped vesicles are visible, more so at the pH 4.8 than 7.6, as seen in Figure 6.2-6.15. Again, these findings are consistent with the fluorescence results.

If one combines the TEM and fluorescence results, it can be seen that the increased fluorescence, which means increased leakage of fluorescent dyes, and hence, increased biomembrane perturbation, is associated with smaller and distorted vesicle shape. Small and distorted vesicles were not present in the initial vesicle mixture before exposure to HA-capped NPs, as evidenced by the light scattering data and TEM images presented in Chapter 2 (Figures 2.1, and 2.2); however, smaller and distorted vesicles are observed in the presence of HA-capped NPs, as is an increase in the observed leakage. This leads to the empirical finding that the observed leakage can be correlated with smaller and distored vesicles. The HA biomembrane perturbation put forward in Chapter 2 can be further refined with these data it was in Chapter 3. The observed vesicle distortion is consistent with the HA on the surface of a nanoparticle absorbing into the bilayer of the vesicles, as discussed in Chapter 2 and 3, and perturbing the membrane's structural integrity, leading to a weakening of the vesicle, and hence, the observed distorted shape. This perturbation may lead to formation of pores large enough to allow for the dye leakage and give rise to some of the fluorescence seen in the fluorescence leakage

experiments. The observation of smaller vesicles can be explained by building on the above explanation; however, rather than just perturbing the membrane's structural integrity, there is a complete breakdown of the bilayer structure to the extent vesicle rupture, instead of just pore formation. Once the vesicle has been reptured, some of the fragments reform smaller vesicles. In this scenario it would be expected that all the fluorescent dye is released. This means that two different membrane perturbation processes may be at work, which is consistent with the fast and slow leakage stages described in Chapter 2. While the exact attribution of the observed fast and slow leakage stages to catastrophic vesicle failure and pore formation is not possible at this time, the kinetic analysis presented in Chapter 2 may provide some guidance. Nevertheless, the slow stage fluorescence leakage discussed in Chapter 2 would be consistent with the formation of pores, as this stage could be fitted to first order kinetics, which implies a single step process. On the other hand, catastrophic vesicle failure would require at least two steps, namely a bilayer breach, followed by vesicle rapture. This minimum of two steps means that this process could not be fitted by a single component, as required by the kinetic fitting attempted in Chapter 2. In addition, it is expected that a full vesicle rapture would lead to a full and rapid release of the fluorescent dye contained within the vesicle compared to a rather limited amount of dye released during the formation of pores. Both of these conclusions are consistent with the time course data and their kinetic analysis presented in Chapter 2. This implies that it is the HA on the NPs that allow the NPs to perturb the vesicles' bilayer and that the mechanism for perturbation of the biomembanes is rather complex with numerous steps (e.g., an adsorption step through a hydrogen bridge formation, a rapid absorption step, and a slow absorption step) as well trajectory pathways (visicle distortion, vesicle rupture, and vesicle reformation).

The cryo-TEM images also reveal two other interesting findings; there appears to be evidence of direct interactions of the NPs with vesicles and there appears to be vesicle fusion. The direct interaction of HA-capped NPs with the vesicles manifests itself in two different ways. The first is surface sorption; example of this are SWHA-capped Ag NPs at pH 4.8 and LAHA-capped Au NPs at pH 7.6 (Figure 6.3 and Figure 6.12). The second is internalization of the NPs into the vesicle, as seen for the SWHA and FPHA-capped NPs at pH 4.8 Figure 6.3 and 6.8. Also, some of the images, e.g., for the FPHA-capped Au NPs at pH 4.8, may show the crossing of the NPs through the bilayer. While the above observations are not conclusive due to the nature (e.g. lack depth information) of the cryo-TEM images obtained, they are very thought provoking and may allow for new insights into how nanoparticles, naturally coated with organic matter in the environment, may interact with biomembranes. The observation that there may be vesicle fusion is intriguing, as it is seen at both pH 7.4 and 4.8 (see SWHA-capped Au NPs at pH 7.6, FPHA-capped Au NPs at pH 4.8, FPHA-capped Ag NPs at pH 7.6, and LAHA-capped Au NPs at pH 4.8). The large variation in terms of HA, NP type, and pH means that, although the TEM images provide stong evidence for vesicle fusion, the exact meachanism of this fusion is not clear, and hence, generates a direction for a future study. With that said, in addition to causing an increase in membrane permeability, HA (the cryo-TEM images show NPs do not need to play a role) at acidic pH conditions may also induce vesicle, and hence, cell fusion; at the moment, however, this proposal is very speculative and stretches the available data well beyond scientific comfort. Overall, the cryo-TEM imaging provided useful and unique information and the specific nature of cryo-TEM was a good complement to the bulk fluorescence leakage studies.

6.4 Conclusions

The current study demonstrates that Au and Ag NPs synthesized and stabilized with chemically diverse HAs interact with induce a perturbation to the model biomembrane bilayer structure at naturally relevant concentrations as evidenced by the increase in leakage. These leakage studies further revealed that the formation of HA-capped NPs alters the potential of HAs to perturb biomembranes by either changing the potential of the HA present to form the needed hydrogen bridge or changing the potential of HA to absorb into the biomembrane through hydrophobic interactions. These interactions were further confirmed by cryo-TEM imaging. Cryo-TEM images demonstrated that the perturbations of the vesicles were as a result of the interaction of the residual HAs in solution and the HAs coatings on the NPs with the vesicles. The leakage and cryo-TEM imaging results further demonstrate that more HAs-metal NPs interactions were observed at pH 4.8 than at pH 7.6.

6.5 References

1. Elghanian, R.; Storhoff, J. J.; Mucic, R. C.; Letsinger, R. L.; Mirkin, C. A. Selective colorimetric detection of polynucleotides based on the distance-dependent optical properties of gold nanoparticles. *Science.* **1997,** *277* (5329), 1078-1081.

2. Mahtab, R.; Rogers, J. P.; Murphy, C. J. Protein-sized quantum-dot luminescence can distinguish between straight, bent, and kinked oligonucleotides. *Journal of the American Chemical Society.* **1995,** *117* (35), 9099-9100.

3. Gallagher, D.; Heady, W. E.; Racz, J. M.; Bhargava, R. N. Homogeneous precipitation of doped zinc-sulfide nanocrystals for photonic applications. *Journal of Materials Research.* **1995,** *10* (4), 870-876.

4. Williams, R. S. Computing in the 21st century: nanocircuitry, defect tolerance and quantum logic. *Philosophical Transactions of the Royal Society of London Series a-Mathematical Physical and Engineering Sciences.* **1998,** *356* (1743), 1783-1790.

5. Linsebigler, A. L.; Lu, G. Q.; Yates, J. T. Photocatalysis on TIO_2 surfaces-principles, mechanisms and selected results. *Chemical Reviews.* **1995,** *95* (3), 735-758.

6. Mills, A.; LeHunte, S. An overview of semiconductor photocatalysis. *Journal of Photochemistry and Photobiology a-Chemistry.* **1997,** *108* (1), 1-35.

7. Sharma, V. K.; Yngard, R. A.; Lin, Y. Silver nanoparticles: Green synthesis and their antimicrobial activities. *Adv. Colloid Interface Sci.* **2009,** *145* (1-2), 83-96.

8. Sotiriou, G. A.; Pratsinis, S. E. Antibacterial Activity of Nanosilver Ions and Particles. *Environ. Sci. Technol.* **2010,** *44* (14), 5649-5654.

9. Wigginton, N. S.; Haus, K. L.; Hochella, M. F. Aquatic environmental nanoparticles. *Journal of Environmental Monitoring.* **2007,** *9* (12), 1306-1316.

10. Maynard, A. D. Nanotechnology: assessing the risks. *Nano Today.* **2006,** *1* (2), 22-33.

11. Popov, A. P.; Priezzhev, A. V.; Lademann, J.; Myllyla, R. TiO_2 nanoparticles as an effective UV-B radiation skin-protective compound in sunscreens. *Journal of Physics D-Applied Physics.* **2005,** *38* (15), 2564-2570.

12. Zhang, W. X. Nanoscale iron particles for environmental remediation: An overview. *Journal of Nanoparticle Research.* **2003,** *5* (3-4), 323-332.

13. Nowack, B.; Bucheli, T. D. Occurrence, behavior and effects of nanoparticles in the environment. *Environmental Pollution.* **2007,** *150* (1), 5-22.

14. Urban, N. R.; Ernst, K.; Bernasconi, S. Addition of sulfur to organic matter during early diagenesis of lake sediments. *Geochimica Et Cosmochimica Acta.* **1999,** *63* (6), 837-853.

15. Stevenson, F. J. H. C. G. Humus chemistry genesis, composition, reactions. *John Wiley and Sons,* Stillerman. **1994.**

16. Wen, L. S.; Santschi, P. H.; Gill, G. A.; Paternostro, C. L.; Lehman, R. D. Colloidal and particulate silver in river and estuarine waters of Texas. *Environ. Sci. Technol.* **1997,** *31* (3), 723-731.

17. Akaighe, N.; MacCuspie, R. I.; Navarro, D. A.; Aga, D. S.; Banerjee, S.; Sohn, M.; Sharma, V. K. Humic Acid-Induced Silver Nanoparticle Formation Under Environmentally Relevant Conditions. *Environ. Sci. Technol.* **2011,** *45* (9), 3895-3901.

18. Machesky, M. L.; Andrade, W. O.; Rose, A. W. Interactions of gold (III) chloride and elemental gold with peat-derived humic substances. *Chemical Geology.* **1992,** *102* (1-4), 53-71.

19. dos Santos, D. S.; Alvarez-Puebla, R. A.; Oliveira, O. N.; Aroca, R. F. Controlling the size and shape of gold nanoparticles in fulvic acid colloidal solutions and their optical characterization using SERS. *Journal of Materials Chemistry.* **2005,** *15* (29), 3045-3049.

20. Lead, J. R.; Hamilton-Taylor, J.; Davison, W. Harper, M., Trace metal sorption by natural particles and coarse colloids. *Geochim. Cosmochim. Acta.* **1999,** *63* (11-12), 1661-1670.

21. Pallem, V. L.; Stretz, H. A.; Wells, M. J. M. Evaluating Aggregation of Gold Nanoparticles and Humic Substances Using Fluorescence Spectroscopy. *Environ. Sci. Technol.* **2009,** *43* (19), 7531-7535.

22. Stankus, D. P.; Lohse, S. E.; Hutchison, J. E.; Nason, J. A. Interactions between Natural Organic Matter and Gold Nanoparticles Stabilized with Different Organic Capping Agents. *Environmental Science & Technology.* **2011,** *45* (8), 3238-3244.

23. Sanchez-Marin, P.; Beiras, R. Adsorption of different types of dissolved organic matter to marine phytoplankton and implications for phytoplankton growth and Pb bioavailability. *Journal of Plankton Research.* **2011,** *33* (9), 1396-1409.

24. Vigneault, B.; Campbell, P. G. C. Uptake of cadmium by freshwater green algae: Effects of pH and aquatic humic substances. *Journal of Phycology.* **2005,** *41* (1), 55-61.

25. Sanchez-Marin, P.; Lorenzo, J. I.; Blust, R.; Beiras, R. Humic acids increase dissolved lead Bioavailability for marine invertebrates. *Environ. Sci. Technol.* **2007,** *41* (16), 5679-5684.

26. Richards, J. G.; Burnison, B. K.; Playle, R. C. Natural and commercial dissolved organic matter protects against the physiological effects of a combined cadmium and copper exposure on rainbow trout (Oncorhynchus mykiss). *Canadian Journal of Fisheries and Aquatic Sciences.* **1999,** *56* (3), 407-418.

27. Campbell, P. G. C. Interactions between trace metals and aquatic organisms: a critique of the free-ion activity model. Metal Speciation and Bioavailability in Aquatic Systems. ed.; *John Wiley and Sons, New York.* **1995.**

28. Lamelas, C.; Slaveykova, V. I. Comparison of Cd(II), Cu(II), and Pb(II) biouptake by green algae in the presence of humic acid. *Environ. Sci. Technol.* **2007,** *41* (11), 4172-4178.

29. Pempkowiak, J.; Kosakowska, A. Accumulation of cadmium by green algae Chlorella vulgaris in the presence of marine humic substances. *Environment International*. **1998,** *24* (5-6), 583-588.

30. Wang, Z. Y.; Li, J.; Zhao, J.; Xing, B. S. Toxicity and Internalization of CuO Nanoparticles to Prokaryotic Alga Microcystis aeruginosa as Affected by Dissolved Organic Matter. *Environ. Sci. Technol.* **2011,** *45* (14), 6032-6040.

31. Harper, S.; Usenko, C.; Hutchison, J. E.; Maddux, B. L. S.; Tanguay, R. L. In vivo biodistribution and toxicity depends on nanomaterial composition, size, surface functionalisation and route of exposure. *J. Exp. Nanosci.* **2008,** *3* (3), 195-206.

32. Wang, H. H.; Wick, R. L.; Xing, B. S. Toxicity of nanoparticulate and bulk ZnO, Al(2)O(3) and TiO(2) to the nematode Caenorhabditis elegans. *Environ. Pollut.* **2009,** *157* (4), 1171-1177.

Chapter 7. Conclusions

The goals of this study were: 1) to investigate the kinetics and the mechanism of the interaction of humic substances with model biomembranes; 2) to investigate the roles of different moieties within HAs in the interaction of HAs with model biomembranes; 3) to explore the potential of HAs from different sources to form Au and Ag NPs at environmentally realistic pH (both acidic and basic) conditions as well as to determine the importance of both the metal ion and HA concentrations; 4) to investigate the roles of aromatic, aliphatic (alkyl), and carbohydrate (O-alkyl) moieties within HAs in the formation of metal NPs and the stabilization of the formed NPs; and 5) to investigate the interaction of these naturally formed NPs with biomembranes.

The kinetics and the mechanisms of interactions of HAs with model biomembranes were successfully carried out using fluorescence spectroscopy. Fluorescence leakage studies indicated that HAs interacted with and perturbed model biomembranes at acidic pH values (4.8), thus making the model biomembranes permeable which is an effect lacking at a neutral pH (7.6). More leakage occurred due to higher perturbations at temperatures closer to the T_m of POPC, due to the acyl chain packing mismatches at the interfacial region that are caused by the coexistence of both the gel and liquid crystalline phases in the phase boundaries [1-6]. HAs concentrations as low as 0.3 mg C/L caused leakage; the leakage increased with increasing concentration of HAs.

The interaction of HAs with model biomembranes has been shown to occur in two main steps: (1) an initial instant *ad*sorption by hydrogen bridging between the phosphate group and the negatively charged functional groups of HAs followed by (2) a rapid *ab*sorption via hydrophobic interactions along with a slow *ab*sorption via hydrophobic interactions following first order kinetics. These findings agree well with the literature and with the theoretical model postulated

by Elayan, et al.[7]. All three chemically diverse HAs studied here perturbed the model biomembranes at acidic pHs.

Investigations into the roles of different moieties within HAs in perturbing the model biomembranes were investigated. The chemical treatment applied to the HAs investigated in Chapter 3 generated specific structural modifications on the HAs samples: bleaching eliminated a significant portion of the aromatic components; hydrolysis reduced most of the carbohydrates; and lipid extraction removed most of the lipids. The study demonstrated further that the hydrolyzed HAs interact with the biomembranes more than the unmodified HAs, while the bleached HAs interact with biomembranes the least. Data presented in this study serves as strong evidence that aromatic components within the HAs are the major biomembrane disruptors; however, direct evidence is impossible to due to the complex and heterogeneous nature of HAs and NOM as a whole.

All the three chemically diverse HAs studied in Chapter 4 reduced metal cations to their NPs. The metal reduction reactions were faster in the presence of SWHA, compared to FPHA and LAHA, which required almost similar time. We have shown that the NPs formed at both pH 4.8 and pH 7.6 for both silver (for the first time at an acidic pH and at environmentally relevant concentrations) and gold and that the NPs formed at pH 4.8 were mostly aggregated, while the NPs at pH 7.6 were suspended in solution. This study has further demonstrated that the reduction reactions were faster for gold metal, compared to silver metal, which required 4-5 weeks for complete synthesis. In addition, this study has demonstrated that reduction of metal cations to metal NPs is dependent on the metal concentration as well as the source and concentration of HAs, and that, at extremely low concentrations, such as 1 μM, metal cations may not be reduced to metal NPs in the natural environment.

The results from Chapter 5 suggest certain premises but do not provide direct proof of the roles of the aromatic, aliphatic and carbohydrate moieties in the formation of NPs. This is due to the complex, heterogeneous and polydisperse nature of humic substances. However, in all probability, the aliphatic, aromatic, and carbohydrate moieties within HAs are involved in Au and Ag NPs formation for all the HAs studied. The extent of the influences of these different moieties on the formation of Au and Ag NPs is different depending on the origin of the HA. This is due to the complex processes accompanying the formation of NPs by HAs, including binding and reduction of the metal cations by the HAs where, as illustrated by the metal and HA concentration data presented in this chapter as well as in the previous chapter, the secondary and tertiary structures of the HAs also play an equally important role.

Chapter 6 illustrated that Au and Ag NPs formed and stabilized with chemically diverse HAs interact with and induce a perturbation to the model biomembrane bilayer structure at naturally relevant concentrations as evidenced by the increase in leakage. These leakage studies further revealed that the formation of HAs-capped NPs alters the potential of HAs to perturb biomembranes by either changing the potential of the HA present to form the needed hydrogen bridge or changing the potential of HA to absorb into the biomembrane through hydrophobic interactions. These interactions were further confirmed by cryo-TEM imaging. Cryo-TEM images demonstrated that the perturbations of the vesicles resulted from the interaction of the residual HAs in solution as well as the HAs coatings on the NPs with the vesicles. The leakage and cryo-TEM imaging results further demonstrated that more HAs-metal NPs interactions were observed at pH 4.8 than at pH 7.6.

7.1 Future Directions and Ongoing Studies

These studies were done on a very simple model membrane system, POPC. In the future, these studies will be extended to a more complex system that would mimic the real biomembranes in the environment since cell membranes are much more complex than the model biomembranes used the studies in this dissertation. The complexity of the model membranes will be increased systematically by first studying mixed membrane systems with different phospholipids, then adding cholesterol to the phospholipids.

HAs from both aquatic and terrestrial environments were used in this study. Future studies will investigate the formation of NPs using HAs extracted from Pony Lake which are acidic in nature and contain no lignins residuals. The potential of NPs formation from HAs extracted from the discharge of municipal wastewater effluent will also be investigated as this is an important source of ENPs discharge to surface waters, particularly in urbanized estuaries and effluent-dominated rivers, since we anticipate that metal ions may be present in these waste plants. The NPs studied in this thesis were mainly from metal ions. Future studies will investigate the interactions between organic forms of nanomaterial such as fullerenes and carbon nanotubes with model biomembranes in the presence of HAs using fluorescence spectroscopy and cryo-TEM. The NPs formed using chemically edited HAs in this study were only characterized using UV-Vis spectroscopy. We hope to characterize them with TEM to determine their size and size distribution. The crystallinity of the NPs formed in both Chapters 4 and 5 will be determined using TEM. In addition, the chemical composition oxidation state, chemical bonding, and surface properties of the NPs formed in this study will be further investigated with electron energy-loss spectroscopy spectrum imaging. This basically involves the bombardment of a sample with a

monoenergetic beam of electrons which causes the sample to lose energy through various mechanisms. The energy loss by the sample determines the composition of the sample.

7.2 References

1. Papahadj.D; Jacobson, K.; Nir, S.; Isac, T. Phase-transitions in phospholipid vesicles-fluoresence polarizationand permeabilitymeasurements concerning effect of temperature and cholesterol. *Biochimica Et Biophysica Acta.* **1973,** *311* (3), 330-348.

2. Marsh, D.; Watts, A.; Knowles, P. F. Evidence for phase boundary lipid -permeability of tempo-choline into dimyristoylphossphatidylcholine vesicles at phase-transition.. *Biochemistry.* **1976,** *15* (16), 3570-3578.

3. Blok, M. C.; Vanderneutkok, E. C. M.; Vandeenen, L. L. M.; Degier, J. Effect of chain-length and lipid phase-transitions on selective permeability properties of liposomes. *Biochimica Et Biophysica Acta.* **1975,** *406* (2), 187-196.

4. Vanhoogevest, P.; Degier, J.; Dekruijff, B. Determination of the size of the packing defects in dymyristoylphosphatylcholine bilayers present at the phase-transition temperature. *Febs Letters.* **1984,** *171* (2), 160-164.

5. Elmashak, E. M.; Tsong, T. Y. Ion selectivity of temperature-induced and electric-field induced pores in dipalmitoylphosphatidylcholine vesicles. *Biochemistry.* **1985,** *24* (12), 2884-2888.

6. Georgallas, A.; Macarthur, J. D.; Ma, X. P.; Nguyen, C. V.; Palmer, G. R.; Singer, M. A.; Tse, M. Y. The diffusion of small ions through phospholipid-bilayers. *Journal of Chemical Physics.* **1987,** *86* (12), 7218-7226.

7. Elayan, N. M.; Treleaven, W. D.; Cook, R. L. Monitoring the effect of three humic acids on a model membrane system using ^{31}P NMR. *Environ. Sci. Technol.* **2008,** *42* (5), 1531-1536.

Vita

Loice Marklyne Ojwang was born to parents Maurice and Benta Ojwang' in Western, Kenya. She lived her childhood years in Western Kenya where she obtained her high school diploma at Kaimosi Girls High school in Vihiga, Kenya. Upon graduation, she enrolled at Moi University Chepkoilel Campus, Kenya where she obtained her Bachelor of Science degree in chemistry in 2005. In the fall 2006 she began graduate studies at Louisiana State University in the Department of Chemistry, Baton Rouge. Loice M. Ojwang is currently a candidate for the degree of Doctor of Philosophy in analytical chemistry, which will be awarded at the August 2012 Commencement.